Injectable Poly (Ethylene Glycol) Hydrogels for Spinal Cord Injury Repair

Douglas Venters

(MEng)

Submitted in fulfilment of the requirements for the Degree of

Doctor of Philosophy (PhD)

School of Science and Engineering

College of Engineering

University of Glasgow

Glasgow, G12 8LT

Abstract

Poly (Ethylene Glycol) (PEG) hydrogels are becoming more ubiquitous in tissue engineering applications due to their inherent biocompatibility, ability to replicate the mechanical environment of soft tissues and their capacity for a diverse range of modifications which make them useful in numerous biological environments. However, spinal cord injury repair is a branch of tissue engineering that is currently provides very limited options on biomaterial strategies to promote recovery and therefore could benefit from an increased focus on developing new materials. This body of work describes the physico-chemical characterisation of hydrogels based on 4-armed PEG-maleimide (PEG-4MAL) which incorporate matrix metalloprotease sensitive peptide cross-linkers to impart degradability, and further functionalisation with integrin-recognisable peptide ligands.

Formulations of the hydrogels were created to include the fibronectin derived RGD peptide sequence or the laminin derived IKVAV sequence, and additional variants were formed by altering proportions of the degradable VPM peptide cross-linker in substitution for non-degradable PEG-dithiol, which was found to enable tuneability of the hydrogel degradation rate. Degradation of the gels in type 1 collagenase could be tuned to range from hours to months and potentially longer by altering the cross-linker character. Young's moduli in the order of hundreds of pascals to low kilopascal range were achieved to make appropriate substrates that replicate the stiffness of the spinal cord. The gelation properties and swelling behaviour were also characterised and the release profiles of nerve growth factor and brain derived neurotrophic factor from the PEG-4MAL hydrogels were evaluated, demonstrating their capability to be loaded with the neurotrophins and rapidly release them into aqueous environments.

PEG-4MAL hydrogels were used to investigate the 3D behaviour of several cell types derived from neural tissues, to include cortical astrocytes, spinal cord dissociated neurons and dorsal root ganglia explants suspended within the hydrogels, along with additional experiments conducted using mesenchymal stem cells. Each of the cell types analysed confirmed the capability of the RGD-tethered hydrogels to promote cellular adhesion and migration in 3D. Neurite outgrowth from DRGs was promoted in RGD bound gels and further encouraged by the incorporation of nerve growth factor into the hydrogel. Spinal cord neurons displayed extensive neuritogenesis within each of the PEG-4MAL gels with the highest neurite densities observe in RGD-tethered hydrogels.

A microfluidics-based system was devised for creating hydrogel microspheres to expedite the implantation of the material into spinal cord injury *in vivo* models. These devices enabled the reliable production of microspheres with a high throughput and narrow size dispersity. Biocompatibility was also measured using mesenchymal stem cells and high levels of viability were retained after 7 days culture on the hydrogel microspheres. MSCs grown on the RGD functionalised microspheres were observed to adhere to their surfaces and conform to the topography presented by the microspheres.

Finally, the hydrogels were evaluated in pilot *in vivo* studies using rat contusion models of spinal cord injury. Hydrogel microspheres were injected into the injury site of the contused spinal cord and development of the resulting cellular response was observed after 7 weeks. Histological analysis revealed a degree of astrocyte infiltration into the contusion cavities filled with RGD microspheres along with some deposition of laminin around them. The microsphere injected spinal cords also displayed evidence of reduced astrocyte reactivity. Modest evidence of axonal presence within the cavities was also observed. This has laid the groundwork for future studies of a larger scale to fully elucidate the potential of the hydrogels as a therapy for spinal cord injury.

Contents

Author’s Declaration

I hereby declare that the research presented within this thesis is my own work unless otherwise stated and has not been submitted elsewhere for any other academic degree.

Acknowledgements

Firstly I'd like to extend my gratitude to my supervisors Prof. Manuel Salmeron-Sanchez and Dr. John Riddell for pioneering this project and providing me the opportunity to contribute to the under-represented field of spinal cord injury research. Both have worked tirelessly in their efforts to provide the resources, guidance and insights necessary to navigate this undertaking from start to finish, without which the obstacles encountered along the way may have proven too great to surmount. I would also like to thank my secondary supervisor Dr. Cristina Gonzalez-Garcia for everything that she has contributed over the last 4 years to build on my capabilities, to encourage my progress and to provide perspective where it was missing. These have all been invaluable inputs for maintaining the motivation to persevere until my goals could be completed.

For the people in my lab, I couldn't have asked for a better group of people to work with. I don't think I've ever encountered such a frictionless environment and I could rely on anyone for help at any time for any reason. They have all demonstrated time and again that work in the lab doesn't always have to be a gruelling task can actually, on occasion, be quite rewarding. I would also like to give special mention to everyone in Prof. Sue Barnett's group, they made possible many of the experiments that were conducted throughout my PhD by providing more than just generosity but their expertise, patience and some discussions I will never be able to forget.

I have always been able to rely on my family and throughout my PhD this has been no different. It's reassuring to know that regardless of what I achieve or do not achieve that my standing among them will never be diminished, and that anything I can add to that will be a bonus. For raising myself and my brothers I owe my parents a debt of gratitude that can never be repaid and so I will endeavour to pay it forward. From my grandparents I've only seen unwavering kindness, optimism and enthusiasm. Grandad, if you're reading this, you're going to need those if you hope to make it to the end of this thesis!

Last but not least I need to thank my girlfriend Dr. Moya Hay who has been by my side for most of my adult life. It is no exaggeration to say I could not have made it through this undertaking without her and she has imparted all the qualities I could have needed to reach this stage. My work ethic is derived almost entirely from hers and she continues to be an inspiration to myself and all those around her. She has been with me for some of the best times of my life and no doubt many more in the future which cannot come too soon.

List of Figures & Tables

List of Abbreviations

(β)NGF	(Beta) Nerve Growth Factor
A.U.	Arbitrary Units
AFM	Atomic Force Microscopy
ALS	Amyotrophic Lateral Sclerosis
AMPA	α-amino-3-hydroxy-5-methyl-4-isoxazolepropionic acid
BBB	Blood Brain Barrier/ Basso, Beattie and Bresnahan
BDNF	Brain-Derived Neurotrophic Factor
BSA	Bovine Serum Albumin
BSCB	Blood Spinal Cord Barrier
CNS	Central Nervous System
CSF	Cerebrospinal Fluid
CSPG	Chondroitin Sulphate Proteoglycan
DIV	Days *in vitro*
DNA	Deoxyribonucleic Acid
DRG	Dorsal Root Ganglia
E15	Embryonic Day 15
ECM	Extracellular Matrix
EDTA	Ethylenediaminetetraacetic acid
FBS	Foetal Bovine Serum
GFAP	Glial Fibrillary Acidic Protein
GFOGER	Glycine-Phenylalanine-Hydroxyproline-Glycine-Glutamate-Arginine
h	Hour(s)
HA	Hyaluronic Acid
HCl	Hydrochloric Acid
hMSC	Human Mesenchymal Stem Cell
HS	Horse Serum
IKVAV	Isoleucine-Lysine-Valine-Alanine-Valine (Laminin Derived Integrin Ligand)
K	Spring Constant
MMP	Matrix Metalloprotease
MSC	Mesenchymal Stem Cell
MW	Molecular Weight
NDMA	N-methyl-D-aspartate
NF200	Neurofilament 200
NPC	Neural Precursor Cell
NSC	Neural Stem Cell
P1	Postnatal Day 1
PBS	Phosphate Buffered Saline
PDMS	Polydimethylsiloxane
PEG	Poly(ethylene glycol)
PEG-4MAL	4-armed Poly(ethylene glycol)-maleimide

PEG-diSH	Poly(ethylene glycol)-di-thiol
PFA	Paraformaldehyde
pHEMA	Poly(hydroxyethylmethactrylate)
PNIPAM	Poly (N-isopropylacrylamide)
PTFE	Polytetrafluoroethylene
RGD	Arginine-Glycine-Aspartic acid (Fibronectin Derived Integrin Ligand)
ROI	Region of Interest
ROS	Reactive Oxygen Species
rpm	Rotations Per Minute
SCI	Spinal Cord Injury
TNF-α	Tumour Necrosis Factor Alpha
Trk(A,B,C)	Tropomyosin Receptor Kinase (A,B,C)
U/mL	Units/mL
UV	Ultraviolet
VPM	Valine-Proline-Methionine (Degradable Cross-Linker)
wt/vol	Weight/Volume
YIGSR	Tyrosine-Isoleucine-Glycine-Serine-Arginine
C_n	Flory Characteristic Ratio
χ	Flory Polymer-Solvent Interaction Parameter
δ	Indentation Depth
E	Young's Modulus
F	Force
l	Average Bond Length Within the Polymer Chain
$\overline{M_c}$	Average Molecular Weight Between Cross-Links
$\overline{M_n}$	Average Molecular Weight
m_d	Dry Mass
M_r	Monomer Molecular Weight
m_r	Relaxed Gel Mass
m_s	Swollen Mass
$\overline{v}$	Specific Volume
v	Poisson's Ratio
q_f	Ratio of Relaxed/Dry Gel
q_w	Weight Swelling Ratio
r	Radius
$\left(\bar{r}_0^2\right)^{1/2}$	Polymer Chain Length Between Cross-Links in the Unperturbed State
ρ_{PEG}	Density of PEG
ρ_{water}	Density of Water
V_1	Molar Volume of Water
$v_{2,r}$	Volume Fraction of Polymer in Hydrogel Relaxed State
$v_{2,s}$	Volume Fraction of Polymer in Hydrogel Swollen State
ξ	Hydrogel Mesh Size

1. Introduction

1.1 The Spinal Cord

1.1.1 Cellular Environment

The spinal cord is one of two major components that make up the central nervous system (CNS) and is responsible for the reception, modulation and transmission of sensory and motor signals to and from the brain respectively (Shahdoost *et al.*, 2014). It does this through an extensive network of neurons, which can be broadly categorised into sensory neurons, motor neurons and interneurons, each of which can be further subcategorised by factors including function, location, transmitter types or morphology (Osseward and Pfaff, 2019). Neurons typically possess one axon which can project over extremely long distances to form synapses to target innervation sites, which depending on the type can be over a metre from the cell body in human adults (Karamched and Bressloff, 2015). One axon can have a multitude of branches, each possessing synapses with unique targets. Neurons communicate with the apposed cells across the synapse by the release of neurotransmitters from the axon terminal when calcium ion influx is triggered by modulation of the cross-membrane voltage (Mccormick, 2014). The neuronal body has several shorter projections known as dendrites that are equipped to receive signals from axons by presenting a high density of ionotropic or metabotropic surface receptors (Noback *et al.*, 2005; Naser and Kuner, 2018). Activation of these postsynaptic receptors enables ions to enter the cell and depolarise the membrane potential, thereby activating voltage-gated ion channels and mediating a migration of charge, propagating the electrical signal (Bezanilla, 2005). The mechanisms of conduction and cross-synaptic transmission operate at sufficient speed that the timespan between sensation, processing and response can be less than 200ms (Fendrich, Hutsler and Gazzaniga, 2004).

To complement and regulate the function of neurons there are also a variety of supporting cells known as glia which encompass a range of different roles and types. Figure 1.1 provides an overview of the how these cells can be observed within the CNS. Oligodendrocytes are responsible for laminating axons with myelin which behaves as an electrical insulator (Pirko and Noseworthy, 2007). Oligodendrocytes are highly prolific and will myelinate several axonal segments in their vicinity (Felton, O'Banion and Maida, 2016). The myelin sheath is periodically interrupted to expose of the axonal membrane and allow transmembrane ionic transport, giving rise to the characteristic saltatory pattern of conduction (Waxman, 2017). Without myelin, the conduction velocity of the axons is a fraction of those that are wrapped in it and as such disruption of oligodendrocytes will severely impact the ability of neurons

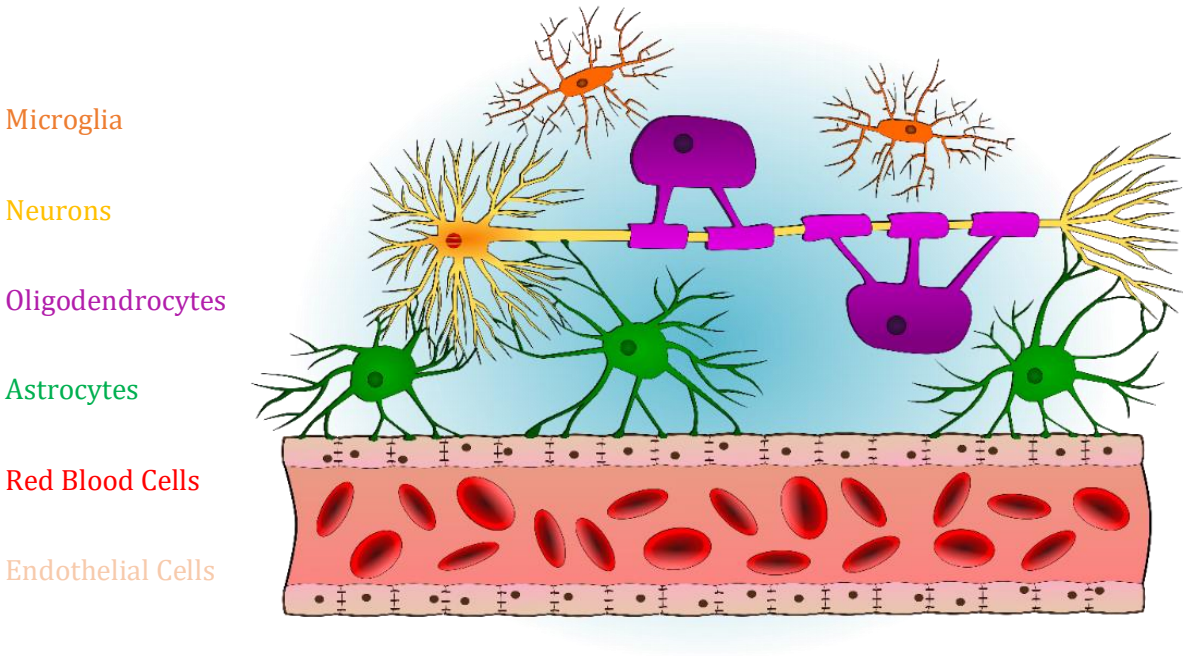

Figure 1.1 *The cellular microenvironment in the spinal cord. The colour legend (left) identifies several key cell types present in the typical spinal cord. Neurons have many postsynaptic dendrites aminating from the cell body and long axons with several presynaptic branches. Oligodendrocytes wrap these axons in myelin to improve conductivity. Astrocytes articulate with neurons, other glia and vasculature to control the extracellular environment in the CNS, in part by regulating the blood brain barrier (BBB) which is characterised by tightly bound capillary endothelia. Microglia are the native CNS immune-type cells and traverse the tissues to response to aberrant environments.*

to communicate. Astrocytes are also present in the spinal cord in high numbers and are heavily involved in the regulation the CNS extracellular environment (Herndon, Tome and Davis, 2017). Astrocytes are known to facilitate the reabsorption of neurotransmitters from the synaptic space which is a useful function in itself, but this can also trigger the release of metabolic components to enhance neuronal respiration, as well as modulating neurovascular tone to increase blood supply when energy requirements are high (Stobart and Anderson, 2013). Beyond this, astrocytes are also instrumental in the formation and maintenance of the blood brain barrier (or in the spinal cord the blood spinal cord barrier) by secreting factors to promote tight junction formation between vascular endothelial cells (Whetstone *et al.*, 2010; Cabezas *et al.*, 2014). Microglia take on a role similar to that of circulatory macrophages in response to immunological threats but are specific to the CNS. In healthy tissues, microglia have been observed to be highly pervasive and constantly monitor their environment for signs of pathology (Popovich, Jakeman and McTigue, 2009). They are also involved in synaptic pruning processes which contribute to neuronal plasticity (Salter and

Stevens, 2017). In abnormal conditions such as injury they rapidly transform into an activated phenotype and engage in phagocytosis of damaged tissue, on top of which they can also release neurotrophic factors into the extracellular environment (Kreutzberg, 1995; Lazarini *et al.*, 2012). However there is a duality in their role in spinal cord injury as they may exacerbate pathologies much more than they prevent it by intensifying neuro-inflammation once in their activated state (Gaudet and Fonken, 2018).

1.1.2 Functional Organisation

The internal architecture of the spinal cord is organised into distinct regions that control its various functions. Looking at a transverse section of the cord reveals a split between white matter at the peripheries of the cord and grey matter in the centre in what is said to resemble a butterfly or an H-shape (Dowlati, 2017). Both sections are occupied by significant numbers of glia, but they can be distinguished by their neuronal content. The white matter is filled predominantly with myelinated axons and are commonly segmented into tracts which usually derive their name from their origin and their terminals (Purves *et al.*, 2001). Figure 1.2 indicates some of the pathways that neurons can follow along the PNS and CNS. Descending tracts are occupied by efferent motor axons that have control over muscular contractility (Sengul and Watson, 2015). The corticospinal tract for example originates in the cerebral cortex and passes down the spinal cord before synapsing with lower motor neurons and exiting the cord through the ventral spinal nerve roots to innervate the outlying musculature (Darby and Frysztak, 2013). The ascending tracts are comprised of afferent sensory fibres that carry information from the periphery first to the cord via the dorsal roots where they link to second order neurons and travel upwards towards the brain, usually onto a third order neuron to complete the pathway (Sengul and Watson, 2015). This includes the dorsal columns of the cord are which responsible for much of the tactile sensory information received from the limbs. Other ascending tracts control the many aspects of somatic sensation including thermoception, proprioception and nociception (Jacobson and Marcus, 2018).

The grey matter is filled with an abundance of neuronal cell bodies which generally innervate the tissues supplied by their nearby spinal nerves or generate local circuitry. The dorsal horns contain second order afferent neurons to receive the input coming from the primary afferents of the dorsal roots while the ventral horns house motor neurons that exit the ventral roots (Krinke and Weber, 2012). Interspersed between these are interneurons which are responsible for the modulation of these signals and are implicated in the

interpretation of sensory signals that determine reflexive actions without the need for superior input (Brownstone and Bui, 2010). The size of these regions is variable throughout the cord and they become enlarged at segments controlling the upper and lower limbs due to the high throughput of sensory and motor information through these areas (Darby and Frysztak, 2013).

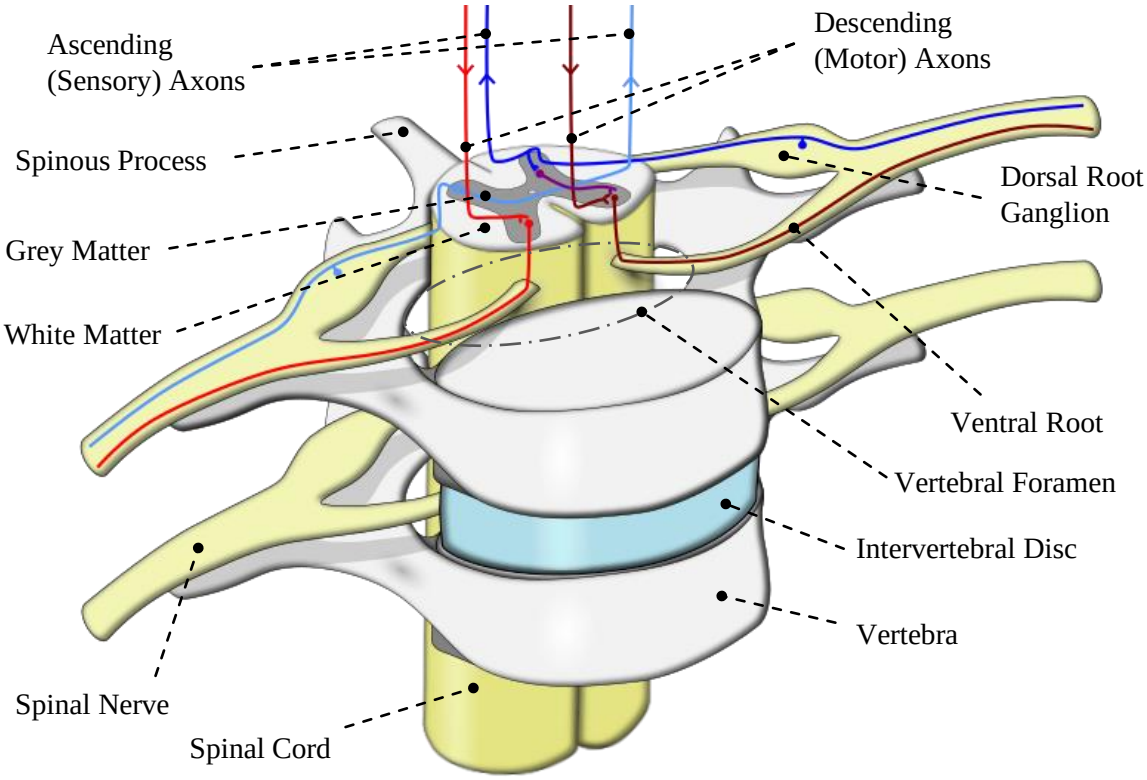

Figure 1.2 *Diagram of the spinal cord and surrounding structures . Ascending pathways (shown in blue) carry sensory information which originates in the periphery and passes through the dorsal roots. Primary sensory neuronal bodies are housed in the dorsal root ganglia and project into the CNS where they will synapse with secondary neurons. Descending paths (shown in red) carry signals to motor effectors, originating in the brain and exiting the cord through the ventral roots as lower motor axons. Sensory and motor axons combined into mixed spinal nerves which extend through the soma. Intermediate neurons (purple) reside primarily in the grey matter and are involved in local processing and coordination. The spinal cord passes through the vertebral foramina of the spinal column, comprised of vertebrae and intervertebral discs which protect the cord while retaining mobility.*

1.1.3 Gross Anatomy of the Spinal Cord and Column

The spinal cord connects to the brain as a continuation of the brain stem as it exits the foramen magnum in the base of the cranium (Mendoza and Foundas, 2008). The spinal cord descends through the neck and trunk within the spinal column which is composed of vertebrae that provide protection to the cord and allow passage through the vertebral foramina. These vertebrae can be numerated and divided into distinct regions that also subsequently allow for indexing of the spinal cord and its nerves. Figure 1.2 shows an overview of the gross anatomy of a typical region of the spinal column. Immediately below the cranium begins the cervical region that contains seven vertebrae and eight pairs of spinal nerves (Jacobson and Marcus, 2018). The cervical vertebrae are relatively small compared to those at other levels which enables a wide range of movement for the head and neck (Gillen, 2016). Spinal nerves exiting this region provide the nervous supply for the neck, the upper torso and the upper limbs. Below this the thoracic region extends with twelve vertebrae that articulate with the ribs and house an equal number of spinal nerve pairs that predominantly supply the trunk. The lumbar region has five large vertebrae and spinal nerve pairs which innervate the lower limbs (Barker *et al.*, 2012). These regions also have neighbouring sympathetic ganglia to perform a range of somatic regulatory functions (Jacobson and Marcus, 2018). Towards the caudal end of the spinal cord, nerve roots are progressively more rostral to the vertebral foramina from which they exit. The cord terminates with the conus medullaris at approximately L1-2 at which point nerves originating from higher levels descend to form the Cauda Equina which contains lower lumbar nerves as well as the nerves passing through sacrum and coccyx, both of which are comprised of fused vertebrae (Diaz and Morales, 2016).

The vertebral column acts as main physical barrier for spinal cord injury by encapsulating it within solid bone channels that can withstand relatively high forces, while the articulations and intervertebral discs allow for sufficient mobility of the column to prevent constriction or compression of the cord (Cramer, 2014). The meninges further protect the cord, with the outermost membrane, the dura mater, acting as a thick elastic barrier (Hartman, 2009). A layer of cerebrospinal fluid (CSF) is held between the innermost layers, the arachnoid mater and the pia mater that is thought to attenuate shock impacts (Jones, Kwon and Cripton, 2012; Wright, Lai and Sinclair, 2012). The cord itself however is extremely fragile, so spinal injuries with sufficient force to break or dislocate the vertebrae will more than likely inflict significant damage to the spinal cord.

1.2 Spinal Cord Injury

1.2.1 Causes, Consequences & Prevalence of Spinal Cord Injury

Damage to the spinal cord causes immediate disruption to the functionality, but the location and severity of the injury will determine the extent to which function is impaired and also how readily it can be restored. Traumatic spinal cord injuries can also be subcategorised as complete if the tissue is completely severed at the site of injury, or incomplete if there is some tissue and function spared (Middendorp *et al.*, 2011). The spinal cord operates hierarchically and communication will be interrupted between the brain and regions of the body that are innervated by nerves originating below the level of injury. Injury to the lumbar or thoracic regions of the spinal cord are often accompanied by paralysis and loss of sensation in the lower limbs - a condition referred to as paraplegia - while cervical level injuries also carry the risk of affecting the upper limbs resulting in tetraplegia (Maynard *et al.*, 1997). Figure 1.3 details how each segment of the spinal cord is responsible for providing sensation to specific regions of the body. Muscular innervation is structured in a similarly layered fashion.

The mechanism of primary injury will also affect the development of the injury as a whole, for example contusion injuries often lead to the formation of central fluid filled cavities within the cord, while lacerations will also affect superficial regions. Ultimately the development and prognosis of injury is highly case specific due to varying levels of severity (Norenberg, Smith and Marcillo, 2004). As axons form distinct white matter tracts within the cord, injury may spare certain functions if the tracts that govern these tasks remain intact. This will have important implications on retention and recovery of function following injury as neuronal plasticity can allow patients to recover a relatively high degree of function in some cases (Lynskey, Belanger and Jung, 2008; Fawcett, 2009).

Spinal cord injury is accompanied by a large range of secondary complications both directly and indirectly associated to the primary injury and add to the already difficult challenge of managing patient treatment. Disuse of musculature in the affected areas leads to tissue atrophy that will exacerbate rehabilitation and contributes to bone mineral loss in the affected limbs (Krassioukov, Furlan and Fehlings, 2003; Sezer, 2015). Globally it has been estimated that there are approximately 180,000 new cases of traumatic spinal cord injury every year (Lee *et al.*, 2014). Typically spinal cord injury is a chronic affliction and can persist

indefinitely, and though there is a wide margin of inaccuracy in estimations of SCI prevalence it is thought to currently affect several million people worldwide (Furlan *et al.*, 2013; Lee *et al.*, 2014; Singh *et al.*, 2014). A contributing factor to this high number is the relatively scarce availability of effective treatments, due in part to the limited number of studies on available therapeutic interventions and as a result there is little consensus on which treatment options hold priority within the clinical community (Fehlings *et al.*, 2017). Therefore, there is an increasingly pressing need to research alternative interventions that demonstrate marked improvement of patient health both in the acute and chronic phases of spinal cord injury.

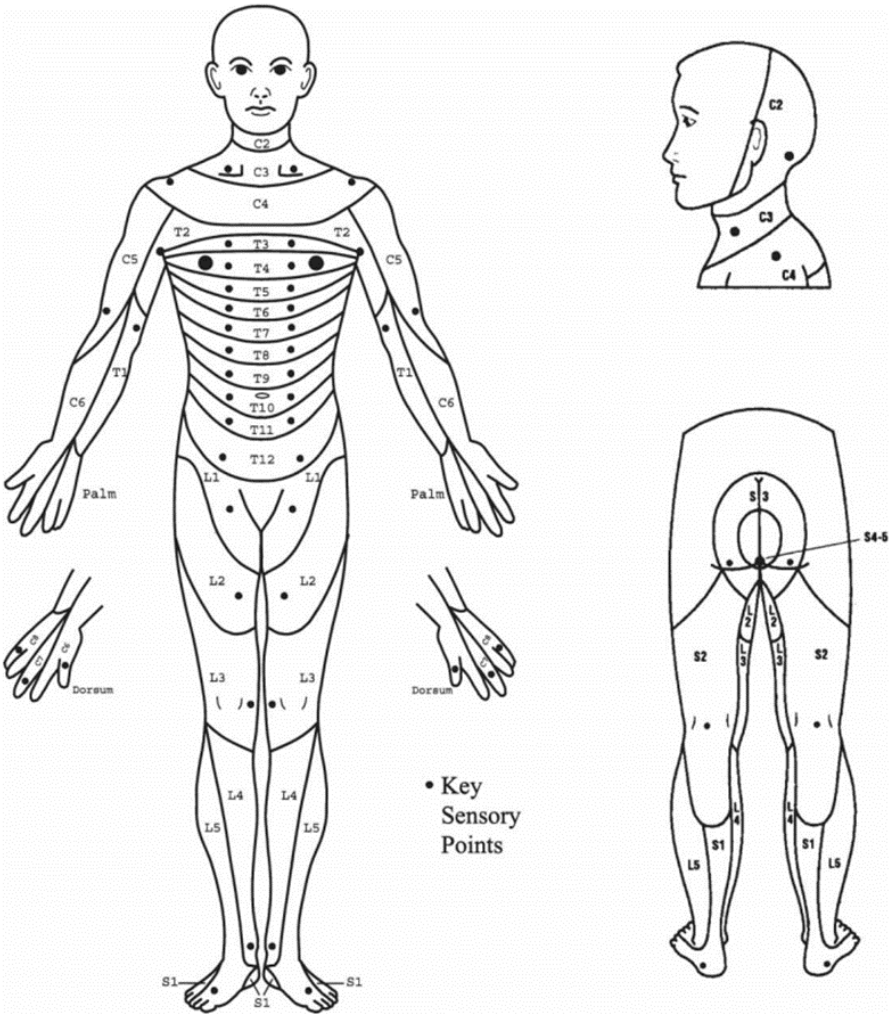

Figure 1.3 *Dermatome representing the map of superficial sensation governed by each nerve root of the spinal cord. Each region corresponds to the specified spinal segment from the cervical level (C1-8) covering the upper body, thoracic segments (T1-12) which mostly cover the trunk, to the lumbar and sacral regions (L1-5, S1-5) which innervate the lower body. Key sensory points are used diagnostically to assess the extent of sensation in the given region. motor equivalent myotome overlaps somewhat with the dermatome but is less easily defined due to muscle orientation and possible innervation by more than one nerve. Image reproduced with permission* (Kirshblum *et al.*, 2011)

1.2.2 Acute Phase of Spinal Cord Injury

The mechanisms of injury progression can be split into primary and secondary phases. The primary phase occurs immediately from the instance of trauma and encompasses the period in which cell death first occurs as a direct response to the damage inflicted by injury (McDonald and Sadowsky, 2002). Mechanical disruption of cell membranes, particularly axons which are especially sensitive to perturbation, interrupts the partitioning of intra- and extracellular environments and interferes with the majority of cellular functions (Jin, 2014). Vascular occlusion or haemorrhage will prevent adequate perfusion of tissues and will ultimately contribute to ischaemia in regions of the cord supplied by the affected vessels (Cao and Dong, 2013). Fluid accumulation begins to exert pressure on tissues and will exacerbate vessel occlusion and hypoxia. In this stage, contents of cells with compromised membranes are exuded locally and begin to instigate reactive behaviour in the surrounding cells in response to the abnormal aqueous factors (Oyinbo, 2011).

The second phase is significantly longer and is initiated several minutes after injury onset but spans a period of days to weeks. The hallmarks of this stage are characterised by dysregulation in the extracellular environment, immune infiltration and reactivity of the native cell populations. The neurotransmitter glutamate normally accumulates in presynaptic vesicles which under normal conditions exhibits a controlled release in response to membrane depolarisation, but injured neurons release an abundance of glutamate into the extracellular environment (Hackett, Ueda and Snare, 2015). This leads to activation of ionotropic glutamate receptors such as NMDA (N-methyl-D-aspartate) and AMPA (α-amino-3-hydroxy-5-methyl-4-isoxazolepropionic acid) receptors which in turn facilitate the influx and accumulation of intracellular calcium, among other ions, that also activate voltage-gated ion channels enacting a positive feedback effect (Siddiqui, Khazaei and Fehlings, 2015). High calcium ion concentrations of can modulate numerous enzymatic and metabolic pathways which precipitate the production of reactive oxygen species (ROS) and accelerate structural deterioration (Mark *et al.*, 2001). This effect can also be amplified by ROS production and other free radicals induced by ischaemic reperfusion which occurs when blood supply is returned to formerly hypoxic areas (Dugan and Choi, 1999). Furthermore, oligodendrocytes are also susceptible to excitotoxicity which will result in the degradation of myelin around the injury site so undamaged neurons may still fail in signal transmission due to poor current insulation around axons (Matute *et al.*, 2007).

In response to the injury many of the cells in the injury site begin to secrete inflammatory chemoattractants including tumour necrosis factor alpha (TNF-α) which initiates the migration of phagocytic cells into the area that can engulf cellular and structural debris which is a key stage in the immune response (David, Zarruk and Ghasemlou, 2012). Activation of the resident microglia also produces cells with a macrophage phenotype which catalyse the inflammation (Okada, 2016). Leukocyte recruitment to the area is enhanced by the disruption of the blood-spinal cord barrier (BSCB) making it an ineffective boundary between circulating cells and the CNS (Bartanusz *et al.*, 2011). There is still controversy over the net effect of leukocytes in spinal cord injury; though there is evidence to support the notion that certain cytokines secreted by these cells will negatively affect the local cell populace while others may provide a benefit (Bastien and Lacroix, 2014). Timings of this activity may be critical in defining the long term effects as a heightened response has proved detrimental when experimentally induced after 24 hours but beneficial after 4 days (Silva *et al.*, 2014), therefore any therapeutic interventions must also consider when exactly administration will be most effective.

1.2.3 Subacute & Chronic Spinal Cord injury

Following the recession of vascular tissue in the injury site over the first few days, angiogenesis is initiated 3-4 days after the primary injury and continues for several weeks, albeit at a gradually diminishing rate (Rocha *et al.*, 2018), however this alone is not sufficient to induce significant regenerative effects. Though blood vessels can enter the injury site, they lack the surrounding cellular architecture of pericytes and astrocytes that they normally possess in healthy tissue (Rauch *et al.*, 2010). These newly formed blood vessels are known to be permeable and again fail to maintain the protection provided by the BSCB (Benton *et al.*, 2010). Additionally, the number of vascular structures in the injured tissue tends to remain significantly lower than in the healthy spinal cord (Loy *et al.*, 2002; Figley *et al.*, 2014). Figure 1.4 highlights some of the key events that take place across the phases of the injury development and the times at which they typically occur.

Reactive astrocytosis becomes pronounced after 1-2 weeks in which resident astrocytes alter their phenotype and function in response to various physiological changes that occur as a consequence of SCI (Sofroniew and Vinters, 2010). Astrocytes with this phenotype become hypertrophied and begin to express several exogenous agents into the region, some of which are beneficial for neuronal repair such as neurotrophic factors, while other promote neuronal apoptosis (Liddelow and Barres, 2017). The most well recognised role of reactive astrocytes

is in their formation of a dense barrier that surrounds what becomes a fluid-filled cavity (syrinx) left in the wake of phagocytic clearance of damaged tissue. The astrocytes mesh together in what is known as the glial scar which is comprised of a fibrotic phase at the cavity surface and astrocytes on the parenchymal side with extracellular matrix (ECM) components distributed throughout both (Yuan and He, 2013). The glial scar is thought to be neuroprotective in the early phase of SCI by blockading the invasion of leukocytes and preventing an intensified inflammatory response (Sofroniew and Vinters, 2010), but in later stages the scar can have negative effects on the tissue recovery.

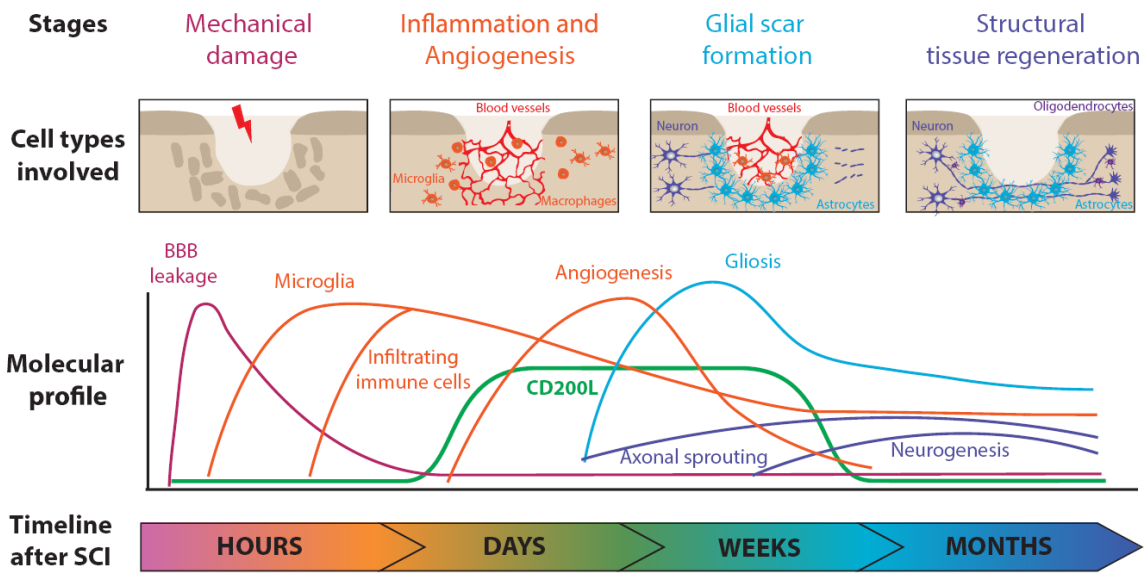

Figure 1.4 *Cellular progression of Spinal Cord Injury. Different phases have defining events in cellular activity and de-escalation. The initial period following injury is hallmarked by direct damage to cells and blood vessels. Shortly after this is the onset of inflammation and the influx of immune cells which can further exacerbate the injury. Beyond this, scar formation and astrogliosis lead to fluid filled cavities in the injury site. In the chronic phases the damaged tissue persistently fails to encourage regeneration of axons. Image reproduced from* (Rust and Kaiser, 2017)

Neurons that survive the primary injury and are sufficiently protected from secondary injury are capable of axonogenesis, however there are many complicating factors that typically prevent this process from occurring to any meaningful extent. The glial scar is densely woven with both cells and ECM components which makes axonal navigation through this barrier more difficult for neurons. Chondroitin sulphate proteoglycans (CSPGs) are a major element of this mesh and are known to have an inhibitory effect on neuronal outgrowth (Thuret, Moon and Gage, 2006). There are also several factors associated with myelin

including Nogo which normally functions as an inhibitory guidance cue for neuronal development but becomes dispersed locally after myelin deterioration and attenuates neurite outgrowth (Schweigreiter and Bandtlow, 2006). The presence of a cavity poses a physical obstacle due to the lack of ECM for cell migration and guidance, and also leads to a lack of trophic support, including growth factor stimulation as a result of cell depopulation.

The long-term condition of the injured tissue typically does not change significantly as it moves into the chronic phase. Cellular activity will reach a state of stability though not necessarily functionality. Astrocytes around the glial scar will remain in the formation around the cavity, as will the deposited ECM and fibrotic scar tissue (Norenberg, Smith and Marcillo, 2004). Neurons may continue in a demyelinated state and signal transduction will be diminished. Axonogenesis also ceases to occur if adequate stimuli are not provided in the earlier stages. Axonal and myelin fragments left from the injury continue to be degraded in the process of Wallerian degeneration for years post injury and neuroinflammation with the presence of microglia and macrophages may persist indefinitely (Schwab *et al.*, 2015). This period of stasis is difficult to escape from so treatment options primarily, though not exclusively focus on avoiding this outcome by intervening early, however the rapidly changing cellular landscape raises questions on exactly the best strategy.

1.2.4 Current Treatments and Therapies

Patients with spinal cord injury have very few options that can prevent the injury progression described in the previous section and typically medical practitioners place more emphasis on the management of secondary problems associated with SCI as opposed to regenerative strategies. In the research community there are a range of approaches that have been targeted with the aim of maximising patient independence in the long term. The most ubiquitous of these is to engage in rehabilitation, ideally as soon as possible after the primary injury as muscle atrophy and demyelination will make this more difficult over time (Ding, Kastin and Pan, 2013). Forms of physical therapy used clinically vary widely as there is yet to be an established common practice (Brogioli *et al.*, 2016), partially due to variability in patient requirements but also because of resource availability and personnel expertise. The general format is to engage in exercises with gradually increasing resistance that can promote the recovery of autonomous functions such as supported treadmill training to enhance walking capability (Gómara-toldrà, Sliwinski and Dijkers, 2014). The upper extremities have several associated degrees of freedom so individual massed practices (resistance training) are used for each type of movement including grip and rotation (Beekhuizen and Field-fote, 2005).

Training can also be augmented by electrical or magnetic stimulation of the cortex or motor nerves which often leads to improved functional outcomes (Hamid and Hayek, 2008; Awad *et al.*, 2013). One of the key factors governing rehabilitation success is that at least some of the neuronal pathways are conserved following the injury, with higher proportions of spared tissue generally forecasting improved functional outcomes in the long-term, though it is still possible to recover a small degree of functionality even with a complete absence of supra-spinal input (Behrman, Bowden and Nair, 2006). While in the majority of cases there is at least some parenchyma remaining (Figure 1.4 illustrates how this may typically occur, particularly in the later stages), this often cannot capably resume the functions of the lost tissue even with extensive rehabilitation programs.

Minimising the damage caused by secondary injury is an effective approach to spare a higher volume of functional tissue and ideally improve the prognosis of patients in the long term. Neuroprotective strategies can take different forms but are typically employed in the late-primary or early-secondary phases of injury when cell death is usually the most accelerated and mitigation will provide the greatest benefit. Surgical decompression is extremely common to alleviate the mechanical stress imposed on the cord by the traumatic displacement of vertebrae or connective tissue into the spinal canal, and can also include durotomy procedures to reduce the high intradural pressures instigated by local oedema (Li *et al.*, 2014). Methylprednisolone is a clinically approved pharmacological neuroprotective treatment which acts by curbing the immune response and diminishing the effects of inflammation at the injury site, however even so there is debate over the pros and cons of steroidal treatment in SCI because of the increased risk of infection (Bowers *et al.*, 2016). Other options are being recruited to seek regulatory approval such as riluzole which is currently used as a treatment for amyotrophic lateral sclerosis (ALS) and is under investigation for use in SCI (Nagoshi, Nakashima and Fehlings, 2015). It serves to inhibit the action of sodium and calcium channels as well as glutamate which minimises the impact of excitotoxicity (Wu, Satkunendrarajah and Fehlings, 2014). It demonstrates limited adverse effects compared to methylprednisolone, yet further research is required before it can be cleared as a SCI treatment. A more unconventional approach considers the use of hypothermia as a means to reduce metabolic activity around the injury site and lessen the effects of ischaemia and inflammation (Ulndreaj, Badner and Fehlings, 2017). There is some evidence that moderate cooling can improve the neurological outcomes following SCI (Levi *et al.*, 2010; Wang and Pearse, 2015), particularly when used in conjunction with other therapies (Cakir *et al.*, 2003). While neuroprotective strategies are unquestionably useful, their effects will rapidly diminish as the window between injury onset and therapy

administration increases and even where its use is effective there is likely to be substantial tissue loss. Therefore, longer term options of treatment are also required which may facilitate regeneration of the spinal cord.

Growth factors are an integral element of neuronal guidance in both development and regeneration. Neurotrophins are a family of growth factors that regulate neuronal survival, neuritogenesis and synaptic plasticity and as such they can be useful agents in spinal cord injury repair (Poo, 2001). Each neurotrophin acts through a cell surface receptor of the tropomyosin receptor kinase (Trk) family and these are expressed in varying amounts by different neuronal populations (Haddad, 2017; Keefe, Sheikh and Smith, 2017). Nerve growth factor (NGF) binds to the TrkA has been demonstrated to promote the regrowth of nociceptive sensory fibres and some motor neuron populations in cases of spinal cord injury (Keefe, Sheikh and Smith, 2017). Brain-derived neurotrophic factor (BDNF) is thought to be even more effective in neuronal regeneration in spinal cord injury as it acts through the TrkB receptor which is expressed by several cell types in the central nervous system and has been demonstrated to enhance axonal sprouting in multiple descending neuronal sub-types (Huang and Reichardt, 2001) as well as being a potent mediator of neuronal plasticity (E and Antila, 2017). Neurotrophin-3 (NT-3) is also capable of encouraging the maintenance and regrowth of neurons, particularly with the corticospinal tract (Grill *et al.*, 1997) and some ascending dorsal column neurons (Bradbury *et al.*, 1999). Furthermore, combinations of neurotrophins will enhance their regenerative capability (Novikova, Novikov and Kellerth, 2000). One of the shortfalls of this approach is that trophic support needs to be continuous in order to have a meaningful impact on neuronal regrowth and administration of neurotrophins or other growth factors is often uncontrolled and require additional mechanisms of delivery.

Cell implantation can be used as a means to provide stimuli that are lacking in the damaged cord. Several cell types have been investigated for their potential to replace populations that are lost due to injury. Neural precursor cells (NPCs) are widely used in cell transplantation models due to their ability to differentiate along neuronal and glial lineages (Temple, 2001). Studies have confirmed that implantation of neural stem cells can lead to improved functional outcomes after spinal cord injury (Abbaszadeh *et al.*, 2018) and that they can also differentiate along several lineages including neurons in response to the local environmental cues (Cummings *et al.*, 2005; Lu *et al.*, 2012). The enhanced functional outcomes can only be partially attributed to replenishing cellular populations however as implanted cells also deliver trophic support to the endogenous cells and consequently stimulate further activity

(Assinck *et al.*, 2017). This paracrine signalling may be of particular importance as similarly improved functional measures can also be observed with implantation of mesenchymal stem cells (MSCs) (Hosseini *et al.*, 2018) which typically do not differentiate into neural cell phenotypes, although this notion remains controversial (Salgado *et al.*, 2015; Ying *et al.*, 2016; Mukhamedshina *et al.*, 2018; Wu *et al.*, 2018). MSCs have been demonstrated to secrete neurotrophic factors and temper inflammation after implantation in SCI models (Qu and Zhang, 2017). Some studies have found evidence that MSCs also have the capacity to provide physical support by forming tube like structures that house and protect neurons (Ma *et al.*, 2018).

Implantation of neural stem cells (NSCs) has already been translated into clinical trials, although the results are somewhat more modest than in animal models (Curtis *et al.*, 2018; Levi *et al.*, 2019). One of the main obstacles in clinical translation is the lack of consensus required to adequately inform decisions on key parameters such as the number of cells required or the timescale of implantation. The cell fate beyond the time of implantation is also difficult to control, and several factors can adversely affect these cells in a realistic setting including patient condition and other concurrent treatments to mitigate the complications of SCI.

Many of the current approaches to treatment of spinal cord injury can be effectively tied together and combined through the use of biomaterials (Führmann, Anandakumaran and Shoichet, 2017). They can act as an appropriate vehicle for pharmacologic agents and cells (Liu *et al.*, 2018), as well as providing an extra degree of control over cell behaviour by directly providing an architecture for engaging integrin activity and cell mobility (Varone *et al.*, 2017).

1.2.5 Rodent Models of Spinal Cord Injury

Researching new strategies for treating SCI can take many avenues. *In vitro* techniques can be used to explore promising systems and there are an abundance of techniques available for culturing neural cells for spinal applications (Gingras *et al.*, 2008; East *et al.*, 2013; Gerardo-Nava *et al.*, 2014). There are some that can also create a reasonable approximation of the complex regenerative environment that follows injury. Boomkamp *et al.* (Boomkamp *et al.*, 2012, 2014; Mccanney *et al.*, 2019)developed an injury model that first establishes a population of myelinated axons before creating a transection in the cell monolayer which can be used for determining the effect of soluble agents on axon regrowth and myelin

reformation. Weightman *et al.* (Weightman *et al.*, 2014) describe a system utilising sagittal slices of neonatal rat spinal cords followed by slice transection to replicate injury. This system could be used in conjunction with an overlaid biomaterial platform to assess the progression of astrogliosis and neurite alignment across the gap. However, these methods can only provide a limited and idealised view of how this would translate to the *in vivo* environment which introduces a host of confounding factors and complexity. For this reason, *in vivo* models of spinal cord injury are highly valued for the insights they can provide.

There are several models that can be implemented to replicate different clinically relevant injury scenarios. One of the most conceptually simple is the transection injury in which the cord is cut to completely separate the spinal cord into proximal and distal segments with a gap in between. This model creates a space that can be used to apply the therapeutic agent being tested but ultimately levels of regeneration seen in this model do not usually match those of other models and it is also a rarity in clinical presentations (Cheriyan *et al.*, 2014). Partial transections can be performed in a similar fashion but with only inflicting damage on a selected region of the cord. Hemisection models have the additional advantage of allowing comparisons of injured and uninjured regions both histologically and functionally (Leszczyńska *et al.*, 2015). Compression models are considered to be more relevant as these types of injuries are relatively common clinically. These involve the application and maintenance of pressure on the spinal cord for a set duration which induces mechanical and ischemic damage and usually produces relatively consistent injuries (Poon *et al.*, 2007). Another similar method that produces very reproducible injuries is the contusion model which is performed by imparting a rapid force onto the spinal cord that again causes mechanical and ischaemic damage. The added benefit of this model is that several methods exist which can provide accurate data on the contusion delivery parameters which makes injuries highly defined (Krishna *et al.*, 2013). However, despite the advantages of certain models over others, choosing the correct approach often comes down to the experimental requirements and as such these models and others are all extensively used.

1.3 Biomaterial Strategies for SCI

1.3.1 What are Biomaterials?

Biomaterials are a class of material that are used to replace or restore the functionality of biological systems. Historically these materials could only replicate very basic functions such as load bearing and they were commonly used as structural elements, for instance as dental implants, prosthesis or tissue sutures (Rezaie, Bakhtiari and Öchsner, 2015). More recently with advances in surgical techniques and medical capability, the additional requirement of biocompatibility became a prerequisite as implantable technologies were developed. The predominant focus was on materials that could remain bio-inert; those that were non-toxic to the surrounding tissues and would cause a minimal immune response. These were used in more complex scenarios such as joint replacement, bone augmentation, vascular stents or hernia meshes (Huebsch and Mooney, David J. Mooney1, 2010; Kalaba *et al.*, 2016). However, these still only performed rudimentary roles in the body by providing mechanical support, but more recent classes of material have focussed on utilising biological mechanisms to enhance the function of implanted materials. Such materials have the capability to encourage cellular processes that can facilitate tissue integration and even regeneration.

The majority of early biomaterials have focussed on replacing damaged tissues and assuming their function. Regenerative strategies aim to promote the recovery of damaged tissue to a healthy state so that normal function can be resumed without the necessity for permanent implants to remain in place. This approach has several advantages as foreign objects typically induce combative responses from the surrounding tissues over time and even state-of-the-art technologies have limited life-spans after implantation (Hu, Eaton and Tang, 2019). More importantly however, the multitude of roles that even relatively simple organs perform cannot yet be recapitulated artificially. Biomaterial-based tissue regenerative strategies are heavily focussed on providing a platform for cellular adhesion and motility, enabling the repopulation of damaged areas by native cell types as migration is directed into material grafts (Nardo *et al.*, 2017). In this manner the materials are intended to replicate the ECM by providing a substrate for cellular attachment. Central to this idea is the inclusion of components that can associate with cell adhesion molecules such as integrins which are one of the most important receptors for the mediation of cellular adhesion.

1.3.2 Cell Adhesion & Migration

Integrins are dimeric transmembrane receptor proteins that have specificity for certain peptide sequences that are embedded in ECM components. Each integrin is comprised of one α and one β subunit, which when combined will determine the molecular epitopes that it can recognise and bind to (Mcever and Luscinskas, 2018). In humans there are 24 identified functional combinations of these subunits, many of which have multi-specificity and can attach to several different ECM proteins (Danen, 2013). Fibronectin is widely distributed in many tissue types and a number of integrins are known to bind to the molecule (Barczyk, Carracedo and Gullberg, 2010), in particular to a sequence of arginine-glycine-aspartic acid (RGD) amino acids (Kapp *et al.*, 2017) which is recognised by several β_1 and α_v integrins (Bharadwaj *et al.*, 2017). Laminin is another abundant ECM protein that includes another notable adhesion sequence of isoleucine-lysine-valine-alanine-valine (IKVAV) amino acids which also binds to several β_1 integrins as their primary ligand (Frith, Mills, Hudson and Cooper-white, 2012). Several other sequences are known to initiate integrin activity such as the GFOGER and YIGSR sequences from collagen (Puranen *et al.*, 2003) and laminin(Kim *et al.*, 2018) respectively. Integrin activation relies on such sequences to act as tethers that allow cells to exert forces on the external environment (Case and Waterman, 2015).

Integrins are closely affiliated with the actin cytoskeleton and play an intrinsic role in actin remodelling. Rho GTPases are activated following integrin binding and are implicated in the process of stress-fibre formation which are necessary to exert tensile forces (Avalos *et al.*, 2004). This process becomes amplified in the generation of focal adhesion which are the main anchorage points for adherent cells. Focal adhesions are supramolecular complexes that combine high numbers of integrins along with a multitude of intracellular stabilising proteins such as talin and vinculin to tether actin filaments to the transmembrane integrins, effectively providing the mechanical bridge between the extracellular environment and the internal cytoskeleton (Turner, 2000). Figure 1.5 illustrates the formation of focal adhesions on a molecular level and a typical distribution of focal adhesions around an adherent cell is also displayed. The cytoskeleton permeates the cell cytoplasm including contact with the cell nucleus and stresses from outside the cell can directly translate into nuclear activity through this system (Wang, Tytell and Ingber, 2009). The application of force through integrins is essential to the maturation of focal adhesions which in turn precipitates numerous signalling pathways to enable cells to sense and respond to the local physical surroundings (Alpin *et al.*, 1998).

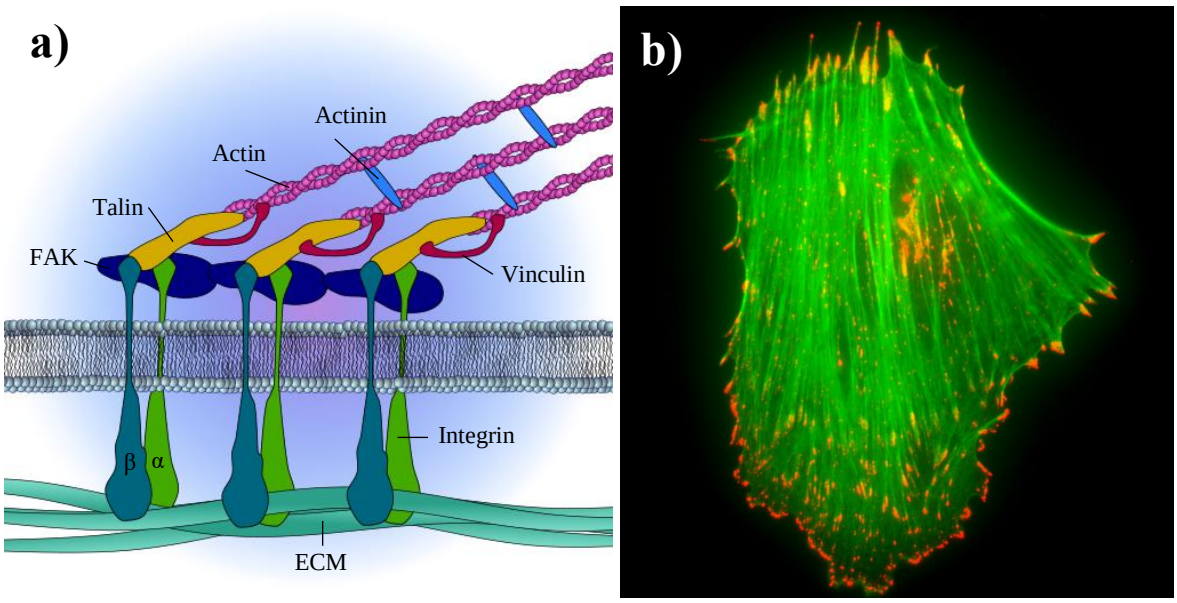

Figure 1.5 a) *Simplified diagram of focal adhesion formation across the cell membrane, connecting the internal architecture with the extracellular matrix. Integrins attach to extracellular matrix through external binding sites which causes internal conformational change. Focal adhesion complexes form by aggregation of integrins and stabilisation with other proteins including FAK, talin and vinculin. This enables formation of actin stress fibres to transmit forces between the cell interior and exterior.* ***b)*** *Image of a cell stained for the cytoskeletal filament actin in green and vinculin in red to visualise the distribution of focal adhesions. Image adapted with permission* (Zaidel-bar, Kam and Geiger, 2005)

Focal adhesions do not only function as anchors to the ECM but are in fact crucial to the motility and migration of cells. They exist in a dynamic equilibrium and are continually being assembled and disassembled in response to migratory cues. Evidence suggests that the formation of focal adhesions and the stabilisation of pathfinding lamellipodia is intertwined and as such constitutes a mechanism of mobilisation (Webb, Parsons and Horwitz, 2002). Rates of formation and turnover can polarise cells along an axis of movement; assembly and stabilisation of focal adhesions is more readily observable on the leading edge of the cells which governs the direction of migration (Broussard, Webb and Kaverina, 2008). Conversely, disassembly or dissociation of focal adhesions occurs at the trailing edge, releasing the tethers to the ECM and contracting the membrane along this axis. These mechanisms are generally responsible for changes in morphology, which is particularly notable in developing axons as they are involved in growth cone pathfinding of neurites (Ganfornina, Sanchez and Bastiani, 1992). These growth cones have high densities of integrins to follow the ECM network and together with chemo-attractants or repellents, integrins enable neurites to navigate with extreme precision over long distances to ultimately

develop into axons (Vanderhaeghen and Cheng, 2010; Raper and Mason, 2019). However, in order to make use of these mechanisms in engineered systems, arguably the most important consideration is choosing the right material substrate to facilitate these processes.

1.3.3 Material Selection

It is important that the micro-environment is able to effectively replicate the ECM not only in the availability of binding sites for integrin coupling but also the mechanical properties of the substrates. It has been demonstrated repeatedly that the elastic modulus of a material will influence cell behaviour including the morphology, mobility and differentiation of the cells (Gray, Tien and Chen, 2002; Schneider *et al.*, 2006; Jalali *et al.*, 2016). This property has been linked to modulation of mechano-transduction and intracellular signalling in response to the apparent deformability of the substrate (Han *et al.*, 2016). One explanation for this is the molecular clutch model of focal adhesion formation; the sustained application of force allows mechanosensitive proteins to unfold, exposing binding sites for other docking proteins to stabilise the complex (Martino *et al.*, 2018). On substrates with low Young's Moduli, the high strain induced in the material leads to an insufficient generation of force to enable the unfolding of focal adhesion stabilisation protein talin (Elosegui-artola *et al.*, 2016). The binding of vinculin to the complex which is required for focal adhesion maturation subsequently fails to occur. For differentiating stem cells, the Young's modulus can be the decisive influence on the lineage of the cells; in the case of MSCs it has been shown the elasticity alone can promote cells to adopt neuronal, muscle or bone phenotypes when adhered to materials with low, intermediate or high stiffnesses respectively (Engler *et al.*, 2006). Materials with low stiffnesses can also stimulate the differentiation of NSCs (Saha *et al.*, 2008) and even embryonic stem cells (Ali *et al.*, 2015) along neuronal lineages. In addition, neuritogenesis is demonstrably improved when cultured on materials that have extremely low Young's moduli of ~2kPa or less (Farrukh *et al.*, 2017). When designing materials to promote growth of specific cell types, it is common practice to tailor the Young's modulus of the material to approximate the tissues in which the cells normally reside.

In the short term, materials have the capability of providing cells with substrates they need to support themselves, but as time progresses and cells attempt to remodel their environment, enduring materials can become more of a limiting factor on tissue regeneration. Repopulation and integration of tissues to a healthy state cannot take place in spaces occupied by implanted structures. Degradable materials are therefore highly valued for their

ability to provide temporally controlled support. They also eliminate the need for surgical re-intervention which is necessary for non-degradable implants. The optimum rate at which the material breaks down is highly tissue specific but a commonly held principle is that the material should be resorbed at a rate on par with the defect recovery so that regenerating tissues can replace the function of the material as it diminishes (Nair and Laurencin, 2007). Several classes of materials exist that can fit this need, many with distinctive mechanisms that can influence their suitability in specific environments. Hydrolytically degradable materials can be constructed from an array of synthetic polymers such as poly (lactic-co-glycolic) acid which has been used in a variety of applications from bone tissue engineering to neural electrodes (Gentile *et al.*, 2014; Koo *et al.*, 2018). Alternatively, enzymatically sensitive materials offer the potential for cellular-mediated remodelling to control degradation rates which can be particularly important for encapsulated cells to forge paths for migration (Schultz, Kyburz and Anseth, 2015). Many biological materials including proteins (Hesse *et al.*, 2010) and polysaccharides (Campbell, Stilhano and Silva, 2018) can take advantage of enzymatic activity to facilitate their degradation, but the use of biological elements can also be translated into synthetic materials for the same purpose (Lin and Anseth, 2009; Feig, Tran and Bao, 2018).

Promoting the activation of integrins is a common focus of biomaterials for improved tissue integration and regeneration, though there are several approaches that can achieve this outcome through different mechanisms. One common method is the modification of surfaces to enhance the adsorption of ECM proteins which enables cells to regulate their own extracellular environment. Factors known to contribute to this process are surface moieties and charge (Li, Yang and Huang, 2011), surface mobility (Bathawab *et al.*, 2016) or surface roughness and topography (Wu *et al.*, 2015; Lizarraga-Valderrama *et al.*, 2019), all of which can be tuned to improve the retention or conformation of matrix proteins to present more binding locations for adhering cells. Changing the topography of the material surface can have the additional benefit of guiding cells through more conventional means by physically constricting their freedom of movement (Wang, Ostuni and Whitesides, 2002). A more direct approach for utilising ECM is to fabricate materials which incorporate integrin binding sites into their structure. Collagen is a ubiquitous ECM protein that is routinely applied to surfaces in cell culture to enhance cellular adhesion and growth. The diverse nature of collagen has led to the evolution of numerous natural composites that incorporate collagen into their structure (Sherman, Yang and Meyers, 2015). Beyond this however, it is also capable of assembly of its own accord into 3D configurations that can be used in biomaterial applications (Doyle, 2017). These belong to a class of materials that are gaining popularity

in biomaterials research due to their extremely versatile nature and their ability to mimic soft tissues; hydrogels.

1.3.4 Hydrogels

Hydrogels are defined by the ability to retain large quantities of water within a hydrophilic macromolecular network (Zustiak and Leach, 2010). These networks arise from the affiliation of long polymeric chains with one another in aqueous media to the point that the relative motion of the chains reduces to near zero. The mechanisms through which this happens determine several material properties of the gel. In physically cross-linked gels the polymer chains are held in place by weak intermolecular forces such as by electrostatic attraction or hydrogen bonds (Hu, Wang and Xiao, 2019). The loose association between the polymer chains mean these gels usually have low elastic moduli and can be dissociated relatively easily. By the same token, this also allows some gels to form in response to distinct and potentially biologically expedient stimuli such as temperature (Ruel-Gariépy and Leroux, 2004), ionic concentration (Henderson *et al.*, 2010), mechanical agitation or even voltage driven gelation (Y. Lin *et al.*, 2014). Figure 1.6 illustrates a handful of mechanisms that can be exploited to synthesise hydrogels.

Much stronger associations can be created through covalent cross-linking of polymer chains. These are highly dependent on the pendent moieties that are available to form covalent bonds; often materials will be synthesised or modified to contain specific functional groups that can participate in cross-linking reactions. Photo-polymerisation can be used to create hydrogels by the incorporation of unsaturated groups such as acrylate into the base polymeric structure (Martens and Anseth, 2000) or they can be integrated into bifunctional chains to become cross-linkers (Fairbanks *et al.*, 2009). Photo-initiators are used to generate free radicals upon exposure to light which initiates the conjugation of the polymer chains and subsequently drives the formation of the hydrogel network. This method gives excellent control over the gelation as the reaction occurs rapidly and can be triggered independently, however it can be harsh on cells that are encapsulated within and requires an initiator for polymerisation which may also be toxic (Nguyen and West, 2002). For this reason, materials that utilise click-chemistry cross-linking methods have been the subject of intense focus due to their spontaneous activity in physiologically benign conditions. These methods rely on the conjugation of reactive groups onto polymer subunits to facilitate the amalgamation of molecules (Moses and Moorhouse, 2007). In hydrogel formation, molecules that are multi-functionalised with reactive groups can form cross-links to assemble hydrogel networks (Xi

et al., 2014). The Diels-Alder reaction is an example of click-chemistry that can be used to form adducts of dienes and dienophiles, so conjugation of groups such as the diene furan onto polymer chains means that cross-linkers with dienophiles like maleimide at the chain ends can link the molecules together (Smith *et al.*, 2018). This approach represents facile methods of gel formation that can be used *in situ* by simply mixing components together. This property makes gels formulated through click chemistry amenable to injection as aqueous components can flow through needles prior to their gelation. During implantation of biomaterials there is associated secondary damage caused by the invasive procedures required to place the implant into lesion sites, therefore injectable options reduce the severity of procedures required and reduce the likelihood of complications.

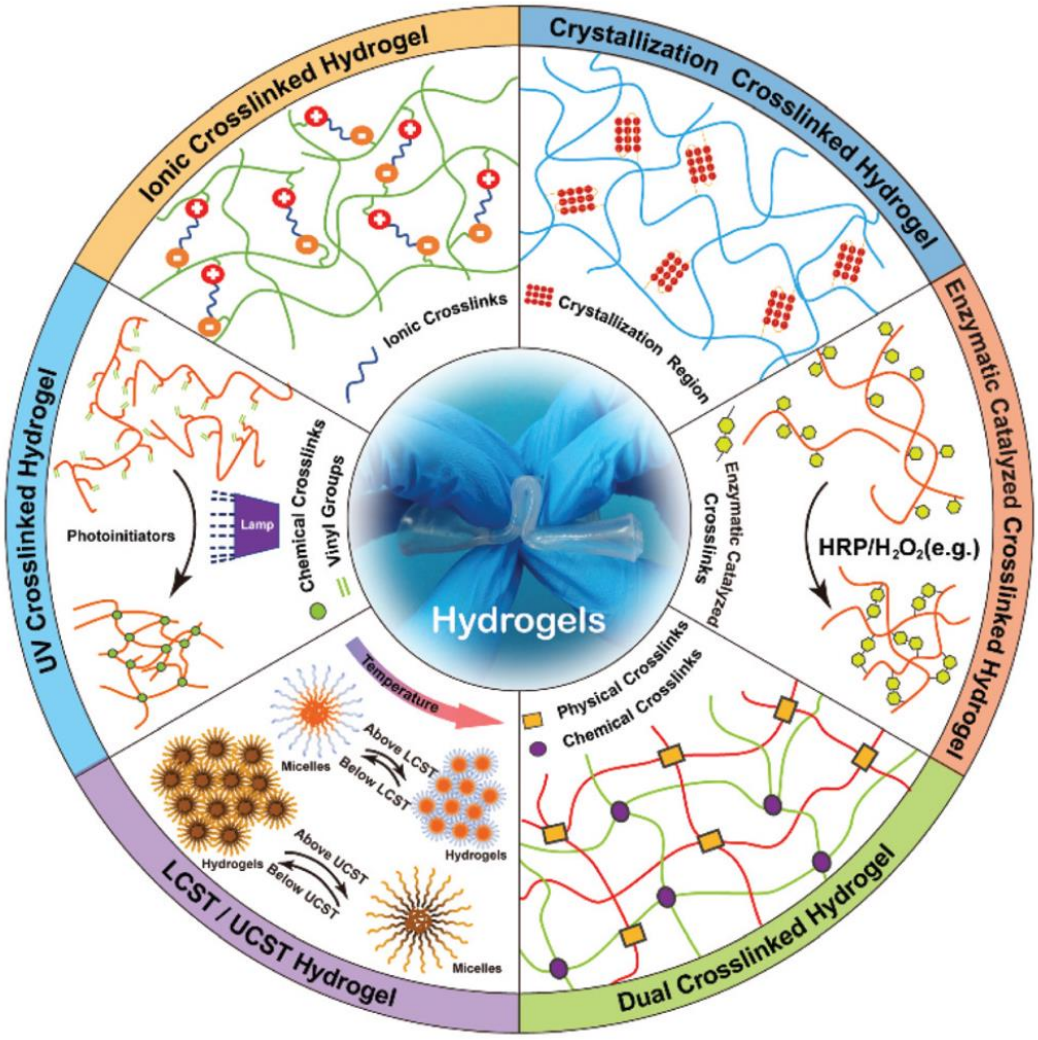

Figure 1.6 *Schematics of several hydrogel cross-linking paradigms, indicating diverse range of mechanism available for hydrogel synthesis. This can include photoinitiated cross-linking to spark radical polymerisation, ionic linking which links chains though ionic ligands, partial polymer crystallisation, enzymatic ligation of polymer chains, cross-linking of chains through intermolecular forces or covalent bonding and temperature phase transition gelation. Image from* (Hu, Wang and Xiao, 2019)

Hydrogels possess a range of properties that make them extremely useful as biomaterials. As the majority of the mass in most hydrogels is water, they are able to participate in diffusion directly without the necessity of porosity to facilitate the movement of solutes. One factor that may limit this however is the mesh size of the hydrogel network which is the average space between cross-links. The mesh size governs the freedom of movement of solutes because smaller mesh sizes equate to a higher density of interlinked polymer chains which ultimately constrict diffusion (Weber, Lopez and Anseth, 2010). This may be further slowed if the solutes have an affinity for the mesh constituents. At the further end of the scale, large molecules such as proteins may become almost completely entrapped if the mesh size is close to the dimensions of the molecule (Witten and Ribbeck, 2017). In some regards this may be a disadvantage if key signalling molecules or nutrients cannot diffuse to reach encapsulated cells, but conversely it makes hydrogels very useful as delivery vehicles for the slow release of agents such drugs, hormones or growth factors. Biodegradable hydrogels can enhance this effect as they subsequently release their contents as they break down (Lu and Anseth, 2000). This has been demonstrated in a wide variety of applications, including delivery of BDNF in injured spinal cords (Jain *et al.*, 2006). Hydrogels that are immersed in water will also tend to swell as the water permeates inwards which will expand the mesh which contributes to increased release rates. These properties will also affect the material stiffness; in general, higher densities of cross-links will lead to less chain mobility and therefore a higher modulus (Uchida *et al.*, 2019). Swelling increases the distance between cross-links and is usually accompanied by a reduction in Young's modulus, however at high degrees of swelling the opposite can happen as stretched chains exhibit strain-hardening behaviour (Hoshino *et al.*, 2018). Designing materials to possess specific properties can often have a knock-on effect as several other properties will also change, therefore the gel composition must be carefully considered.

Hydrogels formed from natural polymers are very often controlled by physical cross-links (Achilli and Mantovani, 2010) and can be made from many different types of polymeric chains from proteins like collagen (Macaya *et al.*, 2013), to polysaccharides such as hyaluronic acid (HA) (Seidlits *et al.*, 2010; Huaping *et al.*, 2012) or even DNA (Lee *et al.*, 2012). Natural polymers provide certain advantages over synthetic ones in biological systems because they can often play several roles simultaneously and may contain domains that can interact with a variety of cell surface receptors or other biomolecules (Sawicka *et al.*, 2015). On the other hand, as they are derived from biological origins, they run the risk of carrying contaminants. Their degradation can be unpredictable due to the volatile changes in enzyme expression at implantation sites (Sarkar, Yingfei and Sant, 2017) and they can

liable to batch variability. Synthetic polymers can be accurately defined during manufacture and often have the additional benefit of being highly modifiable to suit a variety of applications. Poly(hydroxyethylmethactrylate) (pHEMA) (Li *et al.*, 2013), poly (N-isopropylacrylamide) (PNIPAM) (Lanzalaco and Armelin, 2017) and Poly(ethylene glycol) (PEG) (Enemchukwu *et al.*, 2015; Gutowski *et al.*, 2015) have all be fabricated into hydrogels that have proven to be biocompatible. PEG in particular has a long history of use in medical applications having been previously employed for drug modification (Harris and Chess, 2003) and has even been proposed as a fusogen to reconnect the membranes of damaged axons back together in nervous injuries (Lu *et al.*, 2018). The proven track record of PEG *in vivo* and use in the context of SCI, along with its extremely diverse array of potential modifications make it an excellent candidate for investigation as a hydrogel designated for implantation in SCI. PEG-based hydrogels can satisfy all of the criteria required for implantation and provide many additional benefits, hence this body of work is primarily focussed on the fabrication and evaluation of PEG hydrogels for these reasons.

1.3.5 Multi-Arm PEG-Gels

Poly(ethylene glycol) is a polyether comprised of ethylene oxide monomers (Ivanova, Bazaka and Crawford, 2014). PEG chains are hydrophilic which make them suitable for the creation of hydrogels. PEG can be formed into hydrogels by synthesising the polymer in units containing multiple branches with additional modifications at the chain terminals (Tan *et al.*, 2009). These molecules can be linked using multifunctional cross-linkers which must contain at least 2 functional groups that can form a bridge between molecules. As the functional units of the polymer are typically affixed to the chain ends, the binding sites are highly specific and the structure of the material can be well-defined. Many of the properties can be easily tuned by adjusting the chain properties; altering the molecular length of the polymer or cross-linker will directly change the hydrogel mesh size, and therefore will influence the swelling capabilities and the stiffness of the material (Temenoff *et al.*, 2001).
As previously mentioned, multi-armed PEG can be used as the basis of hydrogel formation, however the variety of choice for chain terminus functionalisation enables PEG to participate in a number of cross-linking paradigms. Of particular note in relation to this body of work, Michael-type addition is a highly effective route facilitating PEG hydrogel cross-linking. Michael-type addition is defined as an addition reaction between a nucleophile (Michael donor) and an α-β unsaturated carbonyl (Michael acceptor) (Mather *et al.*, 2006). The Michael donors are often formed by catalysis in a base to accelerate the removal hydrogen ions from the active moieties, enabling the nucleophilic attack of the unsaturated bond and

the conjugation of the two components. This nucleophile can take many forms but in biological systems it is particularly noteworthy that thiolates can initiate this reaction as these can be found in cysteine amino acids. Thiolates are formed by the deprotonation of thiol groups which can be induced with a pH around neutral, though this changes slightly depending on the amino acid sequence that the cysteine is embedded within (Poole, 2015). Several forms of Michael acceptor have also been utilised in biological systems such as acrylates, vinyl sulfones and maleimide groups (Nair *et al.*, 2014), all of which contain α-β unsaturated carbonyls. Figure 1.7 shows a schematic of a Michael-type addition reaction between thiol and maleimide. In particular, maleimide has been demonstrated to be exceptionally reactive with thiols compared to the alternatives and can rapidly undergo addition with extremely high yields (Phelps *et al.*, 2012). As such, multi-arm PEG modified with maleimide functional groups can form an excellent basis for hydrogel synthesis when used in conjunction with di-thiol cross-linkers.

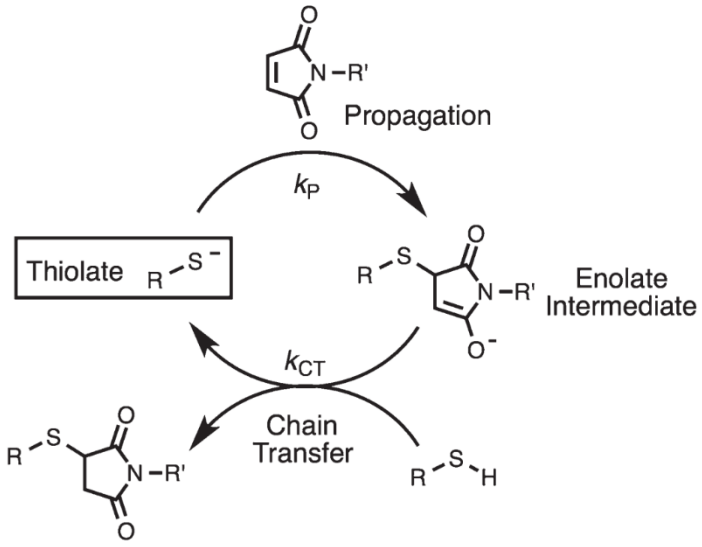

Figure 1.7 *Schematic of the thiol-maleimide Michael-type addition reaction. Deprotonation of thiol groups leads to formation of thiolate ions which initiate nucleophilic attack of the unsaturated bond present in maleimide. The result is conjugation of the two groups and substituent chains. Image adapted with permission* (Northrop, Frayne and Choudhary, 2015)

The thiol content of cysteine amino acids opens up the possibility of using peptides that incorporate cysteines as conjugates for the PEG molecules and as such, essentially any sequence of amino acids can be tethered to the hydrogel covalently (Deforest, Sims and Anseth, 2010). As any bifunctional molecule can act as a cross-linker, peptides containing more than one cysteine can be used to join the polymers together and hence form a hydrogel. Peptides can therefore be synthesised to include bioactive sequences, including those that

are substrates for enzymatic cleavage (Schultz and Anseth, 2013). By severing the cross-links, hydrogels break down into their polymer subunits and therefore using such peptides to form the hydrogel will render them enzymatically degradable. Libraries of sequences that are susceptible to cleavage by matrix metalloproteases (MMPs) have been characterised for their sensitivity to enzymatic cleavage (Patterson and Hubbell, 2010, 2011). As cells are known to secrete MMPs to remodel their environment, cells in the immediate vicinity of the hydrogel will be able to facilitate its degradation. Degradable peptides are not the only useful sequences that can be incorporated into the hydrogels and in fact this mechanism can also be used to engage with integrins and enable their adhesion. As integrins are capable of recognising the short sequences in ECM proteins (RGD, IVKAV etc. (Gunn, Turner and Mann, 2005; Kim *et al.*, 2016)) these truncated sequences can be conjoined with cysteines and bound directly to the hydrogel structure, thereby allowing cells to adhere to the material through the same mechanisms as ECM. Ultimately these gels replicate the ECM in many ways but with completely defined, synthetic components.

The potential of PEG gels in neural studies has been demonstrated using various formulations of the hydrogel. McKinnon *et al.* used MMP degradable PEG gels functionalised with RGD and YIGSR to show extensive neurite outgrowth of embryonic stem cell-derived motor neurons (McKinnon, Kloxin and Anseth, 2013). Mosley *et al.* was able to induce neuronal differentiation and neurite extension on PEG hydrogels in 2D (Mosley *et al.*, 2016). Naghdi *et al.* used RGD bound PEG hydrogels modified with tenascin-C to encourage the differentiation of neural stem cells along a neuronal lineage (Naghdi *et al.*, 2016). Only a limited number of *in vivo* studies have been conducted using PEG hydrogels in spinal cord injury models which give some insight. Park *et al*. employed MMP-degradable PEG-hyaluronan gels modified with IKVAV and loaded with BDNF which were injected intrathecally and demonstrated an early improvement in Basso, Beattie and Bresnahan (BBB) locomotor scores (Park *et al.*, 2009). Dumont *et al.* used a hemi-sectional injury model to implant pre-fabricated aligned PEG gel implants and saw an attenuation of the glial scar and an increase in myelinated axons compared to controls (Dumont *et al.*, 2019). It is notable that the compositions of gel used varies significantly between respective studies and without standardised protocols to make the studies equitable it is difficult to draw firm comparisons, but due to the wide scope of modifications that can be made to PEG hydrogels the diversity is only expanding. However, while the gels may not be precisely the same there is frequently evidence of enhanced growth of neural cells to be seen which does indicate that PEG gels hold the potential to be of therapeutic benefit in SCI.

1.3.6 Injectable Hydrogels

The notion of injectable materials comes with some very attractive advantages over conventional approaches of implantation. They can be significantly less invasive than other surgical alternatives as the target sites do not have to be incised to place the material and they only need to pass through a needle. Additionally, by not having a pre-fabricated structure they can achieve exceptional apposition to tissues as they can flow into the irregular spaces at the peripheries of tissue voids (Liu and Garcia, 2016). This also means they are not limited by manufactured dimensions and can potentially be scaled indefinitely and extemporaneously to meet clinical requirements.

Different approaches can be taken in creating injectable systems. Hydrogels can be injected as precursor agents to solidify *in situ* in response to some form of initiating stimulus, as is the case with thermally gelling hydrogels. Collagen is a notable example that transitions from solid to liquid when the temperature is raised to physiological levels (Yunoki, Ohyabu and Hatayama, 2013). Cornelison *et al.* developed a system that allow them to transform de-cellularised nerve ECM into an inverse thermally setting hydrogel through the same mechanism due to the high collagen content (Cornelison *et al.*, 2019). Hyaluronan-methylcellulose also possesses the same property but has the additional benefit of being shear-thinning which enables the material to switch from solid to liquid as it flows through a syringe and then re-solidify as it exits (Gupta, Tator and Shoichet, 2006).

Alternatively, hydrogels can also be synthesised prior to injection into forms that are small enough to flow through needles which can be in the micrometre range, and this pre-fabrication can have benefits over *in situ* gelation. Production of microgels ex-vivo allows for significantly more freedoms in the gel synthesis as harmful processes or toxic by-products can be eliminated prior to their use which therefore expands the library of potential material candidates. Furthermore, greater control over the reaction kinetics can be achieved in the laboratory than *in vivo* and the hydrogels can be more reliably reproduced. The simplest form for microgels to take is spheres which can be produced in a variety of ways. Emulsions are a straight forward method for rapidly producing microspheres by the agitation of multiphase fluids which prompts the partitioning of the phases into spheres, however these are difficult to control with accuracy and usually result in very high size polydispersity. Wen *et al.* (Wen *et al.*, 2016) produced PLGA microspheres loaded with BDNF and VEGF through this technique and used in conjunction with hyaluronan scaffolds demonstrated an increase in neurite growth through the material compared to the HA alone. Electrospraying

could also be used which accelerate fluid jets to form droplets into a collector bath which can cross-link the material, but these are also not reliably monodisperse (Jain *et al.*, 2015).

Currently the most ubiquitous method for production of microspheres are microfluidics based approaches. Devices based on microfluidics are able to control flows with extreme precision that allow for highly reproducible production of microspheres. Commonly these devices are created using a system developed by McDonald *et al.* (Mcdonald *et al.*, 2000) using polydimethylsiloxane (PDMS) cast onto photolithographic moulds that can be firmly bound to glass substrates to enclose the microscale channels. The device design and operation will be contingent on the mechanisms of gelation for the material in question and whether they are single component gels or if they require mixing with a cross-linker, but the possibilities are potentially limitless. Hong *et al.* (Hong *et al.*, 2012) demonstrated a system for the facile production of cell-laden collagen microspheres by dispersing aqueous collagen droplets in oil flows. Considering the thermally induced gelation they also introduced a heated oil flow downstream to accelerate the hydrogel solidification. Lewis *et al.* described a system that uses photo-polymerisable PEG-based gels that are polymerised by UV irradiation directly onto the polymer droplets within the device after they are formed in a flow focussing regime (Lewis *et al.*, 2010). For Michael-type addition polymerised gels, separation of the polymer and cross-linker are required to prevent device blockages. Such a device has been demonstrated by Foster *et al.* (Figure 1.8) (Foster *et al.*, 2017). to produce 4-armed PEG-maleimide (PEG-4MAL) based hydrogels and as such represents a viable approach for prefabrication of this type of hydrogel into injectable forms.

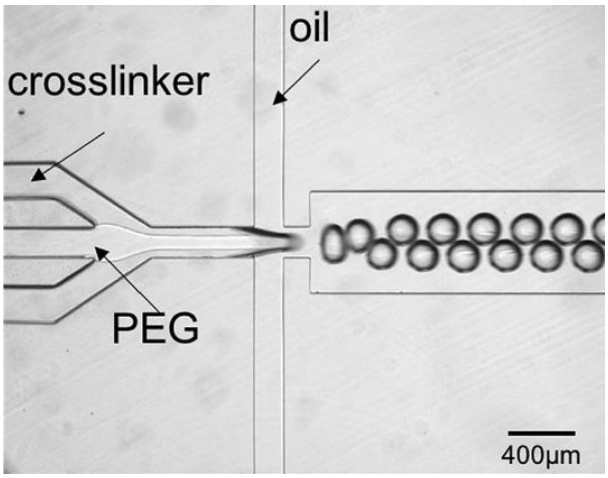

Figure 1.8. *Aqueous-oil flow-focussing microfluidic device with convergent polymer/cross-linker flows to create gel microspheres. PEG and cross-linker streams combine before being continuously formed into droplets by oil forcing through a narrow orifice. Adapted with permission* (Foster *et al.*, 2017)

1.4 Project Aims

The main aim of this project is to establish an injectable form of PEG-4MAL based hydrogel and evaluate the potential for promoting regeneration in the injured spinal cord. To achieve this, the research outline can be divided into 4 distinct sections.

1. Fabrication of PEG-based hydrogels and characterisation of the material properties.

2. *In vitro* analyses to evaluate the behaviour of neural cells cultured within the hydrogels.

3. Establish a protocol to allow for the injection of the hydrogels in a surgical setting.

4. Assess the biological response to the hydrogel *in vivo* using rat models of spinal cord injury.

2. Physico-chemical Characterisation of 4-Armed Polyethylene Glycol Maleimide Based Hydrogels

2.1 Introduction

Polyethylene Glycol is a polymer widely used in the medical industry, in part due to its bio-inert properties (Emilsson *et al.*, 2015), but this property also makes them intrinsically poor at promoting cellular interactions. However, PEG can also be modified with an abundance of chemical moieties that vastly expand the library of chemical processes that it is able to participate in (Bakaic, Smeets and Hoare, 2015). For these properties, synthesis of PEG hydrogels is particularly of interest in the field of tissue engineering (Zhu, 2011). Of all the possible modifications that can be utilised, one that stands out is the use of maleimide groups due to its exceptional capability in conjugating with thiol groups rapidly, efficiently and in biologically benign conditions (Phelps *et al.*, 2012). This enables maleimide groups to tether cysteines and by extension virtually any cysteine-linked amino acid sequence directly to the polymer.

As tissue engineering places a heavy emphasis on biomaterials and their ability to enable cellular colonisation by regulating adhesion and migration, functionalisation with sequences that can facilitate these behaviours is critical. RGD is one such sequence that has been used extensively to induce coupling with integrins and thereby allow cells to move across substrates with tethered RGD through the same mechanisms as they do with natural ECM (Yu *et al.*, 2011). RGD is usually recognised as a derivative of fibronectin, although it can be found in several other proteins (Ruoslahti and Pierschbacher, 1987) and this ubiquity along with the range of integrins that it can engage (Nieberler *et al.*, 2017) make it applicable in many different tissues (Kudva, Luyten and Patterson, 2017; Mauri *et al.*, 2018; Ouyang *et al.*, 2019). IKVAV is another such sequence derived from laminin that is found in abundance throughout the CNS and has been used with the same goal in several studies on neural cells (X. Li *et al.*, 2014; Farrukh *et al.*, 2017). However, just as cells remodel their environment in healthy tissues, so too must they be able to do so within biomaterial scaffolds (Tibbitt and Anseth, 2009). As this is often achieved through matrix metalloprotease activity, peptide sequences that are sensitive to these enzymes such as the VPM (Salimath *et al.*, 2012) sequence have been utilised to allow their passage through the material by degradation of the local environment (Dietrich *et al.*, 2018).

The scope for modification of 4-armed PEG-maleimide gels is incredibly vast, however with each modification the intrinsic properties of the material may also change significantly. In this chapter, different compositions of PEG-4MAL hydrogel modified with the integrin ligand peptides and variable proportions of degradable and non-degradable cross-linker are

examined for some key material properties. Figure 2.1 portrays a schematic of the molecular structure of the hydrogel along with a sample image of the PEG-4MAL hydrogel after formation and swelling. The Young's modulus, degradation profile and gelation rates are measured to ensure they fall within biologically suitable and practically useful ranges. Binding of the peptides to PEG-maleimide is validated through fluorescent thiol detection assays, swelling and mesh size information is calculated and release of the neurotrophins NGF and BDNF are investigated, collectively all of which are used to appraise their suitability as candidates for further exploration *in vitro* and *in vivo*.

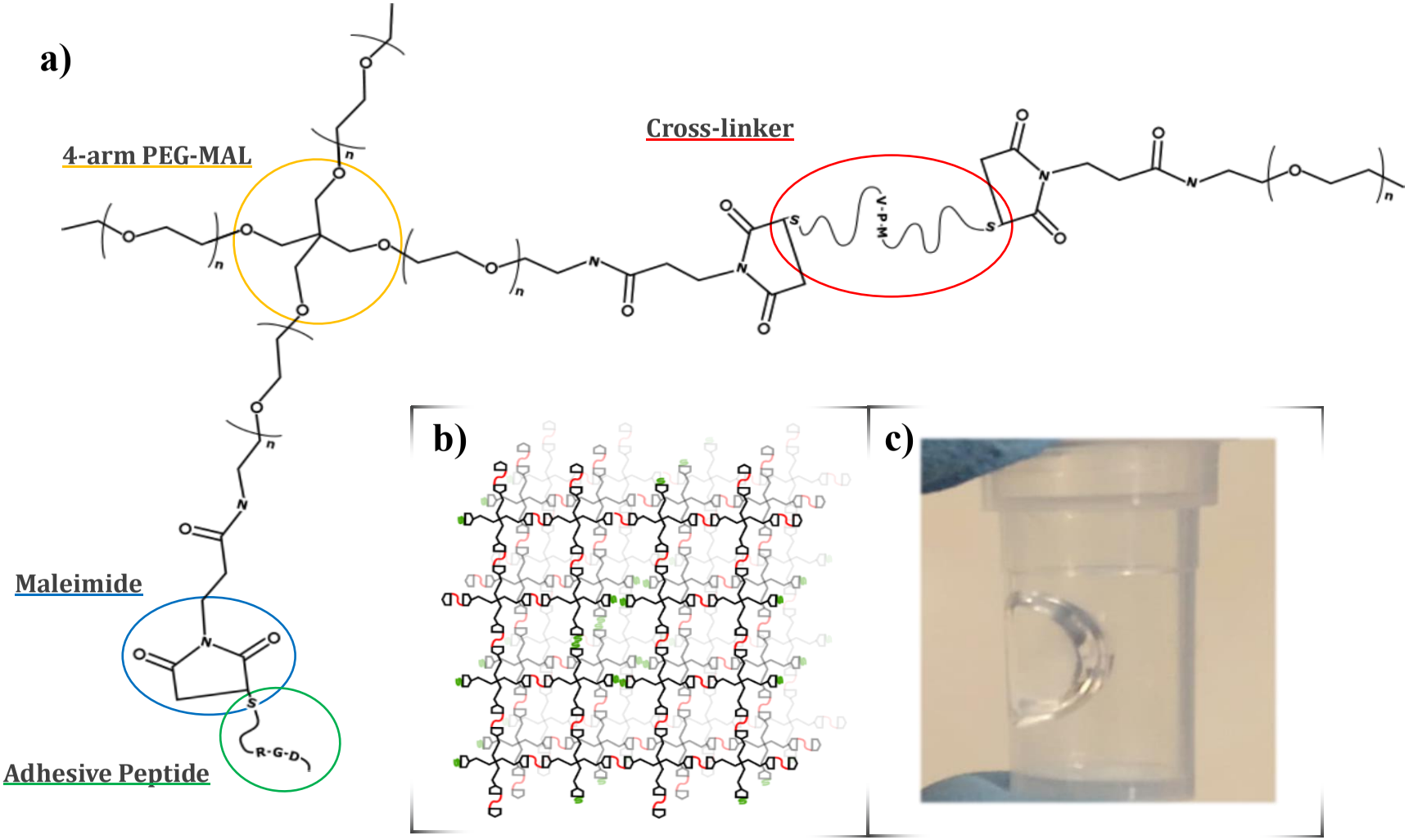

Figure 2.19 a) *Diagrammatic representation of PEG-4MAL gel composition. Peptides can be bound to the maleimide groups via thiols present in cysteine amino acids. The same mechanism is used to link PEG-4MAL molecules together using a dithiol cross-linker.* ***b)*** *Illustration of 3D hydrogel mesh structure, multiple molecules will bind together to form the hydrogel polymer network.* ***c)*** *Photograph of hydrogel after formation and swelling.*

2.2 Material & Methods

2.2.1 Gel Preparation

2.2.1.1 Materials

- 4-armed Polyethylene glycol-Maleimide Macromer (PEG-4MAL, 20kDa, Laysan Bio, USA),
- PEG-dithiol(PEG-diSH, 3.4kDa, Laysan Bio, USA),
- RGD-Peptide(Full Amino Acid Sequence '**GRGDSPC**', Genscript, Netherlands),
- IKVAV-Peptide (Full Sequence '**CSRARKQAASIKVAVSADR**', Genscript, Netherlands)
- VPM-Peptide (Full Sequence '**GCRDVPMSMRGGDRCG**', Genscript, Netherlands)

Each of the peptides is dissolved in PBS and frozen in aliquots. The PEG-4MAL and PEG-diSH are weighed and dissolved in PBS as required on the day of preparation.

2.2.1.2 Calculation of Reagent Quantities

The characterisations details in this chapter have been based on 5% wt/vol PEG-4MAL hydrogels functionalised with 2mM of RGD or IKVAV and non-functionalised controls except where stated otherwise. Different proportions of degradable VPM peptide and non-degradable PEG-diSH cross-linker were also investigated, and consequently the predominant focus of the subsequent characterisations has been based on the hydrogel formulations combinations described in Table 2.1. The control gels (PEG-Only) were created by omitting the peptides from the gel formulation and substituting an equivalent volume of PBS while otherwise using the same quantities of reagents.

	RGD	**IKVAV**	**PEG-ONLY**
100% VPM	R 100V	I 100V	Ø 100V
75% *VPM* : 25% *PEG-DISH*	R 75V:25P	I 75V:25P	Ø 75V:25P
50% *VPM* : 50% *PEG-DISH*	R 50V:50P	I 50V:50P	Ø 50V:50P

Table 2.1 *Principle combinations of hydrogel formulations under investigation, using RGD, IKVAV or unfunctionalised (PEG-Only) gels with varying proportions of degradable VPM and non-degradable PEG-diSH. Their abbreviations are noted in this table.*

To calculate the amount of every reagent required to prepare the different hydrogel combinations presented in Table 1, first the concentration of total maleimide groups available in a 5% wt/vol PEG-MAL hydrogel is calculated. Then, the concentration of maleimide groups that remain unoccupied after binding the 2mM peptide can be determined. Finally, the mass of cross-linker required to cross-link the remaining maleimide moieties is calculated.

1. Determine the molar concentration of PEG-4MAL required in the final gel and subsequently the concentration of individual maleimide groups (4 groups per PEG-4MAL molecule).

$$5\%wt\ /\ vol = 50\ g/L \qquad Molecular\ Weight\ (MW, PEG-4MAL) = 20000\ g/mol$$

$$\frac{50\ (g/L)}{20000\ (g/mol)} = 2.5 \times 10^{-3}\ mol/L\ PEG-4MAL \rightarrow 0.01M\ (10mM)\ MAL$$

2. From this, subtract the molar concentration of RGD/IKVAV that will be used (2mM) this will give the total concentration of unbound maleimide groups after binding with RGD/IKVAV.

$$10\ mM - 2mM = 8mM\ Remaining\ MAL$$

3. Calculate the concentration of cross-linker required to occupy the remaining maleimide groups. Each cross-linker molecule contains 2 thiol moieties. The proportion of degradable cross-linker (VPM) to non-degradable (PEG-diSH) is also calculated.

$$\frac{8mM}{2} = 4mM\ Cross-Linker$$

Table 2.2 *Molar concentrations of cross-linker present in each ratio.*

Cross-Linkers Molar Proportions		
	VPM:	***PEG-diSH:***
100% ***VPM*** ***(100V)***	*4 mM*	-
75% ***VPM*****: 25%** ***PEG-diSH*** ***(75V:25P)***	*3 mM*	*1 mM*
50% ***VPM*****: 50%** ***PEG-DISH*** ***(50V:50P)***	*2 mM*	*2 mM*

4. Convert molar concentrations to units of mass and define the dilutions required, considering the PEG-4MAL and cross-linker solutions are prepared separately and will be diluted when mixed together to form the gel. Detailed below are quantities based on 100µL of gel with the PEG-4MAL and cross-linker diluted as such that they can be mixed in equal volumes to form the final gel.

Table 2.3 *Mass of reagents required to make 100µL of gel for each of the forms described in Table 2.1.*

Integrin Ligand Masses		
Moles Required:	*0.002 M x (100 x 10^{-6} L) = 2 x 10^{-7} mol/100µL*	
Molecular Weight	***RGD:*** *690.73 g/mol*	***IKVAV:*** *2017.33 g/mol*
Ligand Dilutions	*2 x 10^{-7} mol → 138.1 µg*	*2 x 10^{-7} mol → 403.5 µg*
Cross-Linker Masses		
Moles Required:	*0.004 M x (100 x 10^{-6} L) = 4 x 10^{-7} mol/100µL*	
Molecular Weight	***VPM:*** *1696.96 g/mol*	***PEG-diSH:*** *3400 g/mol*
100V	*4 x 10^{-7} mol → 678.8 µg*	*-*
75V:25P	*3 x 10^{-7} mol → 509.1 µg*	*1 x 10^{-7} mol → 340 µg*
50V:50P	*2 x 10^{-7} mol → 339.4 µg*	*2 x 10^{-7} mol → 680 µg*

Table 2.4 *Dilution of reagents required to make 100µL of gel for each of the forms described in Table 2.1. at a 1:1 ratio of functionalised polymer to cross-linker.*

Polymer Functionalisation Dilutions (50uL Total)			
PEG-4MAL	*5mg PEG-4MAL + 25uL PBS*		
Ligand Dilutions	***RGD (20mM Stock):*** *10uL Stock + 15uL PBS*	***IKVAV (20mM Stock):*** *10uL Stock + 15uL PBS*	***PEG-Only:*** *25uL PBS*
Cross-Linkers (50uL Total)			
	VPM (50mg/mL Stock):	***PEG-diSH:***	
100V	*13.55uL Stock + 36.45uL PBS*	*-*	
75V:25P	*10.17uL Stock + 24.83uL PBS*	*0.34mg PEG-diSH + 15uL PBS*	
50V:50P	*6.87uL Stock + 3.13uL PBS*	*0.68mg PEG-diSH+ 30uL PBS*	

5. These quantities can then be scaled to meet the requirements of each experiment.

2.2.1.3 Gel Preparation

PEG-4MAL and PEG-diSH lyophilised powders are weighed and dissolved in PBS, allowing 15 minutes to ensure complete dissolution. Lyophilised peptides previously aliquoted PBS are thawed. RGD or IKVAV peptide solutions are mixed thoroughly with the dissolved PEG-4MAL either by pipette or vortex mixing and given a further 15 minutes to allow the thiol-maleimide reaction to occur. The PEG-Only controls are mixed with an equivalent volume of PBS. The VPM and PEG-diSH are combined in the required proportions. To create the gels, the PEG-4MAL-peptide solution is pipetted into/onto the appropriate vessel/surface then mixed with the cross-linker and allowed to solidify. The gel will solidify spontaneously after mixing over a timescale dependent on the pH (The gelation rates are quantified in Section 2.3.3).

2.2.2 Confirmation of Peptide Binding

The reaction between the peptides' cysteine thiols and the maleimide groups was confirmed using a fluorometric thiol detection kit (Sigma Aldrich, UK). In this assay thiol groups can be detected by reaction with a proprietary fluorophore that will fluoresce with a higher intensity following reaction with thiol moieties (Figure 2.2). Peptides mixed with the fluorophore will yield a high fluorescence intensity due to the presence of unreacted thiol groups whereas peptides that have been conjugated with PEG-4MAL prior to adding the fluorophore should have a significantly reduced intensity if the peptides have successfully bound with the maleimide groups.

Solutions of 20μM RGD and IKVAV were prepared in PBS along with 5μM PEG-4MAL, corresponding to 20μM of maleimide. 25μL of each of the peptide solutions was pipetted into a black-walled 96-well plate and mixed with an additional 25μL of either PBS to quantify the unbound peptides, or with PEG-4MAL to give final concentrations of 10μM peptide and maleimide. This was allowed to react for 15 minutes. A serial dilution of PEG-diSH was prepared in PBS to produce a calibration curve, starting at a concentration of 10μM thiol (5μM PEG-diSH) and diluting by half for each point of reference down to 0.625μM thiol. A blank of PBS, and another blank of 10μM maleimide (2.5μM PEG-4MAL) were also included to observe and deduct any background fluorescence induced by the PEG-4MAL. After the reaction period had elapsed, 50μL of the fluorophore (supplied at 100x concentration and diluted to 1x in PBS) was added to each well bringing the total volume to 100μL per well. This was allowed a further 10 minutes to enable the fluorophore binding

following which the fluorescence intensity was measured in a plate reader (Tecan Infinite® 200 PRO, Switzerland) using an excitation wavelength of 490nm and emission wavelength of 520nm. Each sample was measured in triplicate and the standards were read in duplicate. The measurements from the serial dilution were then used to calculate the linear relationship between fluorescence intensity and sample concentration which in turn was used to calculate the concentration of thiol measured in each sample.

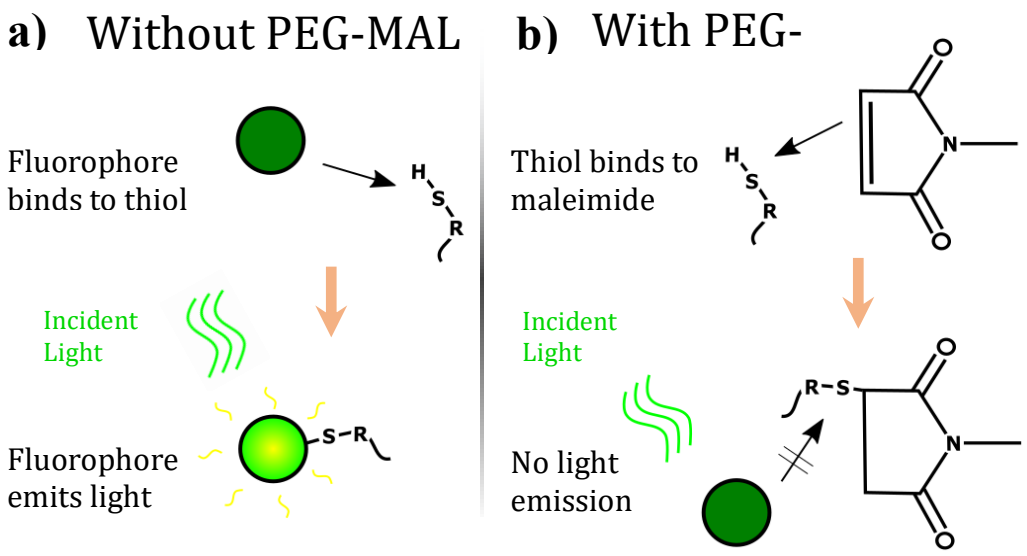

Figure 2.2 a) *Diagram of the thiol detection assay mechanism used to confirm peptide binding to maleimide groups. The fluorophore binds with thiol groups present in the cysteine amino acids in each peptide chain and in doing so creates a strongly fluorescent adduct.* ***b)*** *Following the peptide reaction with PEG-4MAL, the availability of free thiol groups in solution will be greatly reduced therefore the measured fluorescence intensity will be much lower than that of the peptide alone.*

2.2.3 Degradation Profile

2.2.3.1 In-Vitro Degradation

A panel of several hydrogel formulations of various PEG-4MAL concentrations and VPM:PEG-diSH cross-linker ratios to determine which of those measured were capable of maintaining material integrity during *in vitro* culture. PC12 cells (P12, Sigma Aldrich, UK), an immortalised cell line capable of growing in suspension and adherent cultures, were encapsulated within these hydrogels and their degradation was observed over 7-day cultures. Using PEG-4MAL concentrations of 3, 4 & 5 %wt/vol bound with 2mM RGD and cross-linker ratios of 85V:15P (V; VPM, P; PEG-diSH), 75V:25P, 65V:35P and 50V:50P, the time taken for the gel to completely break down was noted so that formulations which failed to

endure 7 days could be discounted from further investigations in favour of more durable gel types. The PC12 cells were expanded in suspension in RPMI 1640 (Thermo Fisher, UK) media with 10% horse serum (HS, Thermo Fisher, UK) in T75 flasks. These were centrifuged to form a pellet and incubated in 5mL of trypsin-EDTA (Sigma Aldrich, UK) for 5 minutes to dissociate the cell clusters before pelleting again. These were re-suspended in RPMI 1640 and adjusted to a density of $5x10^6$ cells/mL. 30μL of gel precursors were prepared as described in Section 2.2.1.3. The volume of PBS added to the cross-linker solution during preparation was reduced by 6μL per 30μL gel to be substituted for the same volume of cell suspension. This cross-linker/cell suspension was then mixed with the PEG-4MAL solution by pipette in a 24-well plate and allowed to solidify for 20 minutes before adding 1mL of RPMI 1640 with 1% HS and 50ng/mL of nerve growth factor (β-NGF, R&D Systems, UK) to each well. The resultant gels contained 30000 cells per sample and the media was exchanged every 2 days for 7 days. The condition of the hydrogels was documented at every media exchange to observe whether they remained intact or if they had degraded.

2.2.3.2 Collagenase Degradation

Based on the outcome of the PC12 gel degradation assay, the formulations of hydrogel that remained stable for the duration of the experiment were further analysed for their degradability using solutions of type-1 collagenase. These were reduced to those designated in Table 2.1, using the 100V gels as a fully degradable comparison and additionally a fully non-degradable equivalent cross-linked with on PEG-diSH (100P). The hydrogel precursor reagents were prepared as described in Section 2.2.1.3 and 30μL hydrogels were formed into centrifuge tubes (Corning® Costar® Spin-X® centrifuge tube filters, Sigma Aldrich, UK). Prior to formation, the empty filtration baskets were weighed so the mass of the basket could be subtracted from the mass of the gel during each weighing. The gels were immersed in PBS overnight to enable them to reach a point of equilibrium swelling. Following this the supernatant was removed from each tube by pipette aspiration and centrifuged for 5 minutes at 5000rpm to fully dispense the supernatant, after which the initial gel mass was recorded. The gels were then immersed in 0.5mL of type 1 collagenase (Thermo Fisher, UK) at concentrations of 30 U/mL, 10 U/mL or PBS as a control. The gel mass was measured at several time points (1h, 3h, 6h, 1d, 3d, 5d, 7d, 10d, 14d then twice weekly), each time removing the supernatant by aspiration and centrifugation which was refreshed after each weighing. This continued until either the gel was degraded, or for those that did not degrade the experiment was terminated after 8 weeks.

2.2.4 Gelation Rate

The speed of gelation was measured by determining the time taken for the gel to resist aspiration by pipette after the PEG-4MAL and cross-linker had been mixed, marking the transition from solution into gel (Figure 2.3). The gel reagents were prepared as described in Section 2.2.1.3 and initially mixed in Eppendorf tubes by pipette for 15 seconds. This was then aspirated and ejected every 15s for the first 5 minutes to determine the point at which the gel could no longer be withdrawn by pipette, and subsequently every minute if gelation had not been reached by this time point. Each formulation of gel designated in Table 2.1 was investigated to observe their gelation rates. Another experiment was conducted using the same methodology to determine the effect of pH on the gelation rate, focussing on the 50V:50P cross-linked gels as these gels displayed the shortest gelation speeds and could maximally discriminate between the anticipated longer gelation times associated with lowering the pH. PBS buffers with pH adjusted to 5, 6 and 7.4 (standard) were prepared using 1M HCl and used to dissolve the PEG-4MAL, peptides and cross-linkers, and subsequently their gelation speeds were measured. Finally, the effect of temperature on the gelation rates was examined, again using the same methodology with 100V gels as these displayed the longest gelation times and could maximally discriminate between the anticipated reduction in gelation times associated with increasing the temperature. Hydrogel precursors were mixed in Eppendorf tubes heated to 37°C and compared to gels formed at ambient temperate (22°C).

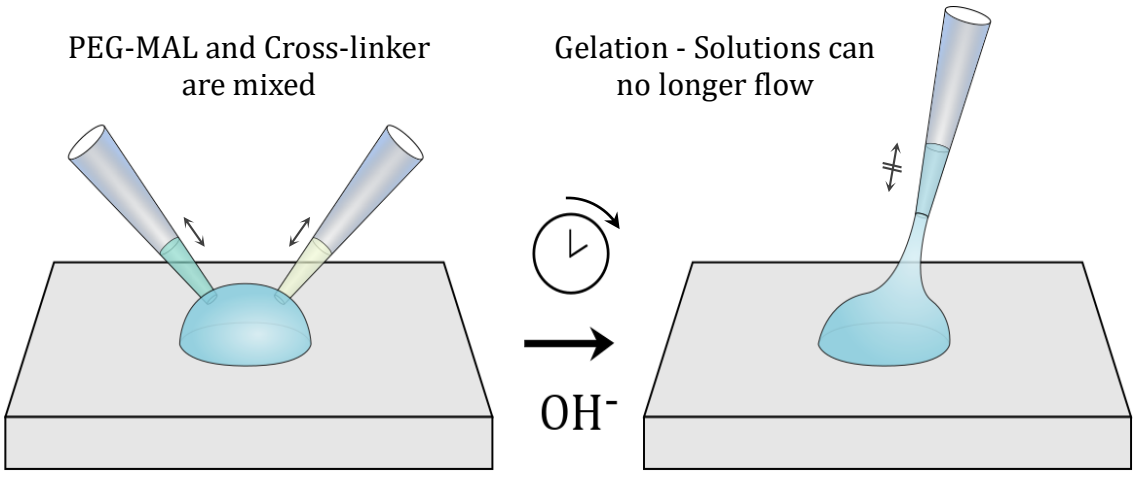

Figure 2.3 *Diagram of gelation measurement. PEG and cross-linker are mixed and the gelation will subsequently occur at a rate dependent on the pH. Gelation will also cause the mixture to resist aspiration by pipette, marking the time point when the material no longer behaves as a liquid.*

2.2.5 Swelling Behaviour

The swelling behaviour of the hydrogels can be adequately described by the swelling ratio which quantifies the relationship between water content and dry mass of hydrogels(Park *et al.*, 2010):

$$Weight\ Swelling\ Ratio\ (q_w) = \frac{m_s}{m_d} \qquad (2.1)$$

Where m_s and m_d are the swollen mass and dry mass of the gel respectively. To measure this, the gel formulation designated in Table 2.1 were formed in triplicate into centrifuge filtration tubes (Sigma Aldrich, UK). Prior to formation, the empty filtration baskets were weighed so the mass of the basket could be subtracted from the mass of the gel during each weighing. 15 minutes after formation of the gels, each sample was weighed in the basket before being immersed in Milli-Q water and incubated at 37°C overnight to allow the diffusion of water into the gels to reach equilibrium. The supernatant was removed from each sample by pipette and was centrifuged at 5000 rpm for 5 minutes to remove any residual water present in the basket or on the gel surface. Samples were then weighed again. Following this each filtration tube was pierced and placed in a vacuum evaporator centrifuge (Eppendorf Concentrator Plus) for 1 hour to dry the samples completely, after which they were weighed for a final time.

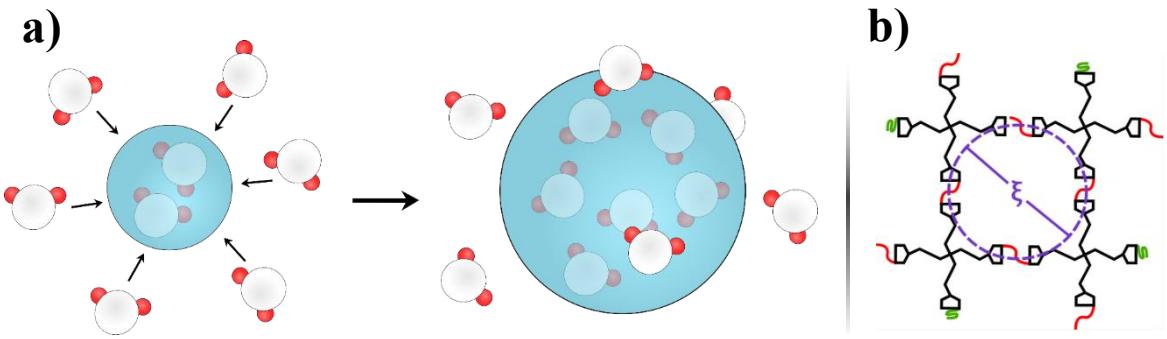

Figure 2.4 a) *Diagram of gel swelling, gel size increases as more water migrates into the structure.* ***b)*** *Illustrative representation of the definition of hydrogel mesh size (ξ), the average distance between cross-links.*

Using the data from the swelling analysis it is also possible to calculate the mesh size (ξ) of the gels which describes the average distance between cross-links of the gel network (Figure 2.4). The calculations were performed as follows:

$$q_w = \frac{m_s}{m_d} \qquad (2.2) \qquad\qquad q_f = \frac{m_r}{m_d} \qquad (2.3)$$

Where q_w is the equilibrium (swollen) weight swelling ratio; the ratio of swollen gel mass (m_s) over dry gel mass (m_d), and q_f is the ratio of the gel mass immediately after formation in the relaxed state (m_r) over dry mass (Caykara and Recai, 2003). From these ratios, the volume fraction of polymer in the hydrogel in the swollen state ($v_{2,s}$) and in the relaxed state ($v_{2,r}$) can be calculated;

$$v_{2,s} = \left[1 + \frac{(q_w - 1)\rho_{PEG}}{\rho_{water}}\right]^{-1} \qquad (2.4) \qquad\qquad v_{2,r} = \left[1 + \frac{(q_f - 1)\rho_{PEG}}{\rho_{water}}\right]^{-1} \qquad (2.5)$$

The density of water (ρ_{water}) is 1 g/mL. The specific volume of amorphous PEG ($\bar{v}$) has been reported(Cruise, Scharp and Hubbell, 1998) as 0.893 mL/g from which the reciprocal can be taken to get the density (ρ_{PEG}) as 1.12 g/mL. Now the Flory-Rehner equation can be used to calculate the average molecular weight between cross-links (Cruise, Scharp and Hubbell, 1998) ($\overline{M_c}$).

$$\frac{1}{\overline{M_c}} = \frac{2}{\overline{M_n}} - \frac{\frac{\bar{v}}{V_1}\left[ln(1 - v_{2,s}) + v_{2,s} + \chi({v_{2,s}}^2)\right]}{v_{2,r}\left[\left(\frac{v_{2,s}}{v_{2,r}}\right)^{1/3} - \frac{1}{2}\left(\frac{v_{2,s}}{v_{2,r}}\right)\right]} \qquad (2.6)$$

In this equation, $\overline{M_n}$ is the average molecular weight of the polymer (20kDa), V_1 is the molar volume of water (18 cm^3/mol) and χ is the Flory polymer-solvent interaction parameter which for PEG has been previously implemented as 0.426 (Lu and Anseth, 2000). The next step is to calculate the polymer chain length between cross-links in the unperturbed state $(\bar{r}_0^2)^{1/2}$:

$$(\bar{r}_0^2)^{1/2} = l\left(2\frac{\overline{M_c}}{M_r}\right)C_n^{1/2} \qquad (2.7)$$

l is the average bond length within the polymer chain (0.146nm) (Raeber, Lutolf and Hubbell, 2005), M_r is the monomer molecular weight (44 Da) (Rehmann *et al.*, 2017) and C_n is the Flory characteristic ratio, reported as 4.0 (Merrill, Dennison and Sung, 1993). From this the mesh size (ξ) can be determined:

$$\xi = v_{2,s}{}^{-1/3}(\bar{r}_0^2)^{1/2} \qquad (2.8)$$

2.2.6 Young's Modulus

In this study the hydrogel Young's Modulus was measured using atomic force spectroscopy. This method uses a cantilever with a spherical tip to indent the hydrogel surface with a defined force. The deformation is measured by deflection of a laser from the cantilever into a calibrated photodiode array, and the depth of indentation can be related with the applied force and tip geometry to calculate the Young's Modulus.

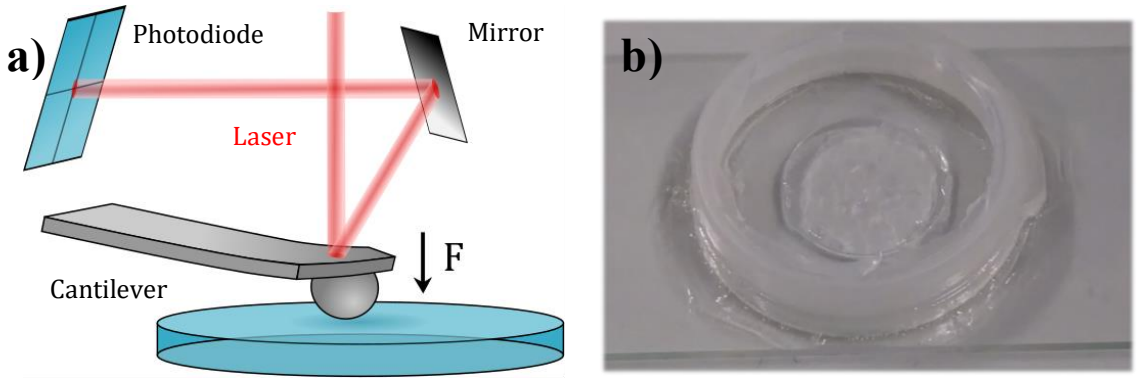

Figure 2.5 a) *Diagram of the AFM operating principles. Laser light is reflected from the surface of a cantilever that deforms on contact with the sample surface. For force spectroscopy, this deflection is deducted from the actual change in height of the cantilever during indentation to give the indentation depth which together with the force of indentation can yield the material Young's modulus by applying the Hertz model of indentation.* ***b)*** *Flat gel samples were mounted on microscope slide in reservoir prior to immersion in water in preparation for AFM measurements.*

2.2.6.1 Cantilever Preparation

Tipless silicon cantilevers (Arrow-TL1-50, k ~ 0.03 N/m, Nanoworld, Switzerland) were prepared prior to measurements with 20μm diameter silica beads (Corpuscular Inc.) mounted on the tip. Firstly, a suspension of beads was prepared by sonication for 5 minutes before

dilution in ethanol and sonication for a further 5 minutes. This suspension was spread onto a microscope slide and dried with nitrogen to disperse the beads across the surface. On a separate area of the same slide, epoxy resin (Araldite) was applied and spread thinly. The cantilevers were mounted on the AFM (Nanowizard® 3 Bioscience AFM, JPK) and manipulated to contact the cantilever tip onto the glue. The silica beads were then attached by aligning the glue-covered tip over the bead and lowering until contact before retracting and unmounting the tip, then leaving overnight to allow the epoxy to cure fully.

2.2.6.2 Sample Preparation

To prepare samples for measurement, gels of each formulation designated in Table 2.1 were formed between 2 glass coverslips to enable the formation of flat surfaces. The 12mm diameter glass was cleaned by sonication in Milli-Q water then absolute ethanol for 15 minutes each then dried in a 120°C oven. The PEG and cross-linker were mixed on the surface of a coverslip before another coverslip was dropped on top prior to gelation to enable the formation of a flat layer. These were allowed to solidify before being immersed in Milli-Q water overnight to reach equilibrium swelling. Following this the gels were removed from the water and the top coverslip was gently dislodged from the gel to leave a flat surfaced sample. These were then mounted onto microscope slides using fixogum (Marabu) and a plastic barrier was glued into place around the sample (Figure 2.5) then filled with Milli-Q water to create a reservoir.

2.2.6.3 Calibration

The JPK SPM NanoWizard® software allows for calibration of the cantilever spring constant using a thermal noise approach. A water reservoir with no sample was created as a calibration surface. The cantilever was mounted on the AFM and lowered into the water until it was fully immersed. The laser was then aligned with the photodiode array and displacement set to zero. The cantilever was set to automatic approach to the glass surface of the microscope slide and a single indentation was performed. The deflection of the cantilever can be related to the measured voltage to get the cantilever sensitivity. From here the spring constant can be calculated by measuring the thermal fluctuation of the cantilever at the resonant frequency and relating this to the thermal energy (Hutter *et al.,* 1998).

2.2.6.4 Data Collection & Analysis

After calibration, the samples were placed on the AFM stage and the tip lowered to contact the hydrogel surface. Indentations of 5nN were performed in a 4 x 4 pixel grid of 100μm x 100μm, with at least 2 samples and 3 areas per sample per condition. The measured indentations were then analysed using JPKSPM Data Processing Software (JPK) software using the Hertz model of indentation for a spherical indenter (Roa *et al.*, 2011):

$$E = \frac{3F(1 - \nu^2)}{4r^{1/2}\delta^{3/2}} \qquad (2.9)$$

Where E is the Young's modulus, F is the force of indentation, r is the radius of the bead on the cantilever tip, δ is the depth of indentation and ν is the Poisson's Ratio (assumed to be 0.5).

2.2.7 Growth Factor Release

To investigate the release profile of selected neurotrophins from these gels, nerve growth factor (NGF, R&D Systems, UK) and brain derived neurotrophic factor (BDNF, R&D Systems, UK) were tagged with fluorescent labels then loaded into the hydrogels and the release was tracked over time by measuring fluorescence of growth factor dispersed into the surrounding supernatant.

2.2.7.1 Growth Factor Tagging

Each of the growth factors was tagged using a Dylight 488 fluorophore conjugated with N-hydroxy succinimide (Dylight 488 NHS Ester, Thermo Fisher, UK) which can bind to primary amines within proteins. The fluorophore was added to 0.05M sodium borate buffer (pH 8.5, Sigma) at a tenfold excess to the growth factors in which the lyophilised proteins were dissolved. This was given 1 hour for the fluorophore to bind to the protein, then the mixture was transferred to dialysis tubes (Slide-A-Lyzer Mini Dialysis Unit 10000 MWCO, Thermo Fisher, UK) where the buffer was exchanged with PBS and the excess unbound fluorophore was removed, refreshing the PBS once an hour for 4 hours.

2.2.7.2 Measurements

30μL of each gel formulation designated in Table 2.1 was formed into centrifuge tubes. These gels were immersed in PBS containing 500ng/mL of tagged NGF or BDNF and left overnight to allow the growth factor to diffuse into the hydrogel. This supernatant was then removed by pipette aspiration and centrifugation for 5 minutes at 5000rpm and was replaced with PBS. This supernatant was removed to be measured for fluorescence intensity after 1, 3, 6, 24, 48, 72, 120 and 168 hours, each time replacing with fresh PBS. A standard curve was generated from 500ng/mL of each growth factor down to 15.625ng/mL, diluting twofold each step, with PBS as a baseline. The fluorescence was measured in a plate reader (Tecan Infinite® 200 PRO) with an excitation/emission of 488/518nm.

2.2.8 Statistical Analysis

Statistical analysis of the data was performed and subsequently plotted using GraphPad Prism Software. Single comparisons were analysed with unpaired t-tests and comparisons of multiple groups were analysed using a 2-way ANOVA with a Tukey post-hoc test. Differences were considered significant if $p < 0.05$ and p-values were annotated as $*p < 0.05$, $** p < 0.01$ and $*** p < 0.001$. Data are presented as mean values + standard deviation.

2.3 Results

2.3.1 Confirmation of Peptide Binding

The covalent attachment of the adhesive peptides to the maleimide groups present on the PEG-4MAL is required to enable cell adhesion and the generation of cellular tension through integrin activity. Untethered peptides will not provide the required physical resistance to facilitate motility mechanotransduction and will conversely behave as integrin inhibitors through occupation of the binding sites (Hatley *et al.*, 2018). The standard curve generated from PEG-diSH with the thiol detection fluorophore was plotted and a linear fit of the data produced a line with the equation y = 3432x, which was then used to convert the fluorescence intensity (A.U.) measured from the samples into the concentration of free thiols (Figure 2.6).

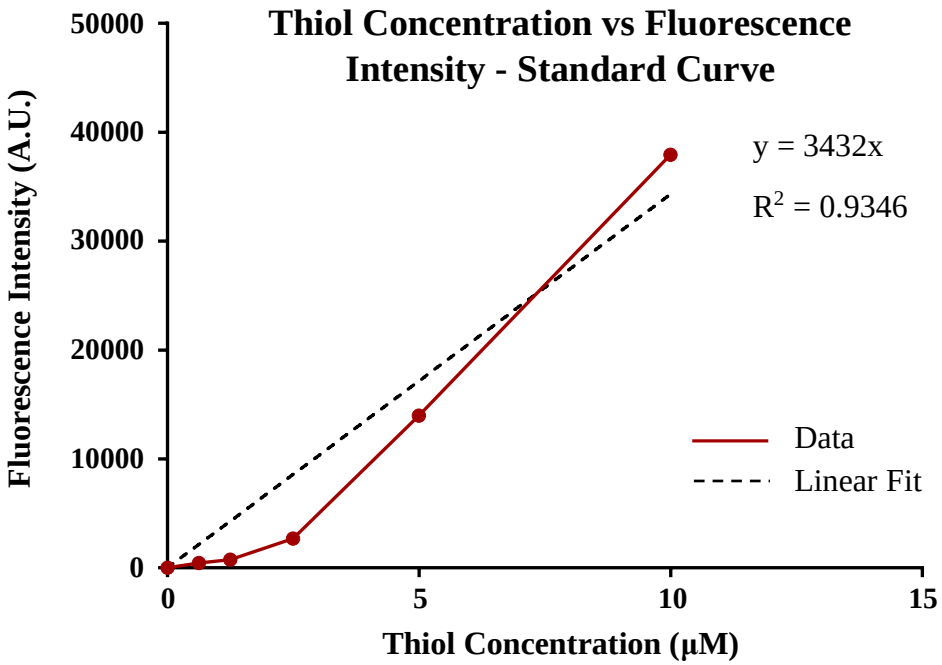

Figure 2.6 *Standard Curve for Thiol Concentration. A linear regression fit was generated using the fluorescence intensity data of a serial dilution from 10µM to 0.625µM, diluted 2-fold in PBS. The fit equation of y=3432x was used to convert fluorescence intensity to thiol concentration. The regression fit produced gave* $R^2 = 0.9346$.

Figure 2.7 shows the concentration of thiol measured for the unbound RGD and IKVAV peptides and for the same peptides combined with the PEG-4MAL. In both cases, the measured free thiol concentration was significantly lower after the peptides were reacted with the PEG-4MAL molecules. This demonstrates that the reaction between thiol and maleimide has taken place and it can be concluded that both the RGD and the IKVAV

peptides have bound to the maleimide. There is some discrepancy between the baseline thiol concentration measure for the RGD and IKVAV peptides which calls into question the accuracy of the assay to effectively quantify the thiol concentration and this indicates that the affinity of the fluorescent probe is different for each of these peptides. Notably however there is a comparable reduction of free thiol concentration between the conditions with and without PEG-4MAL; the RGD peptide sees a measured reduction of 10μM which equates to the concentration of maleimides present and the IKVAV fluorescence drops to zero in the presence of maleimides, demonstrating the capability of each to bind to the PEG molecules.

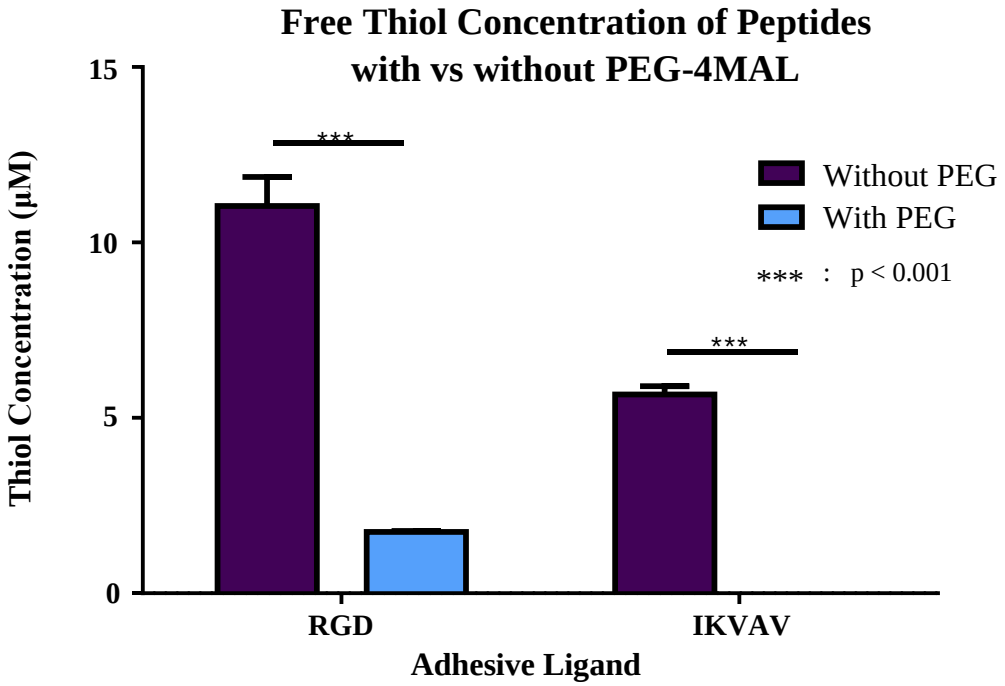

Figure 2.7 *Free Thiol Concentration of RGD and IKVAV with and without being reacted with PEG-4MAL molecules. The measured concentration of thiol in the conditions with peptide and PEG are significantly lower than the peptides without PEG, indicating that the thiol groups have reacted with the maleimide groups. Significance was determined using unpaired T-tests, n = 3 per condition, mean + SD.*

2.3.2 Degradation Profile

The VPM peptide is susceptible to the action of matrix metalloproteases, therefore enzymatic breakdown of the hydrogels can be facilitated by cellular activity in proximity to the hydrogels. Consequently, the degradability of these hydrogels is primarily dependent on the proportion of degradable cross-linker that is used in the gel formulation. To use these hydrogels for in vitro investigation it is essential that the gels can maintain integrity for at least the duration of cell culture likely to be required. The culture of PC12 cells for 1 week

using different concentrations of PEG-4MAL and cross-linker ratios revealed that several of these gel formulations were unable to retain their structure for the full 7 days (Figure 2.8.). This included all of the 3% wt/vol PEG-4MAL hydrogels and all the 4% wt/vol PEG-4MAL hydrogels with the exception of the 50V:50P cross-linked samples. Of the 5% wt/vol PEG-4MAL gels, only the gels with the highest proportion of VPM the 85V:15P gels degraded before 7 days. Consequently the 3 and 4 %wt/vol gels were discounted from further study and of the 5% wt/vol gels the 75V:25P and 50V:50P 5% wt/vol PEG-4MAL gels were selected as potential candidates for implantable materials, retaining the 100V gels as a fully degradable comparison.

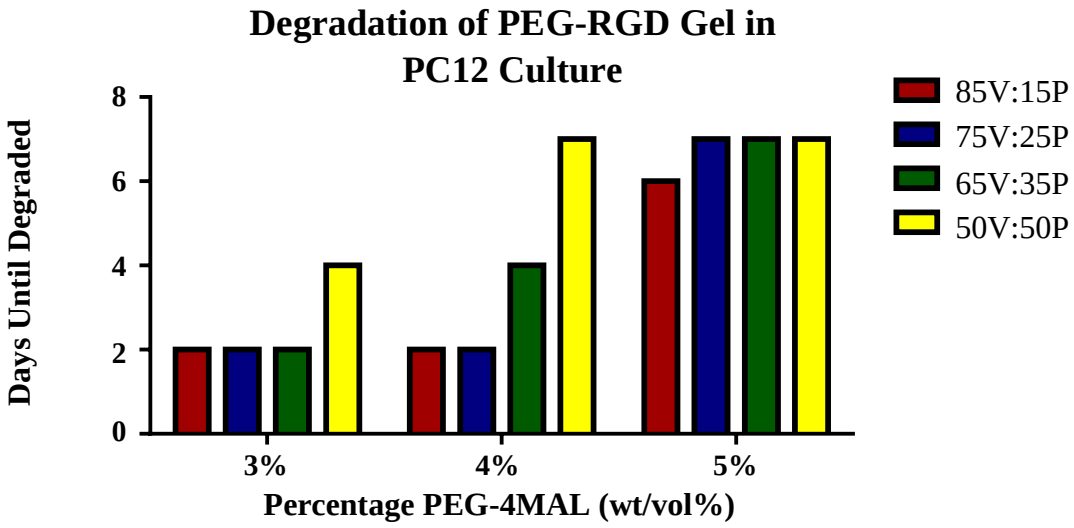

Figure 2.8 *Degradation of PEG-4MAL gels over time in PC12 culture. PC12 cells were cultured for 1 week with a range of PEG-4MAL concentrations and cross-linker ratios and the gels were noted to be present or degraded in 2-day intervals. The 3% PEG-4MAL gels all degraded before the end of the culture as did all but the 50V:50P ratio 4% PEG-4MAL gels, as well as the 85V:15P 5% PEG-4MAL gels. These were all discounted as suitable candidates for investigation due to their short stability period. n = 3 per condition; in each condition degradation occurred on the same day and standard deviation = 0, thus all differences between groups is significant.*

In the presence of type 1 collagenase, the 100V gels were degraded extremely rapidly and the degradation rate increased with the collagenase concentration, (Figure 2.9). At point a) (3h) 30U /mL collagenase samples had significantly decreased in mass compared to 0h and were completely degraded by 6h. At this time point the 10 U/mL collagenase samples had significantly decreased in mass compared to 0h and were completely degraded within 24h. In the presence of PBS the gels crosslinked with fully degradable peptides maintained their mass for 3 days but had degraded after 5 days.

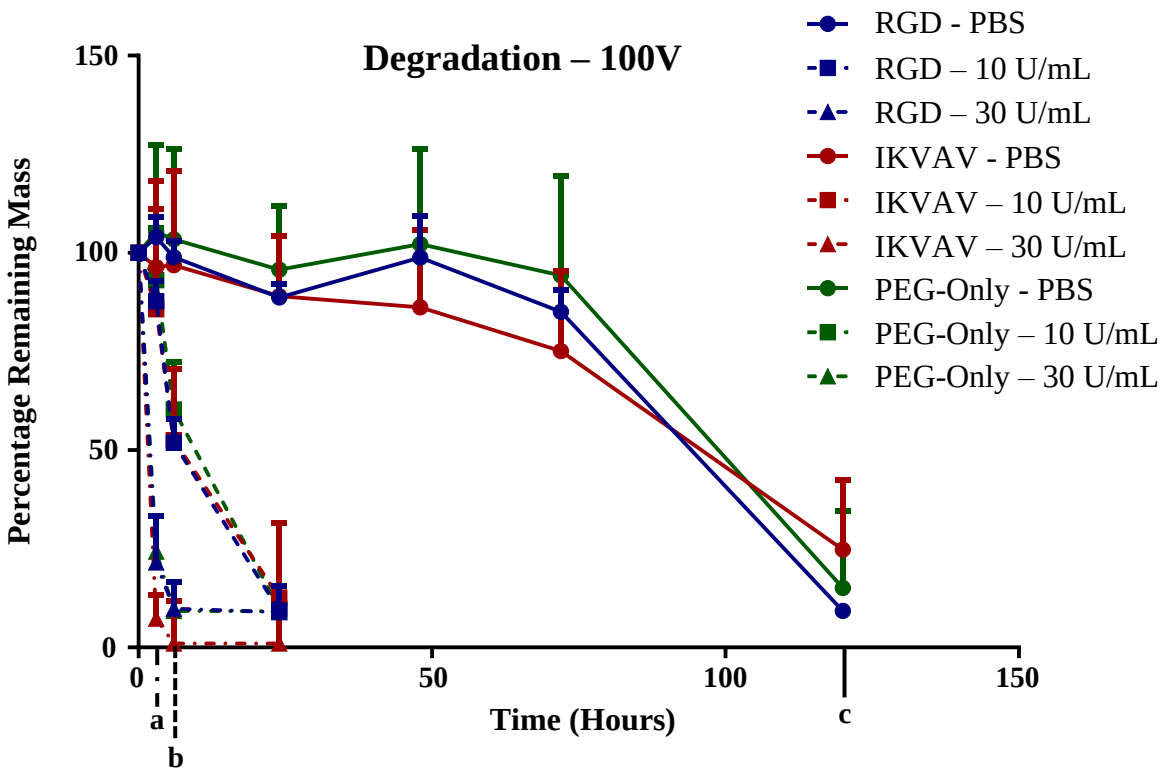

Figure 2.9 *Degradation of the 100V gels. Each of the gels behave similarly to one another in the different concentrations of collagenase, with the trend showing faster degradation with higher collagenase concentrations. The gels are susceptible to breakdown even in PBS, and each gel had degraded by 5 days of incubation. For each collagenase concentration, changing the adhesive ligand did not have a significant effect on the change in mass at any time point. Points* ***a,b & c*** *show the time points that the hydrogel mass was significantly different from the 0h mass for the gels in 30 U/mL collagenase (****a****, 3h), 10 U/mL collagenase (****b****, 6h) and PBS (****c****, 120h). Each data point represents mean percentage mass (n=3) + SD. Statistical significance was determined using 2 2-way ANOVAs to compare between groups and across time respectively, each with a Tukey post-hoc test.*

Incorporating the non-degradable cross-linker into the 75V:25P gels resulted in a slower degradation rate than the 100V gels (Figure 2.10). The gels still retaining mass after 6 hours in 30U/mL (**a**) and up to 120h in the 10U/mL (**c**) though not the IKVAV gels (**b**, 48h). In PBS the mass showed a tendency to increase over time until they broke down after 21 days (**d**). Again, there was very limited difference in mass when comparing different adhesive ligands for each concentration of collagenase at each time point.

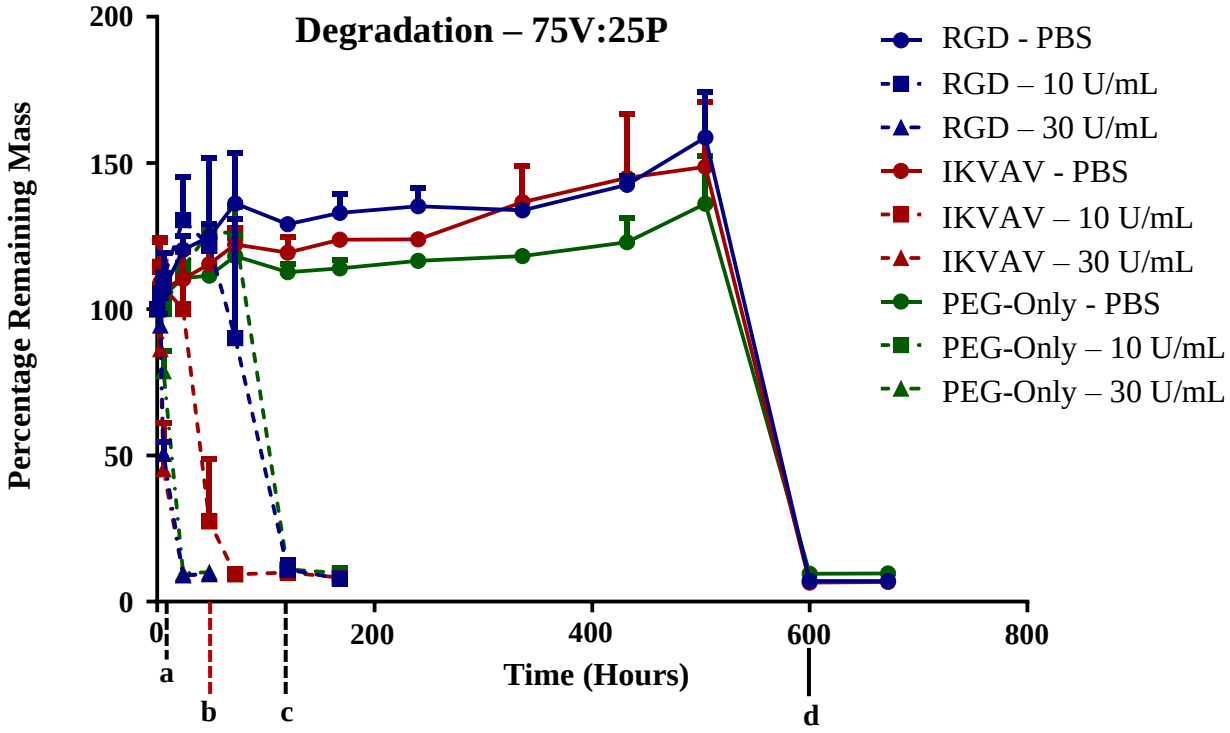

Figure 2.10 *Degradation of the 75V:25P gels. The trends for change in mass are similar for the 75V:25P gels compared to the 100V gels but at a slower rate. The higher concentrations of collagenase take slightly longer to break down each gel, but in PBS the gels are stable for significantly longer than the 100V gels, remaining intact for approximately 3 weeks. For each collagenase concentration, changing the adhesive ligand did not have a significant effect on the change in mass at any time point with exception of the IKVAV – 10 U/mL collagenase gels. Points* ***a-d*** *show the time points that the hydrogel mass was significantly different from the 0h mass for the gels in 30 U/mL collagenase (**a**, 6h), 10 U/mL collagenase IKVAV gels (**b**, 48h), the remaining 10 U/mL collagenase gels (**c**, 120h) and in PBS (**d**, 600h). Each data point represents mean percentage mass (n=3) + SD. Statistical significance was determined using 2 2-way ANOVAs to compare between groups and across time respectively, each with a Tukey post-hoc test.*

Increasing this further to 50V:50P dramatically changed the degradability as each gel only lost a small portion of mass in the initial days, beyond which they did not appreciably degrade any further for the remainder of the 8-week assay, even in the presence of collagenase (Figure 2.11). The only statistically significant differences noted were between the peptide bound gels and the PEG-Only gels in collagenase which did not initially lose mass as the others did.

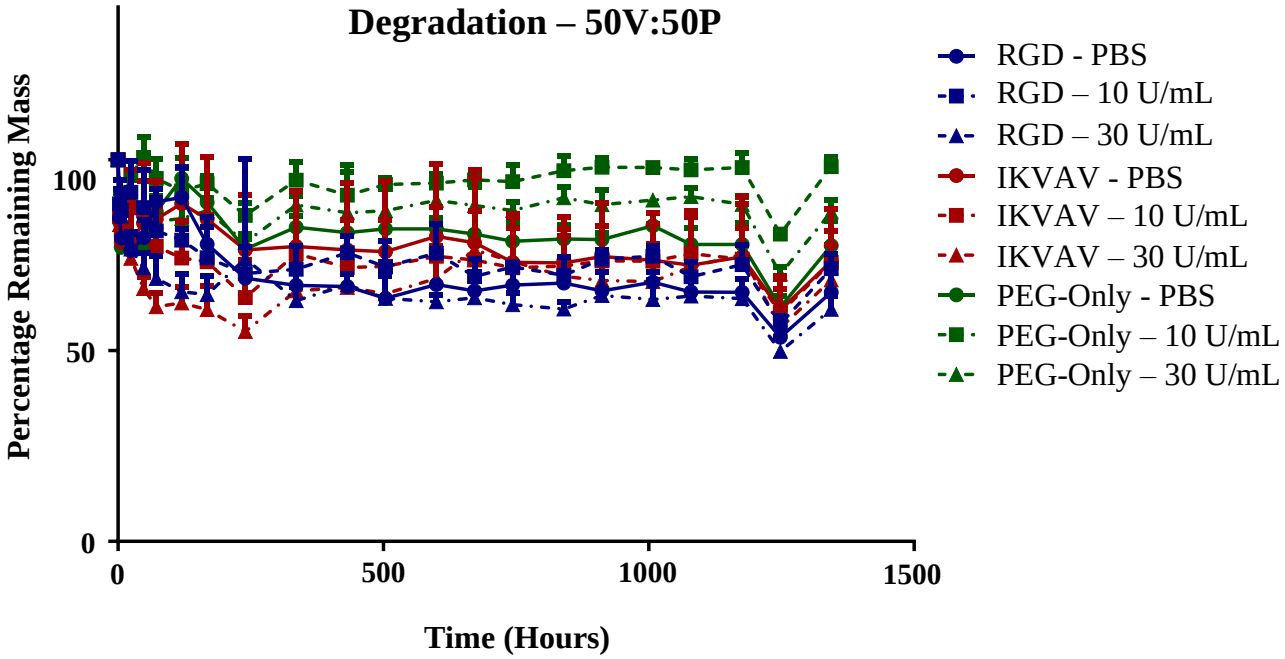

Figure 2.11 *Degradation of the 50V:50P gels. The 50V:50P gels showed a slight reduction in mass initially followed by stabilisation of the gel for the remained of the measurement period which ended after approximately 2 months. By this point it is expected that the VPM would be completely broken down and the gel structure is being maintained by the PEG-diSH alone. Following the initial drop in mass, after 3h the mass is not consistently significantly different from the mass at later time points for any of the measured conditions. The only gels that exhibited differences between adhesive ligands were the PEG-Only gels in collagenase which did not see the same initial drop in mass as other groups. Each data point represents mean percentage mass (n=3) + SD. Statistical significance was determined using 2 2-way ANOVAs to compare between groups and across time respectively, each with a Tukey post-hoc test.*

The 100P gels did not appear to lose any mass for the duration of the experiment irrespective of the solution they were immersed in (Figure 2.12). By the final time point, there was no statistically significant difference compared to the initial time point for any of the measured conditions, nor between each of the conditions.

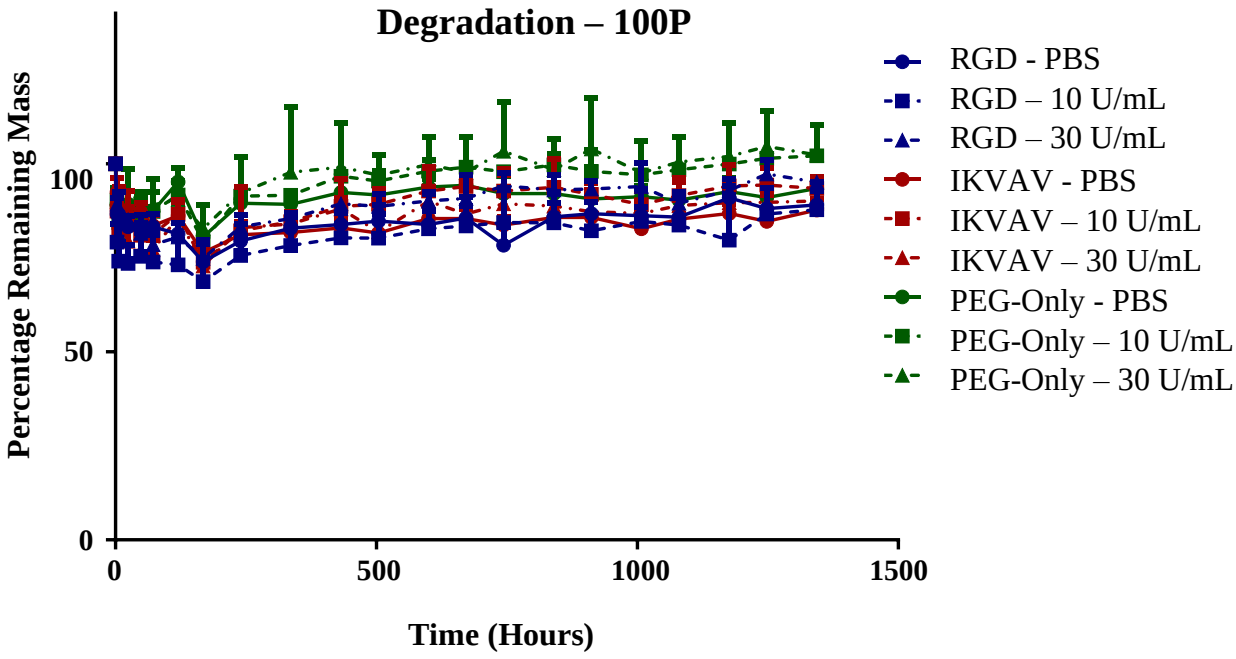

Figure 2.12 *Degradation of the 100P gels (Fully non-degradable cross-linker). The 100P gels showed no evidence of degradation over the full course of incubation irrespective of the concentration of collagenase used. There was a fluctuation in mass initially, however none of the gels had a mass significantly different at the final time point compared to 0h, and there was no significance difference between any of the ligands or collagenase concentrations. Each data point represents mean percentage mass (n=3) + SD. Statistical significance was determined using 2 2-way ANOVAs to compare between groups and across time respectively, each with a Tukey post-hoc test.*

2.3.3 Gelation Rate

The gelation rate is known to be highly dependent on the pH of the solution when the peptide-bound PEG-4MAL and cross-linkers are mixed (Fu and Kao, 2011). This can impose practical limitations on their use as very short or very long gelation times can make them difficult to work with. Each of the lyophilised peptides used, when dissolved, lowers the pH of the solution and slows the cross-linking of the hydrogel. The measured pH of each of the peptide stock solutions can be found in the Supplementary Table 2.1. Because of this, higher peptide content in the hydrogel will be associated with a reduced rate of gelation. The trend for gelation rate follows this rationale that increasing peptide content delays gelation by decreasing the pH (Figure 2.13).

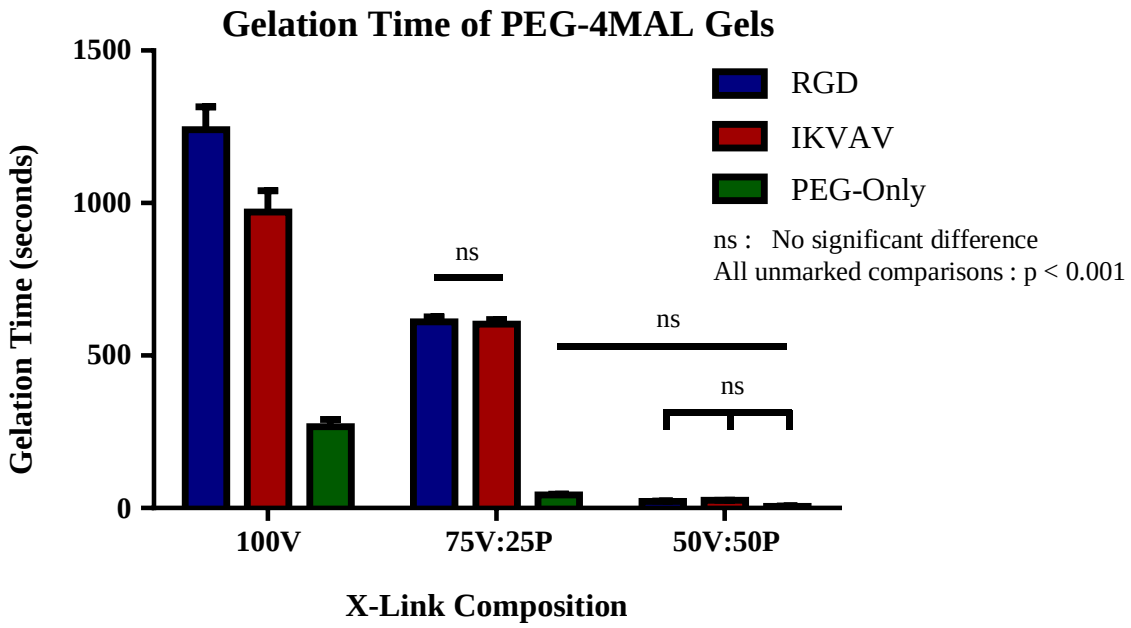

Figure 2.13 *Gelation time of PEG-4MAL gels with different ligands and cross-linker proportions. Significantly faster gelation rates are seen in gels with increasing VPM content which can be attributed to the lower pH with higher concentrations of VPM, delaying the reaction. The RGD and IKVAV peptides also reduce the pH when dissolved and there is a similar observed trend when comparing with the PEG-Only gels. Statistical significance was determined with a 2-way ANOVA using a Tukey post-hoc test. n=3, mean +SD.*

In the 100V gels the gelation times are significantly longer than the 75V:25P samples which are also significantly longer than the 50V:50P samples, which coincides with the reduction in VPM concentration and substitution for PEG-diSH. It is also evident that the PEG-Only gels solidify faster than the peptide bound gels. Reducing the pH of the buffer also had the same effect on gelation rate, with lower buffer pH again slowing the gelation reaction (Figure 2.14). Unaltered PBS with a pH of 7.4 had a gelation time of less than 30s for the 50V:50P gels which was significantly extended when the buffer pH was adjusted to 6, and even more so when reduced to 5. Finally, the temperature is also a known factor in influencing gelation rate(Matsumoto *et al.*, 2016) which is demonstrated here by increasing the temperature of the mixed gel components from ambient temperature (22°C) to 37°C which reduced the gelation time by approximately half for the RGD and IKVAV 100V gels (Figure 2.15).

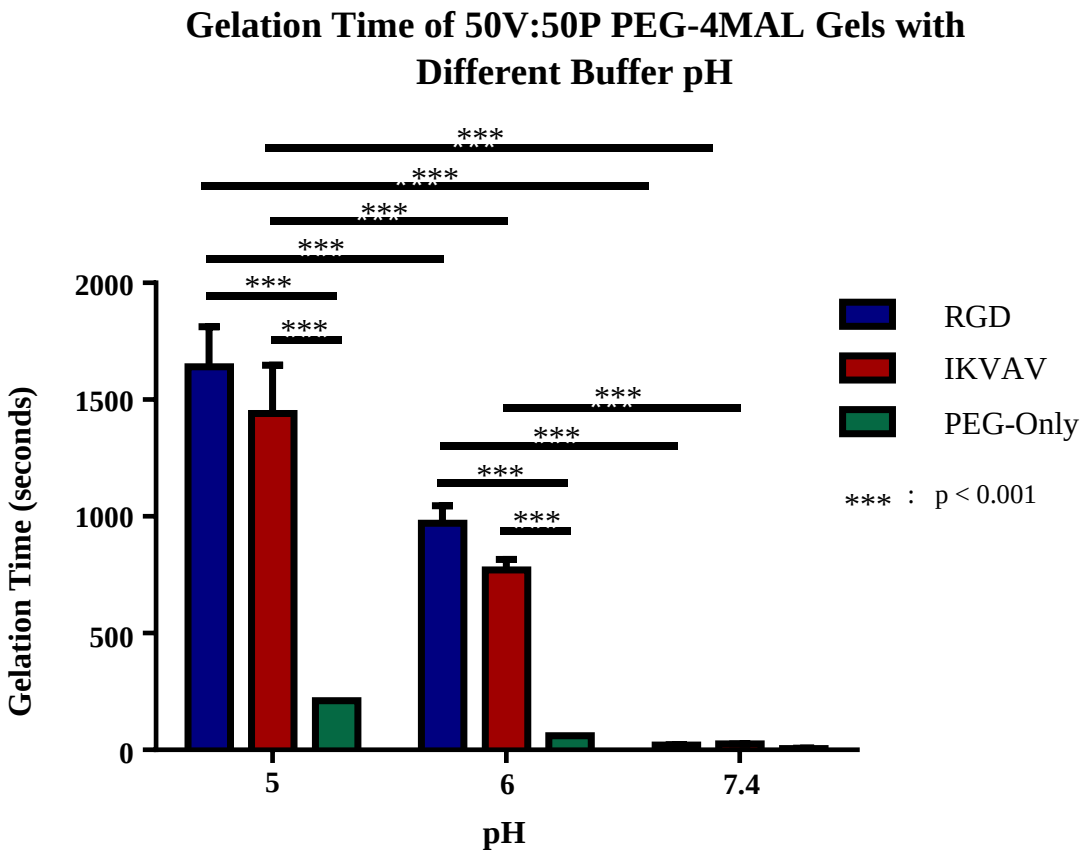

Figure 2.14 *Gelation rate of 50V:50P PEG-4MAL gels with reduced pH buffers. The gelation rate of the hydrogels is predominantly influenced by the pH of the gel after mixing. By lowering the buffer pH, the gelation is significantly prolonged. Statistical significance was determined with a 2-way ANOVA using a Tukey post-hoc test. n=3, mean +SD.*

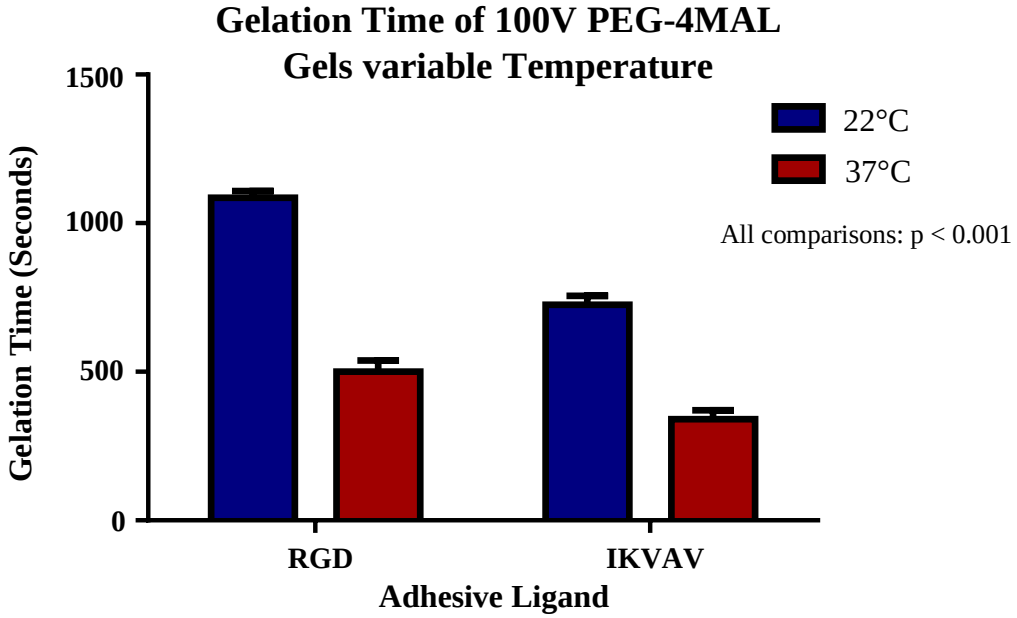

Figure 2.15 *Temperature effect on gelation of 100V PEG-4MAL gels. Temperature can influence the rate of reaction and hence the gelation of these gels. The gelation rate is approximately halved by transitioning from ambient temperature to 37°C. Statistical significance was determined with a 2-way ANOVA using a Tukey post-hoc test. n=3, mean +SD.*

2.3.4 Swelling Behaviour

Hydrogels are principally composed of water and only a small quantity of the material mass is accounted for by the polymeric structure. The degree to which the structure will absorb and retain water is highly dependent on the encapsulating network and can vary significantly between different gel compositions. As a candidate for an implantable material, this can have important implications as swollen gels can exert additional pressure on the local environment which can be particularly detrimental in delicate tissues such as the spinal cord. The hydrogel swelling ratio is significantly lower in the PEG-Only gels than IKVAV in all cases and RGD in the 50V:50P gels, which demonstrates a lower equilibrium level of water sorption in the PEG-Only gels (Figure 2.16). This is likely due to the increase in the number of dangling ends in the polymer structure of the peptide-functionalised gels caused by the binding of the mono-functional peptides to the maleimide groups that subsequently cannot engage in cross-linking mechanisms. Radi *et al.* described this phenomenon and demonstrated increased swelling in gels with higher proportions of dangling ends (Radi, Wellard and George, 2013). Between the different cross-linker ratios there is no significant difference when comparing each adhesive ligand. The swelling ratios are also predominantly similar between the RGD and IKVAV bound gels. The only group that group that saw differences between the RGD and IKVAV were the 100V gels, with the remaining groups being insignificant. The ratio of swollen to relaxed mass also follows similar patterns as the swelling ratio with the PEG-Only gels approximately doubling in mass and the peptide bound gels increasing 2.5-3.5 fold between formation and swelling to equilibrium (Figure 2.17).

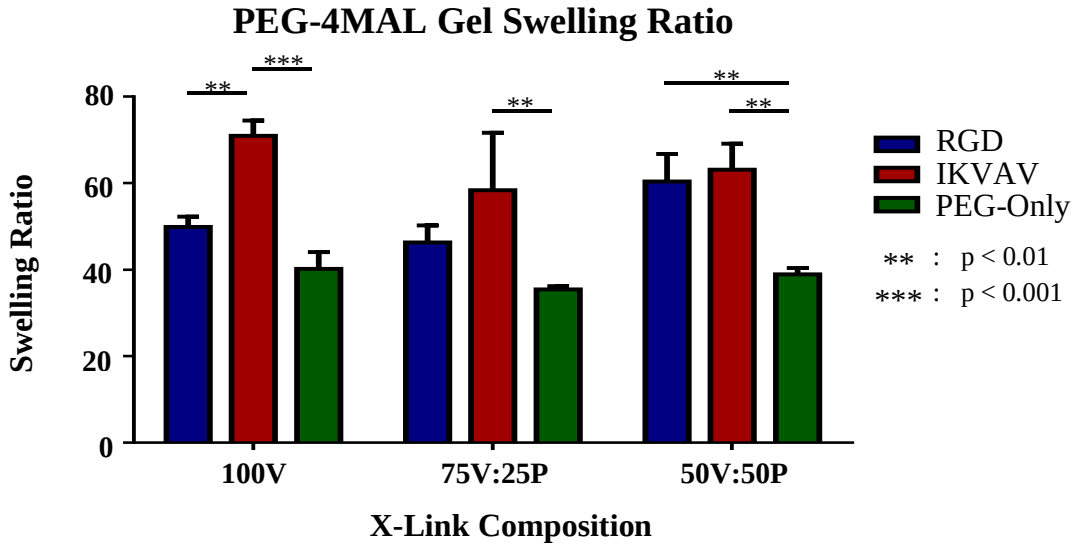

Figure 2.16 *Swelling Ratio of PEG-4MAL gels. The swelling ratio of the hydrogels is the ratio of swollen mass over dry mass. The peptide functionalised gels retain significantly more water than the PEG-only gels for each combination of cross-linker. Statistical significance was determined with a 2-way ANOVA using a Tukey post-hoc test. n=3, mean +SD.*

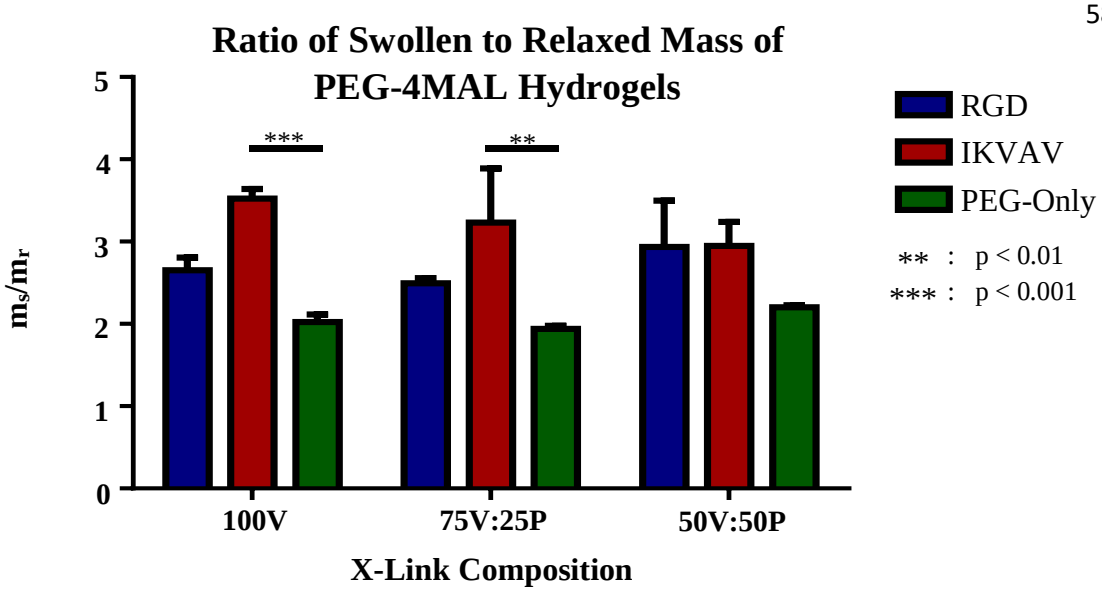

Figure 2.17 *Ratio of swollen (**m_s**) to relaxed (**m_r**) mass of PEG-4MAL gels. As each gel had a very similar relaxed mass, the notable trends in **m_s/m_r** follow those of the swelling ratio. PEG-Only gels swell approximately 2-fold to equilibrium while the peptide bound gels increase between approximately 2.5-3.5 times the relaxed mass. Statistical significance was determined with a 2-way ANOVA using a Tukey post-hoc test. n=3, mean +SD.*

The mesh sizes are derived from the swelling characteristics of the hydrogels and consequently display the same trends seen in the swelling ratio as the mesh size for the PEG-4MAL gels (Figure 2.18). The PEG-Only gels had the smallest mesh size around 15nm while the RGD and IKVAV gels were between 20 and 25nm.

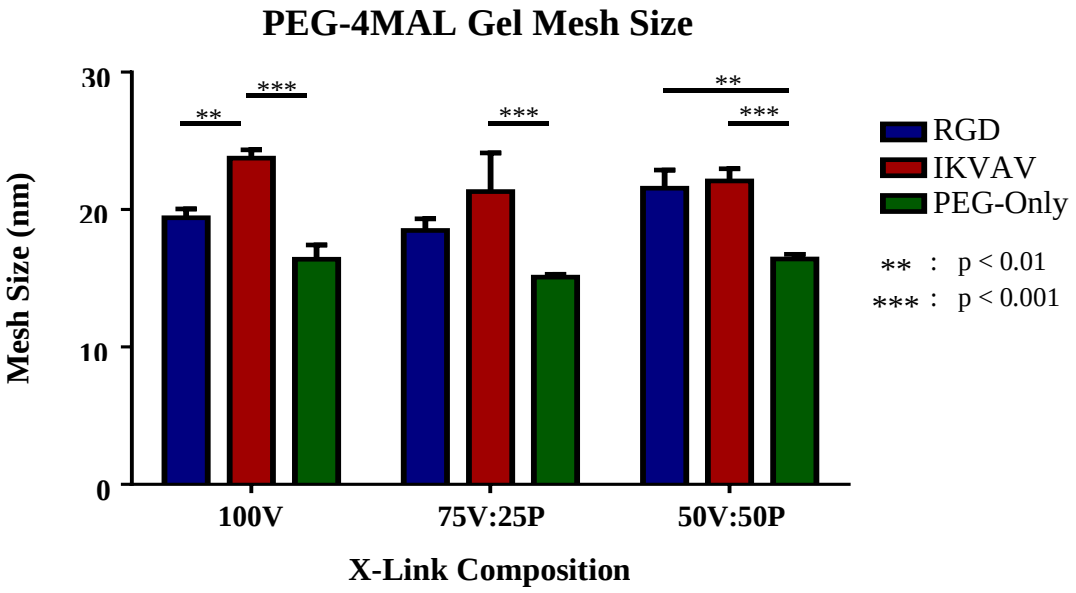

Figure 2.18 *Mesh size of the hydrogels. As the mesh size is directly linked to the swelling behaviour, the trends follow the same pattern. PEG-Only gels have mesh sizes of approximately 15nm while peptide bound gels range from 20-25nm. Statistical significance was determined with a 2-way ANOVA using a Tukey post-hoc test. n=3, mean +SD.*

2.3.5 Young's Modulus

The Young's modulus is a measure of how much a material can be deformed for a certain applied force. In tissue engineering this can define how cells interacting with the material can mobilise and migrate throughout the material and will also influence the cell behaviour through mechanotransduction (Paluch *et al.*, 2015). Matching the Young's modulus of the material to the native tissue of the cell type under investigation is a common approach as it more adequately replicates the mechanical cues that cells would receive *in vivo* (Khan and Tanaka, 2018). The mean Young's modulus of the hydrogels was lowest in the 100V gels giving a mean value of approximately 1 kPa for the peptide bound gels which is in close proximity to reported values of rat spinal cord tissue (T. Saxena *et al.*, 2012) (Figures 2.19). The peptide bound 75V:25P gels were not significantly higher, though the Young's moduli, rose significantly to 2kPa for the 50V:50P peptide bound gels, however there is an overlap in the standard deviation ranges of these data and ultimately the difference is small. For each cross-linker ratio there was an approximately 3-fold increase in the modulus for the PEG-Only gels compared to their peptide bound equivalents, though they still fall within the same order of magnitude. In these gels, the absence of peptides allows for the formation of a more densely cross-linked network as shown in Section 2.3.4, increasing the spatial restriction of the polymer chains and hence leading to a higher modulus.

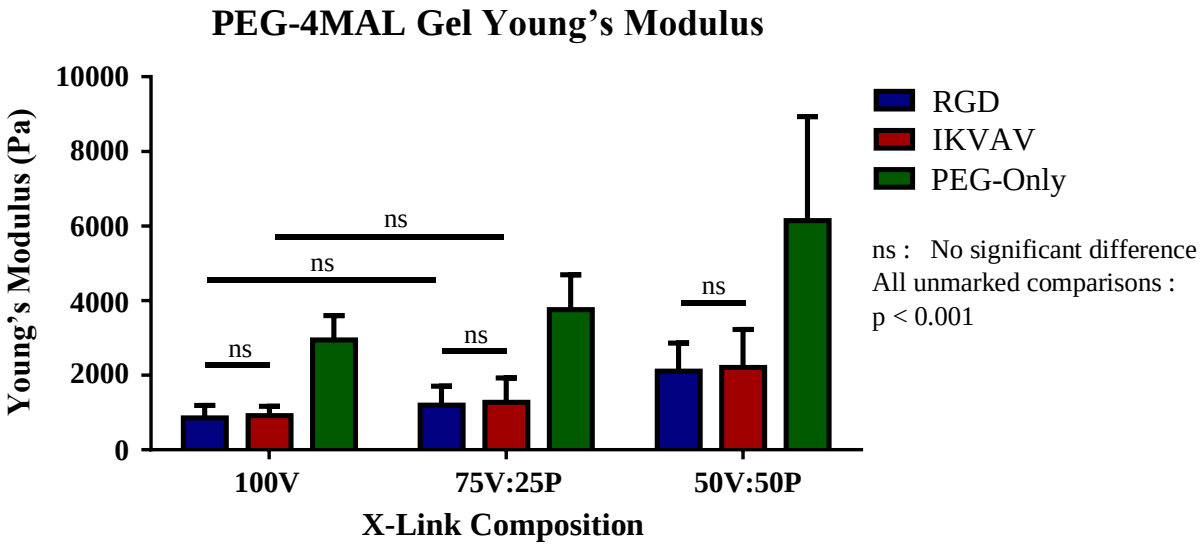

Figure 2.19 *Young's Modulus of PEG-4MAL gels. Increasing the proportion of PEG-diSH leads to a slight increase in the mean modulus, whereas the PEG-only gels have a modulus around 3 times that of the peptide bound counterparts. Statistical significance was determined with a 2-way ANOVA using a Tukey post-hoc test. 101 ≤ n ≤ 175 areas per condition, mean +SD.*

2.3.6 Growth Factor Release

The high water content of hydrogels gives them the capability to capture soluble agents within their network structure and release them by diffusion in target environments at a rate dependent on the capacity of the hydrogel to retain the solutes. Neurotrophins can be delivered using such systems and have the capability to promote neuronal growth which can enhance neuronal cultures *in vitro* or encourage regeneration *in vivo* (Bibel and Barde, 2000). To interpret the data for release of NGF and BDNF from the hydrogels the proportion of growth factor released is expressed as a percentage of the total growth factor released over the course of the experiment. In each case, there is a distinct plateau that marks a cessation of growth factor release from the gel. To qualify this interpretation, the 100V gels had fully degraded over the course of the assay in a manner consistent with the rates demonstrated in Section 2.3.2 and in doing so did not release any extra quantity of growth factor, indicating that all the growth factor initially present in the gel had been dispersed into the supernatant before degradation had occurred. As the release profile is consistent across each of the other gel types this assumption is held for the gels that had not fully degraded by the end time point. Figures 2.20 and 2.21 show that the neither NGF nor BDNF are retained for a significant duration, with both demonstrating release profiles that peak at the first time point before rapidly declining in all conditions.

The PEG-4MAL hydrogels demonstrated nearly instantaneous dispersion of growth factor by releasing the majority of their payload by the first time point, indicating that there is little preventing the diffusion of these molecules from within the hydrogels. To estimate the sizes of each growth factor, the tools available from the RCSB protein data bank were used to measure the span of the proteins at the widest axis which was in the region of ~6-6.5nm for both NGF (Wiesmann *et al.*, 1999; He and Garcia, 2004) and BDNF (Robinson *et al.*, 1999). When comparing with the mesh size of the hydrogels (Section 2.3.4) it is evident that the growth factors will not be spatially restricted from diffusion out of the gels due to the much larger mesh sizes. The polymer or peptides also are not known to have any binding affinity for the growth factors, and the release rates observed in this experiment are corroborated by this.

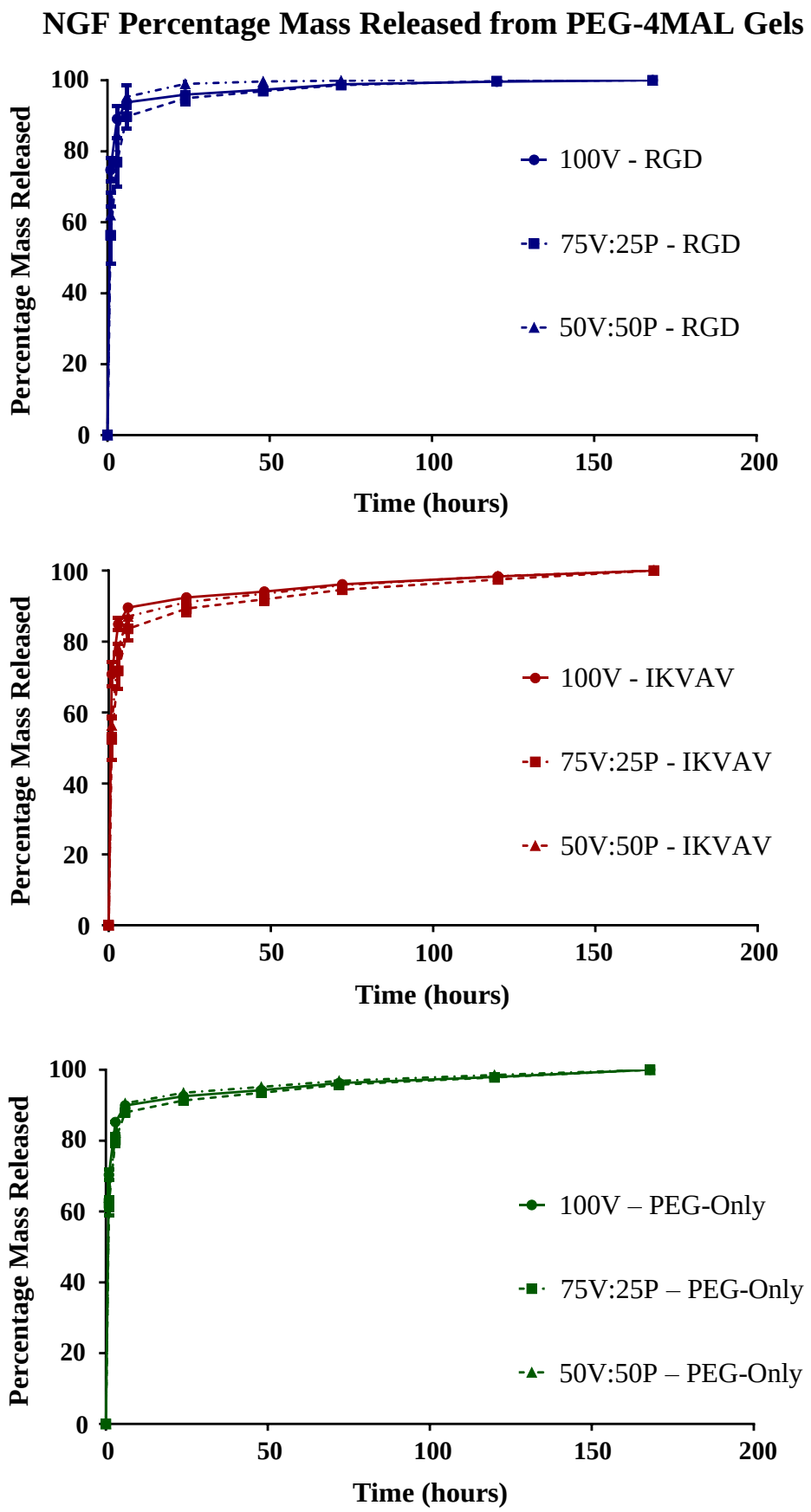

Figure 2.20 *NGF Release from PEG-4MAL gels. NGF release is comparable for all conditions, with the majority exiting the gel within the first hours of immersion in PBS and quickly reaching a plateau where no significant quantity of growth factor is being released.*

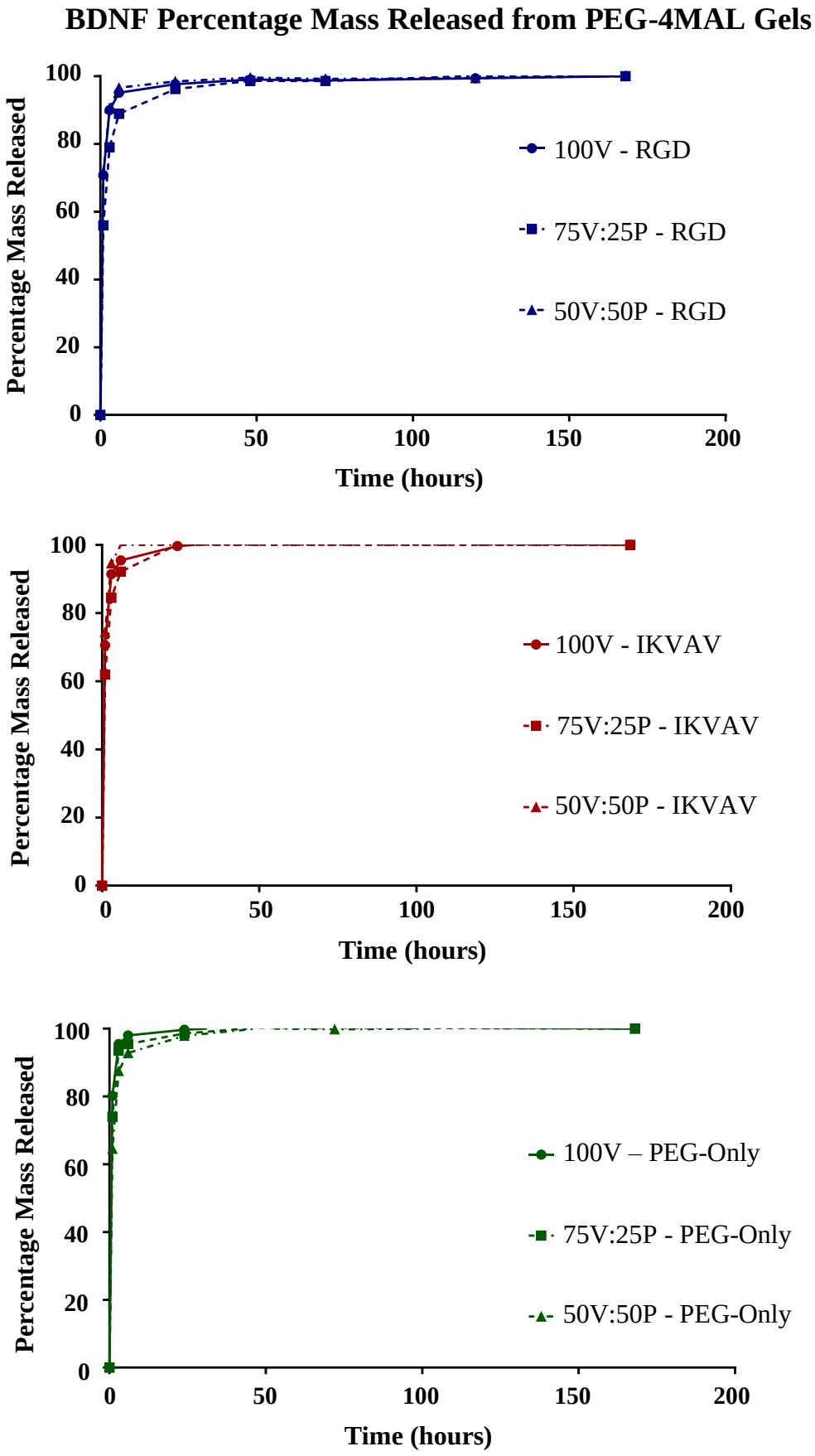

Figure 2.21 *BDNF Release from PEG-4MAL Gels. The same release pattern is observed for the BDNF as the NGF, with the majority of BDNF being released at the earliest time points.*

2.4 Discussion

The free thiol measurement assay successfully demonstrated a clear difference in free thiol content when peptides were in the presence of maleimide and without. However, the differences in baseline fluorescence between the RGD and IKVAV peptides suggest the system of measurement may be influenced by other factors beyond thiol content, though the proprietary nature of the fluorophore means that these factors can only be speculated upon. In trying to determine a possible reason for this discrepancy, the fluorescence intensity of the peptides was measured when dissolved in buffers of various pH. Using the same fluorophore, a notable dependence on pH was observed in the measured intensity particularly when the pH was high (Supplementary Figure 2.1). Even taking this into account however, at the concentrations used for the assay they were measured to be close to neutral and consequently this is unlikely to be a significant factor in the observed deviation. To improve upon the accuracy of these measurements, alternative methods for detection of the thiol-maleimide reaction could be used. Zustiak *et al.* (Zustiak, Durbal and Leach, 2010) used peptides modified with fluorophores and subsequently bound to PEG-vinyl sulfone prior to gelation to confirm the peptide tethering in the absence of a fluorescent signal in the gel supernatant. Baldwin and Kiick (Baldwin and Kiick, 2013) used NMR to confirm the formation of thiol-maleimide binding by observing the disappearance of protons from the respective groups simultaneously which can illustrate both peptide binding and the cross-linking reaction and as such would be a useful tool for this purpose.

The VPM peptide is known to be sensitive to degradation by collagenase as has been demonstrated in Section 2.3.2, however in these degradation studies the fully degradable 100V gels broke down in PBS after 5 days incubation which indicates that the peptide is vulnerable to breakdown through other means. Many studies have conducted similar experiments using collagenase to degrade VPM cross-linked hydrogels, however few if any have reported the long term degradability of these hydrogels in the absence of collagenase (Salimath *et al.*, 2012; L. Lin *et al.*, 2014; Foster *et al.*, 2017; Holyoak *et al.*, 2019). Currently it is unclear what this mechanism of degradation may be. The Michael-type addition can undergo the reverse process but this typically requires a high pH or the presence of high concentrations of free thiols (Zhang *et al.*, 2017), neither of which should is present in these gels. Hydrolytic degradation of PEG can also be discounted as the phenomenon is only seen in VPM bound gels. Subsequently in the absence of enzymatic activity it seems this alternative mechanism is enough to degrade the hydrogels, albeit at a slower rate.

The dangling ends in the polymer structure caused by the incorporation of peptides into the hydrogels can influence their behaviour in many regards. This is demonstrated by Kim *et al.* (Kim *et al.*, 2016) who investigated the effect of maleimide occupation with single cysteine amino acids in PEG-MAL hydrogels and with increasing concentration of blocked maleimides the swelling ratio of the hydrogels increased, gelation rate decreased and shear modulus also decreased. The differences observed between the peptide linked PEG-4MAL gels which would have a relatively high proportion of dangling ends compared to the PEG-Only gels presented in this chapter and are consistent with the findings of this study.

The Young's modulus of the hydrogels is fairly well conserved between the different cross-linker ratios although there are slight differences, unusually however these differences run contrary to expectations. It has been demonstrated that increasing the molecular weight should lead to a decrease in the material stiffness as a consequence of the wider mesh size and higher degree of swelling (Lee, Tong and Yang, 2014), however substituting the relatively small VPM peptide with the larger PEG-diSH cross-linker leads to a slight increase in the Young's modulus. The hydrogels were measured the day after formation and overnight swelling, so it is possible that the onset of degradation initiated a drop in the modulus over this time frame. If this were the case, gels with higher VPM content would degrade to a greater degree over the same time frame and the modulus would be lower than those with lower concentrations which would be in keeping with the observed data. This could be elucidated by measuring the gels at multiple time points to determine the extent of degradation and its influence on the hydrogel stiffness. This information would also be useful for anticipating possible changes in mechanical cues that would be available to resident cells over the course of degradation.

2.5 Conclusions

The hydrogels characterised in this chapter reveal several useful properties in the context of biomaterials for implantation that warrant further investigation into their biological properties. The degradability, when modified with the addition of degradable and non-degradable elements means it could potentially be used in different phases of regenerative support for short- and long-term applications. Due to the dynamic nature of cellular activity in the spinal cord after injury, particularly in the early stages, having the options of a material that can degrade after the sub-acute phase of injury or persist into the chronic phase could drastically alter the impact of the material. Additionally, the Young's modulus of the material matches closely to reported values of the native spinal cord tissue and should adequately mimic the elasticity of the extracellular environment. The option to tune the gelation time of the hydrogels could also be useful, for instance in cell encapsulation applications a rapid gelation reduces the time before media can be introduced which may improve their viability, or conversely a long gelation may be required for implantation in complex *in vivo* procedures. The rapid release of the growth factors from the hydrogels make them unsuitable for long term sustained release however they can still have the potential to be a delivery mechanism for a single dosage. Reducing the mesh size of the gels could be achievable by increasing the PEG-4MAL concentration or changing the cross-linker, but not without compromising the other favourable properties of the hydrogel.

3. In Vitro Analysis of Neurological Cells and Tissues in 3D PEG-4MAL Gel Culture

3.1 Introduction

Neurons are the primary functional unit of the healthy spinal cord and the regrowth of lost neuronal axons is critical to achieving functional recovery following spinal cord injury. However, the environment that is presented to neurons in the spinal cord after injury is inhospitable to axonal regrowth for a number of reasons, particularly in the later stages of injury progression. In order to encourage axonal regrowth, this environment needs to be modulated to overcome the regenerative barriers that arise after injury (Hyun and Kim, 2010; Führmann and Shoichet, 2018). To achieve axonal regrowth there are several possible approaches, many of which do not rely on targeting neurons directly. Cellular activity in the injured spinal cord is highly dynamic and there are several cell types resident in the CNS which can contribute to the matrix remodelling, establishing chemotactic gradients and a host of other regulatory functions which are necessary to promote axonal development. This regenerative activity can even be further enhanced by the introduction of transplantable populations of cells. This chapter details the *in vitro* analyses of several cell types that have been implicated in SCI recovery, which are cultured in PEG-4MAL based hydrogels. These investigations aimed to determine which of the hydrogel formulations described in the previous chapter provide a substrate capable of sustaining healthy cell populations in 3D, and additionally evaluate the extent to which the cells can interact with the material through changes in morphology and distributions.

The role of astrocytes in spinal cord injury has sparked controversy and is not fully understood as their effects are multifactorial and depend on both the phase of injury and cellular phenotype (Nathan and Li, 2017). Previously the association of astrocytes with the formation and maintenance of the glial scar had characterised them as detrimental to SCI recovery but recent research suggests that in their absence, tissue deterioration following injury is exacerbated (Anderson *et al.*, 2016; Adams and Gallo, 2018). They are known to shape the course of neuronal growth both through deposition of matrix components (Powell *et al.*, 1997; Powell and Geller, 1999) and through secretion of growth factors (Yoshida and Gage, 1991). Consequently, therapeutic approaches that facilitate the reorganisation of astrocytes may also provide an avenue for neuronal guidance through the injured spinal cord (East *et al.*, 2010). In healthy tissue the astrocyte network is interwoven with neurons, capillaries and other glia and their typical branching stellate morphology allows them to interface across several intercellular junctions simultaneously (Filous and Silver, 2016).

Therefore, a functional material that can preserve this branching morphology is therefore likely to be beneficial in the context of spinal cord injury.

Spinal cord neurons are capable of growing axons that can extend over distances that are orders of magnitude larger than the cell soma. Multipolar neurons such as those found in the CNS will also possess many much shorter dendrites which enable intercellular communication over shorter distances (Van Der Want *et al.*, 1998). In SCI, axotomised neurons are often capable of stabilising and re-growing their axons to an extent but predominantly fall short of penetrating through the region of injury. Part of the problem is the lack of an appropriate substrate on which axonal development can occur, but biomaterials can be used to resume this function. If re-innervation of denervated regions is to ultimately be achieved, implanted materials must therefore be able to enable the formation and growth of axons.

Dorsal root ganglia are cellular clusters of the peripheral nervous system that are situated at the boundary between the PNS and CNS. As well as housing large quantities of Schwann cells along with glial satellite cells and macrophages, the DRGs contain a dense population of primary afferent neuronal cell bodies (Krames, 2014). As such, DRGs can be cultured as tissue explants which makes them useful for studying neuronal interactions with biomaterials. Though they are not directly analogous to spinal cord tissue, DRGs can be more informative than monocultures due to the multitude of cell interactions taking place. Outgrowth of neurites from DRGs in contact with homogenous materials is typically observed omni-directionally from the explant and is dependent on the trophic and physical cues provided (Yao *et al.*, 2016; Le *et al.*, 2018). Ideally the material can take advantage of several mechanisms to encourage a greater degree of neuronal growth.

Mesenchymal stem cells (MSCs) are multipotent and are able to differentiate into several cell types along the mesoderm lineage. They are commonly used in implantation therapies with the aim to repopulate tissue defects by differentiating into cell types native to the target tissue such as bone or cartilage, though they can also perform other roles (Richardson *et al.*, 2016; Yousefi *et al.*, 2016; Kong *et al.*, 2017). There is a body of research that suggests MSCs can differentiate directly into neural tissues (Dezawa *et al.*, 2004; Taran *et al.*, 2014; Takeda and Xu, 2015; Rao *et al.*, 2016) but this remains under heavy scrutiny (Scuteri *et al.*, 2010; Huda *et al.*, 2016; Luo *et al.*, 2018). In spinal cord injury, MSCs have been implemented as they are able to secrete several growth factors that can encourage the regrowth of neurons and otherwise favourably modulate the wound environment (Hofer and

Tuan, 2016). Hydrogels can also be used as vehicles for transplantation however in order to do so, the minimum material requirements are to maintain high levels of cell viability. Additional benefit can be gained if the cells are able to attach to the material and retain an adherent phenotype which can allow migration, enabling the cells to exit the material and permeate the transplant site.

In this chapter, MSCs, astrocytes, DRGs and spinal cord neurons are cultured in 3D PEG-4MAL hydrogels to certify that viable populations can be maintained and to identify differences in cell morphology and regrowth in gels modified with RGD, IKVAV or no ligand, and different ratios of degradable:non-degradable cross-linkers. Quantification of neurite length and density was also performed for spinal cord neurons, as was outgrowth from the DRGs to assess their ability to promote growth of neural cell types.

3.2 Materials & Methods

MSCs, astrocytes, DRGs and spinal cord neurons were each cultured in 3D PEG-4MAL based gel assays using 5% wt/vol PEG-4MAL tethered with RGD, IKVAV or no ligand and cross-linked with either 75V:25P or 50V:50P cross-linker ratios. . The 100V gels were omitted as these gels were fully degraded by the end of the 7-day culture and no data could be collected. Each formulation of hydrogel was evaluated for the capability to provide a cell responsive environment which was assessed by the adoption morphological features that are characteristic of each cell type analysed. Table 3.1 includes the composition of all the culture media formulations used in the subsequent experiments.

Table 3.1 *List of all culture media compositions used for cell and tissue gel cultures.*

hMSCs *MSC Expansion Media*	Mesenchymal Stem Cell Growth Medium 2 (C-28009, Promocell, Germany) + 1% penicillin/streptomycin (P0781, Sigma, UK)
hMSCs *MSC Culture Media*	DMEM + 4.5 g/L glucose (D5671, Sigma, UK), + 1mM sodium pyruvate (S8636, Sigma, UK) + 1.2 mM L-Glutamine (G7513, Sigma, UK) + 1x Non-Essential Amino Acids (11140035, ThermoFisher, UK) + 0.4% penicillin/streptomycin + 0.125 µg/mL fungizone (15290-026, ThermoFisher, UK)
Astrocytes *Astrocyte Culture Media*	DMEM + 1g/L glucose + pyruvate + glutaMAX (21885-025, ThermoFisher, UK), + 1 % penicillin/streptomycin + 10% foetal bovine serum (FBS)
Spinal Cord Neurons *Neuronal Culture Media*	Neurobasal Media (21103049, ThermoFisher, UK) + 1x B27 Plus Supplement (A3582801, ThermoFisher, UK) + 2mM GlutaMAX (35050-061, ThermoFisher, UK) + 10µg/mL gentamicin (15710-064, ThermoFisher)
Dorsal Root Ganglia *DRG Culture Media*	Neurobasal Media + 1% B27 Plus Supplement + 2mM GlutaMAX + 10µg/mL gentamicin + 10% Horse Serum (ThermoFisher, UK)

3.2.1 Mesenchymal Stem Cells

It is critical that the PEG-4MAL hydrogels can permit cell survival and growth to be suitable for spinal cord implantation. Cell viability assays and morphological analyses of human mesenchymal stem cells (hMSCs, C-12975, Promocell, Germany) were conducted after culturing for 7 days within 75V:25P and 50V:50P gels with RGD, IKVAV or PEG-Only, along with Matrigel (Growth Factor Reduced, 354230, Corning, USA), which is often used in biomaterial studies, as a positive control (S. Dai *et al.*, 2016; Grabowska *et al.*, 2019).

3.2.1.1 Culture Protocol

Each gel was formed as previously described (Section 2.2.1.3) in a 48-well plate along with matrigel controls and allowed to swell to equilibrium overnight at 37°C. The matrigel positive control gels were made by pipetting 30μL of refrigerated liquid matrigel into the 48-well plate and incubating for 30 minutes at 37°C until solidification had occurred. Passage 5 hMSCs were cultured in T75 flasks until confluence in MSC expansion media (See Table 3.1). The cells were trypsinised until detached from the plate and centrifuged for 5 minutes at 1000rpm to form a pellet. The cells were then re-suspended in MSC Culture Media (See Table 3.1) and counted with a haemocytometer. The cell density was adjusted to $2.5x10^6$ cells/mL and 6μL of the suspension was seeded into each gel by inserting the pipette tip within the formed gel and ejecting the suspension into the gel interior, with a resultant density of 15000 cells per gel. 0.5mL MSC Culture Media was then added to each well which was replaced every 2 days for 7 days.

3.2.1.2 Live/Dead Assay

A viability stain was applied using a LIVE/DEAD™ Viability/Cytotoxicity Kit (L3224, ThermoFisher, UK) by adding 2mM Calcein AM which causes living cells to become fluorescent green and 4mM ethidium homodimer which stains dead cells fluorescent red, both dissolved in PBS. These were incubated for 30 minutes at 37°C before imaging each sample with an EVOS microscope (EVOS FL Auto) using the accompanying software. Z-stacks were taken of each gel at 20μm intervals between the uppermost and lowest visible cells which were analysed using ImageJ (Schneider, Rasband and Eliceiri, 2012) image processing software by compressing the stack into a single plane and counting the number of live and dead cells and calculating the percentage of total living cells. Statistical analysis was performed using a 2-way ANOVA with a Tukey post-hoc test.

3.2.1.3 Actin Staining

The cells were fixed in 4% formaldehyde/PBS for 30 minutes before washing 3 times in PBS for 10 minutes each. Cells were permeabilised using a 0.1% Triton-X 100 (Sigma, UK) permeabilising buffer, incubating for 20 minutes at room temperature before rinsing again with PBS. The cells were then stained for actin with rhodamine phalloidin (R415, ThermoFisher, UK) using 0.3mL at a dilution of 1:100 and NucBlue (R37605, ThermoFisher, UK) for nuclei using 2 drops/mL and incubating for 1 hour before rinsing 3 times and storing in PBS. Images were captured using an EVOS microscope to create Z-stacks at 20μm intervals between the uppermost and lowest visible cells. The images were adjusted for brightness and contrast, background fluorescence was subtracted and the stacks were projected into a single plane with a max intensity Z-projection using ImageJ (Schneider, Rasband and Eliceiri, 2012).

3.2.2 Astrocytes

3.2.2.1 Culture Protocol

Cortical astrocytes were harvested from neonatal rats (P1, Sprague Dawley) by Dr. Susan Lindsay (Institute of Infection, Immunity & Inflammation, University of Glasgow) which were donated and cultured in the hydrogels within 1 week of dissection after the astrocytes had reached near-confluency. Cortices were extracted from the neonatal rats and digested in 1.33% type-1 collagenase, then disassociated by trituration before plating in a T75 flask in Astrocyte Culture Media (See Table 3.1) 75V:25P and 50V:50P gels were prepared as described in Section 2.2.1.3 but withholding 12μL of PBS per gel from the gel components to allow for the cell suspension to be added during formation. The cells were trypsinised to dissociate them from the plate and centrifuged for 5 minutes at 1000rpm to form a pellet before re-suspending in DMEM and counted with a haemocytometer. The cell density was adjusted to 10^7 cells/mL and 12μL of this was added to the PEG and cross-linker to form 30μL gels with a density of $1.2x10^5$ cells per gel in a 48 well-plate and allowed approximately 20 minutes to solidify before 0.5mL astrocyte culture media was then added to each well. A matrigel control was prepared by adding 12μL of cell suspension to 18μL of matrigel and incubating for 30 minutes in an incubator before adding 0.5mL of astrocyte culture media to the wells. The media in each well was replaced every 2 days for 7 days.

3.2.2.2 Fluorescent Staining

The cells were fixed using 4% formaldehyde/PBS for 30 minutes before washing 3 times in PBS for 10 minutes each. Cells were permeabilised using a 0.1% Triton-X 100 permeabilising buffer, incubating for 20 minutes at room temperature before rinsing again with PBS. The cells were then blocked for non-specific binding by immersing the samples in a blocking buffer containing 1% bovine serum albumin (BSA, Sigma, UK) in PBS for 1 hour. A primary antibody solution was prepared in blocking buffer using rabbit anti-GFAP antibody (ab116010, Abcam, UK) at a dilution of 1:100 which was added to each sample and stored refrigerated overnight. The primary antibodies were rinsed 3 times with 0.5% tween 20 (Sigma, UK) before adding the secondary antibody goat anti-rabbit Cy3 (111-165-003, Jackson, USA) at a dilution of 1:200 in blocking buffer and Alexa 488 phalloidin (A12379, ThermoFisher, UK) at 1:100 for a further 2 hours at room temperature. These were again rinsed in 0.5% tween 20 before adding 0.5mL PBS with NucBlue (2 drops/mL) to each well for storage. Images were captured using an EVOS microscope to create Z-stacks at 20μm intervals between the uppermost and lowest visible cells. The images were adjusted for brightness and contrast, background fluorescence was subtracted and the stacks were projected into a single plane with a max intensity Z-projection using ImageJ.

3.2.3 Mixed Spinal Cord Culture

3.2.3.1 Culture Protocol

75V:25P and 50V:50P gels along with matrigel were formed into 48 well plates and swollen overnight in PBS as described in Section 3.2.1.1. Additional 50V:50P gels were formed and immersed overnight in 0.5mL 500ng/mL β-NGF (256-GF, R&D Systems, UK) or 0.5mL 500ng/mL of BDNF (248-BDB, R&D Systems, UK). The harvesting of spinal cord neurons was performed by Dr. Susan Lindsay and donated in the form of a cell suspension after processing. Spinal cords from rat embryos (E15, Sprague Dawley) were obtained by dissecting and removing the external tissues surrounding the cord then removing the meninges. Several cords were collected in L-15 media (ThermoFisher, UK) and triturated to disassemble the tissue before incubation with collagenase (ThermoFisher, UK) and trypsin (Sigma Aldrich, UK) for 15 minutes to liberate the cells from the extracellular matrix. The reaction was inhibited by soybean trypsin inhibitor (Sigma Aldrich, UK) with DNAse (Sigma Aldrich, UK) and triturated again for complete cellular dissociation. The cells were centrifuged at 800 rpm for 5 minutes to form a pellet which was resuspended and counted

before the concentration was adjusted to $2x10^4$ cells per mL. The immersing supernatant was removed from the gel well-plates and 6µL of the cell suspension was implanted into each gel by pipette to give a gel cell density of $1.2x10^5$ cells per gel. 0.5mL of neuronal culture media (See Table 3.1) was added to each well which was refreshed every 2 days for 7 days by removing 0.25mL and adding the same volume of fresh media.

3.2.3.2 Immunostaining

The neuronal staining and imaging protocols were conducted in the same manner as the astrocyte staining described in Section 3.1.2.2 but with neuron specific antibody combinations. The primary antibody used was mouse anti-β3-tubulin (ab78078, Abcam, UK) at a 1:1000 dilution and this was bound with donkey anti-mouse Alexa 488 (A21202, ThermoFisher, UK) at 1:200.

3.2.3.3 Analysis

The neuronal clusters that formed within the gels during the 7-day cultures were analysed for the mean neurite length per cluster and the neurite density around the perimeter of the clusters. Neurite length was quantified using the neurite tracing plugin NeuronJ (Meijering *et al.*, 2004) by normalising the image contrast and generating a max intensity z-projection of each stack and selecting a minimum of 10 clusters per condition. Each neurite emanating from the clusters was traced from the cluster periphery to the neurite termination point and the mean neurite length for each cluster was calculated (Figure 3.1). From this the mean total neurite growth per cluster was also calculated. Neurite density was analysed by marking a 60µm boundary around 4 orthogonal edges of 10 clusters per condition, counting each neurite across 4 frames of the z-stack (20µm intervals) equating to a 60x60 μm^2 area and the mean count of each area was calculated (Figure 3.2). Statistical analysis was performed with a 2-way ANOVA using a Tukey post-hoc test.

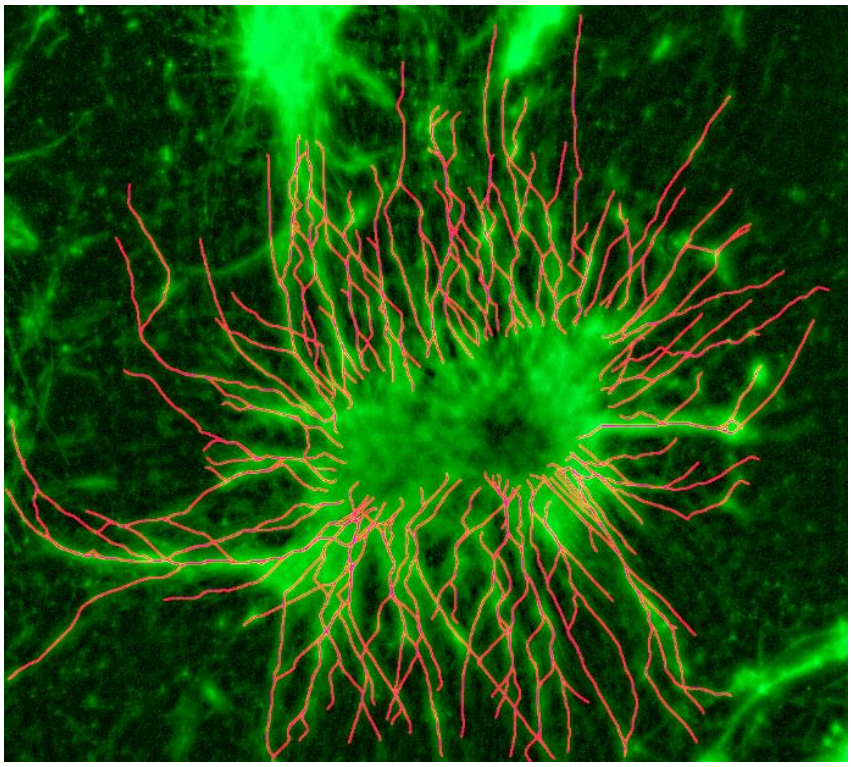

Figure 3.1 *Tracing of neurites from neuronal clusters cultured in PEG-4MAL hydrogels. Each neurite is traced semi-automatically using the ImageJ plugin NeuronJ* (Meijering *et al.*, 2004) *and the mean neurite length for each cluster was calculated.*

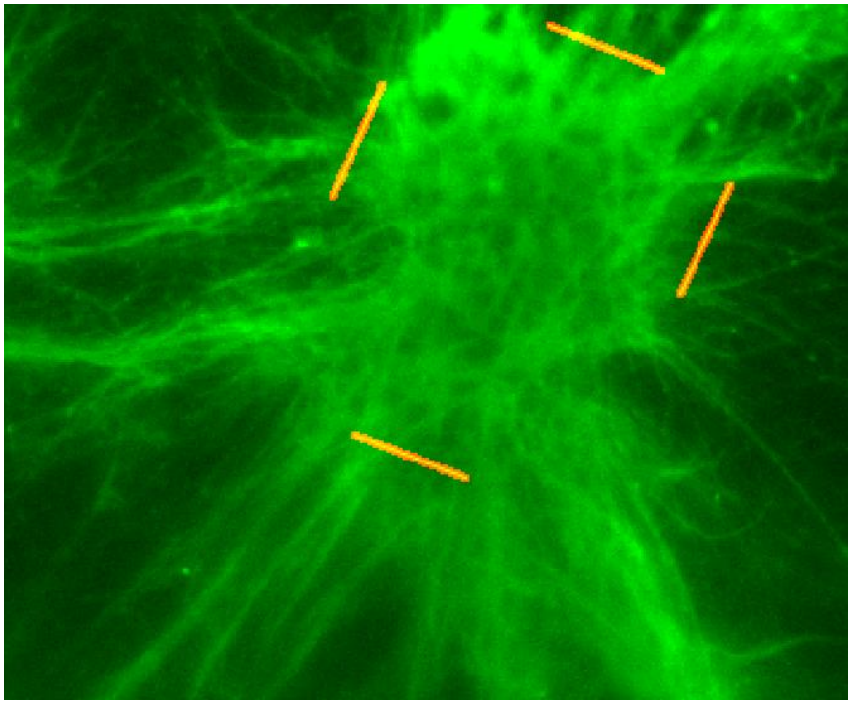

Figure 3.2 *Neurite density counting from neuronal clusters cultured in PEG-4MAL hydrogels. 60µm borders were drawn around orthogonal edges of each neurite cluster and the number of neurites crossing the border was counted across 4 frames of the z-stack, (equivalent to 60µm in the z-axis) totalling a 60x60 µm^{2}area.*

3.2.4 Dorsal Root Ganglia

3.2.4.1 DRG Extraction

Dorsal root ganglia were isolated from neonatal rats (P1, Sprague Dawley) firstly by dissecting the spinal column then debriding and incising the dorsal surface. The spinal cord tissue within the column was excised to reveal the dorsal root ganglia which could be extracted from the intervertebral foramina and collected in L-15 media. The roots were removed from each DRG before implantation into the hydrogels.

3.2.4.2 Culture Protocol

75V:25P and 50V:50P gels along with Matrigel were formed into 48 well plates and swollen overnight in PBS as described in Section 3.2.1.1. Additional 50V:50P gels were formed and immersed overnight in 0.5mL 500ng/mL NGF or 0.5mL of BDNF. In each sample, a single DRG was placed within the gel by grasping with fine tweezers and inserting into the gel interior. Each sample was flooded with 0.5mL of DRG culture media (See Table 3.1) which was refreshed every 2 days for 7 days by replacing half of the media volume with new media (Repic *et al.*, 2016).

3.2.4.3 Immunostaining

The immunostaining and imaging protocols were followed as described in Section 3.2.2.2 using the same neuronal antibodies as described in Section 3.2.3.2

3.2.4.4 Analysis

Cellular growth from the DRGs was quantified by measuring the proportion of the perimeter from which cellular outgrowth could be seen projecting from the DRG surface in brightfield images. The perimeter length of each DRG (n = 6 per condition) was traced using ImageJ, as was the length of the perimeter from which outgrowth could be seen and the percentage of the area with growth was calculated (Figure 3.3).

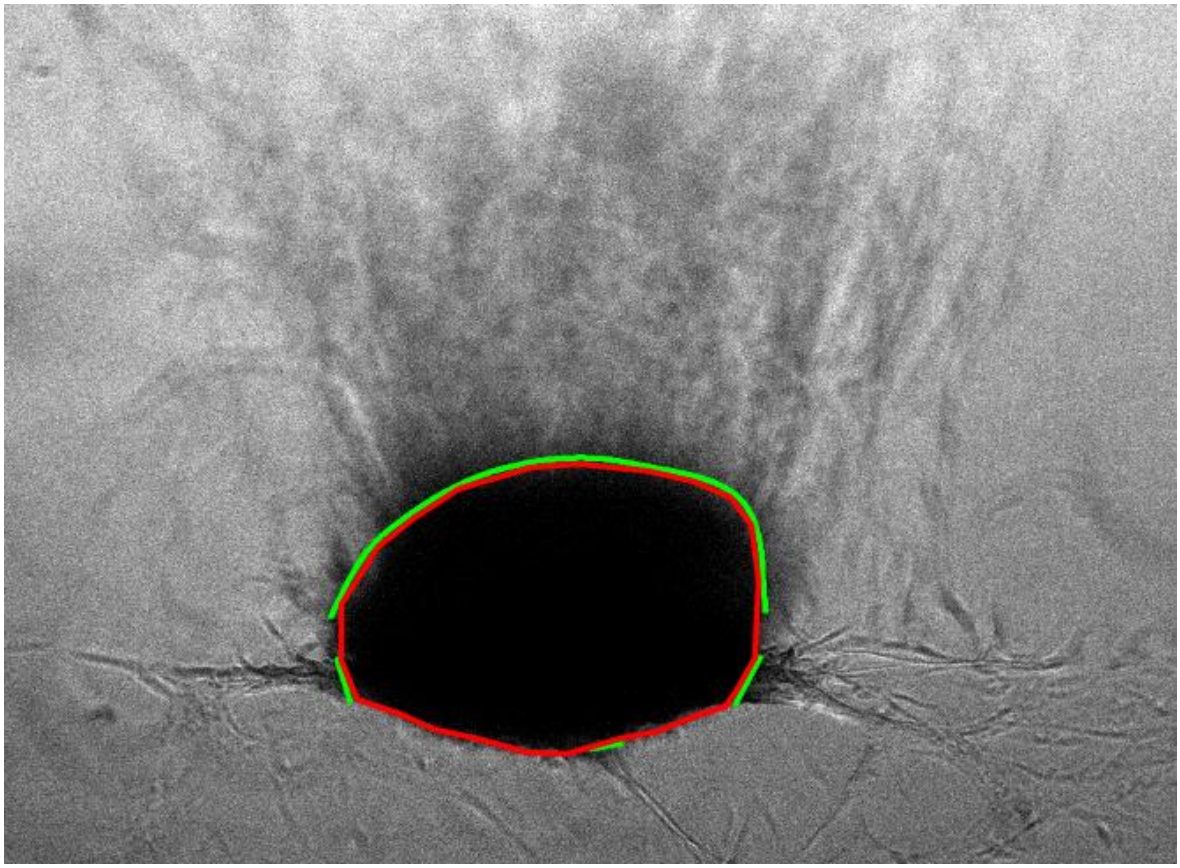

Figure 3.3 *DRG perimeter growth. The area around each DRG is traced (shown in red) and the area of growth is also quantified (shown in green), allowing the proportion of growth to total perimeter length to be calculated.*

3.3 Results

3.3.1 Mesenchymal Stem Cells

3.3.1.1 Live/Dead

The MSCs cultured in the RGD gels were able to maintain high levels of viability after 7 days for both the 75V:25P and 50V:50P gels at approximately 90%, which is comparable to the matrigel positive control and hence demonstrating that the gels are providing adequate support to maintain a viable population (Figure 3.4 & 3.6). In contrast, the IKVAV and PEG-Only gels only sustained viability at around 70% which was significantly lower than the RGD or matrigel. There was no statistical difference between IKVAV and PEG-Only gels indicating the IKVAV is not providing a notable benefit to the viability of the MSCs over the gels with no integrin recognisable sequences. There is no statistical difference between the 75V:25P and 50V:50P gels for any of the ligands used demonstrating that the difference in cross-linker ratio is not affecting the relative viability. The absolute number of cells counted is displayed in Figure 3.5 and the trend of low cell numbers with low percentage viability mostly holds true with the exception of the 50V:50P RGD gels. It should be noted however that the sample variation is relatively high and the standard deviation ranges overlap between many of the groups, particularly with the 50V:50P RGD gels. The distribution of cells within the gels was somewhat heterogeneous and so the variation between image fields is similarly variable and the interpretation of these data should take this into account.

3.3.1.2 Morphology

The trends captured in the MSC viability data (Figure 3.4) are visibly evident when observing their morphology (Figure 3.7). In the RGD gels the MSCs are extending projections throughout the gel and adopting a spindle-like morphology. The majority of the cells are maintaining contact with other cells while adjusting their distribution to position the nuclei relatively evenly along the numerous strands. It is clear that the MSCs are using the gel as a platform for adhesion and reorganisation. This is not the case in the IKVAV or PEG-Only gels as there is very little indication of process formation. The MSCs have instead adopted small clustered formations that exist in isolation from other clusters. The nuclei are densely packed suggesting that the cells are forming intercellular contacts but are not interacting strongly with the material. The congregation of the cells into clusters following

their original dispersion after seeding indicates that they are granted a limited degree of mobility, but beyond this there is no evidence that the cells are indeed binding to the IKVAV as the appearance is similar to the gels with no peptides. The behaviour of the MSCs is again mirrored with the 75V:25P and 50V:50P gels with their respective peptides indicating no substantial impact as a consequence of altering the cross-linker ratios at these proportions. This is at least true for shorter scale studies, but differences could emerge as the more degradable gels break down.

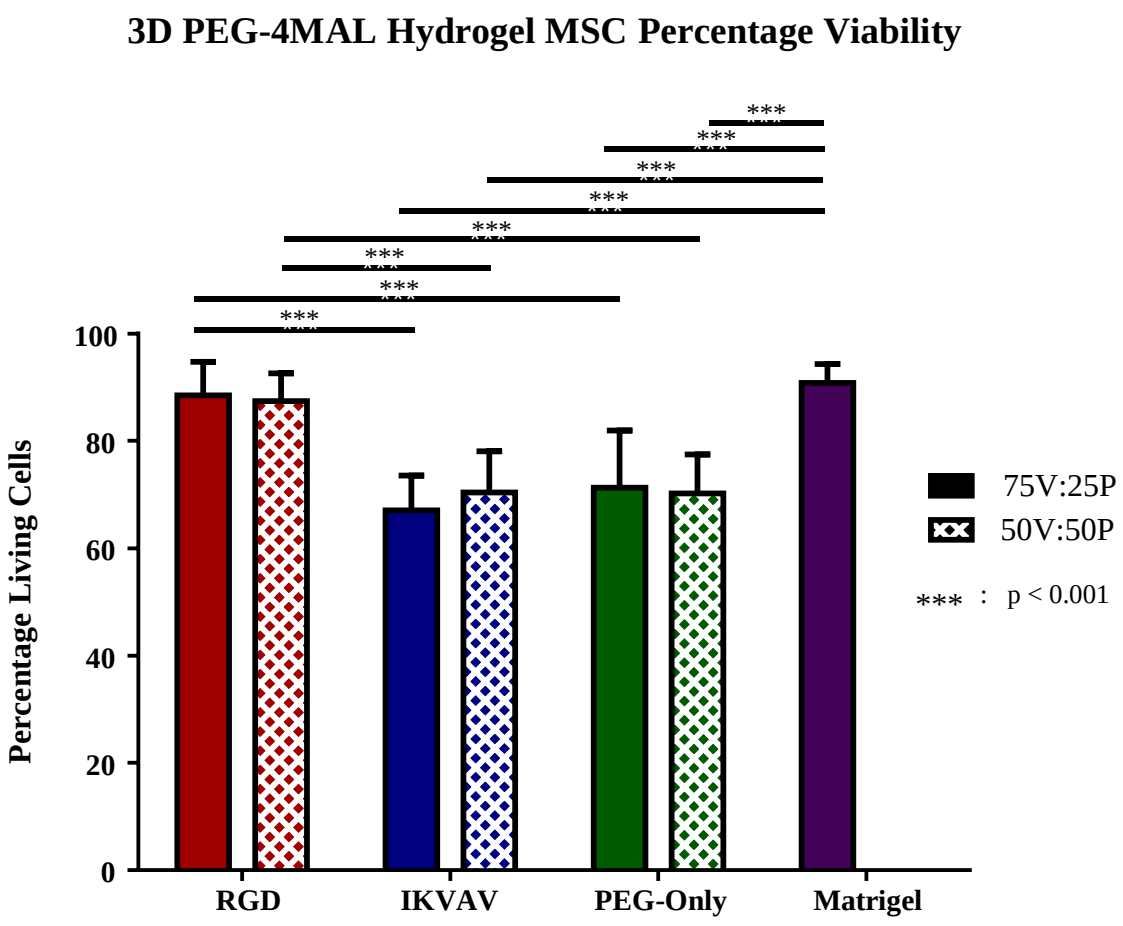

Figure 3.4 *Viability of MSCs in 75V:25P and 50V:50P PEG-4MAL hydrogels. RGD gels have a higher proportion of viable cells after 7 days* in vitro *(DIV) than the other PEG gels, comparable to that of the positive control. Statistical Analysis was performed using a 2-way ANOVA with a Tukey post-hoc test. $7 \leq n \leq 9$ for each condition, some samples were not included as dense cell clustering made counting highly inaccurate. Presented as mean + SD.*

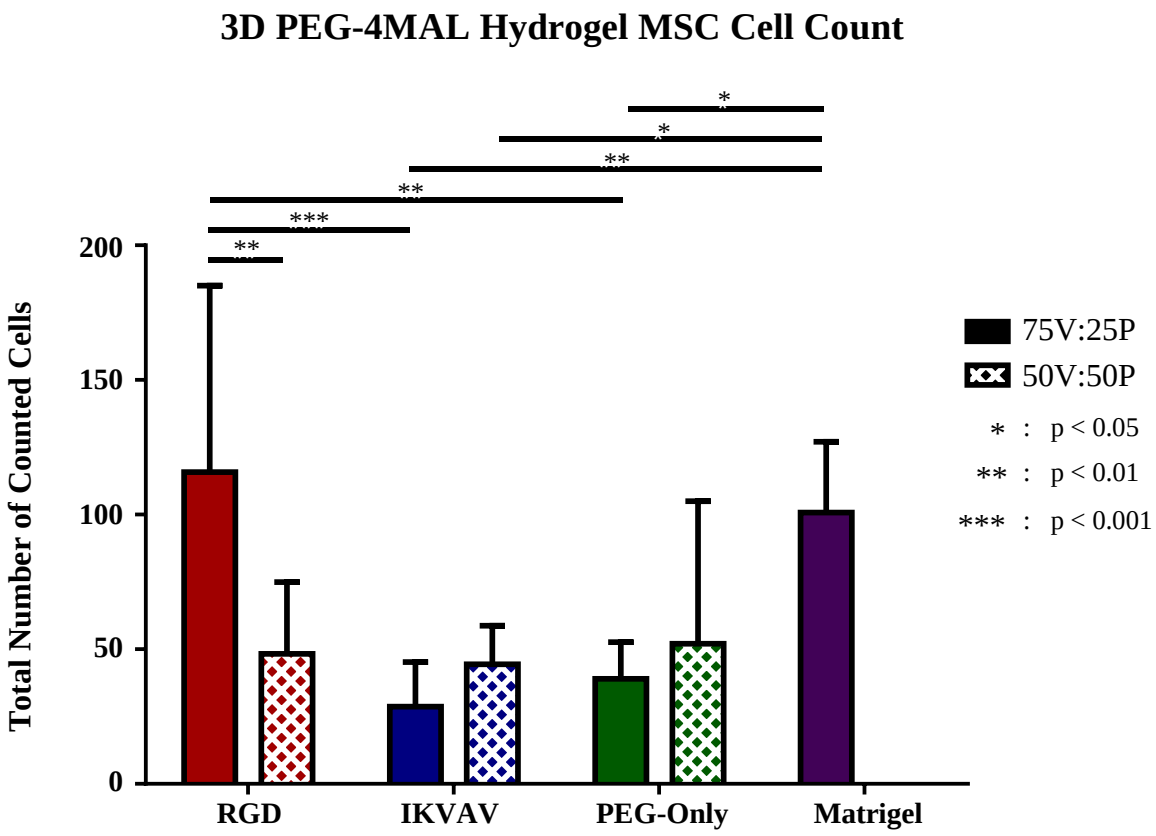

Figure 3.5 *Total Cell Count in MSC Live/Dead Assay. Cell counts are low in the gels with low percentage viability compared to those with high viability. The 50V:50P RGD gel had similar numbers of cells, however it is notable that given the large standard deviation of the 75V:25P that these ranges still overlap. Statistical Analysis was performed using a 2-way ANOVA with a Tukey post-hoc test.* $7 \leq n \leq 9$ *for each condition, some samples were not included as dense cell clustering made counting highly inaccurate. Presented as mean + SD.*

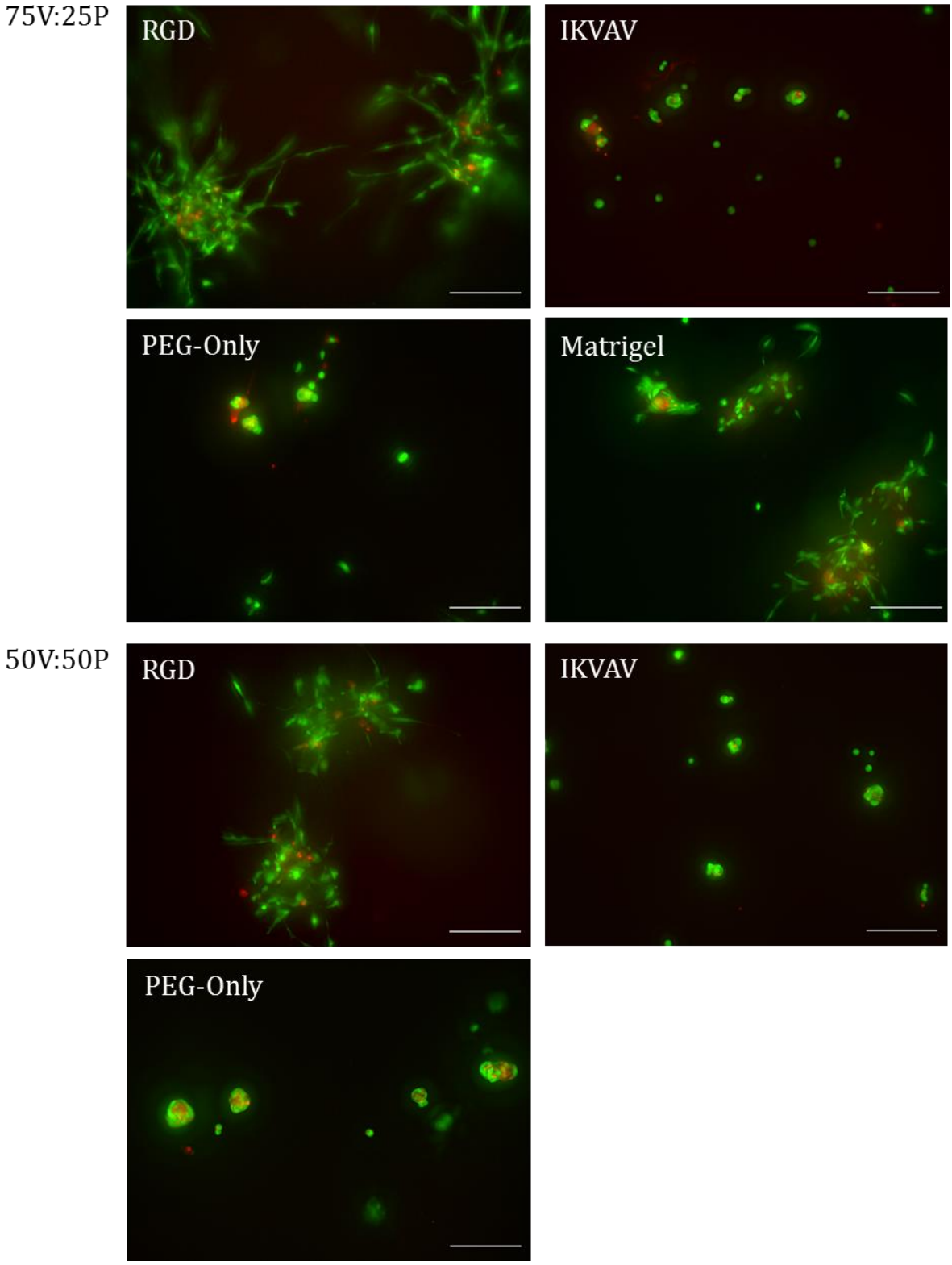

Figure 3.6 *Micrographs of MSC fluorescent live/dead staining in 3D PEG-4MAL hydrogels after 7 DIV presented as max intensity z-projections of captured z-stacks with 20µm increments between topmost and lowest visible cells. Living cell somas are stained green with Calcein AM and nuclei of dead cells are seen in red, stained by ethidium homodimer. Cell viability in the RGD gels is comparable to matrigel while in the IKVAV and PEG-Only gels viability and overall numbers are poor. Scale = 200µm*

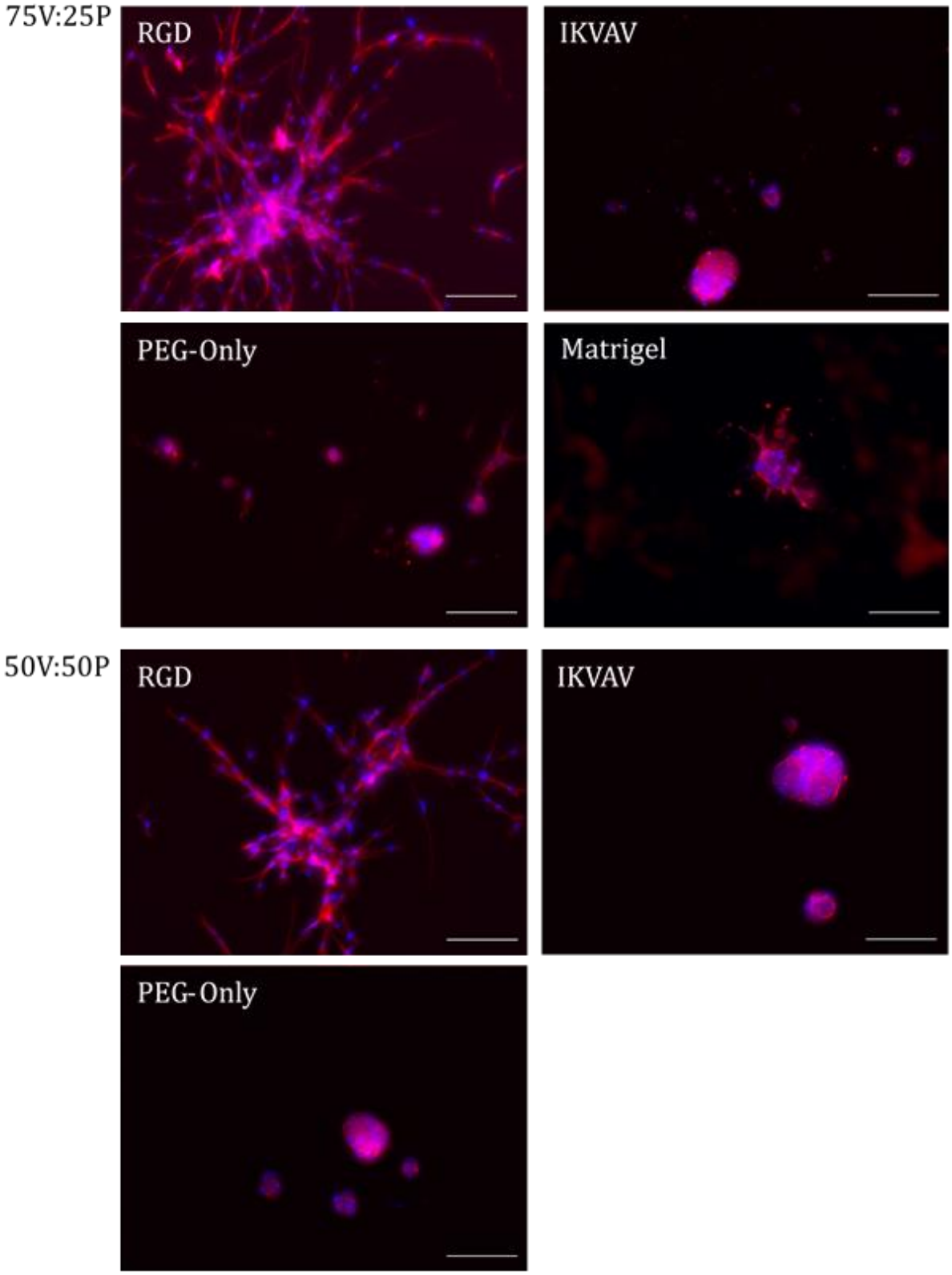

Figure 3.7 *Micrographs of hMSCs in 3D PEG-4MAL hydrogels with 75V:25P or 50V:50P cross-linkers after 7 DIV, stained for actin (red) and nuclei (blue). Presented as max intensity z-projections of captured z-stacks with 20µm increments between topmost and lowest visible cells. RGD gels provide a suitable environment for the hMSCs to elongate and redistribute throughout the gel whereas the IKVAV and PEG-only gels do not provide the same adhesion cues, resulting in densely clustered groupings of rounded cells. These observations are consistent for both cross-linker combinations. Scale = 200µm*

3.3.2 Astrocytes

Several astrocytes in the RGD gels are forming branches and extending through the hydrogels which is something that is not seen in the other PEG-4MAL gels (Figure 3.8). Many of the cells are forming into clusters which indicates that the cells are not fully adherent, but from these groupings there is evidence of cellular processes forming distinct structures in long arcs that contain several nuclei. Astrocytes are known for their arborized morphologies (Sloan *et al.*, 2017) and in the RGD gels there are cells approaching this, forming strands that permeate 3 dimensionally through the material. As with the MSCs, this shows that the astrocytes are capable of using the material for integrin mediated adhesion and spreading to a certain degree. However, these elongated cell structures appear much more prevalent in the Matrigel samples. The rounded clusters are abundant in the IKVAV and PEG-Only gels in similar fashion to those in the MSC cultures (Figure 3.7) which again indicates poor adhesion. There are slight differences in the organisation of the clusters in the IVKAV gels which appear larger and more closely grouped than in the PEG-Only gels, but it is also possible that the slight differences in the material properties detailed in chapter 2 can account for this observation. There are no notable differences between the 75V:25P and 50V:50P gels which once again confirms that the balance of degradable and non-degradable elements is not impacting the astrocyte activity.

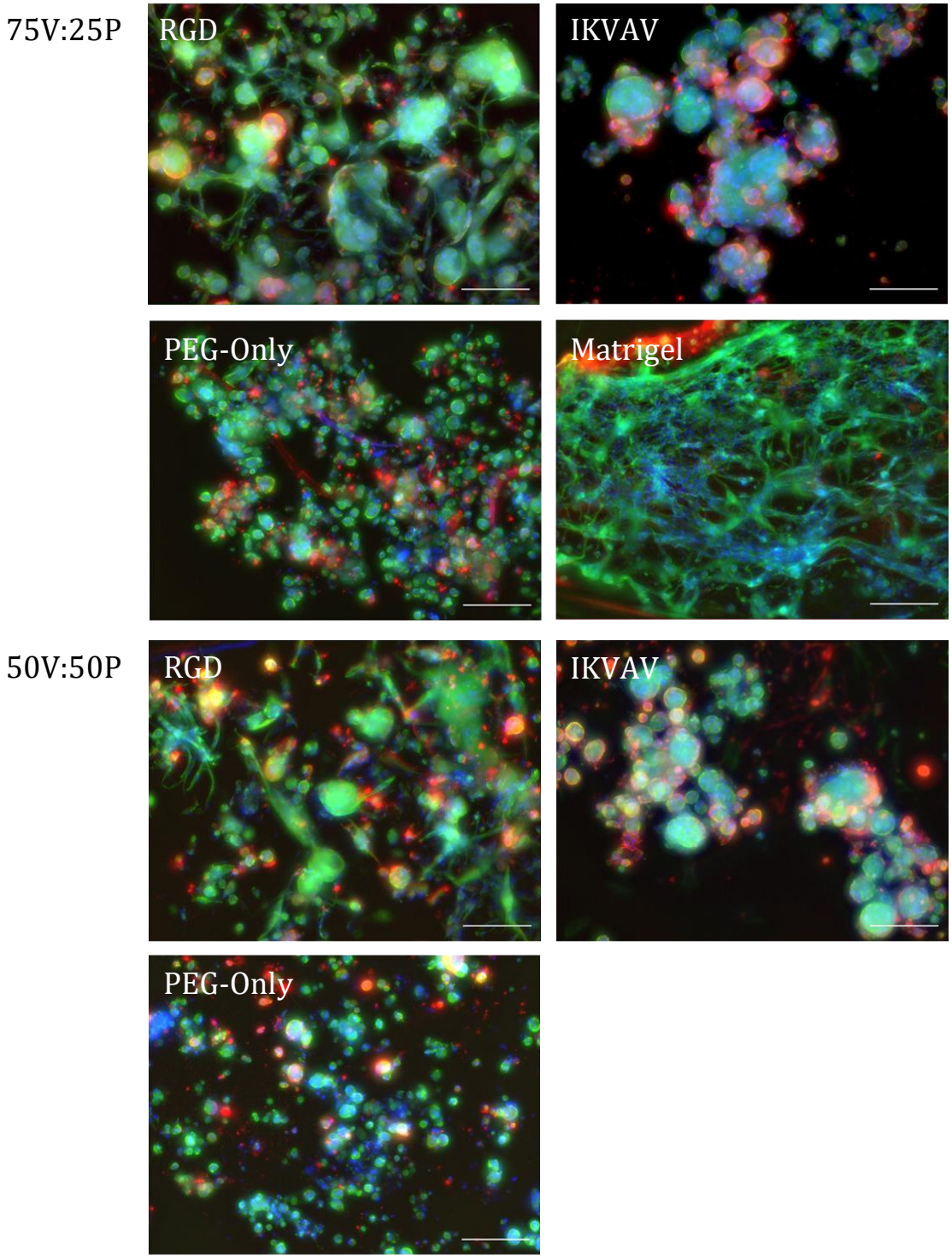

Figure 3.8 *Astrocytes in 3D PEG-4MAL hydrogels with 75V:25P (Top Set, with Matrigel) and 50V:50P (Bottom Set) cross-linkers after 7 DIV, stained for GFAP (red), actin (green) and nuclei (blue). Presented as max intensity z-projections of captured z-stacks with 20µm increments between topmost and lowest visible cells. Astrocytes in the RGD gels can be seen to produce branching morphologies that are indicative of astrocyte adhesion, however there are also several rounded clusters which are not seen in the Matrigel positive control suggesting the RGD gels are not providing the same level of support, although more-so than the IKVAV or PEG-Only gels. In these gels there is no evidence of adhesion and cells are exclusively grouped in rounded clusters. Scale = 200µm*

3.3.3 Mixed Spinal Cord Culture

In each of the gels examined in this study there is extensive neurite outgrowth both in terms of number and length (Figure 3.9 & 3.10) and the distinctions between the gels is not immediately visible as it is with the MSCs and astrocytes. RGD, IKVAV and PEG-Only gels are all capable of supporting 3-dimensional neurite outgrowth and provide sufficient freedom of movement to allow the cell bodies to regroup into clusters from their original dispersion. Neurons in all the PEG-4MAL gels are grouped predominantly into large clusters from which the multi-directional neurites emanate.

Quantification of the mean neurite length per neuronal cluster (Figure 3.11) and the summed total outgrowth per cluster (Figure 3.12) yielded no significant differences between the different conditions due to the wide variability between clusters. However, significant differences were observed when measuring the neurite density. Figure 3.13 details the mean density of neurites over 60x60μm^2 areas measured at neuronal cluster peripheries. Addition of NGF has not demonstrably increased the density of neurite outgrowth compared to the 50V:50P gels with no growth factor. The RGD gels with BDNF are seen to have significantly lower numbers of neurites than those with NGF or no growth factor. Compared to Matrigel, all of the PEG-4MAL gels see significantly fewer neurites with the exception of the 75V:25P and 50V:50P cross-linked RGD gels. Comparing the effect of peptide tethering, in the 50V:50P gels without growth factor there are significant differences between each of the RGD, IVKAV and PEG-only gels, with the highest density in the RGD gels and lowest in PEG-Only. The same is true between the RGD and PEG-Only in gels with NGF. As with the previous experiments, there is no distinction between the 75V:25P and 50V:50P gels as both gel types highlight extensive neurite growth after 7 days. In distinction to the Matrigel control, the PEG-4MAL gels show an absence of cell bodies in the regions between clusters while in Matrigel the neurons are seen to distribute throughout the gel, though there are still clusters present. These data demonstrate that the PEG-4MAL gels are useful platforms for investigating neuronal growth and that in terms of neurite density the RGD gels are comparable to Matrigel, however the addition of growth factor is not enhancing neurite growth within these populations of neurons. This could be due to non-optimal dosage of growth factors and further investigation would be required to determine the optimal concentrations of NGF or BDNF loading into the PEG-4MAL hydrogels to encourage neurite outgrowth.

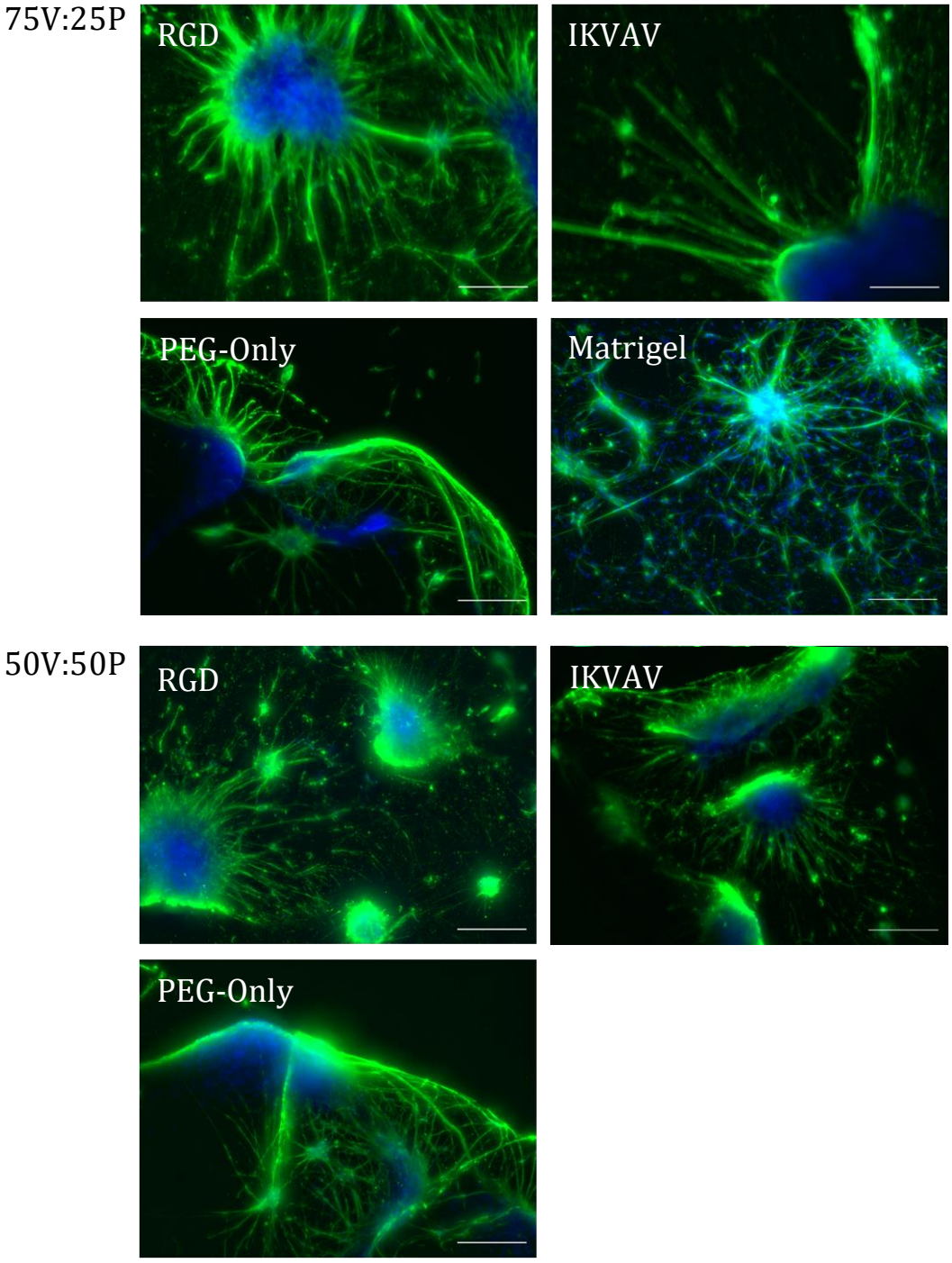

Figure 3.9 *Spinal Cord Neurons in 3D PEG-4MAL hydrogels with 75V:25P (Top Set, with Matrigel) or 50V:50P (Bottom Set) cross-linkers after 7 DIV, stained for β3-tubulin (green) and nuclei (blue). Presented as max intensity z-projections of captured z-stacks with 20µm increments between topmost and lowest visible cells. The evident response to implantation in these gels is for the neurons to form large clusters from which neurites can emanate, and to a certain degree overlap with neurites from neighbouring clusters. This is seen for both cross-linker ratios. Nuclei in the Matrigel controls are very dispersed, indicating that the migration of cell bodies is occurring to distribute more evenly throughout the gel which is not the case for the PEG-4MAL gels, however they are still evidently able to produce large numbers of robust neurites. Scale = 200µm*

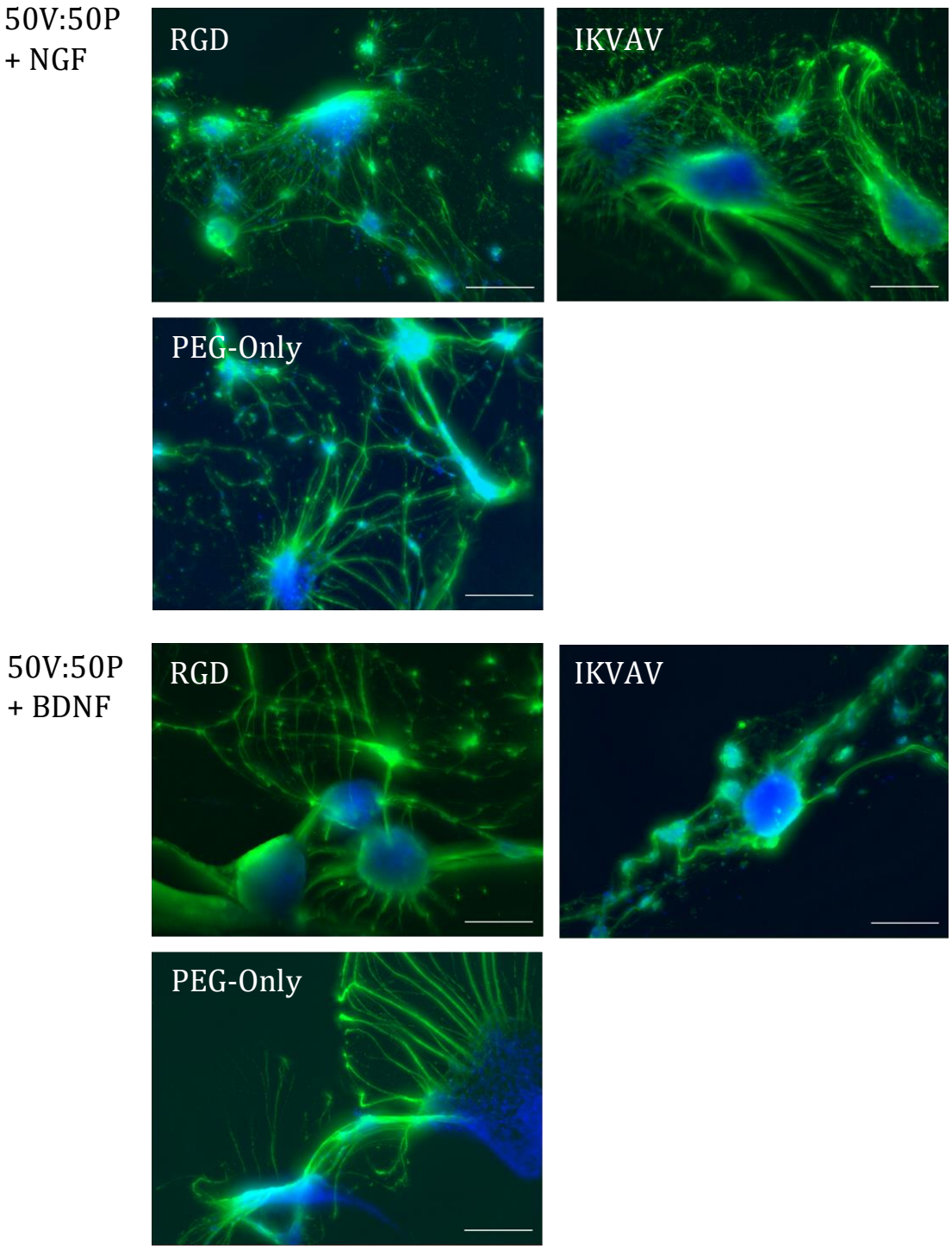

Figure 3.10 *Spinal Cord Neurons in 50V:50P cross-linked PEG-4MAL hydrogels with NGF (Top Set) or BDNF (Bottom Set) after 7 DIV, stained for β3-tubulin (green) and nuclei (blue). Presented as max intensity z-projections of captured z-stacks with 20µm increments between topmost and lowest visible cells. The morphology follows the pattern of large neuron clusters that produce several long neurites projected through the gel as seen in the growth factor-free hydrogels (Figure 3.9). Scale = 200µm*

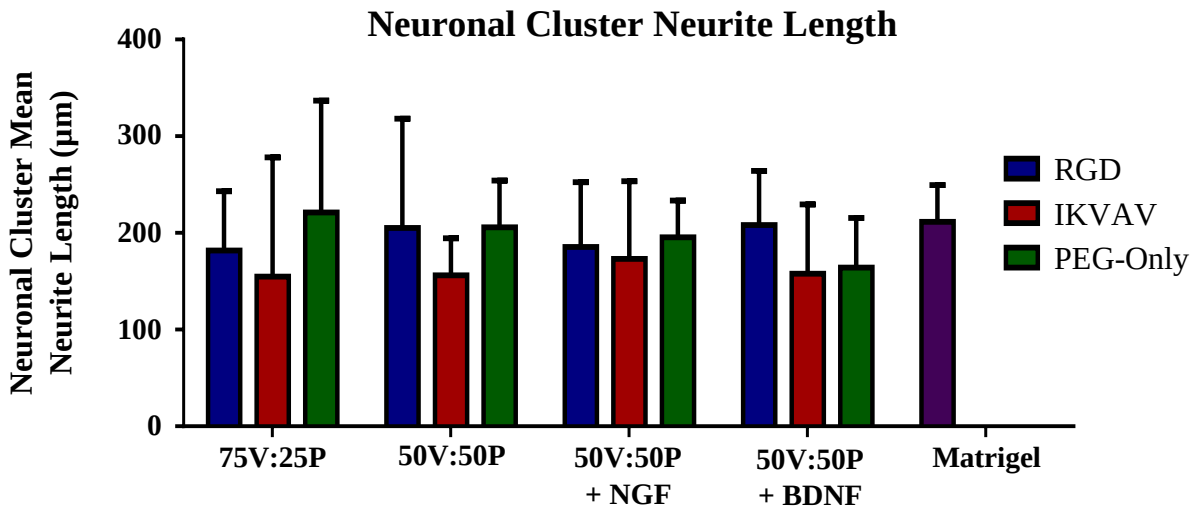

Figure 3.11 *Neuronal Cluster Neurite Length after 7 DIV. Neurite length was traced using NeuronJ* (Meijering *et al.*, 2004) *and the mean length of each cluster was calculated and subsequently average length per cluster. The mean neurite length per cluster is in the approximate range of 160-200µm, however there are no statistically significant differences between any of the measured conditions.) Statistical Analysis was performed using a 2-way ANOVA with a Tukey post-hoc test. Clusters were chosen at random, n ≥ 9 per condition, neurites per cluster 6 < n < 149. Presented is the total mean of the cluster means + SD.*

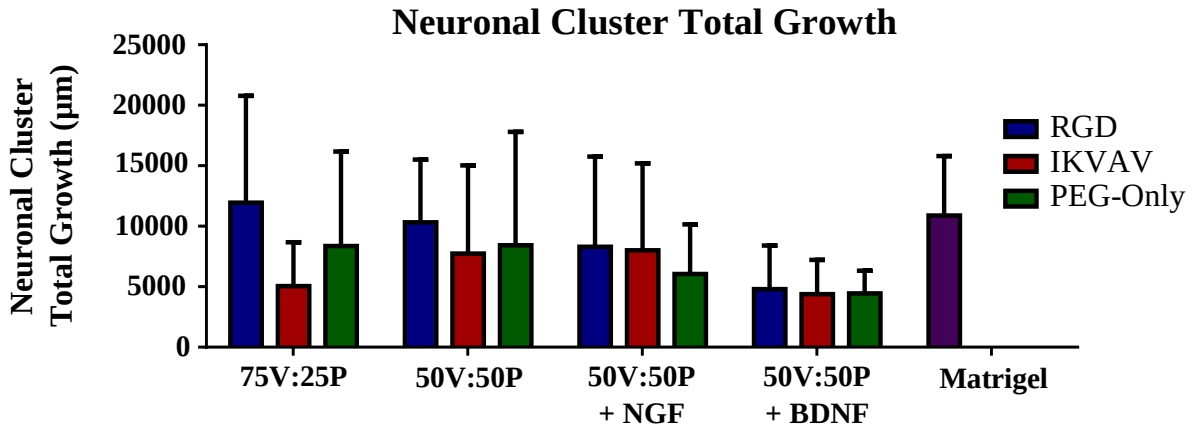

Figure 3.12 *Mean Neuronal Cluster Total Growth after 7 DIV. The cumulative neurite outgrowth is summed for each cluster and the mean growth per cluster is calculated to also take into account discrepancies in cluster size and number of neurites. While there are some notable differences in the mean total neurite outgrowth, particularly the comparatively low outgrowth in gels with BDNF compared to those without, there is no statistical difference between conditions due to the very large variability between clusters. Statistical Analysis was performed using a 2-way ANOVA with a Tukey post-hoc test. Clusters were chosen at random, n ≥ 9 per condition, neurites per cluster 6 < n < 149. Presented is the mean summed cluster growth + SD.*

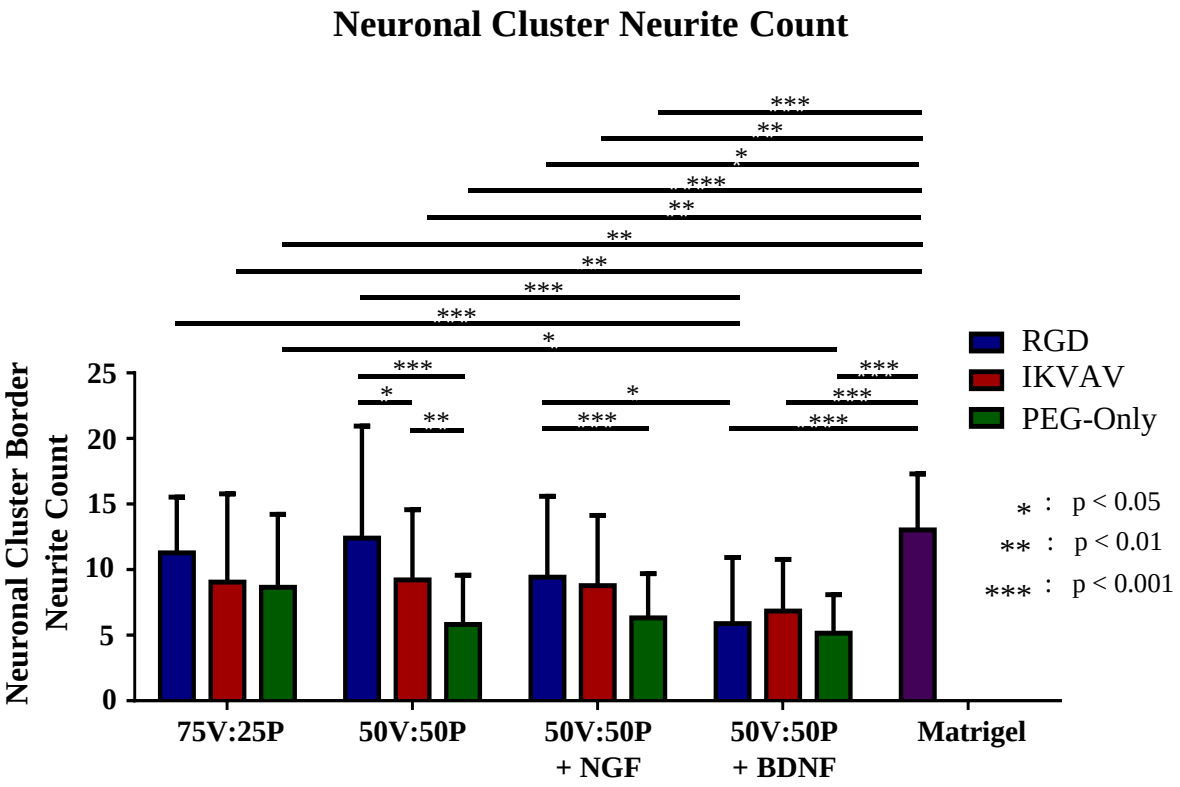

Figure 3.13 *Neuronal Cluster Neurite Count. 60µm borders were drawn around orthogonal edges of each neurite cluster and the number of neurites crossing the border was counted across 4 frames of the z-stack, (equivalent to 60µm in the z-axis) totalling a 60x60µm^2 area. The majority of conditions are statistically significantly different compared to Matrigel with the notable exceptions of the 75V:25P and 50V:50P RGD gels without growth factor. Within the same cross-linker/growth factor groups, significant differences are seen between each RGD, IKVAV and PEG-Only gels, with RGD gels demonstrating the highest density of neurites and PEG-Only the lowest. With NGF there is also a significantly higher neurite density in RGD gels than PEG-Only. The 50V:50P RGD + BDNF has a significantly lower density than with NGF or even without growth factor. Statistical Analysis was performed using a 2-way ANOVA with a Tukey post-hoc test. Clusters were chosen at random, n = 10 clusters, 4 areas each per condition. Presented is the mean neurite count per 60x60 µm^{2}area + SD.*

3.3.4 Dorsal Root Ganglia

In the PEG-4MAL gels, neurite outgrowth from the DRGs is observed in all of the gels functionalised with RGD peptides, including those with no growth factor present. These neurites are accompanied by the presence of cell nuclei into the material (Figures 3.14 & 3.15) which indicates migration of some cell bodies outwith the ganglia. These are likely to be Schwann cells as they are known to move outward from the DRG explants and co-localise with developing axons (Sun *et al.*, 2018), though their character here remains unconfirmed. The addition of nerve growth factor into the gels has contributed to more extensive neuronal growth than can be seen in its absence. NGF has also encouraged growth of neurites from the DRGs in the IVKAV and PEG-Only gels which is scarcely observed with these gel types in any of the conditions without NGF.

Growth from the DRGs is quantified in Figure 3.18, detailing the percentage of the DRG perimeter that has cellular outgrowth. This has confirmed that there is significantly more outgrowth consistently around the DRGs in RGD compared to the IKVAV and PEG-Only gels, except in the presence of NGF where DRG outgrowth in the IKVAV and PEG-Only gels increases significantly compared to other conditions. In these gels however there are no nuclei in the material outside of the ganglia which suggests that this growth is not the consequence of any secreted guidance cues from migratory cells that the neurite growth is mediated directly by NGF supplementation. The distinction is highlighted in the brightfield images (Figures 3.16 & 3.17) where a high density of cells are visible outside of the ganglia in the RGD gels but not so in the IVKAV or PEG-Only gels. This indicates that in the RGD gels the neuronal outgrowth is enhanced by the outward migration of other cells contributing to some form of guidance signalling or matrix deposition which is a role known to be performed by Schwann cells(Ard, Bunge and Bunge, 1987). Again, no differences are notable between the 75V:25P and 50V:50P gels. The BDNF conditions are not distinct from the gels without growth factor which indicates that BDNF is not a potent promoter of growth for these populations of neurons. This has been demonstrated previously by Kimpinski *et al.* (Kimpinski, Campenot and Mearow, 1997) who showed that while NGF was able to enhance neurite outgrowth of dissociated DRG neurons, BDNF had no such effect which is in keeping with the observations of the PEG-4MAL gel cultures. Farinas *et al.* (Farinas *et al.*, 1998) provides more perspective on this having shown that DRGs in later stages of development contain considerably more TrkA expressing neurons than TrkB expressing neurons which are high affinity receptors for NGF and BDNF respectively which gives a possible explanation for the observations made for the DRGs in PEG-4MAL gels.

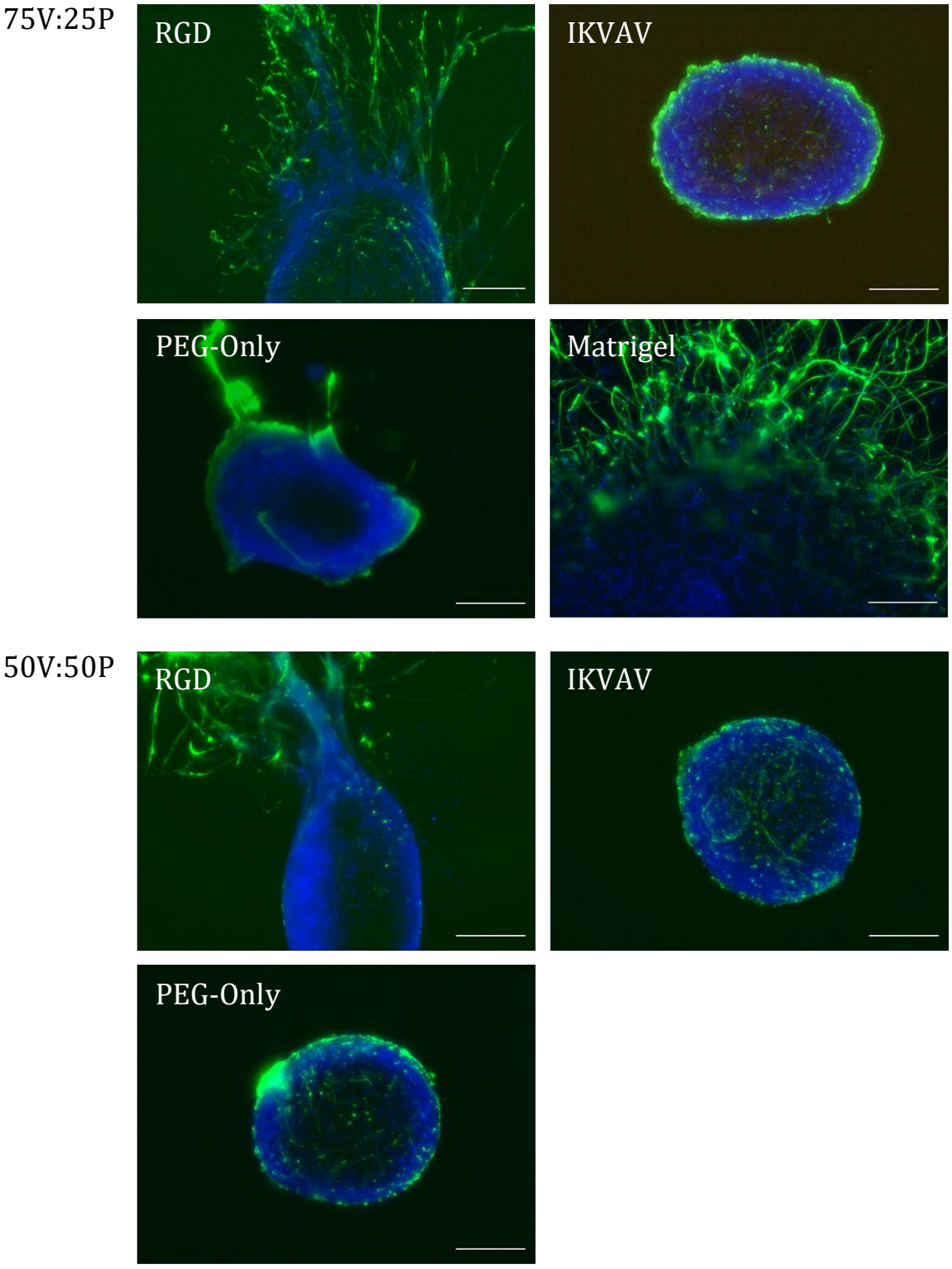

Figure 3.14 *Dorsal Root Ganglia in 3D PEG-4MAL hydrogels with 75V:25P (Top Set, with Matrigel) or 50V:50P (Bottom Set) cross-linkers after 7 DIV, stained for β3-tubulin (green) and nuclei (blue). Presented as max intensity z-projections of captured z-stacks with 20µm increments between topmost and lowest visible cells. In the RGD gels there is fairly extensive neurite outgrowth from the ganglia accompanied by migration of some cells into the surrounding gel as indicated by the nuclei present in areas away from the ganglion body though not to the extent seen in matrigel. This is not seen in the IKVAV or PEG-Only gels which don't show any evidence of outgrowth in the gel. Scale = 200µm*

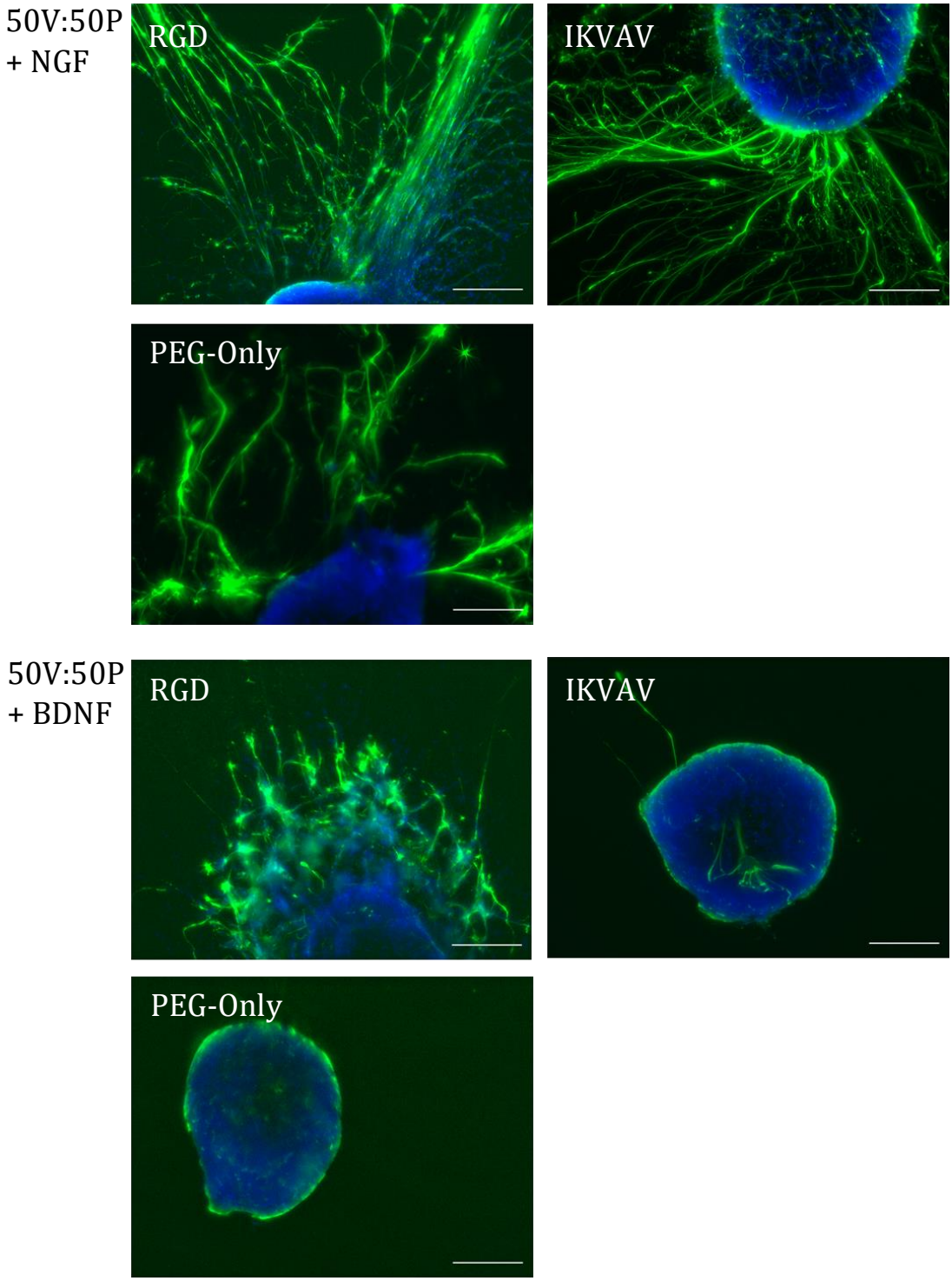

Figure 3.15 *DRGs in 50V:50P cross-linked PEG-4MAL hydrogels with NGF (Top Set) or BDNF (Bottom Set) after 7 DIV, stained for β3-tubulin (green) and nuclei (blue). Presented as max intensity z-projections of captured z-stacks with 20µm increments between topmost and lowest visible cells. Gels cultured with NGF show neurite outgrowth in all conditions though this is particularly evident in the RGD gels. The RGD gels also demonstrate some cell migration from the ganglion with individual nuclei observable outside of the DRG periphery that is not observed in the other gel types. The gels with BDNF do not show such outgrowth in the IKVAV or PEG-Only gels but again there is evidence of activity in the RGD gels, comparably to the samples with no growth factor (Figure 3.14) Scale = 200µm*

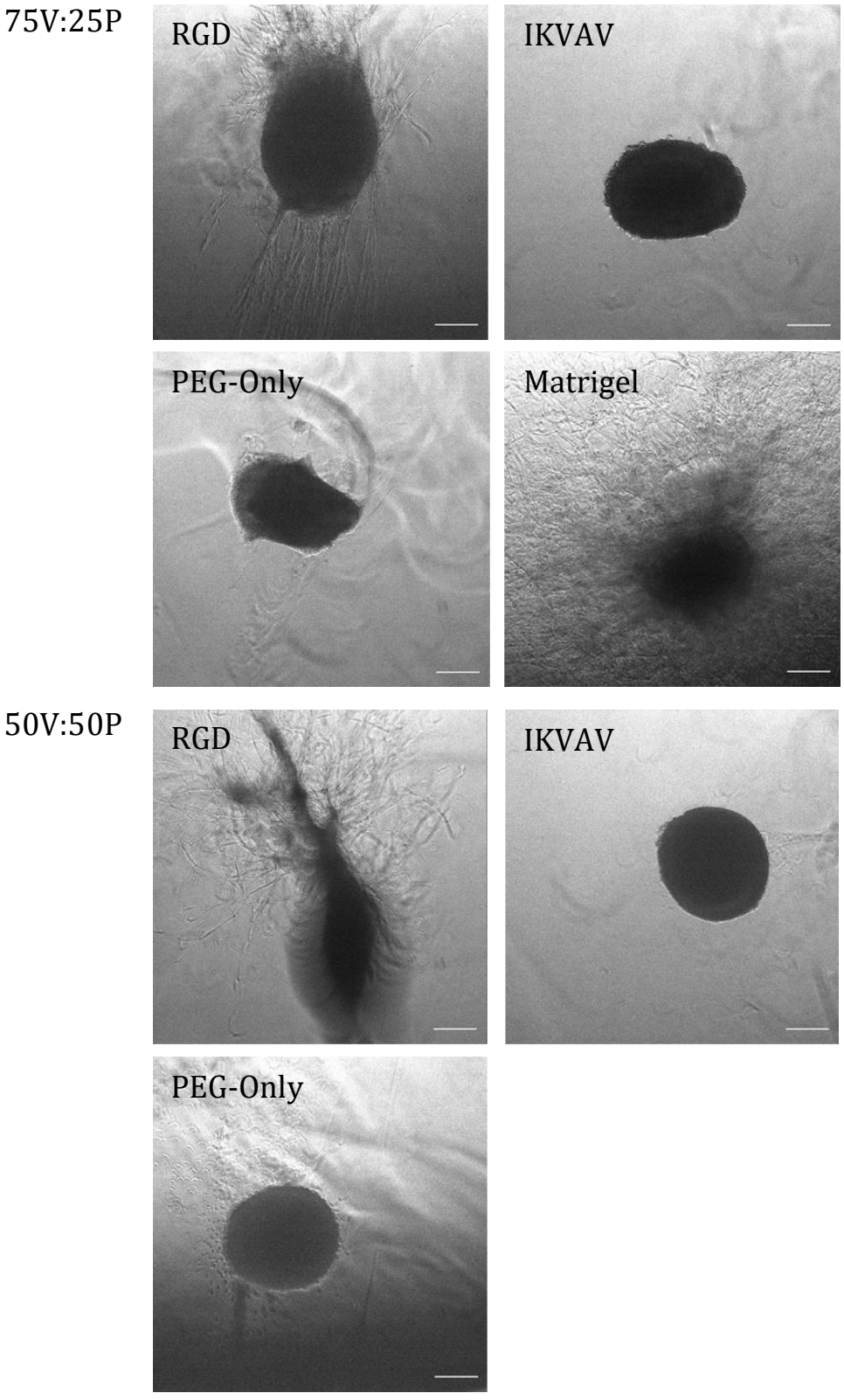

Figure 3.16 *Brightfield images of DRGs in 3D PEG-4MAL hydrogels with 75V:25P (Top Set, with Matrigel) or 50V:50P (Bottom Set) cross-linkers after 7 DIV. Extensive growth is visible from the DRGs in the RGD gels with both cross-linker ratios. Many of the cells were not stained positive for β3-tubulin and so are likely to be Schwann cells. There is very little evidence of outgrowth in the IKVAV or PEG-Only gels. Scale = 200µm*

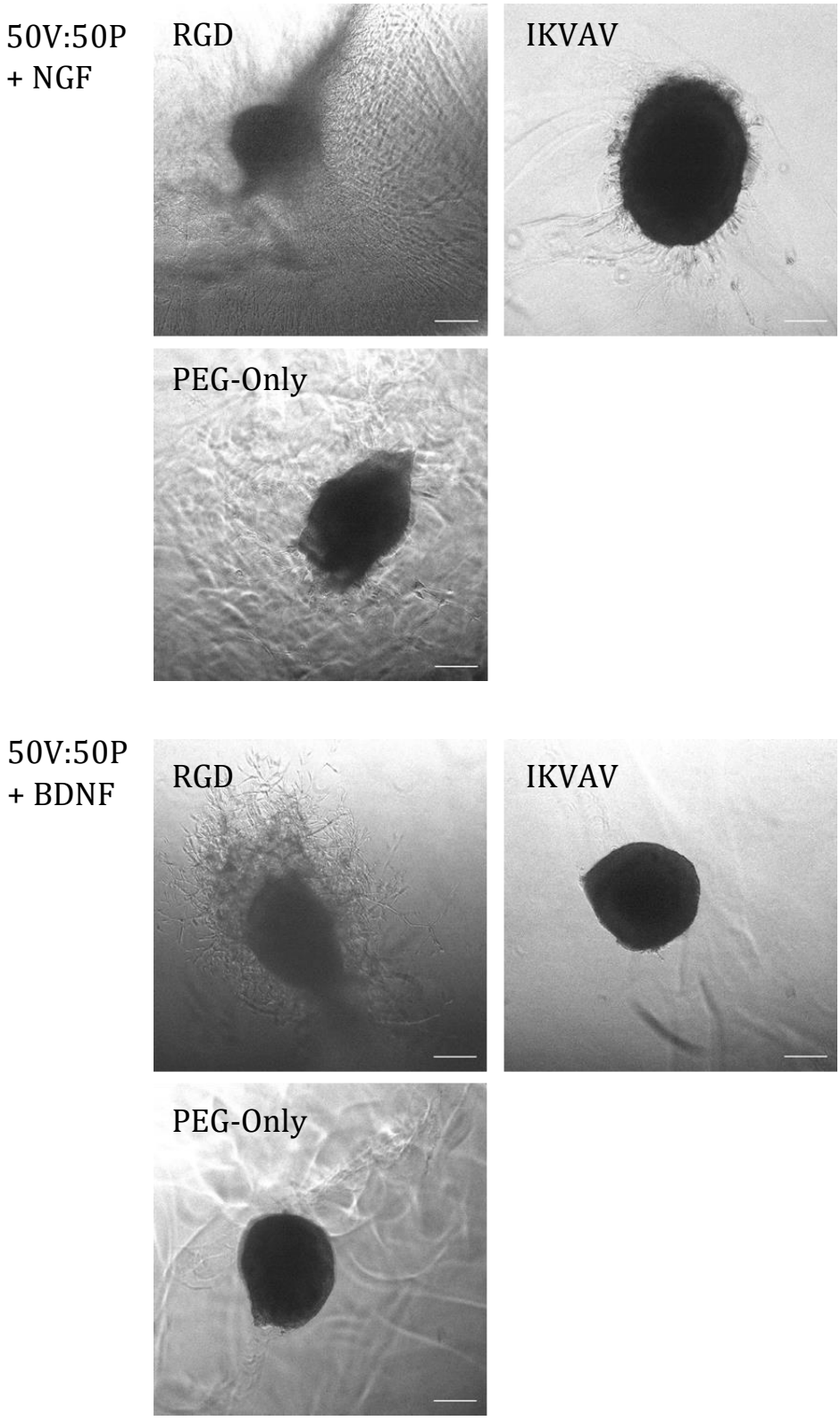

Figure 3.17 *Brightfield images of DRGs in 50V:50P PEG-4MAL hydrogels with NGF (Top) or BDNF (Bottom) after 7 DIV. The most visible growth from the DRGs is visible in the RGD gels with NGF and is even approaching the level seen in matrigel. The BDNF samples are comparable to those with no growth factor (Figure 3.16) The IKVAV and PEG-Only samples show much lower levels of growth, and the neurons are only effectively visible after immunostaining. Note much of the distortion around the DRG in the NGF PEG-Only gel is caused by ripples in the material as opposed to cellular outgrowth. Scale = 200µm*

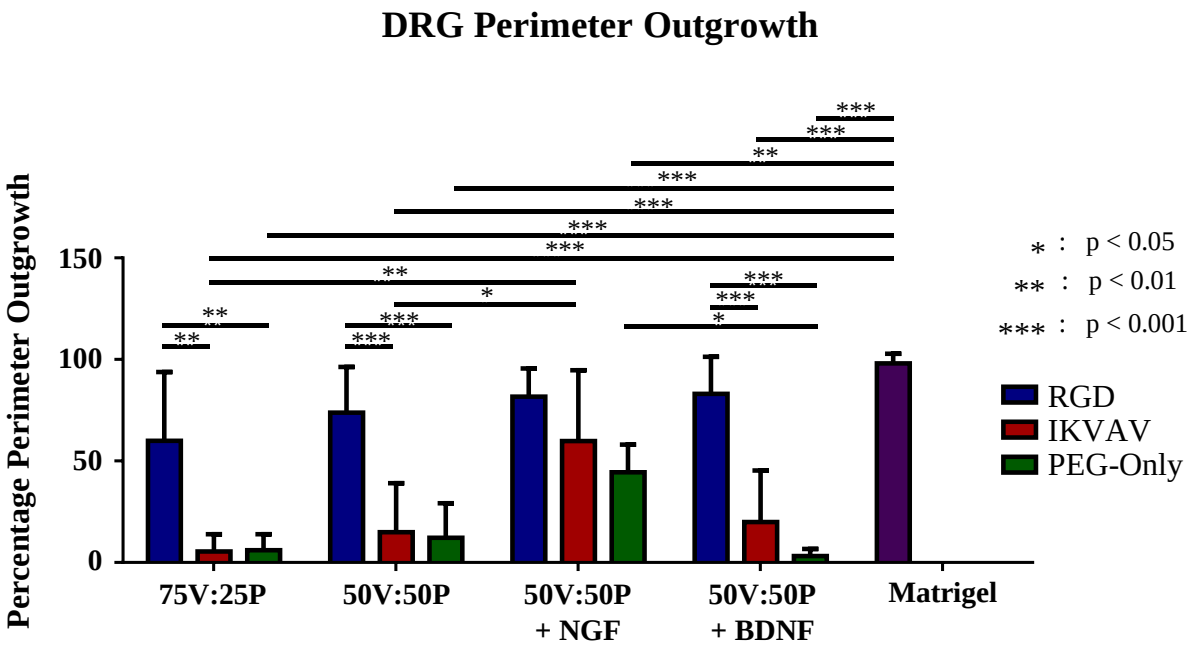

Figure 3.18 *DRG Perimeter Outgrowth. Growth around the perimeter was traced using ImageJ and calculated as a percentage of the total DRG perimeter. Each of the IKVAV and PEG-Only gels had significantly less perimeter growth than Matrigel while the RGD was not significantly difference, neither were any of the RGD gels different from one another. Most notably, the IKVAV and PEG-Only gels with NGF showed greater outgrowth than in other conditions, with statistically higher growth in IKVAV compared to GF free gels and PEG-Only compared to BDNF. Additionally, the outgrowth in the IKVAV and PEG-Only gels is not statistically different compared to the RGD gels. Statistical Analysis was performed using a 2-way ANOVA with a Tukey post-hoc test. Cluster were chosen at random, n = 6 per condition. Presented as mean + SD.*

3.4 Discussion

In vitro investigation of the PEG-4MAL hydrogels has demonstrated that RGD bound gels are capable of supporting cell growth and migration using a variety of cells types that have meaningful implications in the context of spinal cord injury. Each of the cell types tested have been reported to possess α5β1 integrins (and several others) (Feltri *et al.*, 2002; Peng *et al.*, 2007; Frith, Mills, Hudson and Cooper-white, 2012; Tonge *et al.*, 2012) which binds to RGD which was consistently observed to promote the formation of cellular processes and directed the cells towards typical morphological phenotypes. This was not the case for the IKVAV gels despite the fact that α3β1 and α6β1 integrins are known to bind with this sequence and astrocytes, MSCs, immature CNS neurons and Schwann cells express one or both of these integrins (Milner and Campbell, 2002; Peng *et al.*, 2007; Frith, Mills, Hudson and Cooper-White, 2012; Pellegatta *et al.*, 2013). There are several possibilities as to why these integrins may not have been effectively engaged. The affinity of integrin binding to their ligands can be influenced by the surrounding non-binding amino acids, and while the sequence used in these gels is a direct truncation of the sequence present in full length laminin, others have been synthesised which promote neuronal characteristics to a greater extent (X. Li *et al.*, 2014). Furthermore, publications that report modified cellular attachment and proliferation using the same sequence have often relied on peptides tethered to 2D rigid surfaces (Blau *et al.*, 2001; Thid *et al.*, 2008; Jans *et al.*, 2009). Other publications have documented similar differences in cell behaviour between RGD and IKVAV bound hydrogels. Dhillon *et al.* (Dhillon *et al.*, 2019) used chitosan hydrogel tethered with this sequence to culture adipose derived stem cells and the IKVAV bound gels failed to sustain the same number of cells as RGD bound alternatives or in some cases even the un-functionalised gel. Gunn *et al.* (Gunn, Turner and Mann, 2004) used the sequence in PEG-diacrylate hydrogels and also found it to be poor at promoting the formation of neurites when used as a substrate for PC12 cells, and again fared worse than RGD versions. These finding suggest that the efficacy of IKVAV in integrin binding is highly dependent on the presentation of the peptide in terms of both chain conformation and substrate of attachment, and in the PEG-4MAL hydrogels it is likely that neither of these criteria are optimal. Using alternative peptide sequences or changing the tethering mechanism could enable IKVAV peptides to permit more robust cellular adhesion for improved viability and function.

The cell implantation method used for cell seeding into the hydrogels following overnight swelling was adopted after several unsuccessful attempts of mixing the cells in with the gel

precursors before polymerisation, although this was achievable with astrocytes. The working hypothesis is that the relatively low pH of the gel components was detrimental to the cells which were resting within the gels until they had solidified, and the buffered culture media could be applied. Jansen *et al.* (Jansen, Galarza and Shelly, 2019) noted similar findings when they encapsulated SkBr3 cells in PEG-4MAL hydrogels and recorded lower subsequent viability when the hydrogels were prepared using buffers with lower pH. Here, after the gels were swollen in PBS the pH could be neutralised without affecting the gel formation and consequently the same apparent toxicity was not observed. Alternative protocols were also attempted to seed cells on the surface of the hydrogels, but due to the poor adhesion of the cells onto the IKVAV and PEG-Only gels these were quickly displaced as the experiments progressed leaving no cells that could be analysed. Internalising the cells by pipette implantation after swelling enabled them to be retained for the entirely of the cultures and subsequent processing, though additional refinement could be beneficial to achieve a more homogenous distribution.

In the spinal cord neuron cultures, the quantification measures for neurite length did not capture any significant differences between conditions, However, the image processing required to produce quantifiable images introduces several drawbacks as the, notably the z-projections may blur the presence of faint neurites. Furthermore, the z-projection only captures planar growth and not into the z-plane and hence these data may not fully capture the extent of the growth. Additionally, neurites growing in close proximity are also difficult to resolve into separate entities, particularly in dense regions where background fluorescence from out of frame staining is present. This quantification would greatly benefit from more powerful microscopy techniques such as confocal microscopy which could elucidate differences in neurite length in the PEG-4MAL gels.

Other approaches to the experimental model could also be explored, however are not without compromise, for example 2D studies would allow easier quantification but would not resemble *in vivo* conditions. A possible model that could provide more clarity could be a combination of both 2 and 3D could be effective if cells are seeded between flat gels and neurite infiltration is observed into the material. Lampe *et al.* (Lampe, Antaris and Heilshorn, 2013) describes a customised neurite outgrowth quantification that could be applied in the mixed spinal cord cultures that uses DRGs encapsulated in hydrogels within a custom mould that enables the determination of the maximum length of neurite outgrowth as well as the total neuron outgrowth for the whole explant across a z-range of 100μm, providing a thorough overview of the samples as a whole. Time lapse imaging has also been used to

observe axonal development (Turney *et al.*, 2007) and could be developed to observe neuronal growth and migration before new axons get extensively entangled.

The spinal cord neurons cultured with BDNF did not improve the outgrowth of neurites compared to the gels without BDNF even though the TrkB receptor which bind to it is widely expressed throughout the spinal cord (Liebl *et al.*, 2001). Santos *et al.* (Santos *et al.*, 2016) demonstrated a dosage dependent BDNF response in neonatal rat spinal cord explant cultures and found that at concentrations neurite outgrowth increased with increasing concentration up to 50ng/mL after which it decreased. The loading concentration used in the PEG-4MAL gels was 500ng/mL which may have overstimulated the neurons before the BDNF could diffuse into the media. Furthermore, it has been demonstrated that prolonged exposure to concentrations as high as 100ng/mL can induce neuronal injury and death and could have impacted their growth in the PEG-4MAL gels (Hwang, Choi and Koh, 2002; Kim *et al.*, 2003). Therefore, further investigation into BDNF-loaded PEG-4MAL hydrogels should start with BDNF concentration optimisation.

Another notable outcome of the spinal cord neuronal cultures was that neurite growth could be seen in all of the conditions, regardless of the integrin ligands used which runs contrary to the other non-neuronal cell types investigated. As integrins are known to be heavily involved in axonal growth including α5β1as α3β1 that bind to RGD and IKVAV among many other (Myers, Santiago-medina and Gomez, 2011; Nieuwenhuis *et al.*, 2018), this suggests an alternative source of integrin recognisable sequences are present within the gel. It is possible that ECM is being synthesised and deposited within the gels and the neurons are acting upon this. A caveat of this experiment is the lack of purification of the neurons from the dissociated spinal cord and there is likely to be other cell types present in the hydrogels, though the use of neurobasal medium with the B27 supplement is intended to suppress this (Brewer, 1995) and there are no visible nuclei in the PEG-4MAL gels outwith the dense neuronal clusters that subsequently form. However, it cannot be ruled out that there are other populations of cells in the gels that are contributing to the deposition of ECM in each gel. McKinnon *et al.* (McKinnon, Kloxin and Anseth, 2013) demonstrated similar finding when using PEG-4MAL gels to grow embryonic stem cell derived motor neurons and saw neurite outgrowth even on unfunctionalised gels, though they did not suggest a mechanism. Mahoney & Anseth (Mahoney and Anseth, 2006) cultured embryonic cortical neurons in degradable non-functionalised PLA-PGA-PEG hydrogels and noted the formation of neuronal clusters that grew larger over time, deposited fibronectin and

ultimately developed neurites which corroborates the findings here and supports the idea of autologous ECM deposition as a growth substrate in the PEG-Only gels.

In each of the studies in this chapter, the effect of altering the cross-linker degradation ratios was negligible indicating that the properties of the gels that encourage cell attachment are still shared despite some minor differences in physico-chemical properties, at least after 7 days incubation. The degradation profile of the 75V:25P gels make them unsuitable for studies of significantly longer duration but given the similarity of cell behaviour in the early stages it is likely that any study conducted using the 50V:50P ratio would be analogous to the 75V:25P gels which makes the 50V:50P gels ideal for *in vitro* investigations. However, the opposite may be the case for *in vivo* studies of injury models as degradability may be key in such cases. The optimum rate of degradation would be contingent on how rapidly cells could infiltrate and as such the confirmation of similarity between the 2 ratios could allow for either to be used to probe short- and long-term degradation strategies. Nonetheless, one aspect that was not investigated was the long-term response of these cells in the hydrogels and while one week in culture has proven enough to highlight the differences in cell activity between the materials, longer periods of time result in a divergence of behaviour.

3.5 Conclusion

The PEG-4MAL hydrogels bound with RGD have been shown to enable growth and migration of several cell types including some endogenous to the CNS and MSCs which been previously implanted in SCI models. The IKVAV gels however have demonstrated little evidence that they induce distinct cell behaviour compared to the PEG-Only controls, neither of which promote the growth of MSCs, astrocytes or DRGs. As the ultimate goal of these investigations was to establish a candidate material for implantation into SCI, the IKVAV gels were discounted from subsequent study to the leave the RGD gels which have demonstrated efficacy and the PEG-Only gels as a negative control. As well as these considerations, there has been no demonstrable difference between the 75V:25P and the 50V:50P gels in terms of cellular activity. In the interest of observing how the gels modulate the wound environment in SCI models while minimising the number of replicates required, the 50V:50P were pursued for further investigation with the intent of observing material integration with the native tissue as they have a much slower degradation rate and should still remain present after the period of implantation. Therefore, the subsequent preparation SCI implantable hydrogels has been focussed on the 50V:50P RGD and PEG-Only gels.

4. Microfluidics Fabrication of PEG-4MAL-Based Gel Microspheres

4.1 Introduction

Implantable biomaterials most often come in the form of prefabricated solid structures that require extremely invasive surgical procedures to place in their intended site. In fast regenerating tissues this can be an acceptable approach as tissues recover to integrate around the implant, but in areas such as the spinal cord this poses a major problem due to the intrinsically low regenerative capacity of the tissue (Kakulas, 1999). Moreover, sparing the tissue that remains is critically important as any retained functionality can be lost if additional damage occurs during surgery. To overcome this concern, injectable materials hold promise as they can minimise the invasiveness of implantation and limit damage to areas the size of a needle tip. With hydrogels the material can be formed *in situ* if injected in aqueous phase at the injury site before cross-linking, provided the parameters governing gelation align with the physiological environment (Straley *et al.*, 2010).

The alternative is to pre-fabricate the hydrogels into structures that are small enough to pass through a needle. This can be achieved through microfluidics which can be used to generate gel microsphere suspensions that can flow through needles with minimal difficulty. To investigate the PEG-4MAL gels *in vivo,* this approach has been evaluated as a possible mechanism of implantation. The microsphere implantation would be modelled on similar procedures that enabled the successful implantation of populations of cells into the contused spinal cord using the same apparatus that would be available for the microsphere injections (Toft *et al.*, 2013; Lindsay *et al.*, 2017). A size of 50μm diameter was targeted as these would be capable of passing drawn glass capillary needles of the same design used for these studies which had an internal diameter of approximately 70μm. From the literature there is little consensus on which sphere diameter is most appropriate for spinal cord injection and sizes varies wildly from less than 1μm to around 0.5mm (Gwak *et al.*, 2016; Yu *et al.*, 2016; Lan *et al.*, 2017; Kumar *et al.*, 2018), so the 50μm chosen lies within this diverse range and should be appropriate for injection. These microspheres were generated using devices fabricated from PDMS based on moulds created using photolithography. This approach is very commonly used as PDMS devices can be fabricated with extreme precision and the mould casting technique makes devices more easily reproducible compared to alternatives such as glass-capillary devices (Othman, Vladisavljević and Nagy, 2015). More importantly, the generation of gel microspheres by microfluidics-based systems is also more reproducible and lower monodispersities can typically be achieved than with other methods that are not based on microfluidics, for instance emulsion or precipitation (Elbert, 2011). The devices

used here use a flow focussing regime to form microspheres in biphasic oil-gel flows which allows for high production rates of gel spheres that can be collected and stored for later use.

In this chapter, the design, fabrication and operation of PDMS microfluidics devices is discussed. Microspheres produced by these devices are characterised for their size and monodispersity, as well as analysis of microsphere degradation in type-1 collagenase and the assessment of viability of hMSCs cultured atop the microspheres.

4.2 Materials & Methods

4.2.1. Fabrication of Microfluidics Devices

4.2.1.1 Mould Preparation

Figure 4.1 shows a diagrammatic representation of the mould production process. The mould preparation protocol was performed in a Class 1000 clean room to prevent contamination by airborne particulates. Initial designs for the devices were created in AutoCAD (Autodesk) (the full description of design is covered in section 4.3.1) which were used to create an acetate photo-mask for photo-lithography (mask created by Microlithography Services, UK). The devices were patterned into arrays consolidated into 3-inch circles to fit the substrate dimensions.

To begin, 3-inch silicon wafers (UniversityWafer, USA) were sonicated in acetone, isopropanol and reverse osmosis filtered water for 5 minutes per solvent then dried with nitrogen gas. The wafers were then transferred to a spin coater (PMW32, Headway Research, USA) onto an appropriately sized chuck and secured by vacuum. A small quantity of SU8-3050 negative Photoresist (MicroChem, USA) was carefully poured onto the wafer to cover approximately 80% of the wafer surface while avoiding the formation of bubbles. The resist was spun for 30 seconds at 3000 rpm to produce a layer of 50μm thickness(Microchem, 2000) then transferred to a hotplate at 95°C to bake for 15 minutes.

Following this the wafers were transferred to an MA6 mask aligner (Süss, Germany) for photo-patterning. The acetate mask was cut to fit the wafer and placed on the surface, then a blank glass mask was placed over the top to hold firmly in place. The wafer was then exposed to UV (broadband at 7.2mW /cm^3) for 30s to cross-link the resist and transferred to a hotplate to bake at 65°C for 1 minute then 95°C for 5 minutes. The excess SU-8 not exposed to UV was then removed by immersion in the chemical developer EC microposit (Rohm & Haas, USA) for 12 minutes before rinsing with isopropanol to remove dissolved resist then flushing with RO water for 5 minutes and finally baking at 180°C for 2 minutes to complete the mould.

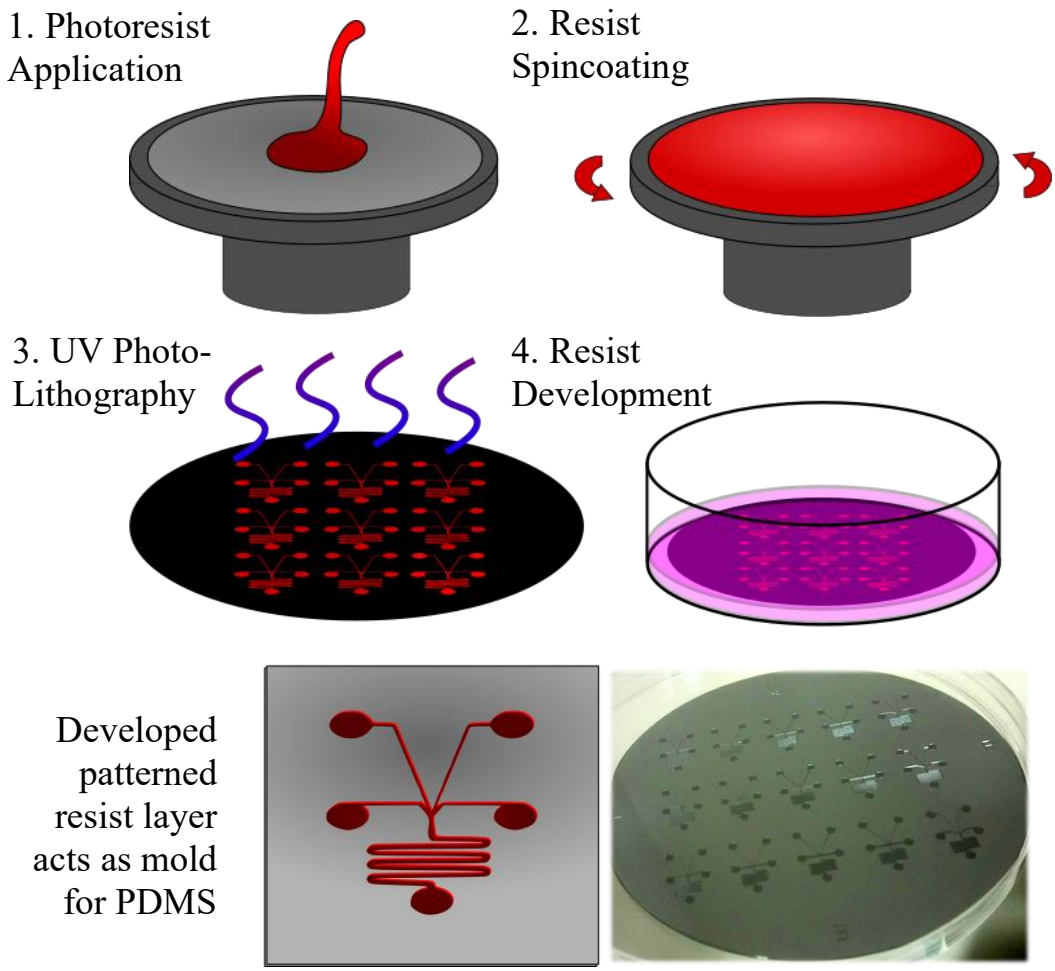

Figure 4.1 *Diagram of device mould production. SU-8 Photoresist is spun on silicon wafers, patterned by UV photolithography using an acetate mask and developed to remove unexposed photoresist and reveal the patterned features. The mould leaves patterned features of 50µm in height to imprint on PDMS which will form the basis of the devices.*

4.2.1.2 Device Fabrication

The prepared moulds were used to cast PDMS as the basis of the devices. Figures 4.2 and 4.3 illustrate the process of device fabrication from casting to complete devices. The PDMS was formed by thoroughly mixing the elastomer base at a ratio of 10:1 with the curing agent (Sylgard 184, Farnell, UK) for several minutes. The mould wafer was placed into a 120mm diameter petri dish and the PDMS mixture was poured over to fully cover the surface and was then degassed in a desiccator until all the air bubbles had evolved and dissipated. Following this, the PDMS was cured at 70°C for 12 hours. Once the material had solidified the PDMS was separated from the mould. On the first run this material was discarded to

ensure that any dust or contamination was clear from the mould surface; after which the process was repeated to pattern the PDMS used to create the devices. The patterned material was cut into rows to fit onto a glass slide and trimmed to remove any uneven sections that could warp the device.

A 1mm biopsy punch (Agar Scientific, UK) was used to create holes in the PDMS at each of the inlets and a 27-gauge blunt tip needle (Fisnar, UK) was used to punch a hole for the outlets. After creating the holes, the devices were washed thoroughly with isopropanol followed by Milli-Q water and dried with nitrogen. The same was done with a 22x64mm microscope slide to act as the device base. The surfaces were then ionised by plasma treatment with a corona discharge from a high frequency generator (BD-20V, Electro-Technic Products, USA) held approximately 5mm from the surface for one minute each on the glass slide and the PDMS imprinted surface followed by an additional 30s each. The ionised surfaces were pressed together tightly, ensuring no air pockets were created between the PDMS and glass. The devices were then incubated at 75°C to complete the bonding of the PDMS to glass. To complete the devices, a hydrophobic silane layer was applied using vacuum deposition to prevent surface adhesion of the aqueous phase by placing the devices in a desiccator along with 30µL of Trichloro(1H,1H,2H,2H-perfluorooctyl)silane (Sigma, UK), placing droplets onto a glass slip then enclosing the desiccator and evacuating the air before sealing to leave in vacuum for 2 hours. The devices were cured for a further 1 hour at 75°C before covering with low adhesive scotch tape until ready to use.

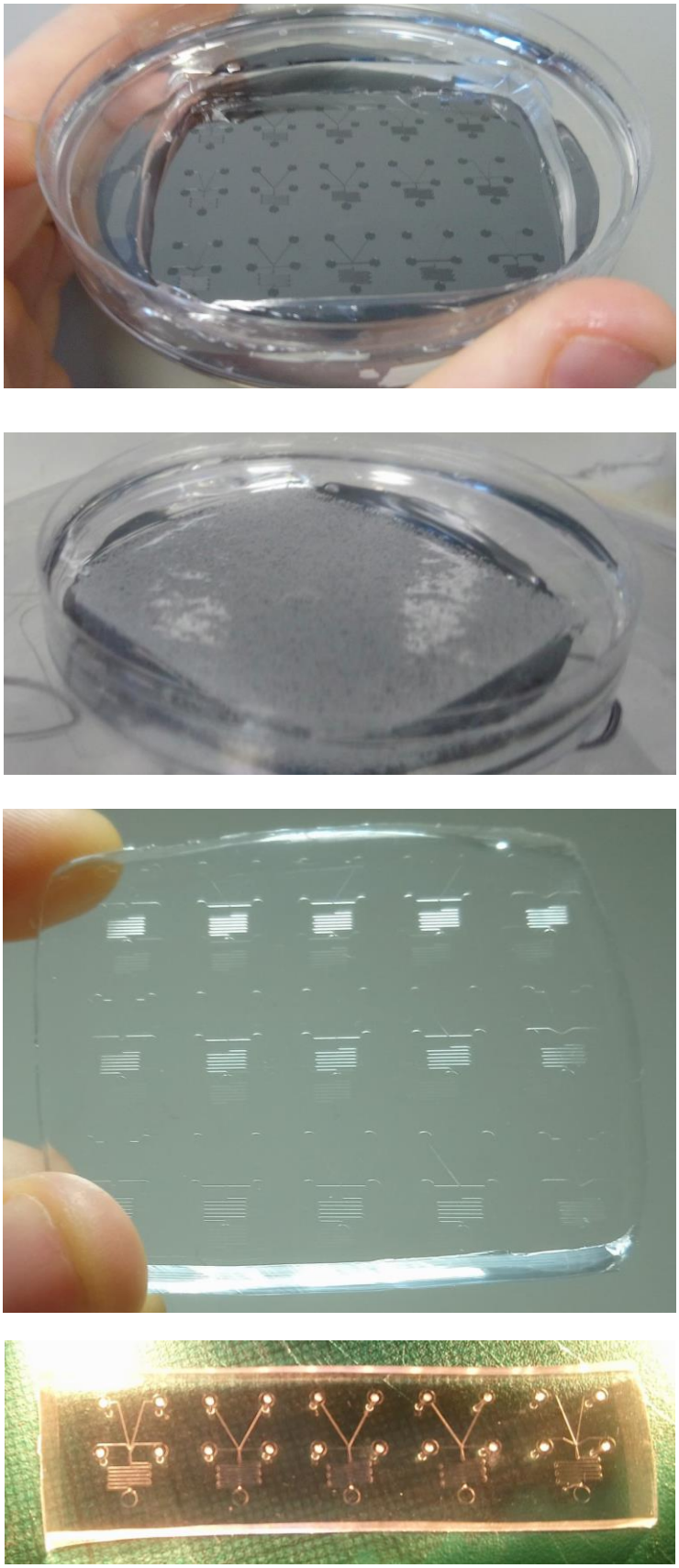

Figure 4.2 *PDMS casting of microfluidic devices. Non-polymerised PDMS base and curing agent are mixed and poured onto the patterned mould, degassed to remove bubbles and cured at 70°C to create the polymerised patterned PDMS. Inlets and outlets are then punched in the cast PDMS*

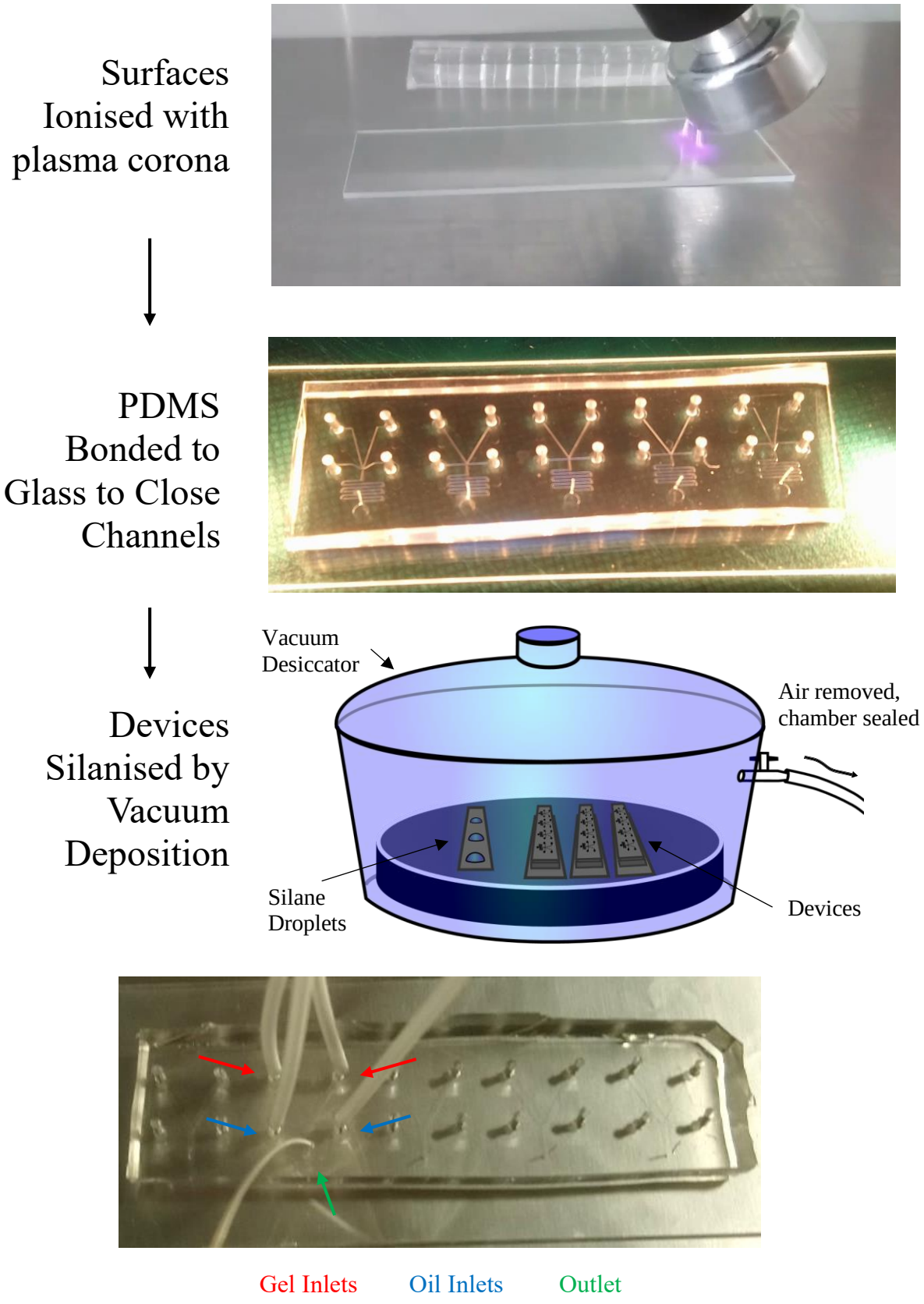

Figure 4.3 *Assembly of microfluidic device. PDMS bound to glass slides by corona plasma treatment followed by incubation 75°C for 1 hour. Devices were silanised by Trichloro(1H,1H,2H,2H-perfluorooctyl)silane vacuum deposition for 2 hours, followed by a final heating step at 75°C for 1 hour to complete the devices. The bottom frame displays the devices ready for use with PTFE tubing inserted.*

4.2.2 Device Operation and Optimisation

4.2.2.1 Device Design

The PEG and cross-linker are constituted so that they can be mixed in equal volumes to obtain the final gels so the devices are designed to enable the gel precursors be pumped into the device through separate channels at equal rates and meet to form a single channel that is 1:1 mix of each of the gel precursor components. This combined stream is then forced through a narrow junction by opposing orthogonal oil flows which prompts the stream to break up into individual droplets in a process that occurs continually as the flows run. These droplets will mix and solidify as they exit the device and can then be collected as gel microspheres. Designs for the devices were created using AutoCAD software. A first iteration was created and evaluated to determine how to set up and run the system to create the gel microspheres. These used layouts based on the flow focussing paradigm of operation using a continuous oil phase to force the aqueous phases of the gel components into segments forming spheres. Several models were patterned onto each wafer to test which parameters were critical to the formation of microspheres and which features were negating the effectiveness of the designs and could be removed. A second set of designs created based on these observations was used to fabricate optimised devices that could function reliably and at high capacity.

4.2.2.2 System Set-Up

The first step of operation was to prepare the gel reagents as described in Section 2.2.1. The PEG (PEG-RGD or PEG-Only) and cross-linker are constituted so that they can be mixed in equal volumes to obtain the final gels. Usual practice was to prepare 100µL of each to produce up to 200µL of microspheres per cycle. Two 1mL gas-tight SGE syringes (Trajan, Australia) were capped with 20-gauge flat tip needles (Fisnar, UK) and filled with Milli-Q water, taking care to expel any air bubbles. Approximately 30cm of PTFE tubing (0.052” OD 0.034” ID, Scientific Commodities, USA) was fit onto each needle tip and flushed through with water. A small volume of air was drawn into the tubing of each syringe to create a gas boundary between the water and PEG solution, which was aspirated into one syringe and cross-linker in the other. Due to the small volume of gel reagents used, the water ensures that the full volume of gel components can be utilised without losing any in the tubing. The loose ends of the tubing were then pushed firmly into the gel inlets of the device.

Two 5mL gas-tight SGE syringes (Trajan, Australia) were filled with mineral oil and 2% Span 80 surfactant (Sigma, UK) which were connected to PTFE tubing and flushed through as with the 1mL aqueous fluid syringes and the loose ends pushed into the oil inlets. A small volume of oil was pushed through the device to expel the air from the channels. Another ~10cm section of PTFE tubing (0.4mm OD 0.2mm ID, VWR, UK) was pushed into the outlet hole. Figure 4.4 shows the typical set-up of the devices during operation to allow for microscopic observation of the fluid flow. To collect the microspheres, a collection medium of 20mM L-cysteine (Sigma, UK) and 2% Tween 20 (Sigma, UK) was prepared in Milli-Q water. These components quench the gelation reaction after leaving the device and prevent the microspheres from aggregating in the collection vessel. The loose end of the tubing was inserted through a hole in the lid of a plastic dish into the collection medium and was sealed in place with Fixogum to enclose the container.

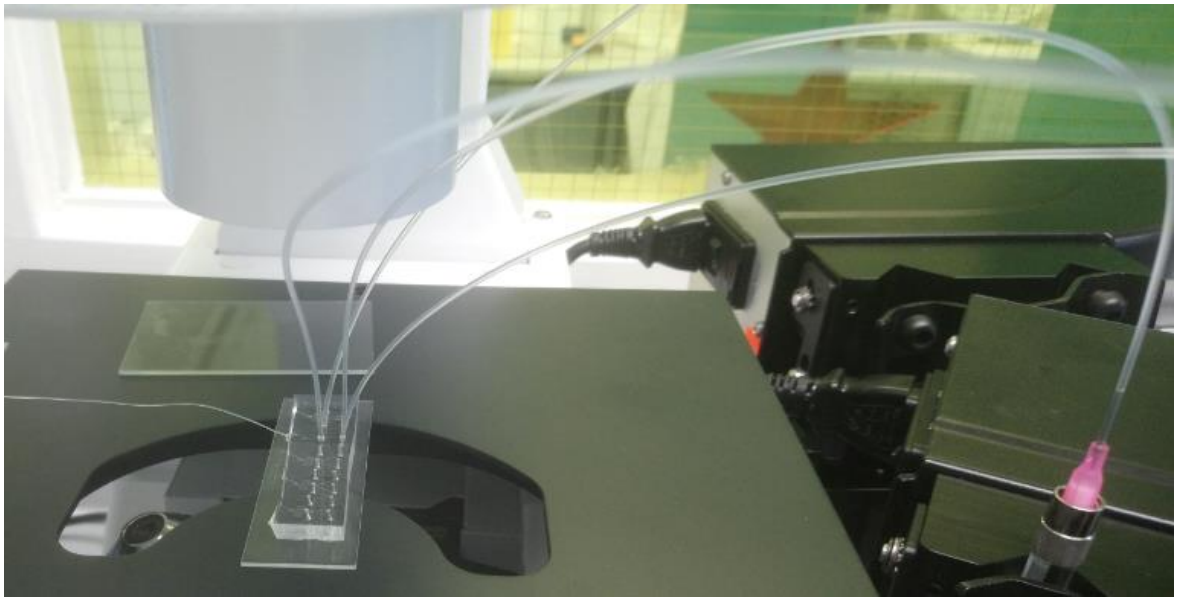

Figure 4.4 *Microfluidic device set-up over microscope lens with attached tubing from syringe pumps (right) and outlet exiting the device (left).*

To produce the microspheres intended for *in vitro* or *in vivo* investigations, each of the steps described above were conducted within a laminar flow cabinet to maintain a sterile environment. Once the tubing is fully connected, the interior of the device is sealed from the exterior and can be transported outside the flow cabinet. All fluids were filtered through a 0.22µm pore membrane. All equipment in contact with the fluids were immersed in ethanol and allowed to dry, accompanied by 30 minutes of UV irradiation and the devices were heated to 125°C to ensure sterilisation. Microspheres produced for this purpose were also irradiated with UV for a further 30 minutes after collection.

4.2.2.3 System Operation

Two syringe pumps (PHD Ultra, Harvard Apparatus, USA) were set up with the 1mL syringes secured into the first pump and the 5mL in the second to ensure symmetrical flow rates for the oil channels and gel channels respectively. The device was placed on the stage of a microscope (Axio Observer, Zeiss, UK) connected to a high-speed camera (Fastcam Mini UX50, Photron, UK) necessary for resolved observation of the high throughput of the device. Each pump was initiated and the nexus of the channels was observed until each channel was confirmed to be flowing in the correct direction and at matching rates, and that droplets were forming. Figure 4.5 displays micrographs of the operation of these devices, highlighting key features of the microsphere production.

Using the camera software (Photron Fastcam Viewer) a scale was overlaid on the video feed to estimate the size of the microspheres and the pump flow rates were adjusted until the microsphere size was approximately 50µm. The optimised flow rates were determined to be 900µL/hour for each oil inlet and 50µL/hour for each gel inlet, resulting in 100µL of microspheres being produced per hour. After the flow rates were established, they were used for subsequent microsphere production runs. The process was continued for approximately 2 hours until the PEG and cross-linker was exhausted. Following this the equipment was detached from the device and the collection medium with microspheres was transferred into a falcon tube to be centrifuged for 5 minutes at 3000 rpm to pellet the microspheres. The supernatant was decanted and replaced with PBS to remove the oil and surfactant from the microsphere suspension, then this process was repeated a further 3 times to ensure complete removal of contaminants. After the final centrifugation the microspheres were transferred to an Eppendorf and stored at 4°C in 1mL of PBS until ready to use. At the time of use, the tube was again centrifuged and the supernatant discarded to leave a maximally condensed stock which was used was used for each subsequent experiment.

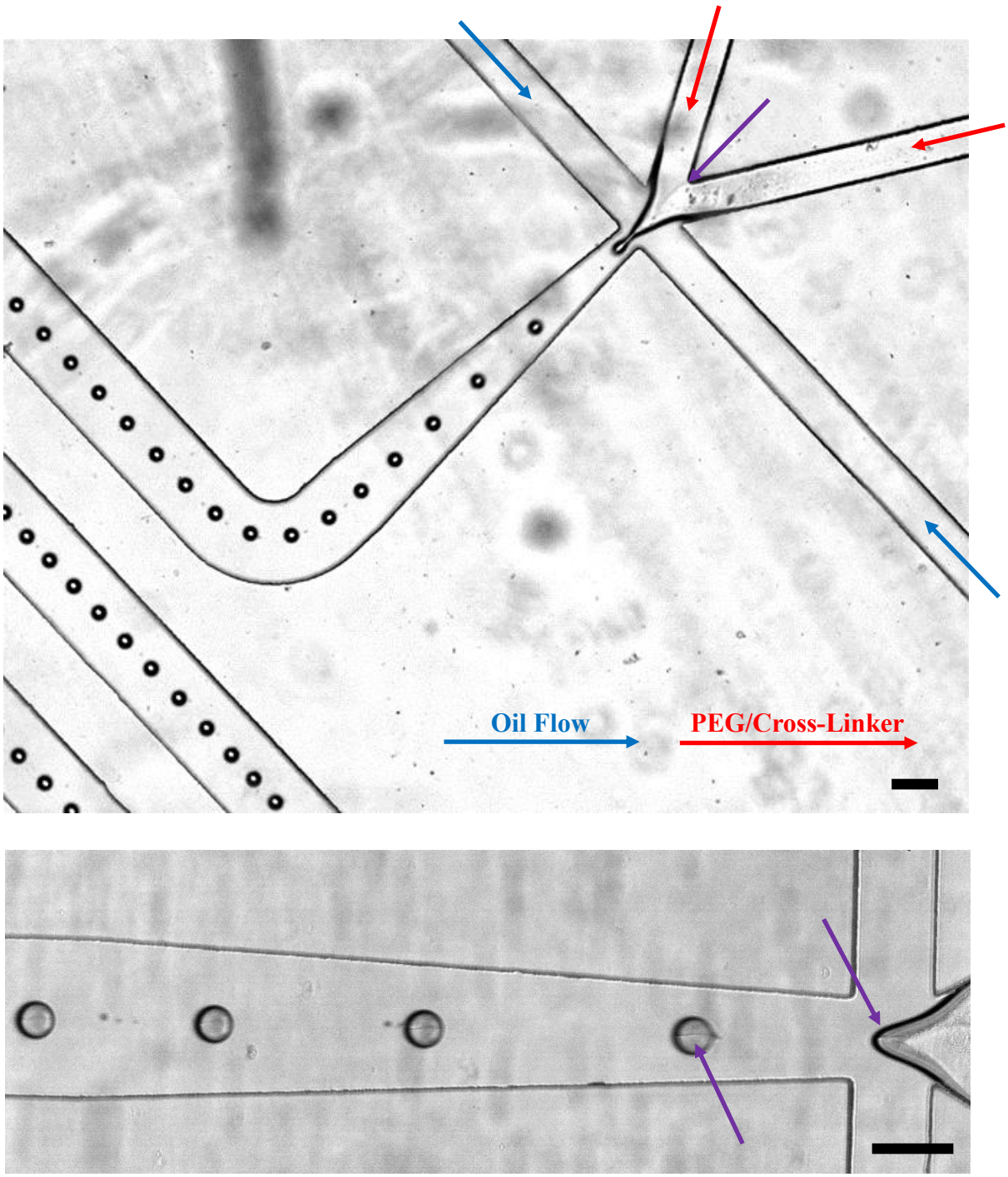

Figure 4.5 Top *Image of microsphere formation at the channel nexus in the microfluidic device. A visible boundary is formed between the PEG and cross-linker phases as they converge before being forced into droplets (purple arrows). The blue and red arrows show the direction of oil and gel flow respectively.* ***Bottom*** *The boundary is still visible in the droplets and bisects the spheres indicating the good proximity to the intended 1:1 ratio of PEG to cross-linker. The boundary quickly disappears as diffusion occurs to mix each component. Scales = 100μm.*

4.2.3 Microsphere Analysis

4.2.3.1 Size & Density

50V:50P RGD and PEG-Only microspheres were generated using the parameters described previously. 10µL of the condensed microsphere suspension was pipetted onto a glass slide and covered with a 12mm glass coverslip. Images of the microspheres were captured in 3 different areas per gel type and from each image 100 particles were measured in ImageJ after establishing a reference scale and the mean size was calculated. The density was evaluated by diluting the suspension 10-fold and placing 10µL into a Neubauer chamber to count the number of microspheres per unit volume.

4.2.3.2 Degradability

20µL of 50V:50P RGD and PEG-Only microspheres were transferred to Eppendorf tubes before adding the same volume of type 1 collagenase at concentrations of 20 units/mL, 2 units/mL or PBS to give final concentrations of 10 units/mL, 1 unit/mL and 0 units/mL. These were then incubated at 37°C. Over several time points, 5µL from each tube was placed on a microscope slide and mixed with 5µL of trypan blue to add contrast then topped by 12mm glass coverslips and images were captured of each sample. The number of microspheres in a $1mm^2$ area were counted at each time point and degradation was observed by the reduction in microsphere suspension density. Statistical significance was determined using 2 2-way ANOVAs to compare between groups and across time respectively, each with a Tukey post-hoc test, with comparisons considered significant at $p < 0.05$. $n = 3$ per condition.

4.2.3.3 MSC Culture on Gel Microspheres

Passage 5 hMSCs were prepared into a suspension of $2.5x10^6$ cells/mL as described in Section 3.2.1.1. 10µL of the 50V:50P RGD and PEG-Only microsphere suspensions were added to a 24-well plate formed into a layer by placing a 12mm coverslip onto the suspension droplet to spread over the surface and removing again. This layer was left in air for 5 minutes to encourage cohesion between the spheres and to the well-plate surface before 6µL of the MSC suspension was seeded onto the microsphere layer giving a density of 15000 cells per well. Control samples were prepared by seeding the cells onto the treated well-plate surface. These were then incubated at 37°C for 7 days in MSC Culture Media (Table 3.1), replacing

the media every 2 days. 2 identical plates were prepared to enable live/dead analysis and actin staining to be performed.

To evaluate biocompatibility of the microspheres with hMSCs, a viability stain was applied using a LIVE/DEAD™ Viability/Cytotoxicity Kit (L3224, ThermoFisher, UK) by adding 2mM Calcein AM which causes living cells to become fluorescent green and 4mM ethidium homodimer which stains dead cells fluorescent red, both dissolved in PBS. These were incubated for 30 minutes at 37°C before imaging each sample with an EVOS microscope (EVOS FL Auto) using the accompanying software. Z-stacks were taken of each gel at 20μm intervals between the uppermost and lowest visible cells which were analysed using ImageJ (Schneider, Rasband and Eliceiri, 2012) image processing software by compressing the stack into a single plane and counting the number of live and dead cells and calculating the percentage of total living cells. Statistical analysis was performed using unpaired student T-tests with significant considered as $p < 0.05$, $n = 3$ per condition.

The cells prepared for actin staining were fixed in 4% formaldehyde/PBS for 30 minutes before washing 3 times in PBS for 10 minutes each. Cells were permeabilised using a 0.1% Triton-X 100 (Sigma, UK) permeabilising buffer, incubating for 20 minutes at room temperature before rinsing again with PBS. The cells were then stained for actin with rhodamine phalloidin (R415, ThermoFisher, UK) using 0.3mL at a dilution of 1:100 and NucBlue (R37605, ThermoFisher, UK) for nuclei using 2 drops/mL and incubating for 1 hour before rinsing 3 times and storing in PBS. Images were captured using an EVOS microscope and were adjusted for brightness and contrast using ImageJ (Schneider, Rasband and Eliceiri, 2012).

4.3 Results

4.3.1 Device Design

The basic features common to all the designs in the first iteration used 2 inlets to supply the PEG and cross-linker which intersect across an axis of symmetry (Figure 4.6). The converged channels immediately bisect a pair of opposing oil inlets to create a nozzle before a serpentine exit channel with 8 turns and a width of 200µm. Each inlet is initiated and the outlet terminated by 1.5mm diameter reservoirs to accommodate the tubing carrying the fluids. The combined gel inlet width was held at 100µm for each layout. Devices based on these parameters were modified in several areas that could influence the formation of the particles to determine which geometries could produce microspheres reliably of the target size of 50µm. The relative angles of the inlets to each other were adjusted, as was the distance between the convergence of the gel channels and the oil channels, the width of the oil channels and the width of the orifice. Of these varying parameters, several observations were made which influenced the design of the second iterations.

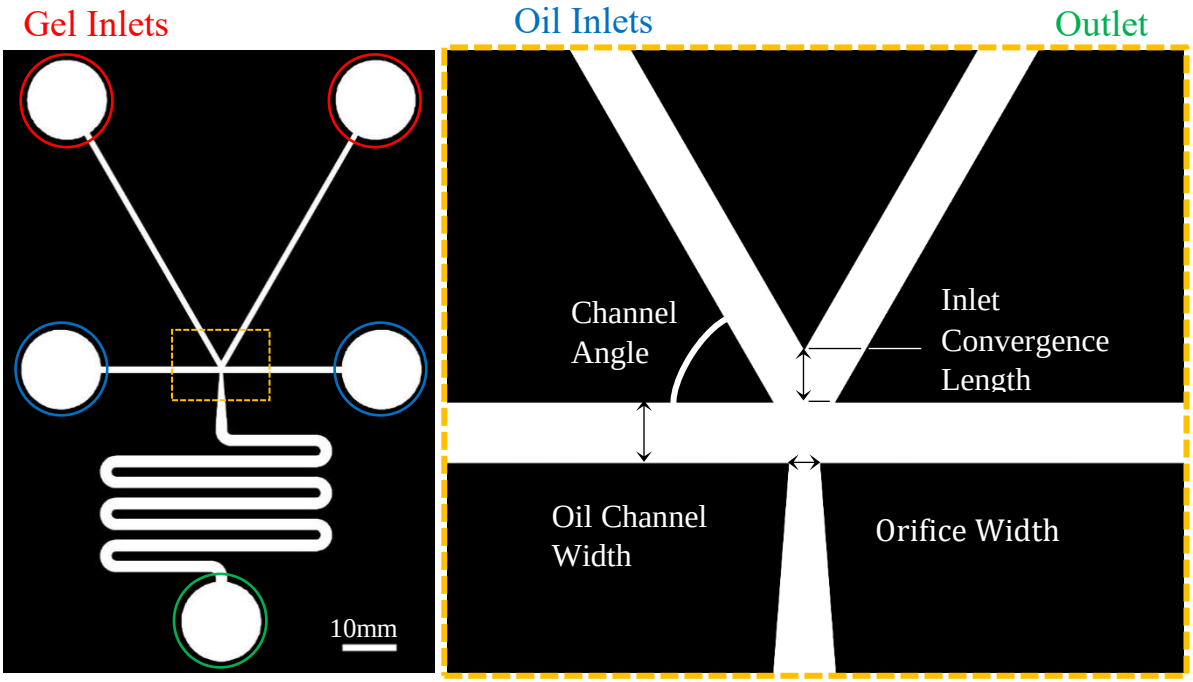

Figure 4.6 Left *Sample design for first iteration of devices.* ***Right*** *Inset schematic of device parameters investigated in the first iteration. These parameters were optimised to reach the final device design.*

Firstly, if the gel components converged at too great a distance from the oil channels then they had the tendency to solidify rapidly and block the devices (Figure 4.7a), so this inlet convergence length was minimised. The oil channel width greatly affected sphere formation (Figure 4.7b) as larger channels prevented the oil flow from effectively shaping the gel streams into droplet which became much larger and this could not be corrected with increased flow rates. Channels of 100µm allowed for the greatest control over droplet size. The orifice width also affected the droplet size but to a lesser extent, however the dilation of the channel after this point reduced the flow speed and caused congestion of the droplets which contributed to aggregation of the gels (Figure 4.7c). This was sufficiently reduced in devices with orifice widths of 100µm and droplets maintained a steady consecutive stream. The channel angle was less consequential and for simplicity they were oriented to have angles of 60° between adjacent channels and the oil channels in direct opposition.

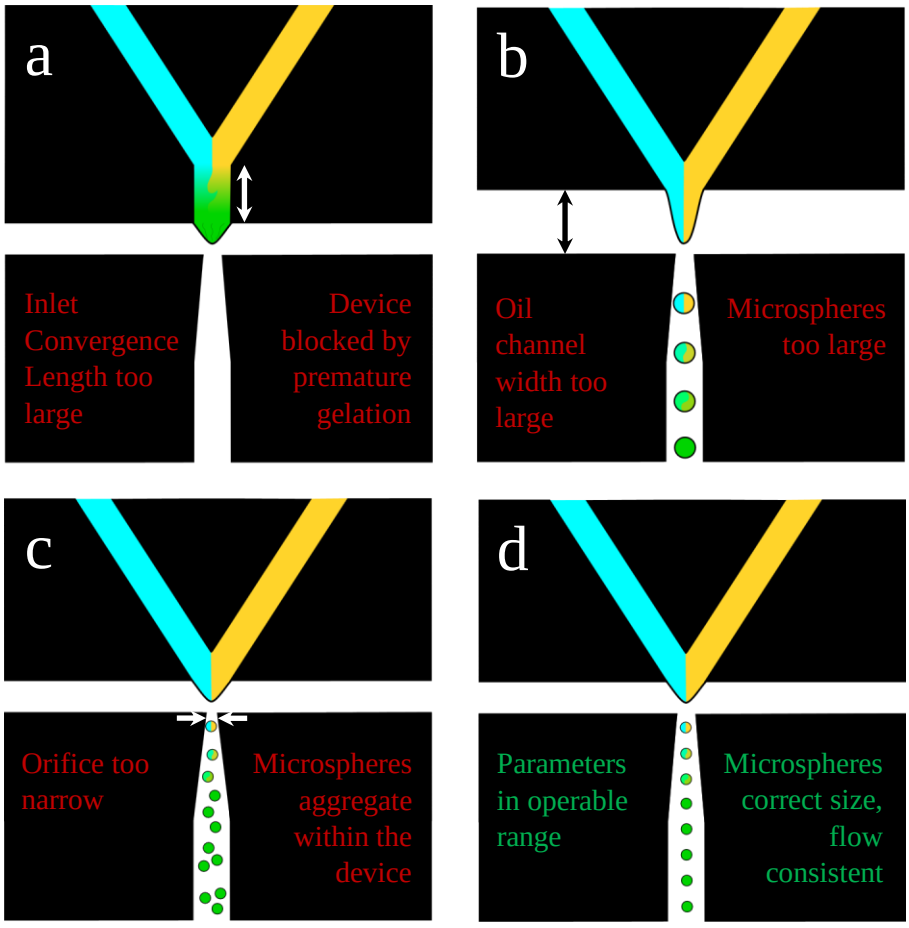

Figure 4.7 *Microfluidic Device Parameter Evaluation.* ***a)*** *Large inlet convergence length caused the gel components to mix before reaching the oil streams and solidify in the channels* ***b)*** *Large oil channels resulted in very large microspheres as the gel streams would bulge further before pinching into droplets.* ***c)*** *Narrow orifice width coupled with channel dilation into the outlet cause the velocity to drop and microspheres would aggregate.* ***d)*** *Devices operating as intended with consistent flow and correctly sized particles with narrow size distribution.*

Several other features were also changed in the second and final iteration to correct some of the problems of the initial design. As the reservoirs capping the inlets were larger than the punched holes these caused stagnation of fluid at the entrance of the device and were subsequently reduced in size to avoid this. The serpentine coil contributed to turbulence at high flow rates, so the number of turns was reduced along with the overall channel length. The reservoir at the outlet terminal was completely removed as the droplets would diverge when the cross-sectional area of the channel enlarged and eliminating this section enabled the droplets to flow in single-file until reaching the collection medium where the reaction could be quenched and gel aggregation could be prevented (Figure 4.8). With these changes, operation of the device was well controlled, droplets could be reliably and rapidly produced, and the collected gels would remain dispersed in suspension without aggregating. The final design schematic is illustrated in Figure 4.9.

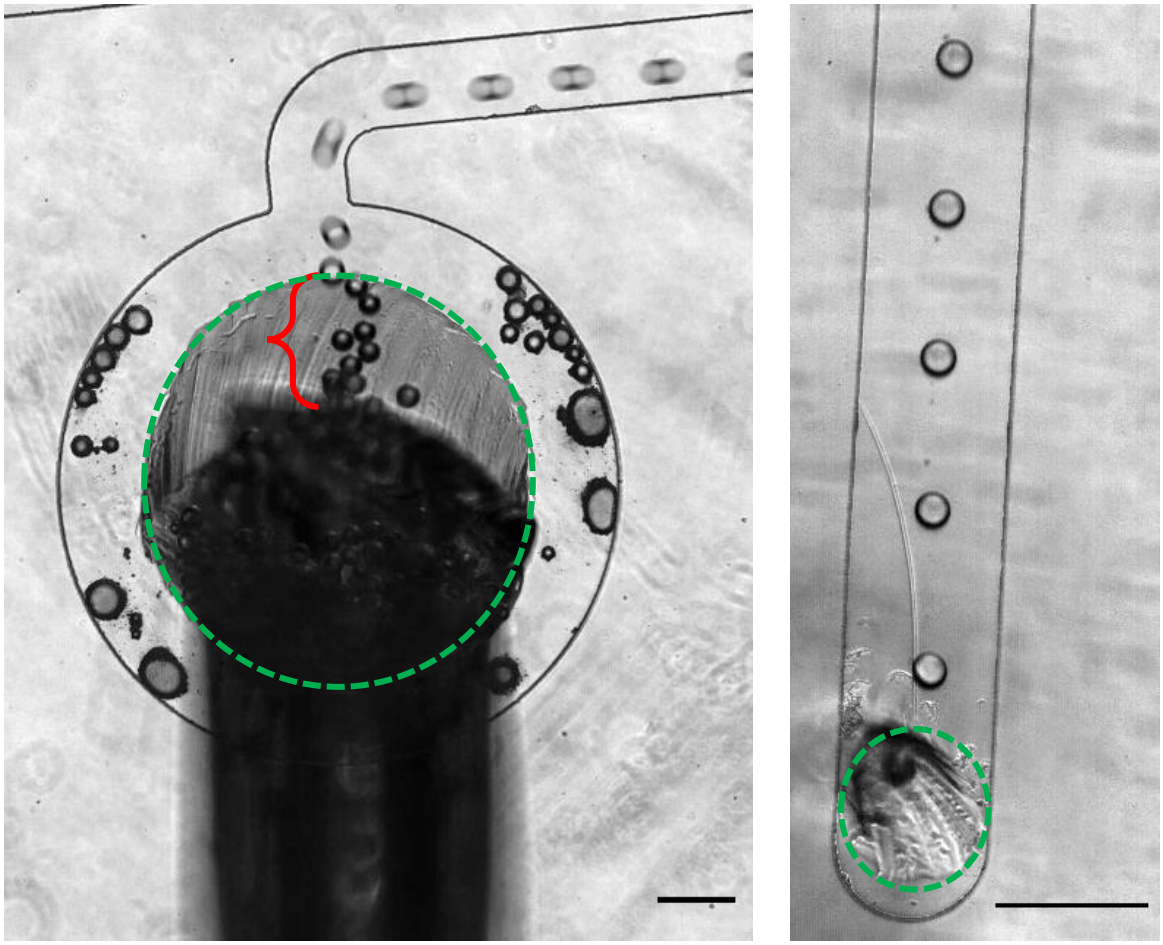

Figure 4.8 *Device Outlets (green ring) with and without reservoir.* ***Left*** *The large reservoir causes the flow velocity to drop and microspheres aggregate as they exit (red bracket). Accumulation of droplets around the edges of the reservoir can also be seen which could allow some microspheres to merge before exiting.* ***Right*** *Reduced outlet size allows for the consistent single-file flow out of the device. Scale = 200µm*

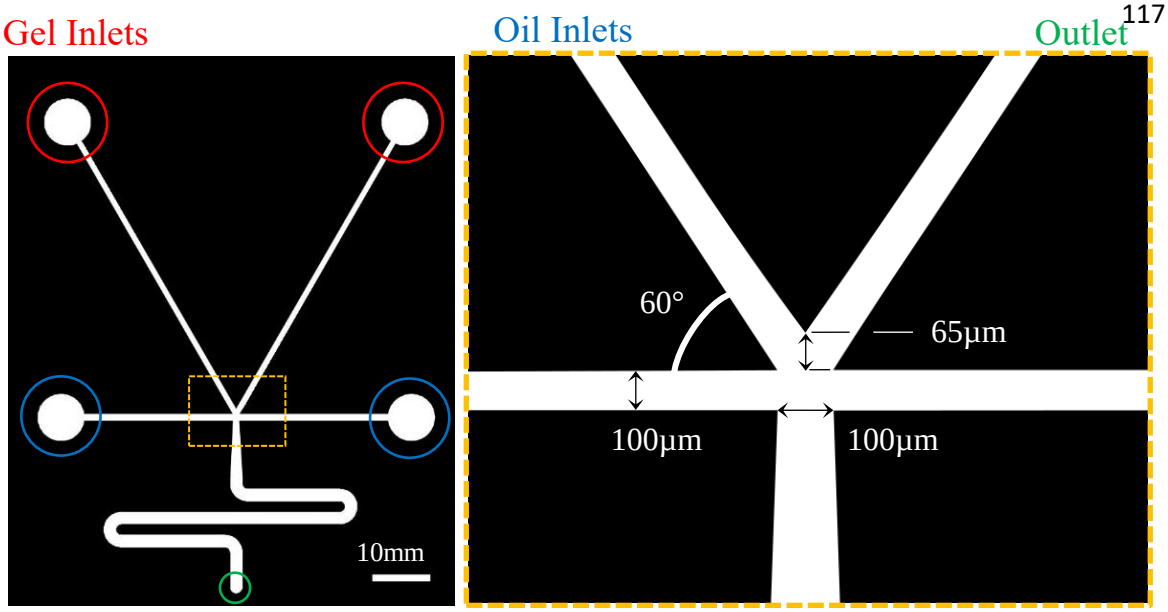

Figure 4.9 *Second and final iteration of device layout. The features that resulted in the best device performance were co-opted into these designs and several others were modified to mitigate notable operational problems (see Figure 4.6 for comparison). The number of outlet coils was reduced, the diameter of the inlet reservoirs were reduced and the outlet reservoir was removed.* ***Inset*** *Channel nexus with optimised sizes.*

4.3.2 Size & Density

The aim of the devices was to produce 50µm diameter microspheres to enable their injection through small diameter needles required for injection, and to be able to produce with them with consistent size. This was successfully achieved using the second iteration PDMS devices. Figure 4.10 shows the collected microspheres after removing the oil and centrifuging several times to produce a maximal density suspension. The 50V:50P RGD and PEG-Only microspheres both had a mean diameter within 2µm of 50µm and a standard deviation of ≤1µm (Table 4.1). Size distribution histograms are also plotted in Figure 4.11.

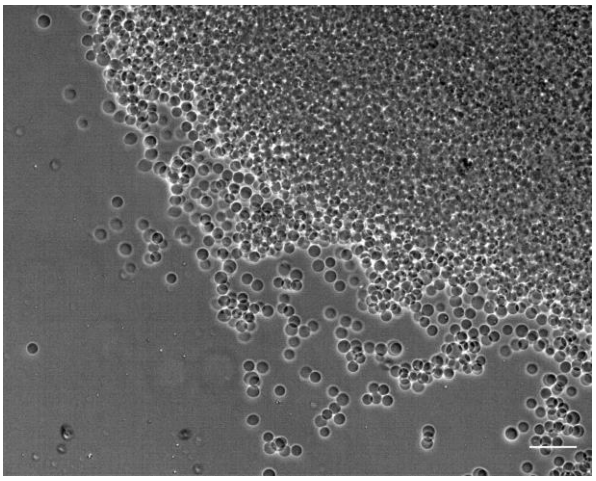

Figure 4.10 *Micrograph of microsphere suspension after collection and centrifugation. Scale = 200µm.*

Table 4.1 Mean size and suspension density of 50V:50P RGD and PEG-Only microspheres.

	RGD	*PEG-Only*
Microsphere Diameter (µm)	51.0 ± 0.6 µm	48.6 ± 1.0 µm
Mean Density (Spheres/mL)	$5x10^6$	$4.7x10^6$

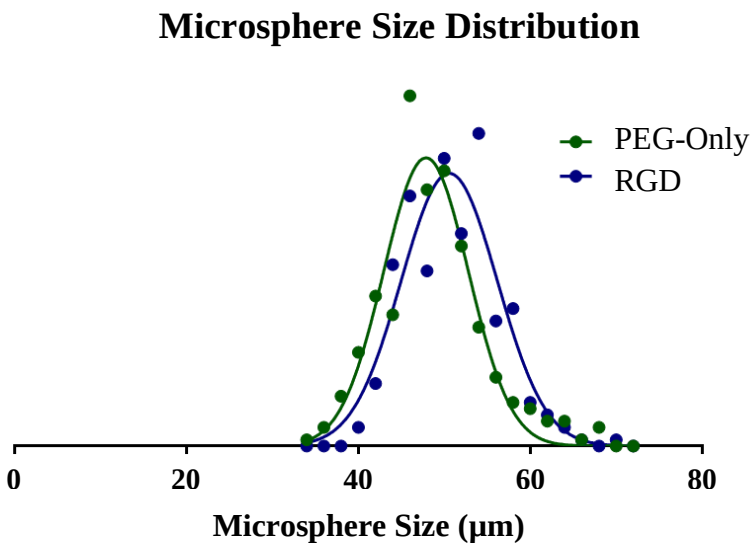

Figure 4.11 Size distribution histogram of 50V:50P RGD and PEG-Only microspheres from 300 individual measurements of each gel type.

4.3.3 Degradability

The microspheres were observed for evidence of degradation for 3 days. Contrary to the bulk degradation experiments, the 50V:50P microgels are seen to degrade over the course of the experiment. (Figures 4.12-4.16). At the initial time point there was an abundance of microspheres with a high opacity after adding the trypan blue contrast. Over time the number microspheres present in each sample with collagenase was seen to decrease. Figure 4.17 displays the reduction in microsphere suspension density over time during collagenase incubation. The 50V:50P RGD and PEG-Only microspheres both have significantly lower densities after 4 hours in 10U/mL collagenase. In the 1U/mL collagenase samples, the RGD microspheres degrade to the point where the density no longer changes within 24h while the PEG-Only gels take 48h to reach this point. In PBS both gel types retain their initial density for the full 72h experiment.

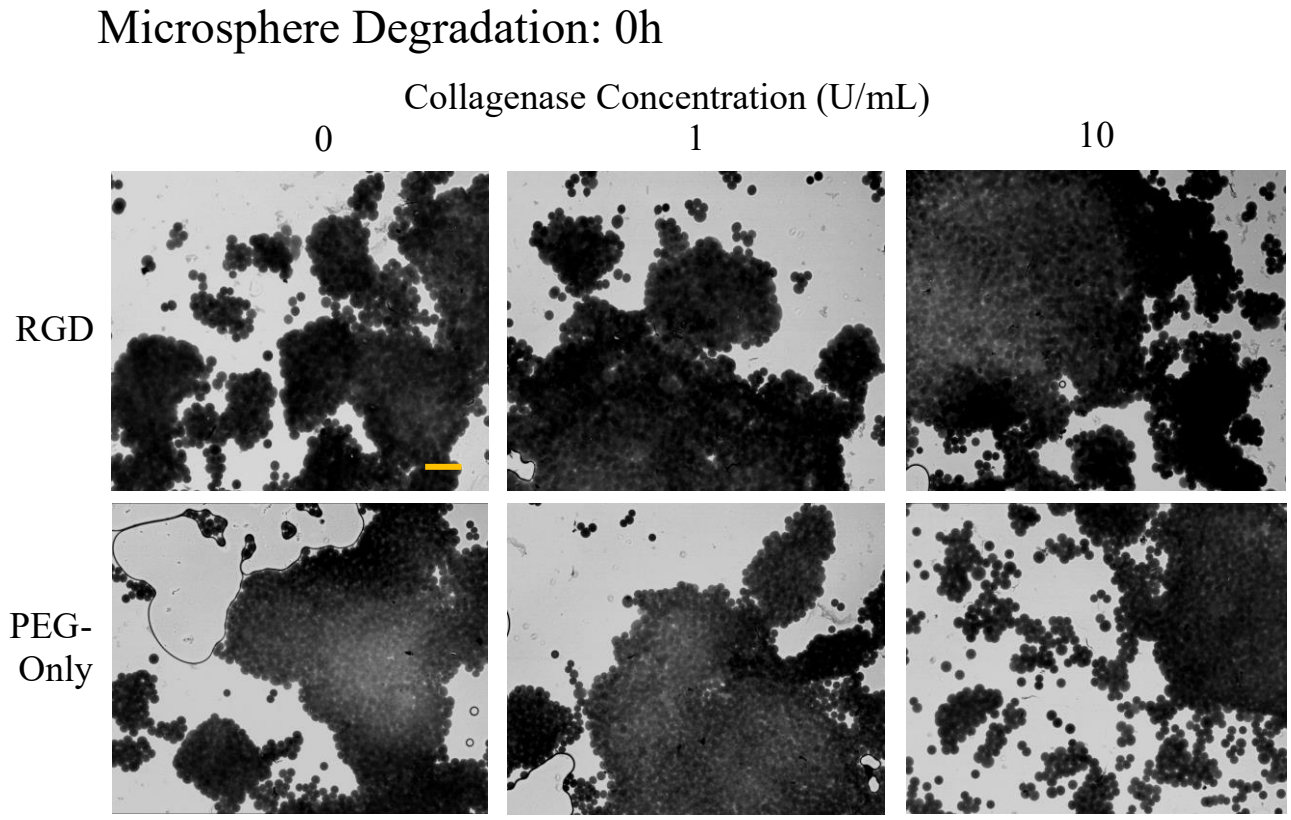

Figure 4.12 *50V:50P Microsphere degradation in collagenase. Time = 0h. At this stage the microspheres are retain high visual contrast and the count density is high. Scale = 200µm.*

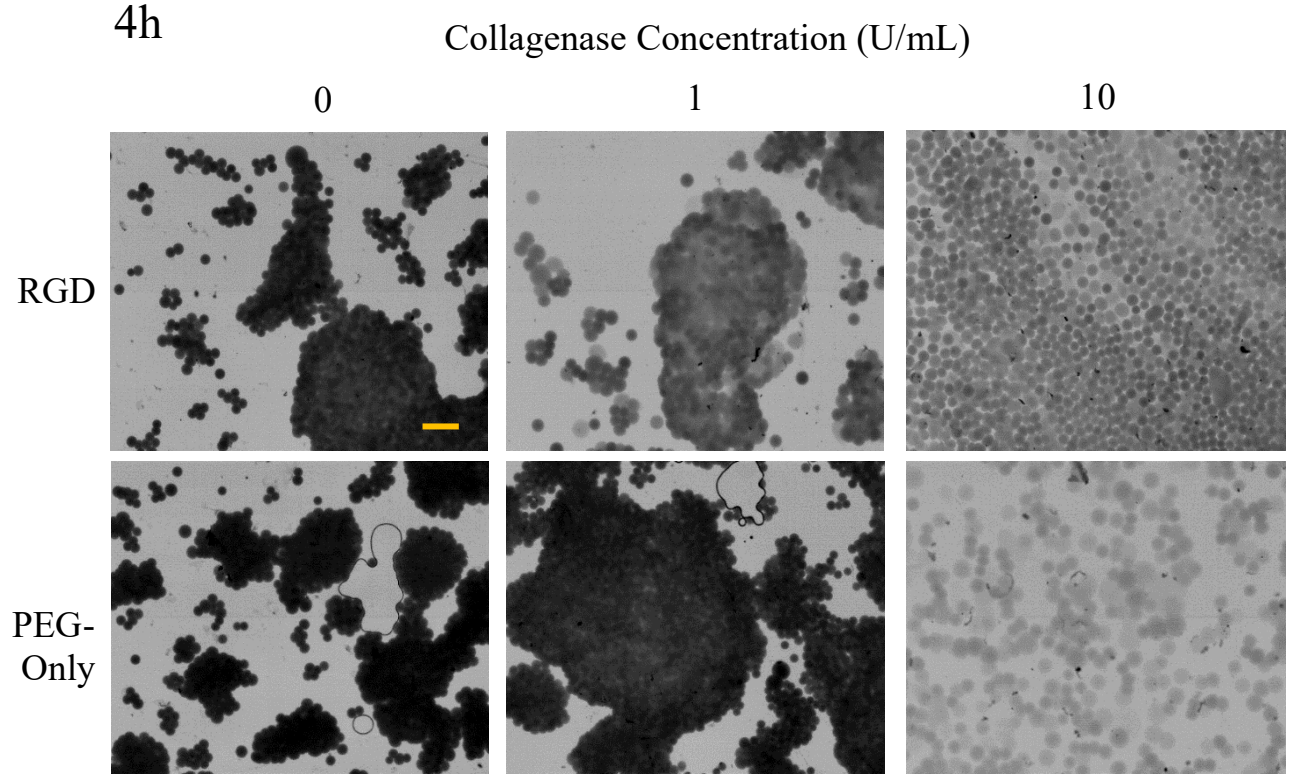

Figure 4.13 *Microsphere degradation, Time = 4h. As the gels degrade, they reduce in number and opacity as the contrast agent retention diminishes. This occurs in a concentration dependent manner as higher concentrations of collagenase accelerate this process. Scale = 200µm.*

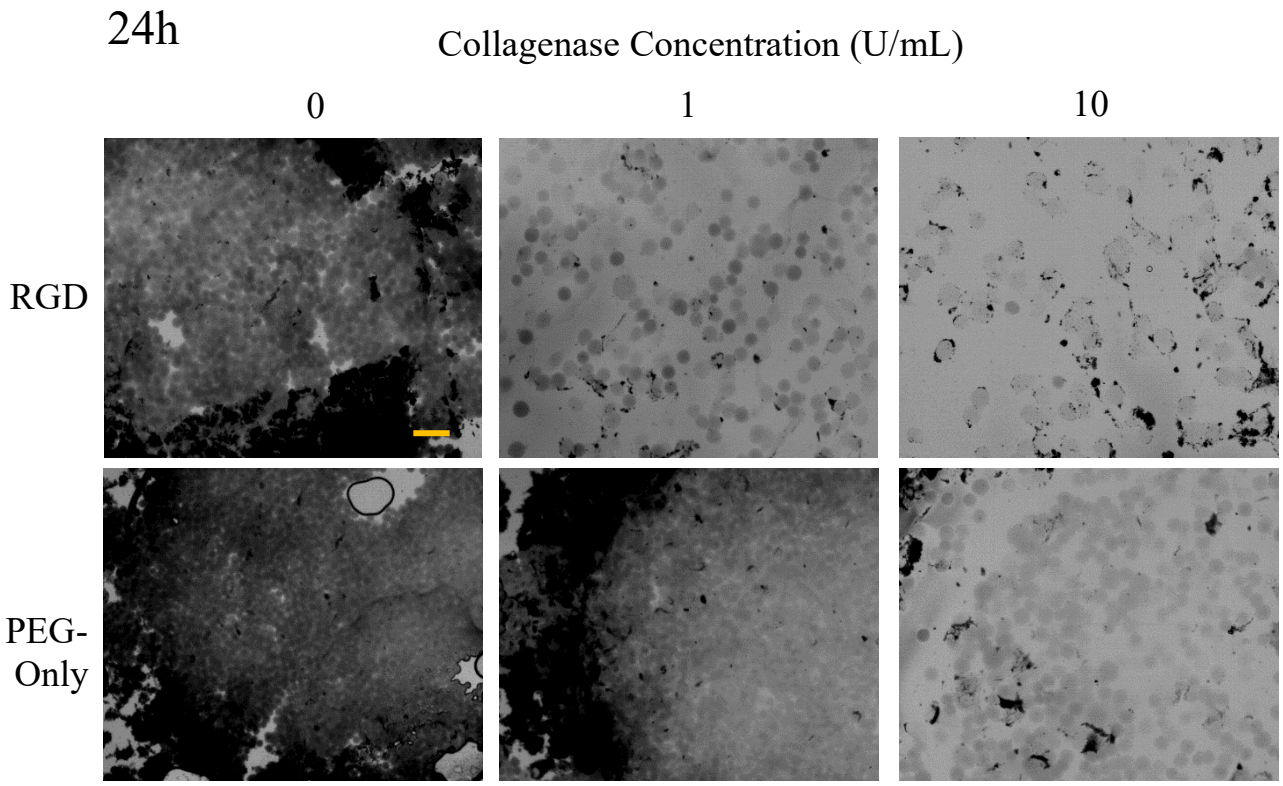

Figure 4.14 *Microsphere degradation, Time = 24h. The collagenase gels continue to degrade. PEG-Only gels lag slightly behind the RGD in terms of reduced microsphere density in 1U/mL collagenase. Scale = 200µm.*

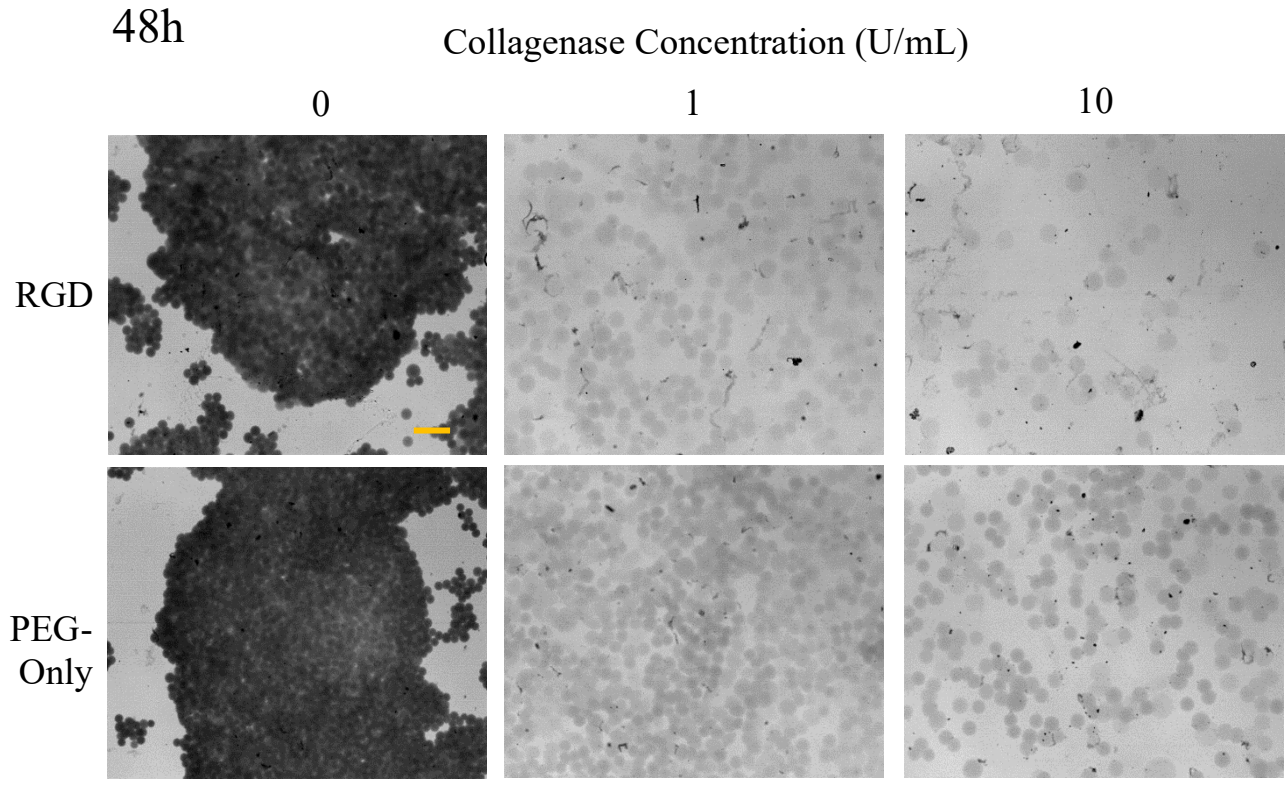

Figure 4.15 *Microsphere degradation, Time = 48h. The collagenase gels continue to degrade. At this stage the RGD and PEG-Only gels appear comparable. Gels in PBS still have high density and visual contrast. Scale = 200µm.*

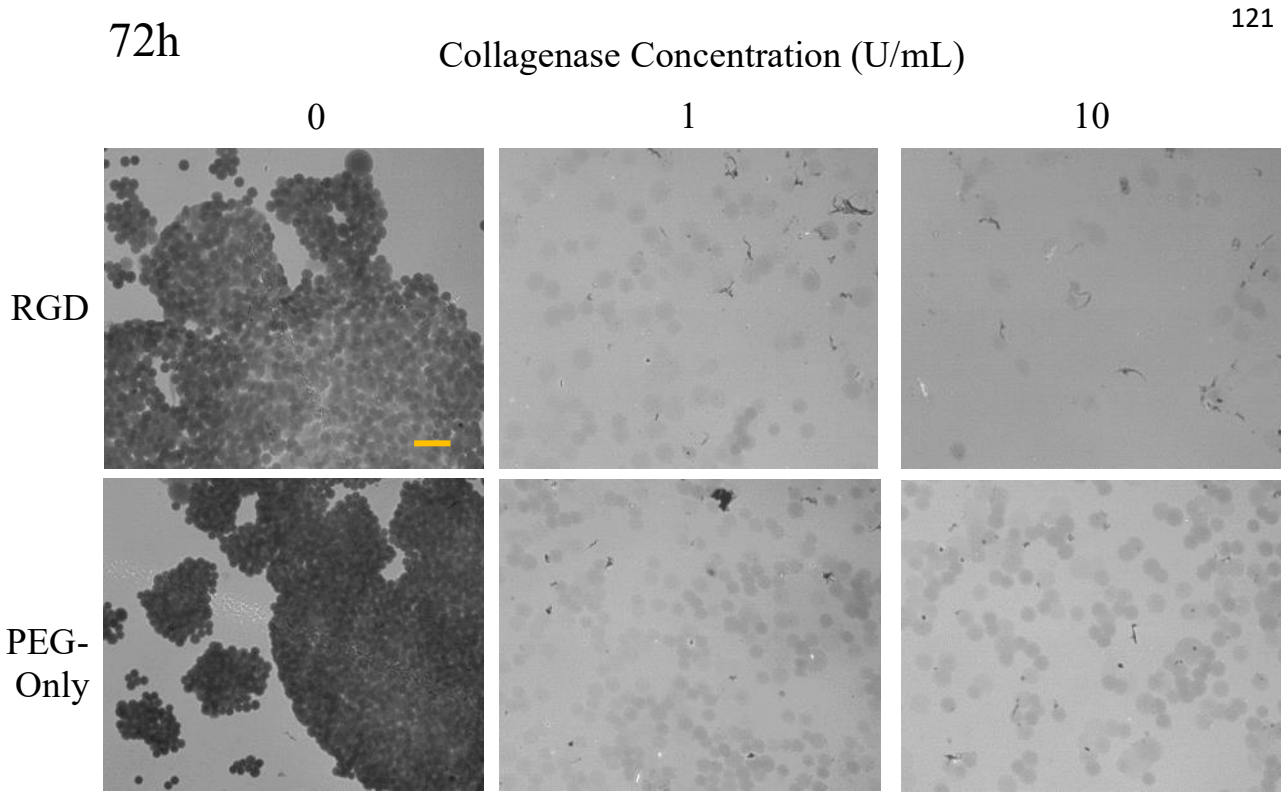

Figure 4.16 *Microsphere degradation, Time = 72h The collagenase gels are still present in small numbers but the majority have degraded. The PBS gels also show signs at this stage that degradation is beginning to occur as visual contrast is diminishing compared to previous time points. Scale = 200µm.*

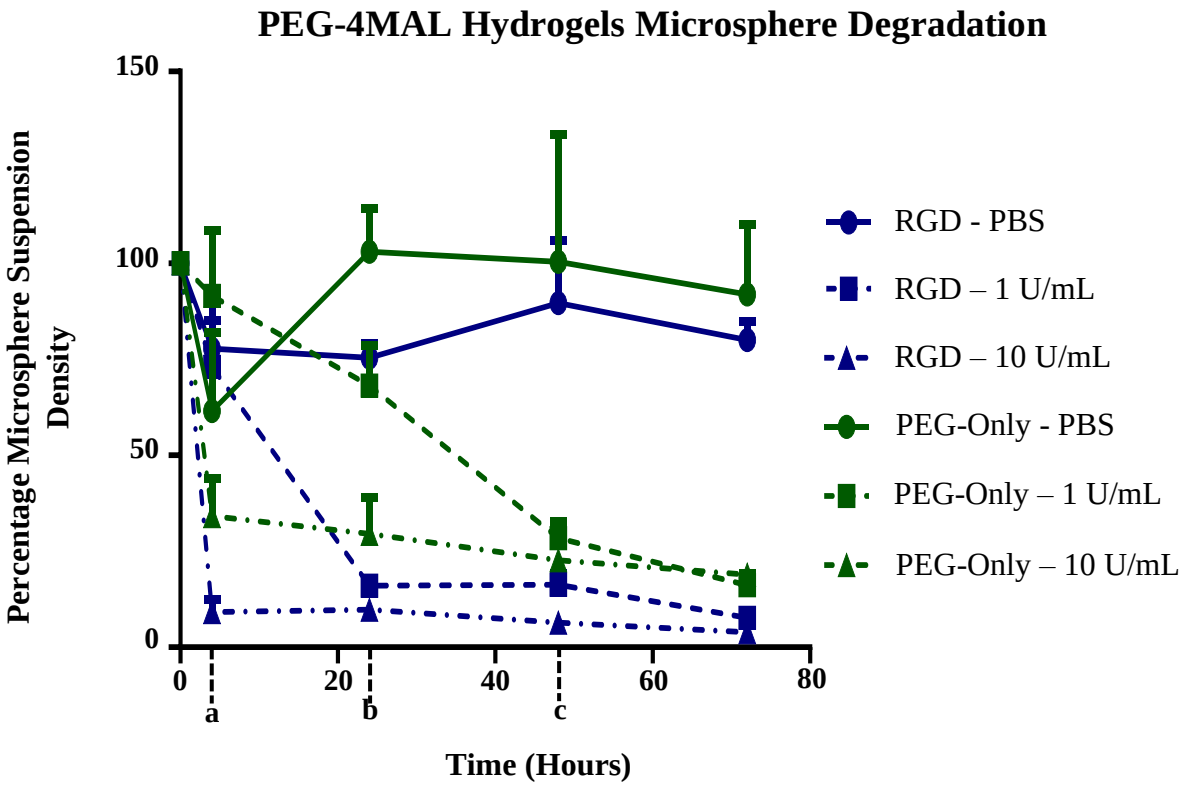

Figure 4.17 *Microsphere degradation quantification. PEG-4MAL gel microspheres were immersed in type-1 collagenase and incubated at 37°C. Degradation was analysed by photographing the microsphere suspension with 10, 1 or 0 (PBS) U/mL type-1 collagenase on a microscope slide and counting the number of microspheres in a 1mm^2 area at several time points. In PBS the microspheres are not a significantly different density after 72h compared each other or compared the initial timepoint. Microspheres in 10U/mL collagenase have a significantly lower density after point* ***a*** *(4h) compared to 0h. At point* ***b*** *(24h), all microspheres in collagenase do not change density significantly at later time points, indicating almost complete degradation, with exception of PEG-Only 1U/mL which occurs at point* ***c*** *(48h). Statistical significance was determined using 2 2-way ANOVAs to compare between groups and across time respectively, each with a Tukey post-hoc test. $p < 0.05$ was considered significant, n = 3 per condition, presented as mean +SD*

4.3.4 MSC Culture on Gel Microspheres

Viability of the MSC cultured on the microspheres was approximately 90% for both the 50V:50P RGD and PEG-Only gels (Figure 4.18). This was comparable to the 2D control as well as the bulk RGD gels and the Matrigel control as described in Section 3.3.1.1.

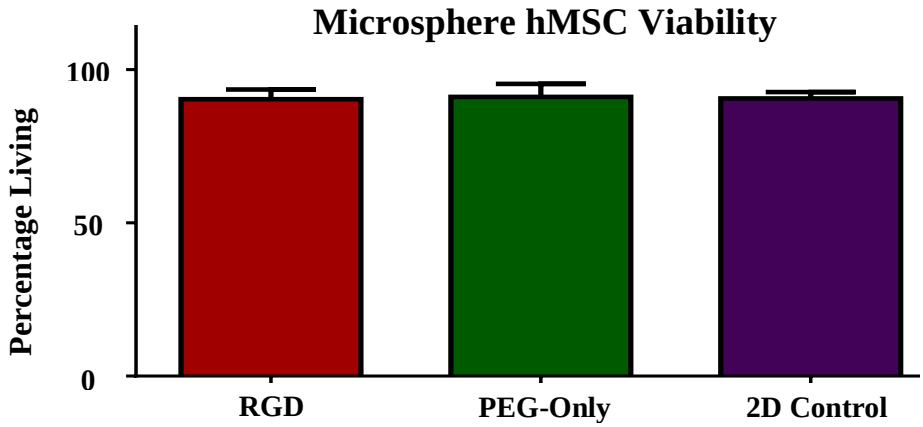

Figure 4.18 *Live/Dead Analysis of MSCs cultured on gel microspheres. Each gel type maintains viability of approximately 90%, comparable to tissue culture plastic controls. Significance was determined using unpaired T-tests, n = 3 per condition, mean + SD.*

There are distinct morphological differences between the RGD gels and PEG-Only gels. The MSCs in the PEG-Only samples have formed a cohesive layer across the surface of the microspheres that appear to be well spread and similar to the 2D controls in appearance (Figures 4.19 & 4.20). It is evident that the microspheres are influencing the cellular morphology to an extent as there are several areas where the cell periphery follows the edges of the spheres, yet they are still confined to a 2-dimensional plane. Conversely, the cells in the RGD samples have interdigitated around the microspheres and adopted a more 3-dimensional distribution. The formation of a monolayer over the microspheres indicate that the cells may be depositing matrix proteins onto the PEG-Only microspheres and binding to this but not directly to the material. MSC are known to secrete ECM proteins to expedite their adhesion (Frith, Mills, Hudson and Cooper-white, 2012) and Hezaveh *et al.* (Hezaveh *et al.*, 2018) have shown that MSCs secrete a range of ECM proteins when cultured in PEG gels which supports the hypothesis they do so in the microsphere cultures. The MSCs on the RGD microspheres are filling the spaces between them and appear to be integrating with the material utilising the entirety of the 3D surface to a much greater extent than the PEG-Only gels. The presence of the cells in 3-dimensions indicates that they have been able to migrate vertically over the spheres or at least remain in place and resist shear forces from media changes after seeding, either of which require the exertion of force on the surfaces and suggest they are binding to the microspheres.

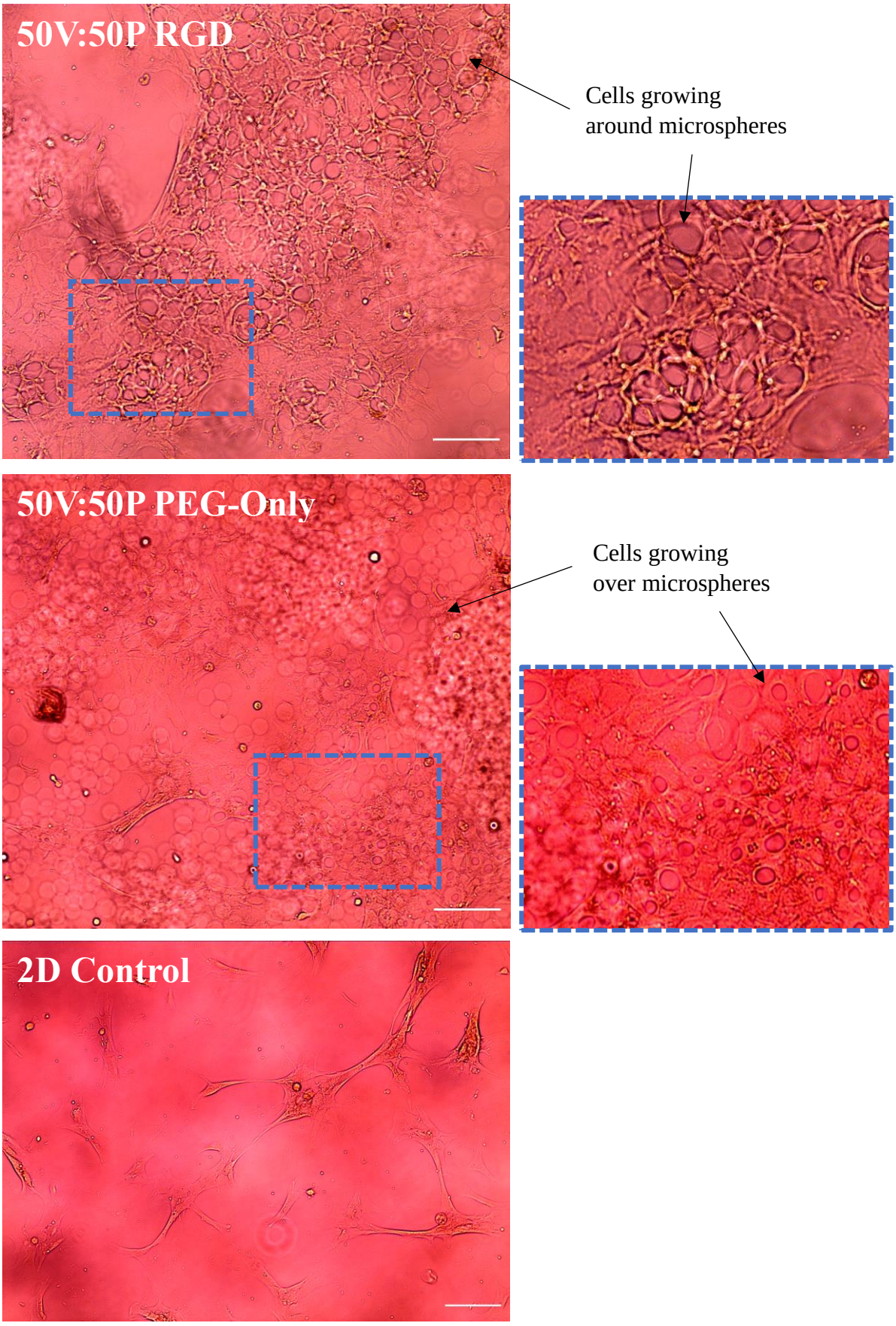

Figure 4.19 *Brightfield images of MSCs cultured on gel microspheres after 7 DIV. Gel conditions also display magnified windows to highlight the cell morphology. Cells in RGD samples surround the microspheres and fill the spaces between them while PEG-Only gels encourage the formation of a cell sheet over the surface. Scales = 200µm.*

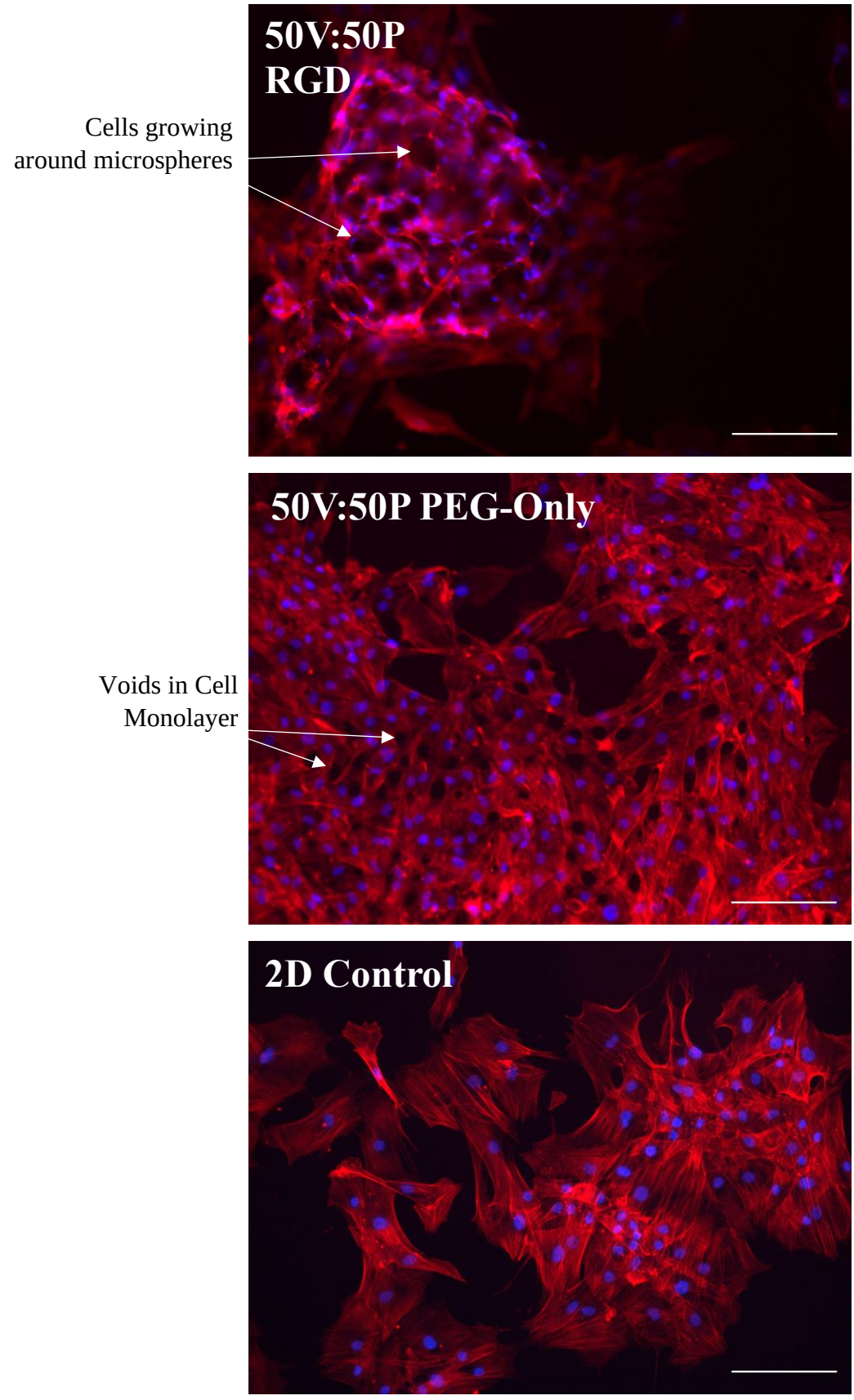

Figure 4.20 *MSCs cultured on gel microspheres after 7 DIV. Stained for actin (red) and nuclei (blue). Differences in cell behaviour are distinct between the RGD gels where growth out of plane and around the spheres is evident and PEG-Only gels where only a 2D cell layer is visible with a number of circular voids that pinpoint the presence of microspheres. Scales = 200µm.*

4.4 Discussion

The devices described in this section are suitable to produce monodisperse suspensions of microspheres with the approximate size of 50μm. There is some discrepancy between the degradation behaviour of the bulk gels and the microspheres. The bulk 50V:50P gels were seen to be resistant to degradation independent of the concentration of collagenase though this was not the case for the microspheres which did degrade over time, however some of these microspheres were still present after 3 days in collagenase. There are several reasons why this may be the case. It is possible that inhomogeneities which are negligible in bulk gels become magnified in the microscale and the cross-linking proportions vary somewhat between each microsphere. The syringe pumps can introduce small oscillations in the flow rate due to the incremental motion of the stepper motor driving the fluid, and though measures were taken to reduce this it may factor into subtle variations. Additionally, the collection medium contains cysteine to stop the gelation reaction after the droplets exit the device which means the gels may not be cross-linked to the same degree as the bulk gels. Without this element however, the microspheres invariably aggregate upon collection rendering them unusable as they become too large for injection and cannot be further analysed without uniformity. Conversely, increasing the gelation rate by modifying the pH also increasing the likelihood of blockages within the device, therefore the correct balance is critical.

The degradation of the microspheres is based on the concentration of type 1 collagenase, however the concentrations used in the degradations assay is somewhat arbitrary as there is very little information on the concentrations of MMPs present in the spinal cord after injury, although they certainly are present as they are required for matrix remodelling (Hsu *et al.*, 2006). In the MSC cultures however the microspheres are still clearly visible after 7 days which suggests that the release of MMPs from the MSCs is low, however in the spinal cord there will be orders of magnitude greater cell numbers of which different types will secrete varying quantities of MMPs. One approach that may shed more light on the matter would be to culture a range of cell densities onto the microspheres and determine if there is a relationship between the disappearance of the spheres and the number of cells present which may allow a greater degree of accuracy in predictions of material degradation *in vivo.*

The observation of degradation by visual inspection was in this case a useful strategy compared to the measurement of change in mass used for the bulk gels as it enabled the use

of much smaller volumes of gel as the starting mass needs to be reasonably high to sufficiently reduce the measurement error while weighing the gels. Additionally, the use of the contrasting agent highlighted different degrees of degradation through the relative visual contrast that became less pronounced as the spheres broke down. This is not something that would be taken into account with mass degradation as the overall mass would not decrease until the gels were fully degraded and the water within their structure was released. This could also enable the possibility of quantification of opacity as a measure of degradation an alternative to microsphere suspension density.

Another aspect that has not been explored is varying the microsphere size. A diameter of 50μm is approaching the same size range of the cells themselves, and the spread MSCs extend over even larger distances than this. While the MSCs grow effectively around the RGD microspheres, if they were to be used as a delivery vehicle then the ideal approach would be to encapsulate the cells within which may not be feasible with smaller spheres. It is likely that the dynamics of adhesion and cell motility around the spheres would vary significantly with different diameters as the forces applied by the cells to smaller spheres may be enough to displace them, but smaller spheres also provide a greater surface area for adhesion to take place. Platen *et al.* (Platen *et al.*, 2015) similarly demonstrated that HEK cells (and to a degree hippocampal neurons) cultured on poly(2-methyl-2-oxazoline) co-polymer microgels of around 50μm have a tendency to envelop the microspheres and appear to sequester them into small aggregates. Dai et al. (Z. Dai *et al.*, 2016) cultured MSCs on PNIPAM microgels of only 1-2 μm and observed they grew as though they were acting on functionalised 2D surfaces. Allazetta *et al.* (Allazetta, Hausherr and Lutolf, 2013) grew MSCs on PEG microgels with diameters of approximately 100μm and at this size scale the cells could be entirely supported by single microspheres as their substrate. The 50μm diameter was chosen as a target for the pragmatic reasons to allow them to easily pass through microscale needles required for surgical injection into the spinal cord, however further investigation could elucidate whether this size is the most appropriate and whether there could be a conceivable benefit to using larger or smaller diameters.

4.5 Conclusion

The goal of the microsphere production was to generate gel microspheres at a size small enough to be easily injectable into a spinal cord injury site for use in *in vivo* models while minimising tissue damage and a 50µm sphere diameter was chosen to fit this requirement. This aim has been met and production of microspheres using the microfluidic devices has been achieved with good accuracy. There is consistency between the 2 gel types created in average size, size distribution and maximum suspension density. The rate of production is sufficient for *in vivo* trials which only require small volumes of microspheres but could be upscaled by adjusting the flow rates or using additional devices in tandem. The spheres also maintain high levels of viability with cultured MSCs and particularly the RGD gels show indications of cellular adhesion to the material surface in a pseudo-3D form. Coupled with the physico-chemical and *in vitro* analyses of the bulk gels of the same material, this provides a basis of evidence to support further investigation *in vivo,* with the goal of evaluating the potential of the PEG-4MAL for neural regeneration in the context of spinal cord injury.

5. *In Vivo* Response to PEG-4MAL-based Hydrogels in Rat Contusion Models of Spinal Cord Injury

5.1 Introduction

The previous chapters have demonstrated several properties that make the PEG-4MAL hydrogels favourable for neural applications including low stiffness, MMP degradability and the ability to promote the adhesion and growth of selected neural cell types. These finding provide validation to pursue further investigation with *in vivo* models of spinal cord injury. These models provide a significantly more detailed picture of the material capability to promote regenerative effects as the complexity of spinal cord injury cannot be accurately modelled *in vitro*. To evaluate the hydrogels *in vivo,* models of contusion injury were surgically induced in rats and allowed to develop through early stages of injury progression before injecting the PEG-4MAL hydrogel into the spinal cord following the formation of a syrinx. Untreated contusion injuries tend to form cavities that contain only CSF, although in some variants of injury progression a degree tissue sparing within these cavities can be observed with regions of intact cells, ECM and multiple spinal syringes separated by tissue bridges (Ellingson, Schmit and Kurpad, 2010).

The lack of intrinsically viable regenerative mechanisms in the spinal cord after injury also introduces additional constrains for possible interventions as any surgical strategy that aims to use direct interventions in the region of injury cannot do so without causing further damage to the remaining structures. Furthermore, as remaining axons can begin to adopt additional roles through plasticity and neurite sprouting, their functional value becomes even greater after injury (Chen and Zhang, 2015). For this reason, minimising the invasiveness of interventions is a high priority and this can be achieved through use of injectable materials. This can be achieved with hydrogels through different means; with injection of the gel precursors to mediate *in situ* gelation, or as described in this chapter, using injectable prefabricated hydrogel microspheres.

Although there are several animal models available to study SCI such as compression, distraction or laceration (Cheriyan *et al.*, 2014), the contusion injury model was chosen over other possible models for several reasons. This model can be one of the most highly reproducible ways to induce SCI due to the availability of apparatus that can reliably apply an impact with tightly constrained force and velocity to the same location across different animals. Additionally, this model has been studied fairly extensively and the development of the injuries into enclosed cavities can be reliably anticipated (Talac *et al.*, 2004). The formation of these cavities makes them well suited to study the injection of materials as they

act as their own enclosures to hold the injected matter in place, which should remain within the cavity without going off target. Beyond this, contusion is a more clinically relevant model of injury than other potential options such as transection or laceration and the delayed injection to allow wound maturation following injury is also more representative of current approaches to treatment which usually cannot be implemented in the acute stages (Alizadeh, Dyck and Karimi-abdolrezaee, 2019).

The recovery of the injured spinal cord can be assessed at the cellular level by looking at the extent to which the cavity is repopulated by infiltrating cells and other structures. The formation of neuronal axons through the cavity may be the long-term goal of regenerative strategies but other events will usually precede this. The formation of vasculature in the wound site is a positive indicator of recovery as this is a pre-requisite to the formation of healthy tissue and areas that are re-vascularised after injury can also increase axonal growth in later stages (Zhang and Guth, 1997). Astrocytes are known to congregate at the periphery of these cavities to carry out their role in establishing and maintaining the glial scar (Sofroniew, 2009). Migration of these cells away from the boundaries and further into the cavities can provide a foundation for other cells to follow suit by the secretion of chemotactic factors and ECM including fibronectin and laminin (Lukovic *et al.*, 2015). In this regard, the addition of the biomaterial into the syrinx supports this role by providing the physical structures needed to facilitate rapid migration through the cavity which both serves as a substitute for the ECM in the short term and encourages the deposition of additional ECM which can remain in place after the material degradation has occurred. To investigate the effect that injected PEG-4MAL hydrogel into the spinal cord after injury would elicit on these cellular processes, tissue sections of the afflicted areas were cut and stained using immunohistochemistry to highlight axons, astrocytes and accumulation of laminin in and around the spinal syringes.

This chapter details the investigation of PEG-4MAL microsphere delivery into the spinal cord following induction of contusion injury in rats. Firstly, a mechanism of delivery was established, following which *in vivo* trials were commenced using the injectable PEG-4MAL hydrogel microspheres. Immunohistochemistry was utilised to highlight variation in the spinal cord tissues at the wound site between 50V:50P RGD microspheres, PEG-Only microspheres and PBS injected controls. Astrocyte reactivity was also analysed through GFAP intensity analysis and the average cavity size was quantified.

5.2 Material and Methods

5.2.1 Pipette Preparation

Glass capillaries (1mm OD, 0.78mm ID, Harvard Apparatus, UK) were formed into pipettes required for the hydrogel injection into the spinal cord. The capillaries were placed into a capillary pulling apparatus (PE-2, Narishige, Japan) with a heating filament encircling the capillary centre. A current of 20A was run through the filament to heat the glass until melting which was then drawn to a fine point by the weighted grip attached to the bottom of the capillary (Figure 5.1). The capillaries were placed under a microscope and the tip was broken back to form a pipette with an outer diameter of between 80-100µm and inner diameter of approximately 60-80µm using the eyepiece graticule to scale the diameter. These were inspected for regularity and any with cracks or serrated edges were discarded. The pipettes were marked every 2mm to denominate 1µL divisions so injected volumes could be quantified. Prior to use for injection, these were flushed through with ethanol and heated to 125°C for sterilisation.

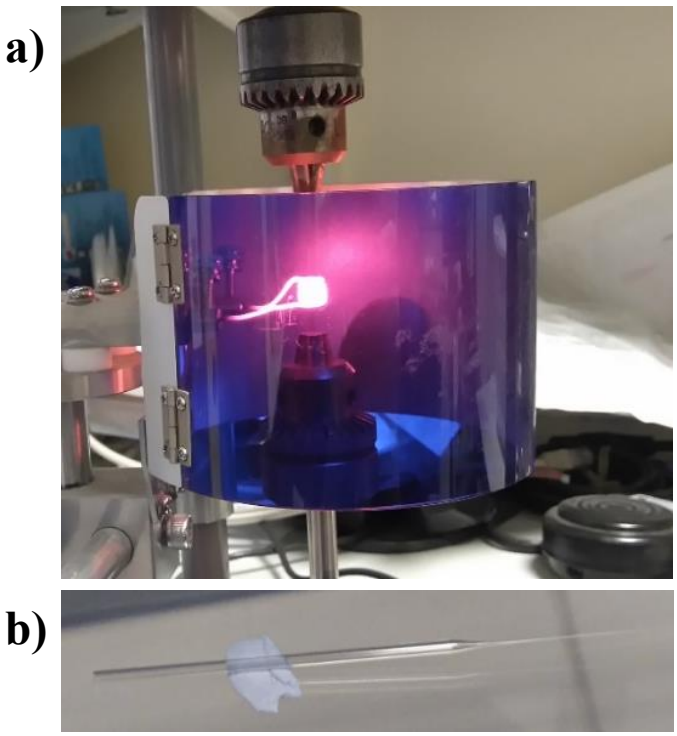

Figure 5.1 a) *Glass pulling apparatus heating the glass capillaries until melting point.* ***b)*** *A newly formed glass pipette.*

5.2.2 Contusion Injury Model

All surgical procedures were performed by Dr. John Riddell (Institute of Neuroscience and Psychology, University of Glasgow) with assistance from myself to prepare the surgical theatre and the materials for injection, and technical staff at the central research facility to oversee animal welfare before, during and after the procedures. They were conducted in accordance with the UK Animals (Scientific Procedures) Act 1986 under the authority granted by the Home Office personal licences, establishment license and project licence following approval from the Ethical Review Process Applications Panel of the University of Glasgow. Animals were housed in procedure-matched pairs where possible with free access to food and water in 12-hour cycles of light/dark. The study with gel microspheres involved 14 male Charles Dawley rats (Charles River, UK) (5 with RGD microspheres, 5 with PEG-Only microspheres, 4 PBS injected shams). As a pilot study, power calculations to determine the ideal sample size were not performed, however similarly structured experiments from literature have used equivalent sample sizes (Jain *et al.*, 2006; Seong *et al.*, 2019).

Prior to surgery the rats were administered Buprenorphine (Vetergesic, 0.05mg/kg, Alstoe Animal Health, UK) and Carprofen (Rimadyl, 5mg/kg, Pfizer, UK) for pre-emptive analgesia and Saline (0.2-0.4 ml/100 gm) to prevent dehydration. Anaesthesia was induced with 5% isofluorane (Abbot Laboratories, UK) in oxygen and the fur covering the incision site was clipped. The animals were transferred to a stereotaxic headframe (Kopf, USA) with an in-house built spinal frame and anaesthesia was maintained by 2% isofluorane in oxygen supplied via face mask. The skin and musculature overlying the cervical vertebrae were incised and a laminectomy of the C5-C6 vertebrae was performed to remove the spinous processes and reveal the spinal cord dorsal surface. The vertebral column was stabilised with Adson's forceps gripped to the C4 and C7 vertebrae and an Infinite Horizon Impactor (Precision Systems and Instruments, USA) was manoeuvred into position centrally over the C6 spinal cord region. An impact of 1.75N was delivered with a 1.5mm diameter circular impactor tip at 100mm/s then a 10-0 marking suture (Ethicon, USA) was placed into the dura over the contusion area centre to denote the injury location for the subsequent gel injection surgery, similarly to previously published procedures (Lindsay *et al.*, 2017). Subcutaneous tissue was closed by 3-0 suture (Ethicon, USA) and cutaneous tissue was closed by application of wound clips. The pre-operative analgesia regimen was also administered one day post-operatively along with saline. Following this, daily assessments were made to judge whether further doses of Carprofen were required.

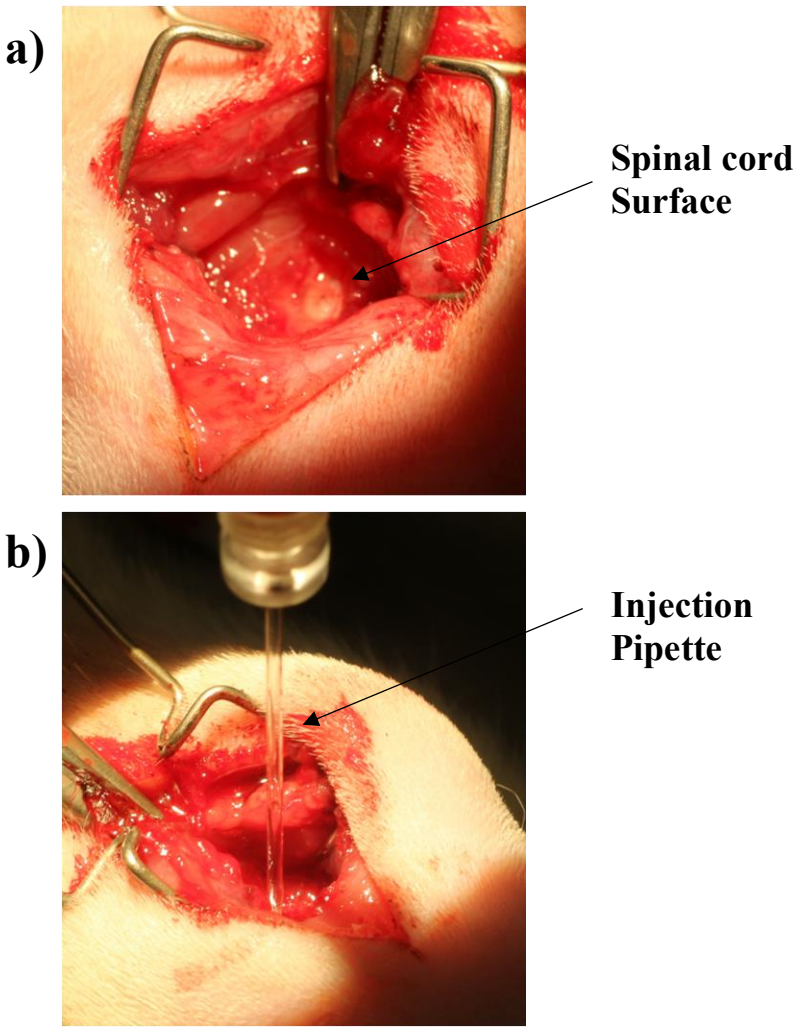

Figure 5.2 a) *Photograph of the surgical site following contusion of the spinal cord.* ***b)*** *Photograph of the gel injection using the glass pipette apparatus.*

5.2.3 Gel Injection

Three weeks after the initial contusion injuries another surgical procedure was performed to inject the hydrogel. This time frame is intended to allow the formation of a syrinx in the spinal cord which can be filled with gel. By this time the cavity has reach a point of stabilization and previous work has demonstrated the cavity size remains consistent with later intervals (Mohamad, 2014). The same pre-operative and post-operative care measures were performed in the injection procedures as with the contusion surgeries. Following onset of anaesthesia, the superficial tissues were incised to reveal the spinal cord and the 10-0 marking suture was located. The surface of the cord was punctured with an insulin syringe needle at this location to create an opening for insertion of the pipette. To perform the injections, the pipettes were loaded with the required volume of gel and were transferred and secured to a motorised stereotactic arc manipulator capable of microscale position adjustment for accurate alignment of the pipette with the punctured opening in the cord

surface. The pipette was lowered approximately 1mm into the opening and gel was slowly injected in the form pre-fabricated microspheres with a pneumatic pump (PV820 Pneumatic PicoPump, World Precision Instruments, USA) which dispenses liquid from the pipettes by the application of pressurised air pulses, until the intended volume was dispensed. Figure 5.2 illustrates the use of the pipette apparatus for surgical injection of the microspheres. 5 animals were injected with 20μL of 50V:50P RGD gels, 5 with 50V:50P PEG-Only gels with the same microsphere densities as described in Section 4.3.2 and 4 with PBS as sham controls. Following this the pipette was withdrawn and the incised tissues were closed by sutures and wound clips as in Section 5.2.2. Animals were perfused with fixative seven weeks after injection.

5.2.4 Tissue Processing

After the designated time period the rats were perfused with 4% paraformaldehyde (PFA) in 0.1M phosphate buffer to fix the spinal cord tissue. Each animal was anaesthetised with 5% isofluorane in oxygen before administering 300mg of sodium pentobarbital (Euthatal, Merial Animal Health, UK) via intraperitoneal injection. The rats were then perfused through the left ventricle with mammalian ringer to expedite exsanguination immediately prior to perfusion with 1L of fixative. After fixation they were dissected to extract the spinal cord tissue. The injury site was located and a section of spinal cord between the C2 and T2 vertebral levels was removed from the vertebral column while leaving the dura behind. The extracted tissue was transferred to a post-fixative solution with 4% PFA and 30% sucrose for cryo-protection and refrigerated overnight. Subsequently the cords were stored in 30% sucrose in 0.1M phosphate buffer without PFA.

From these tissues blocks of 6-7mm were cut from the cord to fully contain the injured region of the spinal cord. A notch was cut in the ventro-rostral corner of the block to identify orientation after sectioning and each of the dorsal and ventral roots were removed. Each block was then cut into 60μm thick parasagittal sections and placed into 0.1M phosphate buffer. Alternating sections were split between 2 containers to allow separate antibody combinations to be used. The sections were then immersed in 50% ethanol for 30 minutes before washing 3 times in 0.3M phosphate buffered saline (double salt PBS). Primary antibody solutions were prepared in double salt PBS with 0.3% Triton-X 100 and spinal cord sections were incubated for 3 days at 4°C using different combinations of the antibodies from Table 5.1. The primary antibodies were washed from the sections 3 times with double salt PBS before adding the secondary antibodies prepared in double salt PBS with 0.3%

Triton-X 100. Section were incubated for 4 hours at 4°C with secondary antibodies using the corresponding species to the primaries with non-overlapping fluorescent dyes as indicated in Table 5.2.

Sections were washed 3 times in double salt PBS and once in 0.1M phosphate buffer, at which point they were mounted onto microscope slides in Vectashield anti-fade medium (Vector Laboratories, UK), sealed and stored at -20°C until ready for microscopy. Tiled epifluorescence image scans for spinal cord sections were taken on an EVOS microscope (EVOS FL Auto) which were stitched together to create images of the full sections using the accompanying software. Additional selected sections were imaged using an LSM 710 confocal microscope (Zeiss, Germany) in tiled scans with 2µm slices of the full section thickness that were combined into a single plane image by max intensity z-projection using the accompanying Zen Black software (Zeiss).

Table 5.1 *List of primary antibodies used for spinal cord section staining.*

Target	*Antibody*	*Dilution*
Neuronal Axons	Mouse Anti-NF200 (N0142, Sigma, UK)	1:1000
Astrocytes	Mouse Anti-GFAP (G3893, Sigma, UK) Rabbit Anti-GFAP (Z0334, Agilent, USA)	1:500 1:1000
Blood Vessels/ Extracellular Matrix	Rabbit Anti-Laminin (L9393, Sigma, UK)	1:100
Neuronal Nuclei	Guinea Pig Anti-NeuN (266 004, Synaptic Systems, Germany)	1:500

Table 5.2 *List of secondary antibodies used for spinal cord section staining.*

Fluorescent Label	*Target (all Abs from Donkey, purchased from Jackson, UK)*	*Dilution*
AlexaFluor 488	*Anti-Rabbit (711-545-152)* *Anti-Guinea Pig (706-545-148)*	*1:500*
Dylight 647	*Anti-Rabbit (711-605-152)* *Anti-Guinea Pig (706-605-148)*	*1:500*
Rhodamine Red-X	*Anti-Mouse (715-295-151)*	*1:100*

5.2.4.1 Tissue Section Analysis

An intensity profile of the GFAP immunostaining was measured to quantify the astrocyte reactivity. This was done with tiled epifluorescence micrographs with imaging parameters kept constant for each section. ImageJ was used to segment regions of the GFAP stained tissue sections of 0.4 x 0.5 mm along the edges of the cavity in each quadrant of the ventro-dorsal and rostro-caudal axes. Figure 5.3 illustrates the process of segmentation and analysis. The intensity was averaged in line-by-line cross-sections (single pixel lines across the width of the boxes) in the orientation parallel to the cavity wall. These boxes were positioned centrally to measure 0.2mm on either side of the cavity boundary. The peak cross-section intensity from each measured area was analysed along with the mean binned integrated intensity profile (summed intensity over 15 cross-section intervals) to display the average intensity profile across the measured areas for each condition. $n \geq 30$ per condition (injected with RGD microspheres, PEG-Only microspheres or PBS), 4 animals each with 2-3 sections per animal and 4 measured regions per section. Some sections were discounted from analysis due to the presence of air bubbles artificially inflating the intensity at the interfaces. Statistical significance was determined for the peak intensity with a one-way ANOVA and two-way ANOVA (condition and distance from cavity border) for the binned integrated intensity, each with a Tukey post-hoc test. The average cavity length was also determined by measuring the largest section cavity of each animal (Figure 5.3). Statistical significance was determined by one-way ANOVA with a Tukey post-hoc test.

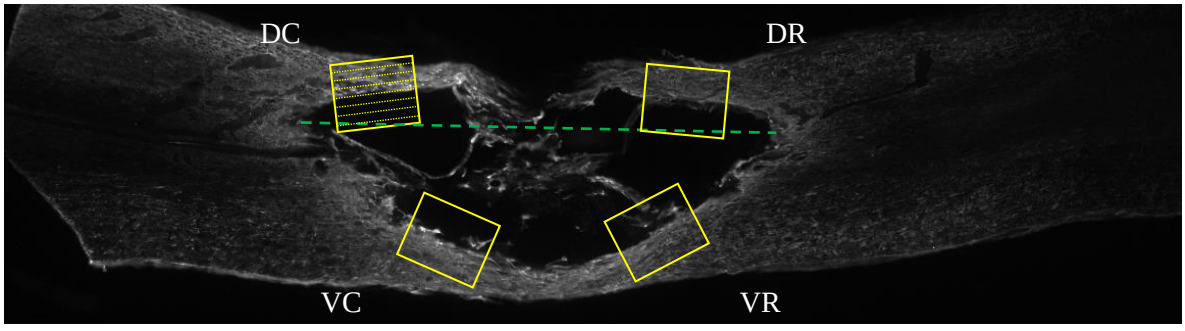

Figure 5.3 *Sample image of SCI Tissue quantification. 4 boxes of 0.4 x 0.5mm (shown in yellow, 268 x 335 pixels) were drawn in the dorso-caudal (DC), ventro-caudal (VC), dorso-rostral (DR) and ventro-rostral (VR) edges of the injury cavity. The boxes were positioned parallel to the cavity border and the image intensity was averaged in line-by-line cross-sections (in pixels) through the box (illustrated by dashed yellow lines), 0.2mm on either side of the cavity border. The binned integrated intensity is comparable to the summed intensity of the areas between he dashed yellow lines (Not to scale). The green dashed line illustrates how the cavity length was measured from end to end.*

5.3 Results

5.3.1 Immunohistochemistry

The microspheres were successfully injected into each of the animals with minimal difficulty. Out of the 14 animals that underwent the injections, 1 from the RGD group did not survive and was found dead without obvious cause the day after surgery. One from the PEG-Only group had an incomplete perfusion and the spinal cord was damaged so tissues could not be processed. Finally, 4 animals from each condition were processed for immunofluorescent staining. In each of the conditions there was considerable variability between each of the replicates. In this section, confocal images have been taken of selected tissue sections that have demonstrated the greatest degree of laminin deposition, astrocyte migration into the cavities and signs of axonal presence in the injured regions of the cord. Epifluorescence photographs of sections from each animal have also been included in the Supplementary Figures (S. Figures 5.1-5.6) to demonstrate the variations between animals for a more complete perspective.

5.3.1.1 Remaining Gel

While the gel is not present in all of the sections with the RGD microspheres, evidence of the gel can be observed in S. Figure 5.1c & d in the form of cohesive patches. Furthermore, the gel is present distinct gel-filled voids that are not enclosed by astrocytes. These appear to be extensions of the original syrinx and the dense accumulation of gel indicates that their presence are the consequence of the injection. Pockets of gel appear to extend along the centre of several sections and it is likely that the microspheres have over-filled the cavity leading to their intrusion along the spinal cord central canal. Gel can also be observed in some of the PEG-Only spinal cords where there are significant quantities of gel remaining within the cavities (Figure 5.5a, S. Figure 5.3a & c). Where gel is visible it does not appear to be well integrated with the surrounding tissue as there is relatively little evidence of cellular infiltration and the boundaries of the cavity abutted abruptly against the gel. They also show no signs of the microsphere accumulation in the central canal observed in the RGD treated groups, however overall the cavities appear larger than in the RGD or negative control. In the RGD animals the laminin deposition and astrocyte morphologies highlight areas that have been filled with microspheres for a period of time but are no longer evidently present.

5.3.1.2 Laminin

The presence of laminin is fairly extensive and particularly highlights the prior presence of the injected microspheres as laminin can be seen as a meshwork in the spaces between the spheres in the RGD injected animals (Figure 5.4b, S. Figure 5.2). In some sections (in particular S. Figure 5.2b) the laminin takes on a somewhat fibrillary appearance that could indicate the formation of vasculature, though elsewhere it is difficult to determine whether the laminin originates in nascent blood vessels or is deposited by other cells to form an ECM. The deposition of laminin is not heavily pronounced in the PEG-Only microsphere animals, though some laminin is evident in Figure 5.5b. In some areas the silhouette of the microspheres can be seen in the distributions of the laminin within the cavity, though to a lesser extent than in the RGD conditions. In S. Figure 5.4c there is particularly abundant regions of laminin in the rostral segment of the cavity, however this is likely to be spared rather than recent deposition. When compared to the alternate staining combination of the same animal in S. Figure 5.3c, a strand of tissue that runs between the dorsal and ventral cavity surface can be seen occupying the same region which has dense astrocytic boundaries on either side. This suggests multiple regions of cavitation as opposed to a single continuous one. In addition to this, similar densities of laminin to those seen in S. Figure 5.3c can be observed in the spared tissue bridging across the dorsal regions in several of the sections, suggesting this region is not composed of tissue that has developed after the injury. The control animals have some similar areas of dense laminin that also follow the areas where axonal staining has been observed (Figure 5.6b, S. Figure 5.6) but there no interlacing distributions as seen in the microsphere injected cords.

5.3.1.3 Astrocyte Infiltration

In the spinal cords injected with RGD microspheres there is evidence of astrocyte migration into the cavities fairly consistently between replicates (Figure 5.4, S. Figure 5.1). In some instances, the distribution of the astrocytes can be seen to highlight the surfaces of the microspheres, particularly at the peripheries of the cavities where they have moulded to the form of the spheres. Astrocytes can also be seen closer to the centre of the cavities in several of the sections and the boundaries of the glial scar appear diffuse as the astrocytes are seen to move further away from the cavity edges. In the PEG-Only gel injected cords the presence of astrocytes in the cavities is significantly less pronounced (Figure 5.5, S. Figure 5.3). They are predominantly distributed around the edges forming a rigid glial scar boundary with little evidence of remodelling. The confocal image of the control animal section (Figure 5.6)

shows a fairly full cavity, however there appear to be voids that are encapsulated by dense layers of astrocytes suggesting these regions mark the boundaries of smaller cavities, though it is not clear whether this is a consequence of regeneration into a wider cavity after injury whether it constitutes spared tissue. The control animals (S. Figure 5.5) display only a modest presence of astrocytes within the cavity and the abrupt delineation of the glial scar is comparable to the PEG-Only animals.

5.3.1.4 Axonal Growth

In the RGD groups the majority of the animals have regions where some axonal growth is evident and can be seen to project into the cavities. Whether these are preserved from prior to the injury is unclear though their presence in multiple replicates highlights some interesting commonalities between the animals as the axons are present in grouped strands along ventral portion of the cavities. In the PEG-Only gel cords there is little to no evidence of axonal infiltration into the cavities, with the exception of those seen in S. Figure 5.3c where there is strand that runs between the dorsal and ventral cavity surface, though as described in Section 5.3.1.2 this is likely to be an area of spared tissue. Similar areas of axonal growth can be seen in some of the control cords in segments between the dorsal and ventral surfaces rather than along the rostro-caudal axis which further suggests the axonal presence seen in S. Figure 5.3c is not a consequence of the gel injection. The confocal imaging for the control animals (Figure 5.6) highlights the presence of axons, though similarly to the astrocyte presence it is not clear whether this is from regrowth or sparing.

RGD Microspheres

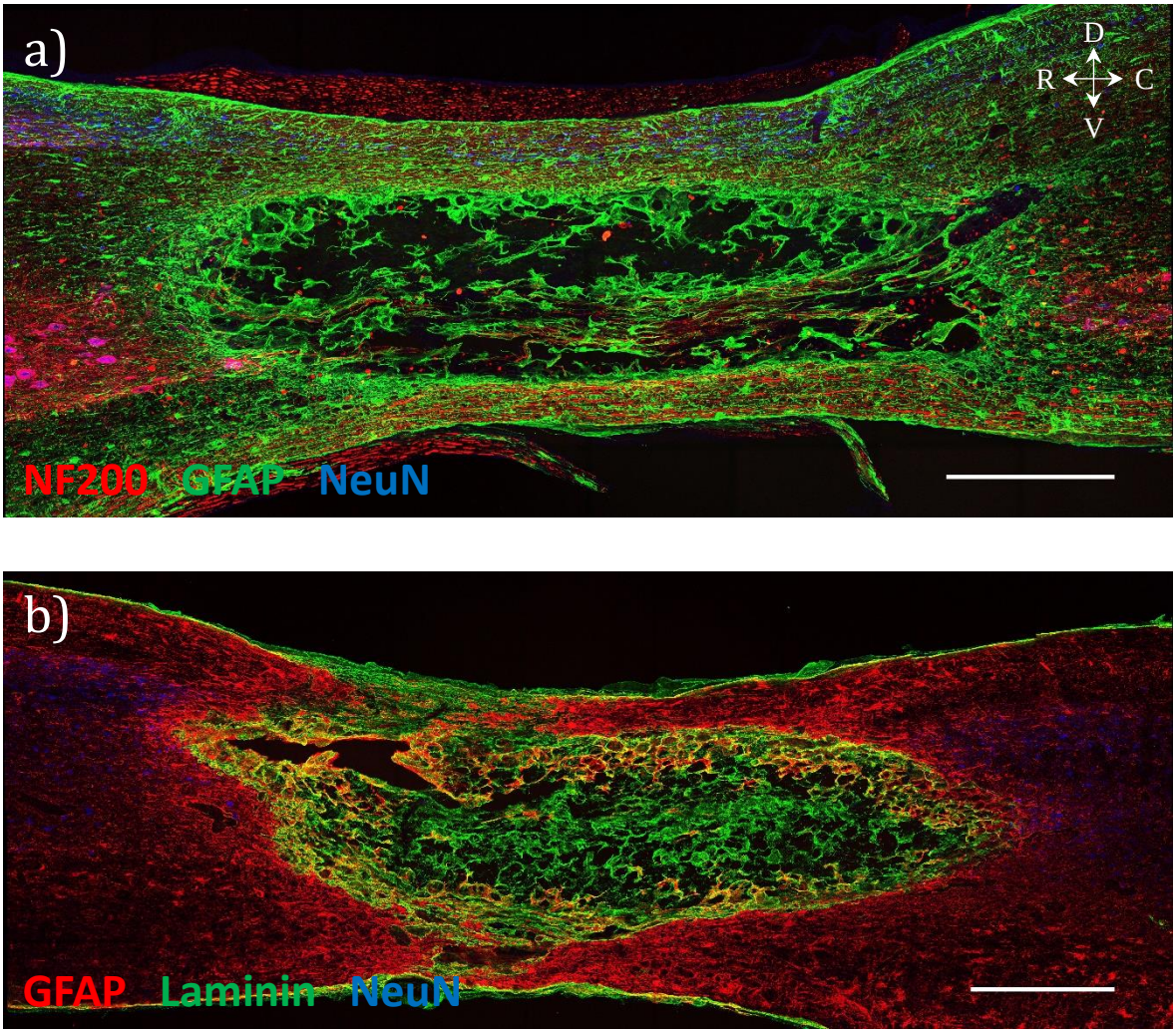

Figure 5.4 *Confocal images of spinal cord sections 7 weeks after injection of 20µL 50V:50P RGD microspheres using tiled 2µm sliced z-stacks with a max intensity z-projection.* ***a)*** *Stained for NF200 (red), GFAP (green), NeuN (blue). Astrocyte infiltration into the injury cavity is fairly wide and in some areas can be seen to follow the microsphere distribution. There is a degree of axonal growth through the injury close to the ventral surface of the cord that traverses the whole cavity.* ***b)*** *Stained for GFAP (red), Laminin (green) and NeuN (blue). The presence of laminin can be clearly seen to follow the outline of the microspheres and permeates the majority of the cavity. Some astrocytes are seen to follow this as well albeit to a lesser extent. Arrows in the top right panel indicate the rostral (R), Caudal (C), Dorsal (D) and Ventral (V) orientations. Scale = 0.5mm*

PEG-Only Microspheres

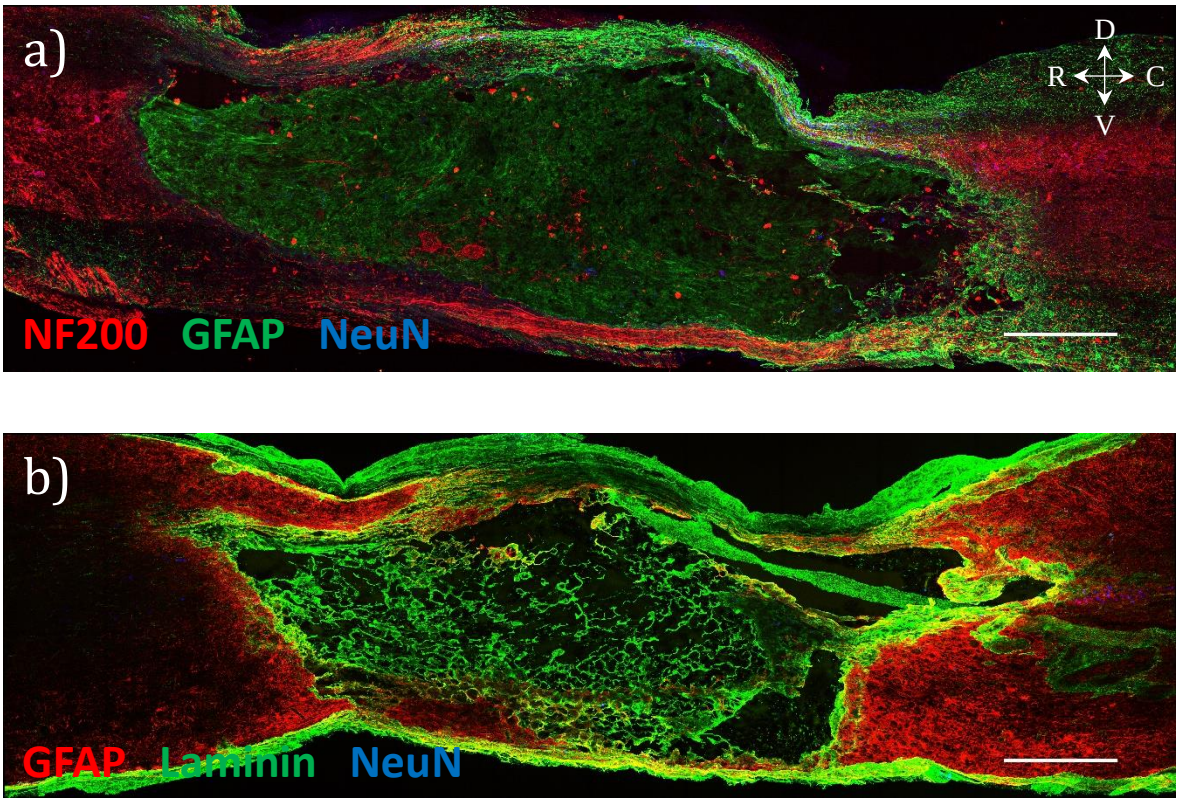

Figure 5.5 *Confocal images of spinal cord sections 7 weeks after injection of 20µL 50V:50P PEG-Only microspheres using tiled 2µm sliced z-stacks with a max intensity z-projection.* ***a)*** *Stained for NF200 (red), GFAP (green), NeuN (blue). The injury cavity is extremely large and contains a large quantity of the gel. There is very little indication of astrocyte migration into the cavity and the boundaries of the cavity are abrupt. There is some sporadic NF200 staining but this does not appear to present a typical pattern of growth.* ***b)*** *Stained for GFAP (red), Laminin (green) and NeuN (blue). The outline of the microspheres can be observed in the deposition of laminin similarly to the RGD microsphere injected sections. The sharp boundaries of the cavity can be observed in the laminin staining and there appears to be poor integration between the cavity edges and the material. Again the astrocytes are constrained to these regions and do not migrate to a large extent into the injured region. Arrows in the top right panel indicate the rostral (R), Caudal (C), Dorsal (D) and Ventral (V) orientations. Scale = 0.5mm*

PBS Controls

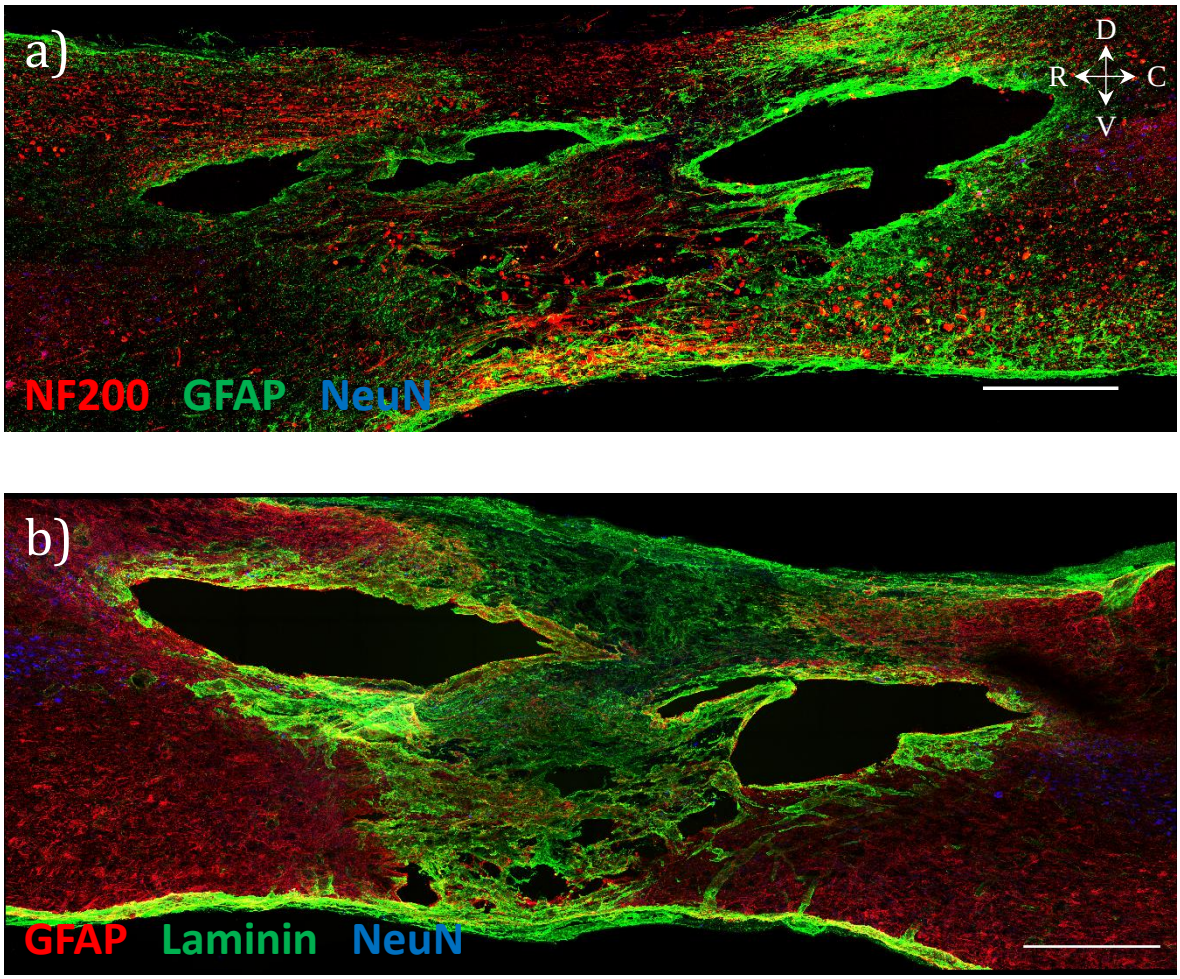

Figure 5.6 *Confocal images of spinal cord sections 7 weeks after 20µL PBS injection using tiled 2µm sliced z-stacks with a max intensity z-projection.* ***a)*** *Stained for NF200 (red), GFAP (green), NeuN (blue). In this section the cavity is fairly well filled and includes both astrocytes and some axons.* ***b)*** *Stained for GFAP (red), Laminin (green) and NeuN (blue). Here the cavity occupies only a small proportion of the section with the rest being filled with laminin and some astrocytes, however there is a visible area of the dorsal portion that does not contain any astrocytes. Some major vessels are also visible on the ventral portion however it is likely these were formed pre-injury due to their size. Arrows in the top right panel indicate the rostral (R), Caudal (C), Dorsal (D) and Ventral (V) orientations. Scale = 0.5mm*

5.3.2 Image Quantification

Quantification of the GFAP intensity has revealed some distinctions between the different injected groups. The intensity was quantified as the averaged intensity of 1-dimensional lines of pixels (cross-sections) running parallel to the cavity border within a bounded area of $0.4x0.5mm^2$ (0.2mm on either side of the cavity boundary, an illustration can be found in Figure 5.3). The peak GFAP intensity highlights the cross-section of the tissue with the highest intensity, which corresponds to the region at the edge of the cavity border where presence of scar forming astrocytes is most pronounced (Figure 5.7). Both types of gel injected animals were similar in their peak GFAP intensity while the PBS injected animals had a higher mean peak intensity. In the PBS injected spinal cords, there are typically very abrupt boundaries which is reflected in the accumulated intensity of the reactive astrocytes while in the gel injected cords the edges are more diffuse in several of the sections.

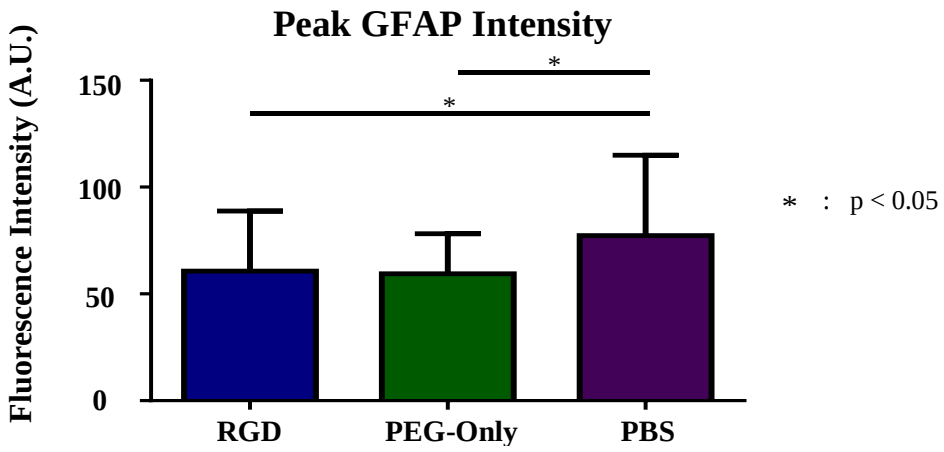

Figure 5.7 *Peak GFAP intensity around SCI injury cavities. The highest peak intensity is seen in the PBS injected animals while the gel injected animals have comparatively lower peaks. n ⩾ 30 per condition (injected with RGD microspheres, PEG-Only microspheres or PBS), 4 animals each with 2-3 sections per animal and 4 measured regions per section. Statistical significance was determined for the peak intensity with a one-way ANOVA with a Tukey post-hoc test.*

The average profile of intensity of the measured areas was generated by binning the individual profiles into summed intervals of 15-cross sections and taking the mean of each interval for all the measured areas of each condition. Figure 5.8 shows the mean intensity profiles for each condition, plotted by the distance of each interval from the cavity boundary. Notably, when quantified using the summed intervals there is no significant difference in the

intensity peak at the cavity boundaries and the majority of the profile is the same for each of the conditions. However, the RGD does have a significantly larger intensity than the PEG-Only or PBS samples immediately adjacent to the boundary in the cavity interior. Overall, the decay of intensity from the edge of the boundary towards the centre is also more gradual for the RGD sections than the PEG-Only or PBS. This could be interpreted as an increased presence of astrocytes having migrated from the cavity wall towards the injury centre. In the images of the RGD samples, there are several areas where astrocytes can be seen to be moving towards the injury core which is not seen to the same extent in the other conditions.

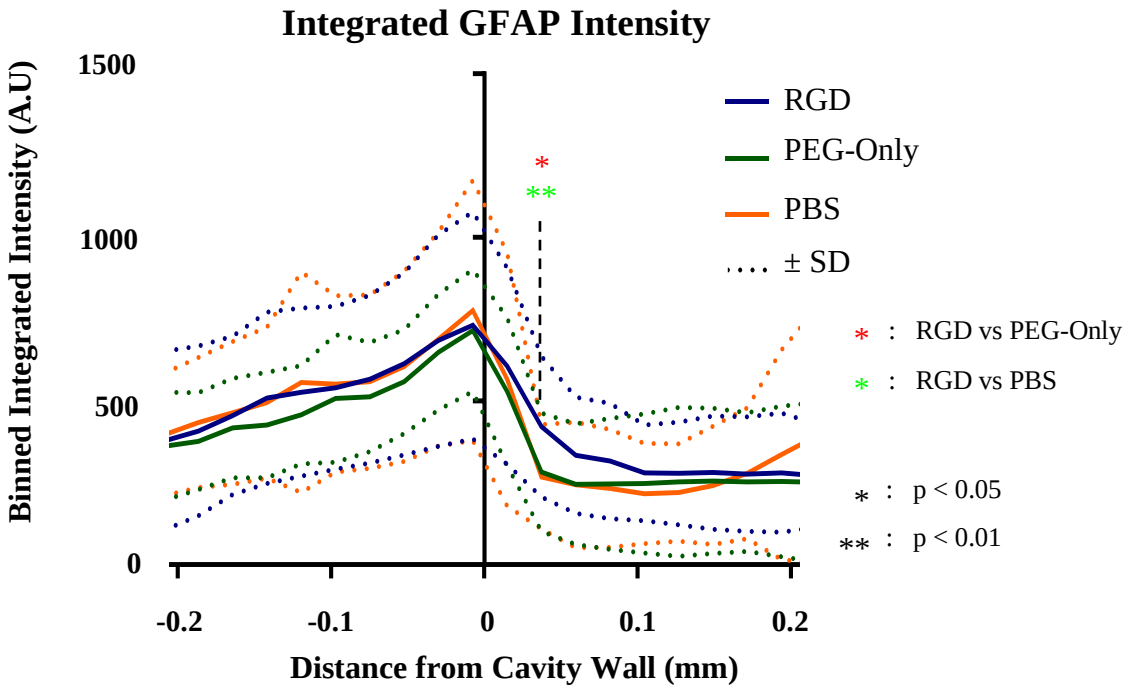

Figure 5.8 *Mean GFAP intensity profiles across SCI cavity boundaries. The GFAP intensity across the SCI cavity peripheries was measured using ImageJ and summed into 15 cross-section intervals (Full description in section 5.2.4.1). Positive values denote distance towards the cavity centre from the boundary and negative values away from the cavity. Dotted lines represent the margins of standard deviation. The mean profiles are predominantly the same for each injected material, exhibiting a gradual intensity decrease moving further into the tissue from the boundary and a sharp decrease moving into the cavity. The RGD cords have a significantly higher intensity on the cavity side of the boundary compared to the PEG-Only or PBS sections. This could be indicative of an increased presence of astrocytes migrating towards the injury centre. n ≥ 30 per condition (injected with RGD microspheres, PEG-Only microspheres or PBS), 4 animals each with 2-3 sections per animal and 4 measured regions per section. Statistical significance was determined for the peak intensity with a 2-way ANOVA with a Tukey post-hoc test.*

The maximum cavity length was also measured for each injured spinal cord. Figure 5.9 shows the mean cavity length, without taking into account the ruptures observed in the cords injected with RGD microspheres, which could be delineated by glial boundaries. Figure 5.10 shows an example of the boundary delineation. By this measure there was no significant difference in the cavity size. If the ruptures in the RGD samples were included in the measurements however, the mean cavity size would increase, possibly significantly, though this was not achievable as the ruptures extended beyond the end of the tissue sections and could not be adequately quantified.

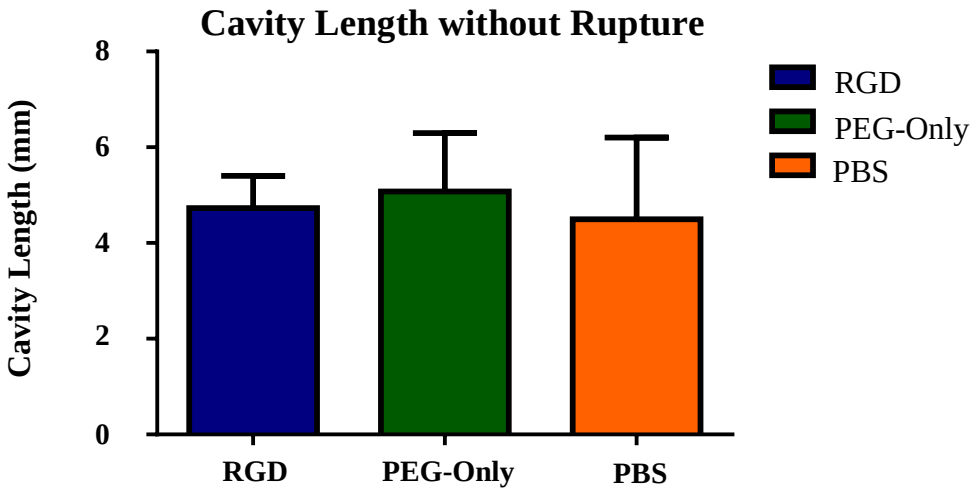

Figure 5.9 *Maximum cavity length, not including ruptured RGD segments. No significant differences were measured in the cavity length of the injured spinal cords, however with the ruptured areas the RGD mean cavity length would be much larger and could become significant. n = 4 per condition,*

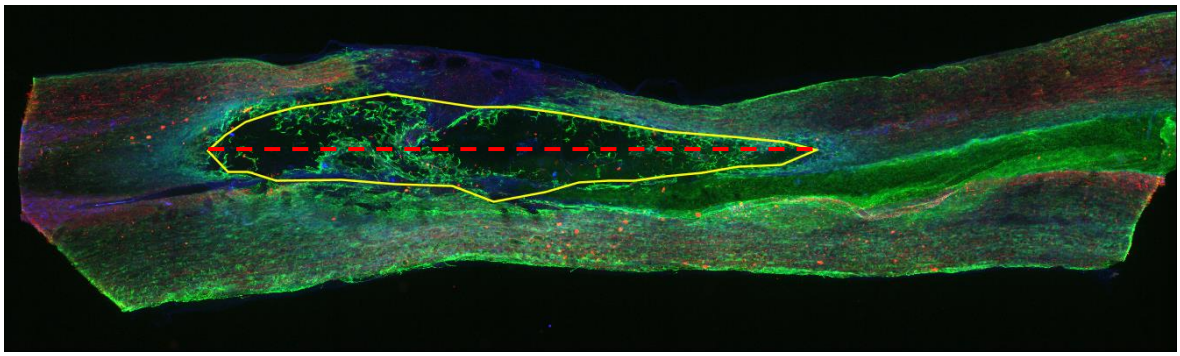

Figure 5.10 *Non-Ruptured Cavity Boundary. The yellow border outlines the formed cavity which is encircled by glia, while the ruptured cavity extends beyond the end of the section.*

5.4 Discussion

Prior to establishment of the microsphere injection protocol some earlier preliminary studies were conducted using the mixed hydrogel precursors in liquid form prior to gelation. Ultimately these studies were not informative towards the efficacy of the gel and were discounted from further study, but they did highlight some problems in the injection protocol and influenced the decision to use microspheres as an alternative option for the injectable PEG-4MAL hydrogels. Firstly, the constraints for injection of the *in situ* gelling mixture were dictated by the gelation time and as such the success of injectability could be predicted from the gelation times seen in Section 2.3.3. The injection procedure took approximately 10 minutes to fully eject the gel volume and only the 100V RGD and IVKAV gels could be successfully mixed, connected to the pump and ejected before the onset of gelation and blockage of the pipette. This determined a large drawback in the injectability of the bulk hydrogel and limited the early *in vivo* trials exclusively to the 100V RGD and IKVAV gels. The same constraints were not placed on the microsphere injections as the pre-fabrication of the gels removed the possibility of premature gelation in the pipettes.

During the surgical injections of the liquid gel precursors there were some notable events that informed the subsequent decisions regarding the injection protocol. While performing the injections, the pipettes encountered repeated blockages despite the non-surgical trials suggesting otherwise. Upon further observation it became evident that a gel plug was forming in the pipette tip stopping any further flow. The likely cause was the buffering of the gel mixture caused by the cerebrospinal fluid as gel could be seen to form rapidly after exiting the pipette. CSF has a pH of approximately 7.4 and is known to buffer the pH of the CNS under normal homeostasis (Siesjo, 1972). Further to this, the repeated blockages made the technique difficult to control and somewhat wasteful if blocked pipettes needed to be discarded. Additionally, mixing the hydrogel precursors with cerebrospinal fluid (CSF) prior to gelation would have an unknown effect on the hydrogel composition. The buffering effect seen by the CSF also ruled out the possibility of modulating the pH of the gel mix for other the gel compositions with faster gelation rates as the same outcome would be inevitable. These factors led to the conclusion that the PEG-4MAL hydrogels in liquid form would ultimately not suitable for large scale investigation. These problems could potentially be overcome using different gelation mechanisms that are not dependent on pH as a catalyst, however when using aqueous constituents there will always be an unavoidable dilution of the gelling substances for hydrogels formed *in situ*. Other models of injury that do not have

enclosed boundaries such as transection may allow more effective CSF drainage, but would also impose the need for a method of containment to hold the material in its intended location.

One of the main issues with regards to the model has been the determination of the optimal gel dose. As the cavity is hidden under the dorsal surface of the spinal cord it not possible to visually gauge how much material has gone into the spinal cord or how much is required to fill it. The original decision on the appropriate volume for injection was a rough estimation of the cavity sizes observed in experiments previously conducted using the same model (Mohamad, 2014). It was anticipated that some indication of outward flow would indicate complete filling of the void with gel however this was not observed, and it was unclear that the gel introduced to the cord had adequately filled the available space. Hence in the microsphere study the volume was increased to 20μL and again no backflow from the cavity was observed, however in this instance it was clear upon inspection of the tissue sections that the volume exceeded the cavity capacity in some cases and intruded the central canal. The fact that this was observed in some of the animals but not all highlights the problem of variability between injury development in the cords, and what may be too much in one instance might be insufficient in another. Therefore, a method of verification to determine the dimension of the cavities preoperatively or the extent of cavity filling intraoperatively with the material would be highly beneficial for pursuing further study.

The cavity size measurements made here are complicated by the rupturing of the spinal cords around the central canal in some of the RGD sections. In each of the sections measured there was evidence of a glial scar rim persisting around an enclosed region of the spinal cord which was taken as the actual cavity size, while the gel filled ruptures did not show an evidently increased glial presence around the boundaries. However, even given this, it is still possible that these ruptures did contribute to a change in size of the portion of the cavity bound by the glial scar and so interpretation of these measurements should acknowledge this. The cavity area or cavity volume were not estimated here as several of the sections, particularly those with large cavities, exhibited buckling of the thin subpial rim upon mounting the sections which would artificially alter the dimensions of the cavity in the ventro-dorsal axis. Were this not the case however, these measures would provide a more detailed picture of the overall injury size.

Fluorescence intensity of GFAP is a commonly used measurement to determine the reactivity of astrocytes in pathological CNS tissue with lower values interpreted as reduced

activation, however even given the frequency of its use there several differing ways it can be computed. Lee *et al.* (Lee *et al.*, 2018) used several measures to define the reactivity of astrocytes based on GFAP fluorescence intensity in a region of interest (ROI), including the number of GFAP positive cells (after intensity thresholding), the mean grey scale values of the ROI and the proportional of the ROI occupied by the thresholded GFAP positive cells. They also observed the establishment of statistical significance between the same measured groups when comparing each quantification method. Li *et al.* (K. Li *et al.*, 2014) used integrated intensity as opposed to mean grey scale value of the ROIs. Jain *et al.* (Jain *et al.*, 2006) used a segmented ROIs to draw an intensity profile and determine statistical significance of intensity based on sub-regions of various distances from the injury boundary in a similar approach to that used here. Ultimately, as the intensity is a product of the imaging systems used and RIOs are highly variable between publications to fit specific tissue dimensions, these measures will not be directly comparable between publications and the key is experimental consistency.

Another issue that was noted was the microsphere adhesion to surfaces including the glass pipettes used for injection. The spheres were seen to stick to the walls of the vessels they were in and as such some would be lost during the injections. Additionally, the microspheres would loosely stick to one another and though they could be separated by mechanical agitation they could still gather and may not have been fully dispersed as they entered the spinal cord. A potential solution to this would be to use an alternative carrier phase or introduction of an additional surfactant to maintain dispersion (Kim *et al.*, 2008). This would ensure that the microsphere suspension is highly uniform and that accumulation or blockages at the pipette tip would be eliminated. However, this may also reduce the likelihood that the microspheres will aggregate within the cavity and it is possible that if the microspheres cannot adhere to each other or be otherwise constrained that they may shift around the which would most likely detrimental to recovering axons due to their fragility.

One potential flaw of using microspheres as a regenerative platform in spinal cord injury is that the regeneration of axons through the spheres is unlikely to be linear across the injury site. The dispersion of the spheres creates a porosity in the space between them and it has been observed in several of the tissue sections that cells follow this pattern as was the case for astrocytes. Heavy laminin deposition into these areas was also observed which would make these avenues for migration and growth even after the degradation of the spheres. Due to the highly directional alignment of axons in healthy tissue this could make re-innervation of the distal segments more laboured. This is one of the main supporting arguments for using

pre-fabricated structures that incorporate guiding structure such as aligned nanofibers (Nguyen *et al.*, 2017) but unlike injectable materials they usually do so at the expense of invasiveness and apposition to the tissues, so a combination of these approaches would be the ideal scenario. Rose *et al.* (Rose *et al.*, 2017) demonstrated a novel system using magnetically oriented anisotropic hydrogels that were also amenable to injection to align neurite outgrowth *in vitro* which could ultimately be a promising line of research if translated *in vivo*.

It is notable that gel can be seen in some of the tissue sections but is absent from others. The evidence of microsphere presence during at least the early period after implantation can be inferred by the meshwork organisation of laminin within the cavities where spherical voids are evident. A possible explanation for this is variable expressions of MMPs within the injury sites that has led to the degradation of the gels more rapidly in some than in others. Both the RGD and PEG-Only microspheres used were produced from single batches so large variations in degradability of the microspheres is unlikely to be the cause. Another possibility could be that loosely integrated microspheres were dislodged during the tissue processing, however as extensive deposition of laminin around the spheres was visible in several sections this is also unlikely to be the case.

Another aspect of study that could have enhanced discrimination between the gel conditions would have been to include behavioural testing in the evaluation of functional recovery following hydrogel injection. Models of contusion injury in the cervical region are commonly used to assess motor function (Nakae *et al.*, 2011) and analysis could be performed using the BBB locomotor scale (Koopmans *et al.*, 2005) to observe differences. However, with the relatively low sample sizes this still would have run the risk of being lost within the variability between each replicate therefore a larger sample size would be required to utilise this measure effectively.

The microspheres used in this study were implemented only in their most basic form and would be likely to benefit from a combination of strategies to deliver growth factors or cells into the environment. Yu *et al.* (Yu *et al.*, 2016) observed an increase in vascularisation, decreased cavitation and improved locomotor scores by implantation of VEGF releasing PLGA microspheres. Jose *et al.* (Hidalgo San Jose *et al.*, 2018) successfully encapsulated and differentiated NSCs into neurons within alginate-collagen microgels and showed promise for translation *in vivo.* From the PEG-4MAL experiments the positive response observed with the MSCs opens up the possibility of stem cell delivery into the cavities using

the microspheres as a vehicle. Additionally, the packing of the spheres throughout the available space would allow cells to remain well distributed throughout the entirety of the cavity and prevent cell sedimentation to the peripheries of the wound. Growth factor release was seen to occur rapidly from the bulk gels and in the microspheres the release of growth factor would be even faster with the increased surface area, but used in conjunction with cell transplants could have a combinatorial enhanced effect *in vivo.*

5.5 Conclusion

The use of PEG gels in the *in vivo* models has given some insight into their potential as a regenerative tool in spinal cord injury. However, although the findings from the data collected are promising, further studies would be required to draw firm conclusions. The evidence suggests that the RGD hydrogels are enhancing astrocyte infiltration into the injury cavity to a certain degree and the images point towards increased deposition of laminin throughout the injury site compared to the other conditions. However, the effects of the material on influencing axonal development in the injury site are not clear. In order to conclusively determine the impact of the material on regeneration within the cord, it is imperative that a method of establishing optimised dosages can be implemented that can ensure there is neither too much nor too little gel placed within the injury. Following this, a larger sample size that could take account of the variability between injuries would also be required. Beyond this, additional modifications or components, such as growth factor loading, could be incorporated into the gel for implantation that could further enhance the regenerative capacity of the material.

6. Final Discussion and Conclusion

6.1 General Discussion

6.1.1. Overview

Overall this body of work has elucidated the character of PEG-4MAL hydrogels using modifications of peptide integrin ligands and variants with different rates of degradability through use of combinations of degradable and non-degradable cross-linker elements. This has laid the foundations for conducting *in vitro* and *in vivo* analyses using these hydrogels and elucidated the favourable interactions that can be achieved using these gels. However, it has also identified several of the limitations that need to be considered and built upon to pursue further investigation and optimisation of the material.

6.1.2. Gel Synthesis and Characterisation

In the characterisation of the hydrogels there were some parameters that were considered to be critical to the utility of the material and so the fabrication was tailored to try and meet specific ranges for these properties. The Young's modulus of a substrate is known to influence the behaviour of cells that attach to it and for neurological tissues the bounds for Young's modulus that have been found to encourage processes such as neurite outgrowth have been reported in the hundreds of pascals to low kilopascal range (Ali *et al.*, 2015; Mosley *et al.*, 2016). Hence the hydrogels were produced to match these values. The degradability of the hydrogels as demonstrated in Section 2.3.2 also restricted the options of available gel formulations to those that were able to remain cohesive for the week of cell culture that was used, though for short term applications such as cell transplantation delivery vehicles this might have been a viable option. Another additional constraint was initially placed on the gelation type as the protocol for injection of the bulk gel *in vivo* required the gel to remain in liquid form for at least 10 minutes. This changed however in the fabrication of microspheres as the rapid gelation was desirable to prevent aggregation, highlighting the benefits of materials with tuneable gelation kinetics. The other measured properties were informative but less critical to the material implementation. The growth factor release from the PEG-4MAL hydrogels was rapid and sustained growth factor release would have been a desirable capability. The materials could have been tuned to maximise this aspect, but doing so would lead to knock-on effects of each of the other properties, for example decreasing the mesh size would increase the material stiffness. However, there may be approaches that could minimise these differences, such as physical tethering of the growth factor to the

hydrogel (Seliktar *et al.*, 2004). Although neither the NGF nor BDNF have unbound cysteines that could participate in the thiol-maleimide addition, a commonly used conjugate for biomolecules is N-Hydroxysuccinimide which can bind to primary amines such as those found in lysine amino acids and protein N-terminals (Morpurgo and Veronese, 2004). PEG bifunctionalised with NHS and thiol could therefore tether the molecules directly, however not without causing an unknown effect on the growth factor presentation.

It must be said however that there are a lot of caveats that come attached to the optimal Young's modulus values for spinal cord applications. Koch *et al.* (Koch *et al.*, 2012) showed that the neurons from dorsal root ganglia show preferential neurite growth on polyacrylamide substrates of 1kPa over a range of 150 to 5000 Pa while hippocampal neurons demonstrated no preference over the same range. Conversely, Zhang *et al.* (Zhang *et al.*, 2014) show improvements in a host of neuronal functions on much stiffer PDMS substrates of ~450 kPa. Koser *et al.* (Koser *et al.*, 2016) have found seemingly paradoxical behaviour in *Xenopus* brains that show axons growing faster in stiffer regions while also being repelled by stiffer substrates in the presence of a softer alternative course. To further complicate matters, astrocytes have been observed to show preference for stiffer materials than those commonly reported for neurons (Georges *et al.*, 2006; Moshayedi, Costa and Christ, 2010). From a physical perspective, the choice of measurement instrumentation will inevitably influence the measurements themselves, as demonstrated by Kingsley *et al.* (Kingsley *et al.*, 2019) who showed the discrepancy between methodologies when measuring hydrogel moduli, and in particular the over-estimation of magnitude when using AFM compared to other common techniques. Therefore, reaching a consensus for tailoring material stiffness in neural applications is not immediately straight forward.

One improvement that could have been made overall to the experimental design would be to incorporate a scrambled peptide into the hydrogels as a negative control to the functionalised peptide gels instead of instead of the non-functionalised PEG-Only gels (Singh *et al.*, 2015). This could have more adequately replicated the properties of the other gels and still remained inactive. While it can't be ruled out that this may have affected behaviour of the cells *in vitro*, the IKVAV gels possessed the same physical properties as the RGD gels yet cells exhibited behaviour very similar to the PEG-Only counterparts, indicating their property differences was not a decisive factor for the poor growth in the PEG-Only gels but was rather a consequence of inadequate integrin ligand availability.

The choice of microsphere size used for injection was a pragmatic decision to accommodate for the size of pipettes used to minimise damage to spared tissues in the contusion SCI models, however using a different model where needle size was not consequential such as a transection model would a wider size range of microspheres to be investigated. This could have been achieved with the existing designs by adjusting the fluid flow rates, or by optimising the device dimensions for larger droplet production (Lashkaripour *et al.*, 2019). Exploring the effect of microsphere size on the interactions with the various cells used could be a useful endeavour as 50μm approaches the approximate size of several mammalian cells (Liu *et al.*, 2016; Placone *et al.*, 2016) the interface dynamics between the spheres and cells would be altered drastically. Moreover, for cell encapsulation applications changing the microsphere size could ultimately affect the delivery and viability of cells as higher flow rates or smaller channels generate higher shear stresses which have been shown to negatively impact cells that flow through them (Varma and Voldman, 2018).

6.1.3 Neural Cell Response to Hydrogels

The poor survival of the encapsulated cells necessitated their implantation via pipette after the hydrogel formation and swelling which introduced some limitations to the experimental model. Cell encapsulation has been demonstrated before using a version of these gels (Phelps *et al.*, 2012), but not with the same cell types and neurons are known to be particularly delicate. The pH is likely to be a factor in this as too long spent in a low pH environment presented by the gel precursors will inevitably impact the viability of cells, and even when steps were taken to minimise the time spent in the hydrogels before addition of media the neuron survival remained low. However, increasing the pH also increases the gelation rate and reduces that practical manageability of the hydrogels and gelation that occurs too rapidly also leads to poor structural homogeneity (Jansen, Galarza and Shelly, 2019) and inevitable experimental errors. Therefore, the alternative route of implantation into the gels was the preferred option over cell encapsulation.

The growth factor release experiments revealed the near immediate release of the growth factors and while this makes them unsuitable for sustained release they could still be used as mechanisms for immediate growth factor delivery. Coupled with cellular implantation this could compound their efficacy, and in the case of stem cells encourage their differentiation along the preferred lineage (Rosner *et al.*, 2012). Their ability for delivery was highlighted with the dorsal root ganglia experiments where differences between the conditions with and without NGF were immediately visible, particularly for the IKVAV and PEG-Only gels.

Additionally, even single dose injections of growth factor have been demonstrated to contribute to positive outcomes following SCI (Widenfalk *et al.*, 2003) so their delivery in the PEG-4MAL gels could still be beneficial.

There has long been a consensus that laminin plays a more dominant role in the regulation of neuronal activity than fibronectin (Rogers *et al.*, 1983; Flanagan *et al.*, 2008) so the resulting findings that the RGD peptide encouraged the formation of neurites in DRG neurons while the IKVAV peptide did not was unexpected. The RGD-bound gels were also seen to result in higher neurite densities for some of cross-linker combinations than the IKVAV-bound gels. The confirmation that the peptides had bound to the maleimide with the thiol analysis presented in Section 2.3.1, along with the concurrence of other physical properties with the RGD hydrogels and the literature that has demonstrated similar findings (Dhillon *et al.*, 2019) lead to the conclusion that this IKVAV peptide is not effective as a hydrogel bound integrin ligand. This raised the possibility that other sequences may be more effective and so a derivate of the looped sequence described by Li *et al.* (X. Li *et al.*, 2014) was trialled that could be implemented as a cross-linker due to cysteine terminations at either chain end, however this sequence proved to by insoluble in PBS and quickly precipitated, making it also inappropriate for use in hydrogel functionalisation. An avenue of research that could lead to improved IKVAV-integrin coupling would therefore be beneficial for hydrogels with neural applications.

6.1.4 *In Vivo* Investigations

The problems noted with bulk gel injections into the injured spinal cord represent an intrinsic flaw with pH driven gelation of hydrogels intended for *in situ* applications as in the presence of biological fluids there will inevitably be a modulation of the pH that will disrupt gelation kinetics. This may be overcome in certain applications where there is sufficient ability to aspirate excess fluid from the implantation site but in the case of the spinal cord, at least in rats, the constant accumulation and replenishing of CSF in the wound site made this untenable. Another model of injury was attempted using a wire knife model of injury to the dorsal columns as described by Toft *et al.* (Toft *et al.*, 2007) to try and elucidate a solution to these issues in the hope that gel distribution could be more easily visualised. While they were informative to a degree, they encountered the same problem with the CSF accumulation and ultimately it was concluded that they would not provide an additional benefit over the contusion models.

The data gathered from the microsphere injection experiments did point towards a net positive effect of these RGD gel microspheres by the reduction in peak GFAP intensity and indications of encouraging the infiltration of astrocytes into the cavities. There were additionally signs that the RGD gels could promote the deposition of laminin around the microspheres and some evidence of axonal growth was also observed. This corroborates with the *in vitro* analyses that the RGD hydrogels enabled adhesion and spreading of astrocytes as well as neurite development from spinal cord neurons and DRGs. However, while these observations provide a basis of support for the efficacy of the RGD PEG-4MAL microspheres as a potential implantable material for SCI repair, further investigation is needed to confirm this effect with greater certainty. A follow up study with higher numbers of replicates would be required to overcome the impact of intrinsic variability of injury progression that comes with the contusion model. Furthermore, an additional body of evidence needs to be generated to determine suitable microsphere dosages, and to confirm that the behaviour of the neural cells seen in the bulk gels is analogous to the gel microspheres. Another line of investigation could also be directed towards microglial activation in response to the hydrogels and indications of other neuroinflammatory events.

One unknown of the microsphere injections is the ability of the spheres to remain in a cohesive formation or whether there was any internal movement and readjustment of the sphere distribution. As they are essentially untethered to one another it is possible that the spheres did not remain in the same position as the animals became more active following the surgeries. This could pose an issue to regenerative efforts, particularly to re-growing axons which are sensitive to mechanical perturbations (A. Saxena *et al.*, 2012). Countering this notion however was the presentation of the laminin as observed in the tissue sections which was seen to be interlaced around what had been the microspheres and this structure would impart some stability to the material overall. Whether this process had begun immediately after injection or if the spheres were sequestered later on is unclear however, and to fully understand this process it would be beneficial to look at additional time points after the gel injections.

The main focus of the histological analysis has aimed to identify and characterise the cellular repopulation of the spinal cord in regions affected by cavitation, but there are other aspects that could also have been investigated beyond those that were chosen for this study. Other options may have shed more light on the differences between conditions such as fibre myelination by staining for myelin basic protein (Bajaj *et al.*, 2013), alternative markers for astrocytic reactivity such as nestin (Cho *et al.*, 2013) or identifiers of new axonal growth or

collateral sprouting using GAP-43 staining (Benowitz and Yin, 2006). Additionally, other outcome measures could be implemented such as locomotor assessment or measurement of stimuli sensitisation to quantify functional restoration. Future experimental designs would benefit from the inclusion of these considerations to gain a more complete assessment of the microsphere efficacy in promoting regeneration after SCI.

6.2 Thesis Conclusions

This body of work has focussed on producing PEG-4MAL hydrogels that are suitable for injection into the injured spinal cord and can enhance the intrinsically low levels of spontaneous regeneration that is usually observed in such cases. Gel formulations have been established to optimise their Young's modulus in the context of the spinal cord to lie between 1-2 kPa and their degradability to be tuneable with the modulation of cross-linker character. These formulations have been evaluated to determine their efficacy in maintaining healthy populations of MSCs, astrocytes and neurons which represent some key potential targets for spinal cord injury repair. The findings determined the ability of RGD bound gels to support each of these cell types. These gels were trialled to be injectable *in vivo* and subsequently modified using a microfluidics-based system to produce gel microspheres to facilitate their expedient delivery into the spinal cord. Finally, these microspheres were used to conduct further *in vivo* studies. Tentative increases in the level of laminin deposition and astrocyte migration into the spinal cord cavity were observed, as well as lower levels of astrocyte reactivity being noted in the gel injected cords, leaving the door open for further investigation.

6.3 Future Work

Due to the observed shortcomings of the IKVAV peptide in comparison to RGD bound hydrogels, a continuation of this project could investigate different forms of the IKVAV peptides with alternative peripheral sequences. This would aim to elucidate one or more sequences that can be incorporated into the PEG-4MAL hydrogels to enable effective peptide-integrin binding and facilitate cellular migration and growth. Additionally, the hydrogels could be modulated to incorporate varying concentrations of these peptides to determine an optimum and could even consider co-functionalisation with RGD.

In vitro work should focus on refinement of the 3D culture protocols to enable additional quantification of outcomes, particularly with astrocytes which were too densely grouped to

enable meaningful analysis. Additionally, co-cultures of several neural cell types could be investigated to elucidate combinatorial effects of neurons and glia presented with different integrin ligands. Further to this, *in vitro* SCI models could be built upon to evaluate these hydrogels more thoroughly.

The microfluidics system developed is capable of producing a variety of gel formulation that could also be used to create spheres of different gel types for implantation and this could make an addition facet to many other concurrent hydrogel projects. Further developing the microspheres by incorporating growth factors and fine-tuning the degradability would also expand the potential applications and efficacy in *in vivo* systems.

The *in vivo* investigations require additional research into a method of evaluating the correct dosage requirements for delivery into the injured cord, or alternatively different models could be investigated provided containment measures could be implemented to prevent microspheres from going off target. The experiments should then be reassessed using this methodology and behavioural testing should also be considered to enhance the experimental impact.

Appendices

RGD (20mM)	*IVKAV (20mM)*	*VPM (50mg/mL; 29.4mM)*
pH = 2.9	*pH = 3.21*	*pH = 3.01*

Supplementary Table 2.1 *pH of custom peptides used in PEG-4MAL gel synthesis.*

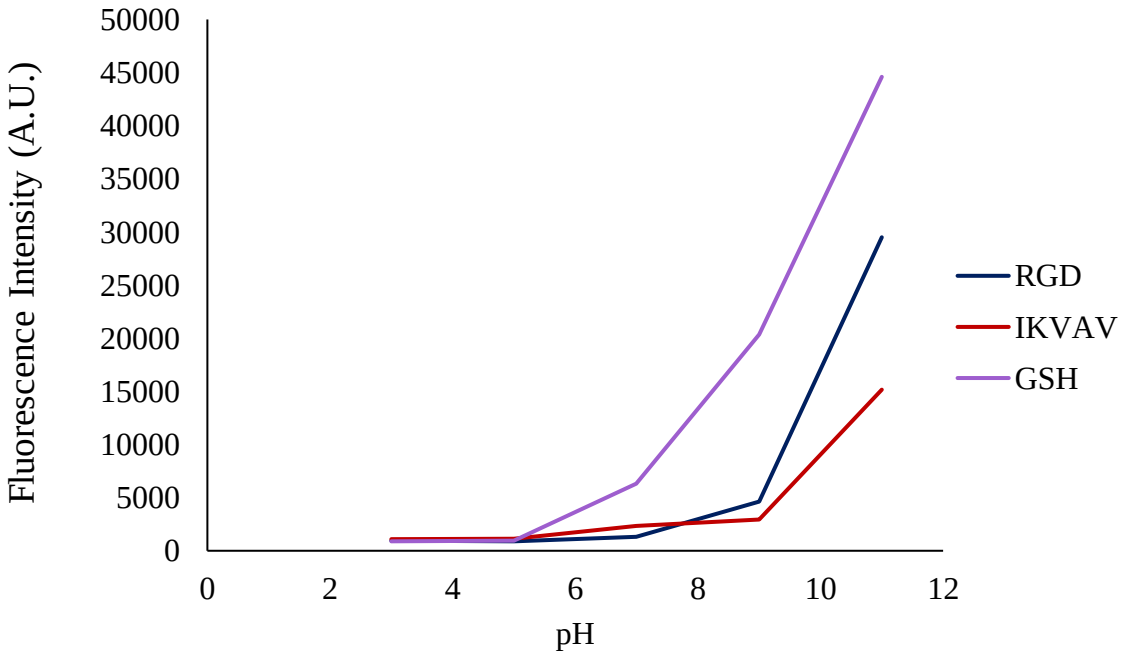

Supplementary Figure 2.1 *Effect of buffer pH on measured fluorescence intensity of 10µM thiol containing components RGD peptide, IVKAV peptide and Glutathione (GSH), diluted in PBS at pH 3,5,7,9 & 11.*

Microsphere Contusion Sections - RGD

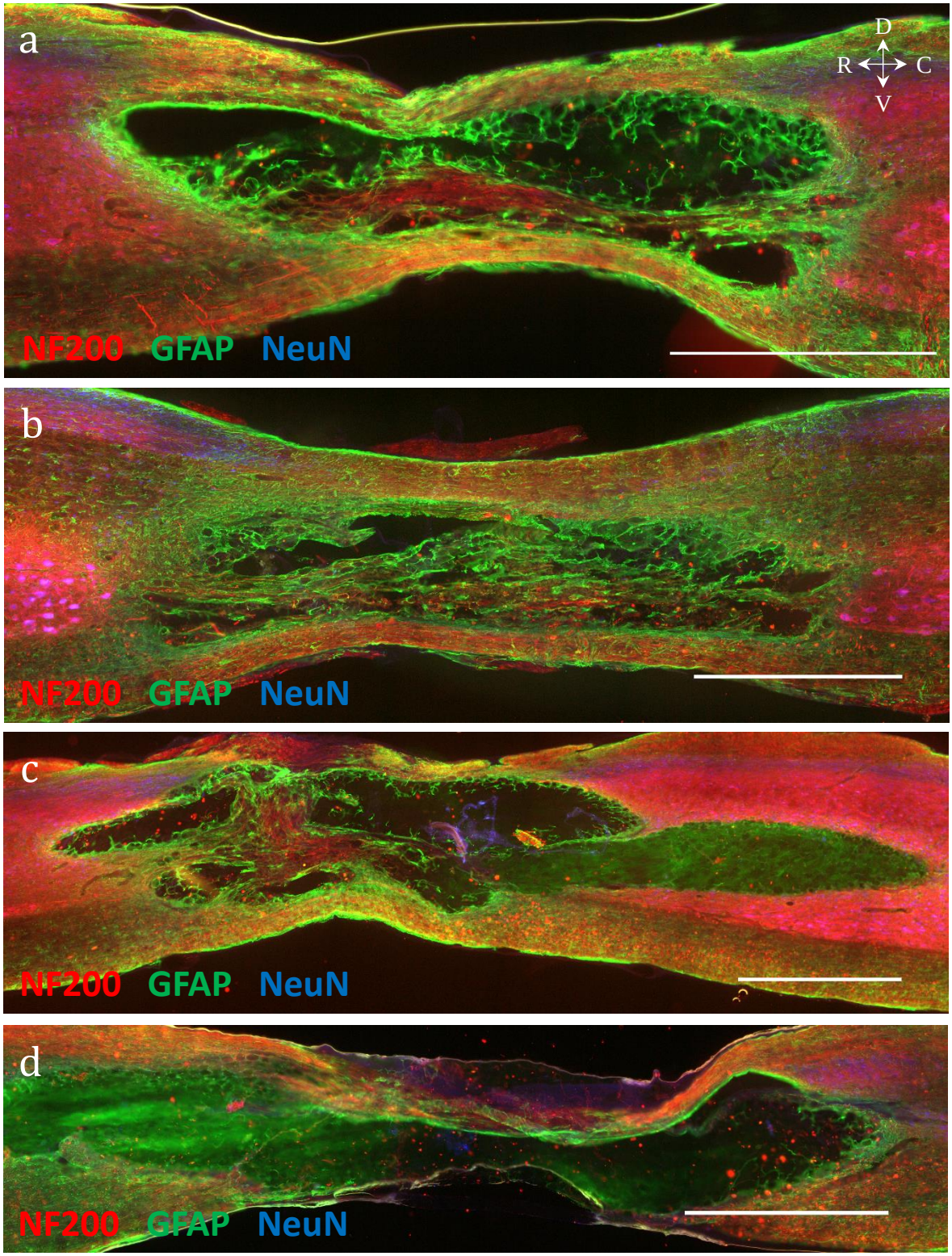

Supplementary Figure 5.1 *Spinal Cord sections from each animal injected with 20µL 50V:50P RGD gel microspheres (a,b,c,d). Stained for NF200 (red), GFAP (green) and NeuN (Blue). Arrows in the top right panel indicate the rostral (R), Caudal (C), Dorsal (D) and Ventral (V) orientations. Scale bars = 1mm*

Microsphere Contusion Sections - RGD

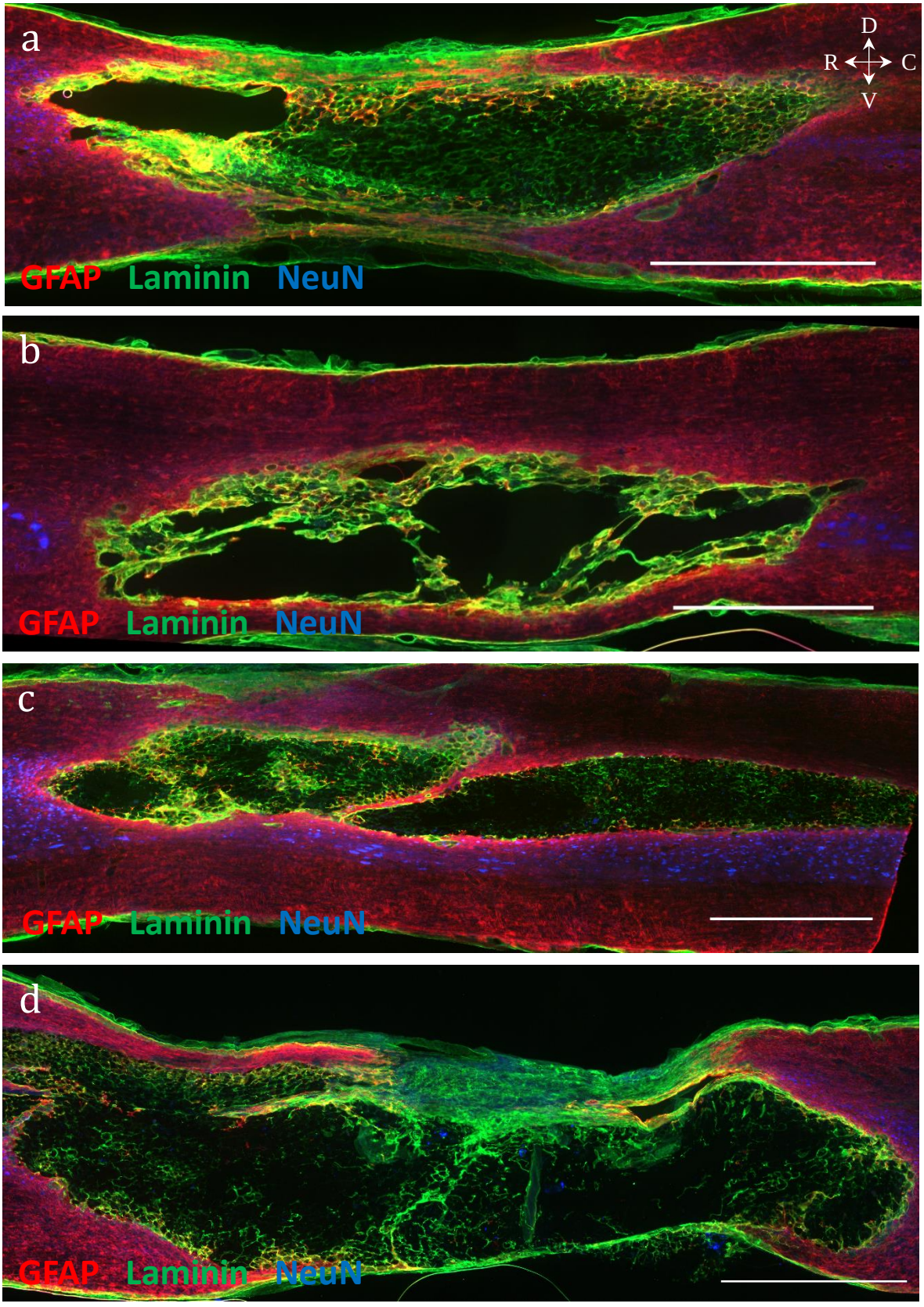

Supplementary Figure 5.2 *Spinal Cord sections from each animal injected with 20µL 50V:50P RGD gel microspheres (a,b,c,d). Stained for GFAP (red), Laminin (green) and NeuN (Blue). Arrows in the top right panel indicate the rostral (R), Caudal (C), Dorsal (D) and Ventral (V) orientations. Scale bars = 1mm*

Microsphere Contusion Sections - PEG-Only

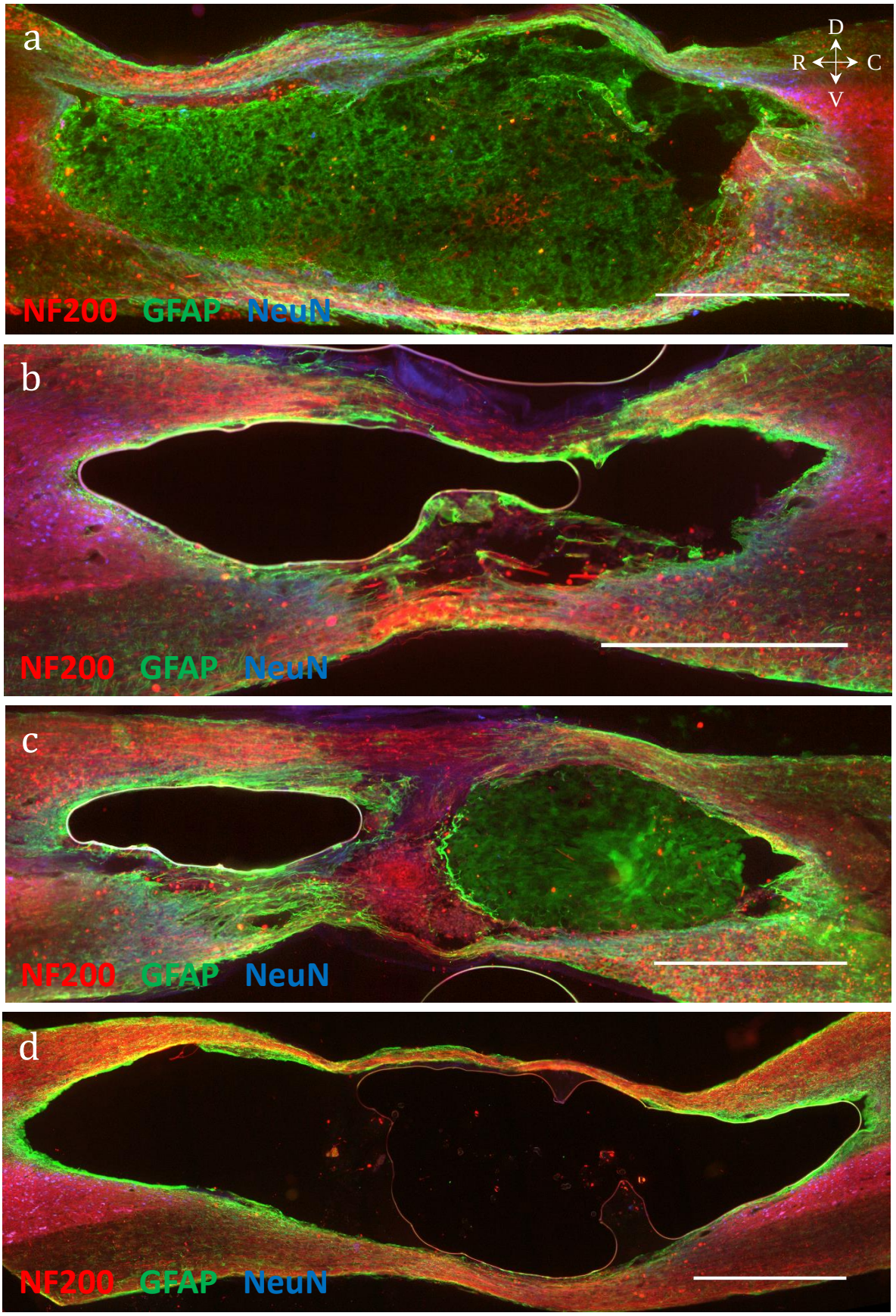

Supplementary Figure 5.3 *Spinal Cord sections from each animal injected with 20µL 50V:50P PEG-Only gel microspheres (a,b,c,d). Stained for NF200 (red), GFAP (green) and NeuN (Blue). Arrows in the top right panel indicate the rostral (R), Caudal (C), Dorsal (D) and Ventral (V) orientations. Scale bars = 1mm*

Microsphere Contusion Sections - PEG-Only

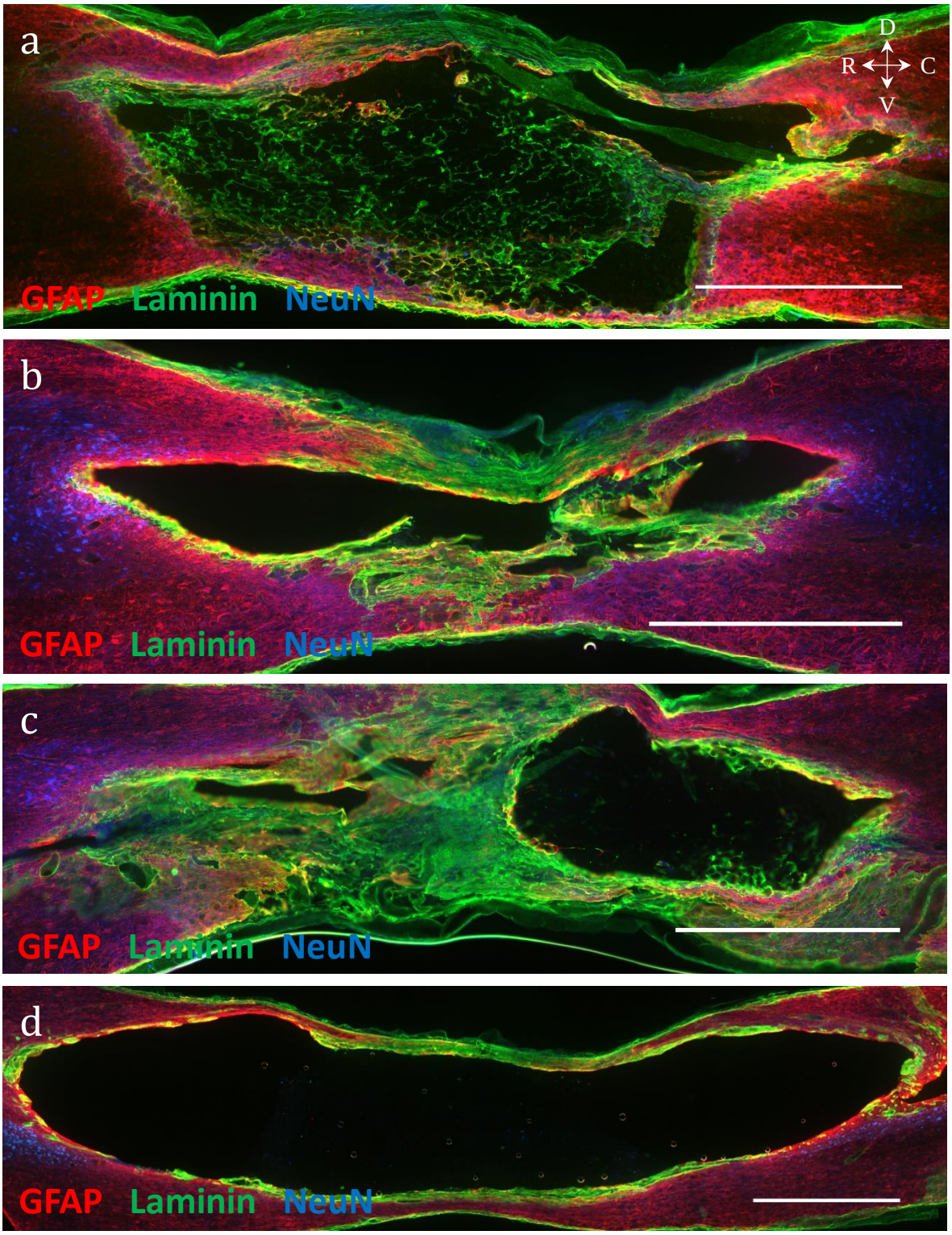

Supplementary Figure 5.4 *Spinal Cord sections from each animal injected with 20µL 50V:50P PEG-Only gel microspheres (a,b,c,d). Stained for GFAP (red), Laminin (green) and NeuN (Blue). Arrows in the top right panel indicate the rostral (R), Caudal (C), Dorsal (D) and Ventral (V) orientations. Scale bars = 1mm*

Microsphere Contusion Sections - PBS Control

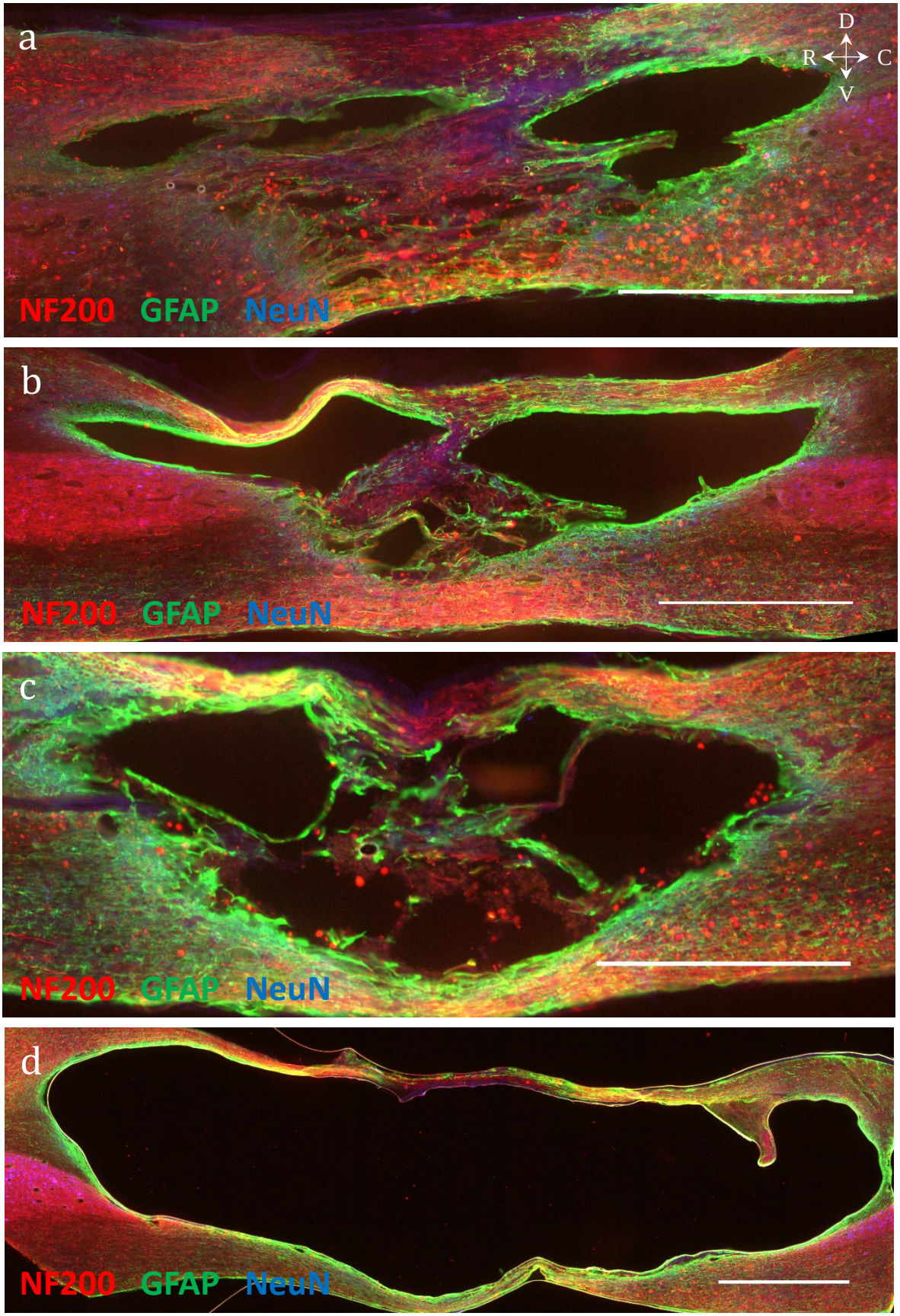

Supplementary Figure 5.5 *Spinal Cord sections from each animal injected with 20µL PBS (Sham Control) (a,b,c,d). Stained for NF200 (red), GFAP (green) and NeuN (Blue). Arrows in the top right panel indicate the rostral (R), Caudal (C), Dorsal (D) and Ventral (V) orientations. Scale bars = 1mm*

Microsphere Contusion Sections - PBS Control

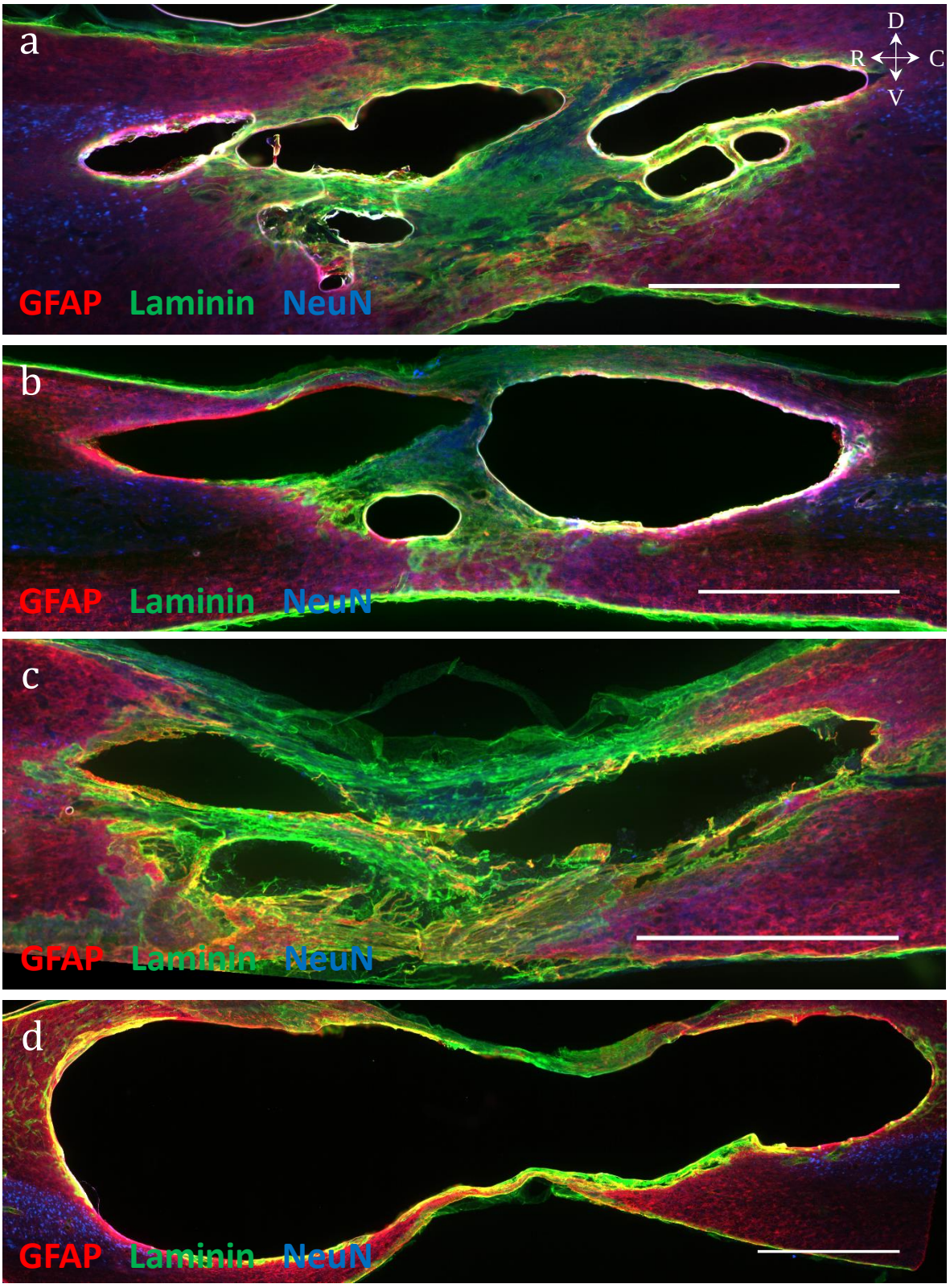

Supplementary Figure 5.6 *Spinal Cord sections from each animal injected with 20µL PBS (Sham Control) (a,b,c,d). Stained for GFAP (red), Laminin (green) and NeuN (Blue). Arrows in the top right panel indicate the rostral (R), Caudal (C), Dorsal (D) and Ventral (V) orientations. Scale bars = 1mm*

References

Abbaszadeh, H. *et al.* (2018) 'Stem cell transplantation and functional recovery after spinal cord injury : a systematic review and meta-analysis', *Anatomy & Cell Biology*, 51(3), pp. 180–188.

Achilli, M. and Mantovani, D. (2010) 'Tailoring Mechanical Properties of Collagen-Based Scaffolds for Vascular Tissue Engineering: The Effects of pH, Temperature and Ionic Strength on Gelation', *Polymers*, 2, pp. 664–680. doi: 10.3390/polym2040664.

Adams, K. L. and Gallo, V. (2018) 'The diversity and disparity of the glial scar', *Nature Neuroscience*. Springer US, 21(January), pp. 9–15. doi: 10.1038/s41593-017-0033-9.

Ali, S. *et al.* (2015) 'The effect of Young's modulus on the neuronal differentiation of mouse embryonic stem cells', *Acta Biomaterialia*. Acta Materialia Inc., 25, pp. 253–267. doi: 10.1016/j.actbio.2015.07.008.

Alizadeh, A., Dyck, S. M. and Karimi-abdolrezaee, S. (2019) 'Traumatic Spinal Cord Injury : An Overview of Pathophysiology , Models and Acute Injury Mechanisms', *Frontiers in Neurology*, 10(March), pp. 1–25. doi: 10.3389/fneur.2019.00282.

Allazetta, S., Hausherr, T. C. and Lutolf, M. P. (2013) 'Microfluidic Synthesis of Cell-Type-Specific Artificial Extracellular Matrix Hydrogels', *Biomacromolecules*, 14, pp. 1122–1131.

Alpin, A. E. *et al.* (1998) 'Signal Transduction and Signal Modulation by Cell Adhesion Receptors : The Signal Transduction and Signal Modulation by Cell Adhesion Receptors : The Role of Integrins , Cadherins , Immunoglobulin-Cell Adhesion Molecules , and Selectins', *PHARMACOLOGICAL REVIEWS*, 50(2), pp. 199–252.

Anderson, M. A. *et al.* (2016) 'Astrocyte scar formation aids central nervous system axon regeneration', *Nature*. Nature Publishing Group, 532(7598), pp. 195–200. doi: 10.1038/nature17623.

Ard, M. D., Bunge, R. P. and Bunge, M. B. (1987) 'Comparison of the Schwann cell surface and Schwann ceil extracellular matrix as promoters of neurite growth', *Journal of Neurocytology*, 16(4), pp. 539–555.

Assinck, P. *et al.* (2017) 'Cell transplantation therapy for spinal cord injury', *Nature neuroscience*, 20(5), pp. 637–647. doi: 10.1038/nn.4541.

Avalos, M. A. *et al.* (2004) 'Aggregation of Integrins and RhoA Activation Are Required for Thy-1-induced Morphological Changes in Astrocytes *', *THE JOURNAL OF BIOLOGICAL CHEMISTRY*, 279(37), pp. 39139–39145. doi: 10.1074/jbc.M403439200.

Awad, B. I. *et al.* (2013) 'Transcranial Magnetic Stimulation After Spinal Cord Injury', *World Neurosurgery*. Elsevier Inc, 83(2), pp. 232–235. doi: 10.1016/j.wneu.2013.01.043.

Bajaj, A. *et al.* (2013) 'Identification of the Protein Target of Myelin-Binding Ligands by Immunohistochemistry and Biochemical Analyses', *Journal of Histochemistry & Cytochemistry*, 61(1), pp. 19–30. doi: 10.1369/0022155412467353.

Bakaic, E., Smeets, N. M. B. and Hoare, T. (2015) 'Injectable hydrogels based on poly(ethylene glycol) and derivatives as functional biomaterials', *RSC Advances*. Royal Society of Chemistry, 5, pp. 35469–35486. doi: 10.1039/c4ra13581d.

Baldwin, A. D. and Kiick, K. L. (2013) 'Reversible maleimide-thiol adducts yield glutathione-sensitive poly(ethylene glycol)-heparin hydrogels', *Polymer Chemistry*, 4(1), pp. 133–143. doi: 10.1039/c2py20576a.

Barczyk, M., Carracedo, S. and Gullberg, D. (2010) 'Intregrins', *Cell Tissue Res*, 339, pp. 269–280. doi: 10.1007/s00441-009-0834-6.

Barker, R. A. *et al.* (2012) *Neuroanatomy and Neuroscience at a Glance*. 4th edn. Wiley-Blackwell.

Bartanusz, V. *et al.* (2011) 'The Blood – Spinal Cord Barrier : Morphology and Clinical Implications', *ANN NEUROL*, 70, pp. 194–206. doi: 10.1002/ana.22421.

Bastien, D. and Lacroix, S. (2014) 'Cytokine pathways regulating glial and leukocyte function after spinal cord and peripheral nerve injury', *Experimental Neurology*. Elsevier Inc., 258, pp. 62–77. doi: 10.1016/j.expneurol.2014.04.006.

Bathawab, F. *et al.* (2016) 'Lateral Chain Length in Polyalkyl Acrylates Determines the Mobility of Fibronectin at the Cell/Material Interface', *Langmuir*, 32, pp. 800–809. doi: 10.1021/acs.langmuir.5b03259.

Beekhuizen, K. S. and Field-fote, E. C. (2005) 'Massed Practice versus Massed Practice with Stimulation: Effects on Upper Extremity Function and Cortical Plasticity in Individuals with Incomplete Cervical Spinal Cord Injury', *The American Society of Neurorehabilitation*, 19, pp. 33–45. doi: 10.1177/1545968305274517.

Behrman, A. L., Bowden, M. G. and Nair, P. M. (2006) 'Neuroplasticity After Spinal Cord Injury and Training : An Emerging Paradigm Shift in Rehabilitation and Walking Recovery', *Physical Therapy*, 86(10), pp. 1406–1425. doi: 10.2522/ptj.20050212.

Benowitz, L. I. and Yin, Y. (2006) 'Combinatorial Treatments for Promoting Axon Regeneration in the CNS : Strategies for Overcoming Inhibitory Signals and Activating Neurons ' Intrinsic Growth State', *Developmental Neurobiology*, 67(9), pp. 1148–1165. doi: 10.1002/dneu.

Benton, R. L. *et al.* (2010) 'Neutralizing Endogenous VEGF Following Traumatic Spinal Cord Injury Modulates Microvascular Plasticity but not Tissue Sparing or Functional Recovery', *Curr Neurovasc Res.*, 6(2), pp. 1–13.

Bezanilla, F. (2005) 'Voltage-Gated Ion Channels', 4(1), pp. 34–48.

Bharadwaj, M. *et al.* (2017) 'αV-class integrins exert dual roles on α5β1 integrins to strengthen adhesion to fibronecti', *Nature Communications*, 8, pp. 1–10. doi: 10.1038/ncomms14348.

Bibel, M. and Barde, Y. (2000) 'Neurotrophins : key regulators of cell fate and cell shape in the vertebrate nervous system', *Genes & Development*, (14), pp. 2919–2937. doi: 10.1101/gad.841400.lated.

Blau, A. *et al.* (2001) 'Promotion of neural cell adhesion by electrochemically generated and functionalized polymer films', *Journal of Neuroscience Methods*, 112, pp. 65–73.

Boomkamp, S. C. *et al.* (2014) 'Epac and the high affinity rolipram binding conformer of PDE4 modulate neurite outgrowth and myelination using an in vitro spinal cord', *British Journal of Pharmacology*, 171, pp. 2385–2398. doi: 10.1111/bph.12588.

Boomkamp, S. D. *et al.* (2012) 'The Development of a Rat In Vitro Model of Spinal Cord Injury Demonstrating the Additive Effects of Rho and ROCK Inhibitors on Neurite Outgrowth and Myelination', *Glia*, 456(December 2011), pp. 441–456. doi: 10.1002/glia.22278.

Bowers, C. A. *et al.* (2016) 'Patients with Spinal Cord Injuries Favor Administration of Methylprednisolone', *PLOS ONE*, (Nascis Ii), pp. 1–12. doi: 10.7910/DVN/B5KEYD.Funding.

Bradbury, E. J. *et al.* (1999) 'NT-3 promotes growth of lesioned adult rat sensory axons ascending in the dorsal columns of the spinal cord', *European Journal of Neuroscience*, 11, pp. 3873–3883.

Brewer, G. J. (1995) 'Serum-Free B27lNeurobasal Medium Supports Differentiated Growth of Neurons From the Striatum , Substantia Nigra , Septum , Cerebral Cortex , Cerebellum , and

Dentate Gyrus', *Journal of Neuroscience Research*, 42, pp. 674–683.

Brogioli, M. *et al.* (2016) 'Monitoring Upper limb recovery after cervical spinal cord injury : insights beyond assessment scores', *Frontiers in Neurology*, 7(142), pp. 1–12. doi: 10.3389/fneur.2016.00142.

Broussard, J. A., Webb, D. J. and Kaverina, I. (2008) 'Asymmetric focal adhesion disassembly in motile cells', *Current Opinion in Cell Biology*, 20, pp. 85–90. doi: 10.1016/j.ceb.2007.10.009.

Brownstone, R. M. and Bui, T. V (2010) *Spinal interneurons providing input to the final common path during locomotion*, *Breathe, Walk and Chew: The Neural Challenge: Part I*. Elsevier B.V. doi: 10.1016/B978-0-444-53613-6.00006-X.

Cabezas, R. *et al.* (2014) 'Astrocytic modulation of blood brain barrier : perspectives on Parkinson ' s disease', *Frontiers in Cellular Neuroscience*, 8, pp. 1–11. doi: 10.3389/fncel.2014.00211.

Cakir, O. *et al.* (2003) 'Neuroprotective effect of N-acetylcysteine and hypothermia on the spinal cord ischemia – reperfusion injury', *Cardiovascular Surgery*, 11(5), pp. 375–379. doi: 10.1016/S0967-2109(03)00077-2.

Campbell, K. T., Stilhano, R. S. and Silva, E. A. (2018) 'Biomaterials Enzymatically degradable alginate hydrogel systems to deliver endothelial progenitor cells for potential revasculature applications', *Biomaterials*. Elsevier Ltd, 179, pp. 109–121. doi: 10.1016/j.biomaterials.2018.06.038.

Cao, H.-Q. and Dong, E.-D. (2013) 'An update on spinal cord injury research', *Neuroscience Bulletin*, 29(1), pp. 94–102. doi: 10.1007/s12264-013-1366-3.

Case, L. B. and Waterman, C. M. (2015) 'Integration of actin dynamics and cell adhesion by a three-dimensional , mechanosensitive molecular clutch', *Nature Publishing Group*. Nature Publishing Group, 17(8), pp. 955–963. doi: 10.1038/ncb3191.

Caykara, T. and Recai, I. (2003) 'Determination of Average Molecular Weight Between Crosslinks and Polymer – Solvent Interaction Parameters of Poly (acrylamide- g -ethylene diamine tetraacetic acid)', *Journal of Applied Polymer Science*, 91, pp. 2168–2175.

Chen, M. and Zhang, B. (2015) 'Axon Plasticity in the Mammalian Central Nervous System after Injury', *Trends Neurosci.*, 37(10), pp. 583–593. doi: 10.1016/j.tins.2014.08.008.Axon.

Cheriyan, T. *et al.* (2014) 'Spinal cord injury models : a review'. Nature Publishing Group, 52(8), pp. 588–595. doi: 10.1038/sc.2014.91.

Cho, J. M. *et al.* (2013) 'Characterization of nestin expression in astrocytes in the rat hippocampal CA1 region following transient forebrain ischemia', *Anatomy & Cell Biology*, 46, pp. 131–140.

Cornelison, R. C. *et al.* (2019) 'Injectable Hydrogels of Optimized Acellular Nerve for Injection in the Injured Spinal Cord', *Biomed Mater.*, 13(3), pp. 1–26. doi: 10.1088/1748-605X/aaab82.Injectable.

Cramer, G. D. (2014) 'General Characteristics of the Spine', in Cramer, G. D. and Darby Spinal Cord, and Ans (Third Edition), S. A. B. T.-C. A. of the S. (eds) *Clinical Anatomy of the Spine, Spinal Cord, and ANS*. Saint Louis: Mosby, pp. 15–64. doi: https://doi.org/10.1016/B978-0-323-07954-9.00002-5.

Cruise, G. M., Scharp, D. S. and Hubbell, J. A. (1998) 'Characterization of permeability and network structure of interfacially photopolymerized poly (ethylene glycol) diacrylate hydrogels', *Biomaterials*, 19, pp. 1287–1294.

Cummings, B. J. *et al.* (2005) 'Human neural stem cells differentiate and promote locomotor recovery in spinal cord-injured mice', *PNAS*, 102(39), pp. 14069–14074.

Curtis, E. *et al.* (2018) 'Clinical Progress A First-in-Human , Phase I Study of Neural Stem Cell Transplantation for Chronic Spinal Cord Injury Clinical Progress A First-in-Human , Phase I Study of Neural Stem Cell Transplantation for Chronic Spinal Cord Injury', *Stem Cell*. Elsevier Inc., 22(6), pp. 941-950.e6. doi: 10.1016/j.stem.2018.05.014.

Dai, S. *et al.* (2016) 'One-step seeding of neural stem cells with vitronectin- supplemented medium for high throughput screening assays', *J Biomol Screen.*, 21(10), pp. 1–24. doi: 10.1016/j.physbeh.2017.03.040.

Dai, Z. *et al.* (2016) 'Effects of Culture Substrate Made of Poly(N- isopropylacrylamide-co-acrylic acid) Microgels on Osteogenic Differentiation of Mesenchymal Stem Cells', *Molecules*, 21, p. 1192. doi: 10.3390/molecules21091192.

Danen, E. H. J. (2013) 'Integrins: An Overview of Structural and Functional Aspects. In: Madame Curie Bioscience Database [Internet]. Austin (TX): Landes Bioscience; 2000-2013.', in *Madame Curie Bioscience Database*. Landes Bioscience.

Darby, S. A. and Frysztak, R. J. (2013) *Neuroanatomy of the Spinal Cord*. Third Edit, *Clinical Anatomy of the Spine, Spinal Cord, and ANS*. Third Edit. Elsevier Inc. doi: 10.1016/B978-0-323-07954-9.00009-8.

David, S., Zarruk, J. G. and Ghasemlou, N. (2012) *Inflammatory Pathways in Spinal Cord Injury*. 1st edn, *Axon Growth and Regeneration: Part 2*. 1st edn. Elsevier Inc. doi: 10.1016/B978-0-12-407178-0.00006-5.

Deforest, C. A., Sims, E. A. and Anseth, K. S. (2010) 'Peptide-Functionalized Click Hydrogels with Independently Tunable Mechanics and Chemical Functionality for 3D Cell Culture', *Chemistry of Materials*, 22, pp. 4783–4790. doi: 10.1021/cm101391y.

Dezawa, M. *et al.* (2004) 'Specific induction of neuronal cells from bone marrow stromal cells and application for autologous transplantation', *The Journal of Clinical Investigation*, 113(12), pp. 1701–1710. doi: 10.1172/JCI200420935.The.

Dhillon, J. *et al.* (2019) 'Peptide-modified methacrylated glycol chitosan hydrogels as a cell-viability supporting pro-angiogenic cell delivery platform for human adipose-derived stem/stromal cells', *Journal of Biomedical Materials Research - Part A*, 107(3), pp. 571–585. doi: 10.1002/jbm.a.36573.

Diaz, E. and Morales, H. (2016) 'Spinal Cord Anatomy and Clinical Syndromes', *Seminars in Ultrasound, CT, and MRI*. Elsevier, 37(5), pp. 360–371. doi: 10.1053/j.sult.2016.05.002.

Dietrich, M. *et al.* (2018) 'Guiding 3D cell migration in deformed synthetic hydrogel microstructures', *Soft Matter*, 14, pp. 2816–2826. doi: 10.1039/c8sm00018b.

Ding, Y., Kastin, A. J. and Pan, W. (2013) 'Neural Plasticity After Spinal Cord Injury', *Curr Pharm Des.*, 11(11), pp. 1441–1450.

Dowlati, E. (2017) 'Spinal cord anatomy , pain , and spinal cord stimulation mechanisms', *Seminars in Spine Surgery*. Elsevier, 29(3), pp. 136–146. doi: 10.1053/j.semss.2017.05.002.

Doyle, A. D. (2017) 'Generation of 3D collagen gels with controlled, diverse architectures', *Curr Protoc Cell Biol.*, 72, pp. 1–22. doi: 10.1002/cpcb.9.Generation.

Dugan, L. and Choi, D. (1999) 'Free Radicals in Hypoxia-Ischemia', in *Basic Neurochemistry: Molecular, Cellular and Medical Aspects*. 6th edn. Philadelphia: Lippincott-Raven. Available at: https://www.ncbi.nlm.nih.gov/books/NBK28241/.

Dumont, C. M. *et al.* (2019) 'Aligned hydrogel tubes guide regeneration following spinal cord injury', *Acta Biomaterialia*. Acta Materialia Inc., 86, pp. 312–322. doi: 10.1016/j.actbio.2018.12.052.

E, C. and Antila, H. (2017) 'Neuronal plasticity and neurotrophic factors in drug responses', *Molecular Psychiatry*, 22, pp. 1085–1095. doi: 10.1038/mp.2017.61.

East, E. *et al.* (2010) 'Alignment of Astrocytes Increases Neuronal Growth and Is Maintained Following Plastic Compression to Form a Spinal Cord Repair Conduit', *Tissue engineering. Part A*, 16(10), pp. 3173–3188. doi: 10.1089/ten.tea.2010.0017.

East, E. *et al.* (2013) 'A 3D in vitro model reveals differences in the astrocyte response elicited by potential stem cell therapies for CNS injury', *Regen. Med.*, 8(6), pp. 739–746.

Elbert, D. L. (2011) 'Liquid-liquid two-phase systems for the production of porous hydrogels and hydrogel microspheres for biomedical applications: A tutorial review', *Acta Biomaterialia*, 7(1), pp. 31–56. doi: 10.1016/j.actbio.2010.07.028.

Ellingson, B. M., Schmit, B. D. and Kurpad, S. N. (2010) 'Lesion growth and degeneration patterns measured using diffusion tensor 9.4-T magnetic resonance imaging in rat spinal cord injury', *Journal of Neurosurgery: Spine SPI*. American Association of Neurological Surgeons, 13(2), pp. 181–192. doi: 10.3171/2010.3.SPINE09523.

Elosegui-artola, A. *et al.* (2016) 'Mechanical regulation of a molecular clutch defines force transmission and transduction in response to matrix rigidity', *Nature Cell Biology*, 18(5), pp. 540–550. doi: 10.1038/ncb3336.

Emilsson, G. *et al.* (2015) 'Strongly Stretched Protein Resistant Poly(ethylene glycol) Brushes Prepared by Grafting-To', *Applied Materials & Interfaces*, 7, pp. 7505–7515. doi: 10.1021/acsami.5b01590.

Enemchukwu, N. O. *et al.* (2015) 'Synthetic matrices reveal contributions of ECM biophysical and biochemical properties to epithelial morphogenesis', *The Journal of Cell Biology*, 212(1), p. jcb.201506055. doi: 10.1083/jcb.201506055.

Engler, A. J. *et al.* (2006) 'Matrix Elasticity Directs Stem Cell Lineage Specification', *Cell*, 126, pp. 677–689. doi: 10.1016/j.cell.2006.06.044.

Fairbanks, B. D. *et al.* (2009) 'Biomaterials Photoinitiated polymerization of PEG-diacrylate with lithium phenyl-2 , 4 , 6- trimethylbenzoylphosphinate : polymerization rate and cytocompatibility', *Biomaterials*. Elsevier Ltd, 30(35), pp. 6702–6707. doi: 10.1016/j.biomaterials.2009.08.055.

Farinas, I. *et al.* (1998) 'Characterization of Neurotrophin and Trk Receptor Functions in Developing Sensory Ganglia : Direct NT-3 Activation of TrkB Neurons In Vivo', *Neuron*, 21, pp. 325–334.

Farrukh, A. *et al.* (2017) 'Bifunctional Hydrogels Containing the Laminin Motif IKVAV Promote Neurogenesis', *Stem Cell Reports*, 9, pp. 1432–1440. doi: 10.1016/j.stemcr.2017.09.002.

Fawcett, J. W. (2009) 'Recovery from spinal cord injury: regeneration, plasticity and rehabilitation', *Brain*, 132(6), pp. 1417–1418. doi: 10.1093/brain/awp121.

Fehlings, M. G. *et al.* (2017) 'A Clinical Practice Guideline for the Management of Acute Spinal Cord Injury : Introduction , Rationale , and Scope', *Global Spine Journa*, 7, pp. 84–94. doi: 10.1177/2192568217703387.

Feig, V. R., Tran, H. and Bao, Z. (2018) 'Biodegradable Polymeric Materials in Degradable Electronic Devices', *ACS Cent. Sci.*, 4(3), pp. 337–348. doi: 10.1021/acscentsci.7b00595.

Felton, D. L., O'Banion, K. and Maida, M. S. (2016) 'Neurons and Their Properties', in *Netter's Atlas of Neuroscience*. 3rd edn, pp. 1–42. doi: 10.1016/B978-0-323-26511-9.00001-1.

Feltri, M. L. *et al.* (2002) 'Conditional disruption of β1 integrin in Schwann cells impedes interactions with axons', *The Journal of Cell Biology*, 156(1), pp. 199–209. doi: 10.1083/jcb.200109021.

Fendrich, R., Hutsler, J. J. and Gazzaniga, M. S. (2004) 'Visual and tactile interhemispheric transfer compared with the method of Poffenberger', pp. 67–74. doi: 10.1007/s00221-004-1873-6.

Figley, S. A. *et al.* (2014) 'Characterization of Vascular Disruption and Blood – Spinal Cord Barrier Permeability', *JOURNAL OF NEUROTRAUMA*, 31(6), pp. 541–552. doi: 10.1089/neu.2013.3034.

Filous, A. R. and Silver, J. (2016) 'Targeting astrocytes in CNS injury and disease : A translational research approach', *Progress in Neurobiology journal*, 144, pp. 173–187. doi: 10.1016/j.pneurobio.2016.03.009.

Flanagan, L. A. *et al.* (2008) 'Regulation of Human Neural Precursor Cells by Laminin and Integrins', *J Neurosci Res.*, 83(5), pp. 845–856.

Foster, G. A. *et al.* (2017) 'Biomaterials Protease-degradable microgels for protein delivery for vascularization', *Biomaterials*, 113, pp. 170–175. doi: 10.1016/j.biomaterials.2016.10.044.

Frith, J. E., Mills, R. J., Hudson, J. E. and Cooper-White, J. J. (2012) 'Tailored Integrin–Extracellular Matrix Interactions to Direct Human Mesenchymal Stem Cell Differentiation', *Stem Cells and Development*, 21(13), pp. 2442–2456. doi: 10.1089/scd.2011.0615.

Frith, J. E., Mills, R. J., Hudson, J. E. and Cooper-white, J. J. (2012) 'Tailored Integrin – Extracellular Matrix Interactions to Direct Human Mesenchymal Stem Cell Differentiation', *STEM CELLS AND DEVELOPMENT*, 21(13), pp. 2442–2456. doi: 10.1089/scd.2011.0615.

Fu, Y. and Kao, W. J. (2011) 'In situ forming poly (ethylene glycol)-based hydrogels via thiol-maleimide Michael-type addition', *Journal of Biomedical Materials Research Part A*, 98A(2), pp. 201–211. doi: 10.1002/jbm.a.33106.

Führmann, T., Anandakumaran, P. N. and Shoichet, M. S. (2017) 'Combinatorial Therapies After Spinal Cord Injury: How Can Biomaterials Help?', *Advanced Healthcare Materials*, 6(10), pp. 1–21. doi: 10.1002/adhm.201601130.

Führmann, T. and Shoichet, M. S. (2018) 'The role of biomaterials in overcoming barriers to regeneration in the central nervous system The role of biomaterials in overcoming barriers to regeneration in the central nervous system', *Biomed. Mater*. IOP Publishing, 13, pp. 13–16.

Furlan, J. C. *et al.* (2013) 'Global Incidence and Prevalence of Traumatic Spinal Cord Injury', *The Canadian journal of neurological sciences*, 40(4), pp. 456–464. doi: DOI: 10.1017/S0317167100014530.

Ganfornina, M. D., Sanchez, D. and Bastiani, M. J. (1992) 'The Role of the Cell Surface in Neuronal Pathfinding', *BioScience*, 46(5).

Gaudet, A. D. and Fonken, L. K. (2018) 'Glial Cells Shape Pathology and Repair After Spinal Cord Injury', *Neurotherapeutics*. Neurotherapeutics, 15(3), pp. 554–577.

Gentile, P. *et al.* (2014) 'An Overview of Poly (lactic- co -glycolic) Acid (PLGA) -Based Biomaterials for Bone Tissue Engineering', *International Journal of Molecular Sciences*, 15, pp. 3640–3659. doi: 10.3390/ijms15033640.

Georges, P. C. *et al.* (2006) 'Matrices with Compliance Comparable to that of Brain Tissue Select Neuronal over Glial Growth in Mixed Cortical Cultures', *Biophysical Journal*. Elsevier, 90(8), pp. 3012–3018. doi: 10.1529/biophysj.105.073114.

Gerardo-Nava, J. *et al.* (2014) 'Biomaterials Spinal cord organotypic slice cultures for the study of regenerating motor axon interactions with 3D scaffolds', *Biomaterials*. Elsevier Ltd, 35(14), pp. 4288–4296. doi: 10.1016/j.biomaterials.2014.02.007.

Gillen, G. (2016) 'Trunk Control: Supporting Functional Independence', in Gillen, G. B. T.-S. R. (Fourth E. (ed.) *Stroke Rehabilitation*. 4th edn. Mosby, pp. 360–393. doi: https://doi.org/10.1016/B978-0-323-17281-3.00018-6.

Gingras, M. *et al.* (2008) 'In Vitro Study of Axonal Migration and Myelination of Motor Neurons in a Three-Dimensional Tissue-Engineered Model', *Glia*, 364(August 2007), pp. 354–364. doi: 10.1002/glia.

Gómara-toldrà, N., Sliwinski, M. and Dijkers, M. P. (2014) 'Physical therapy after spinal cord injury : A systematic review of treatments focused on participation', *The journal of spinal cord medicine*, 37(4), pp. 371–379. doi: 10.1179/2045772314Y.0000000194.

Grabowska, I. *et al.* (2019) 'Adipose tissue-derived stromal cells in matrigel impacts the regeneration of severely damaged skeletal muscles', *International Journal of Molecular Sciences*, 20, pp. 1–22. doi: 10.3390/ijms20133313.

Gray, D. S., Tien, J. and Chen, C. S. (2002) 'Repositioning of cells by mechanotaxis on surfaces with micropatterned Young ' s modulus', *Journal of Biomedical Materials Research - Part A*, 66A(3), pp. 605–614.

Grill, R. *et al.* (1997) 'Cellular Delivery of Neurotrophin-3 Promotes Corticospinal Axonal Growth and Partial Functional Recovery after Spinal Cord Injury', *The Journal of Neuroscience*, 17(14), pp. 5560–5572.

Gunn, J. W., Turner, S. D. and Mann, B. K. (2004) 'Adhesive and mechanical properties of hydrogels influence neurite extension', *J Biomed Mater Res A*, 72(1), pp. 91–97. doi: 10.1002/jbm.a.30203.

Gunn, J. W., Turner, S. D. and Mann, B. K. (2005) 'Adhesive and mechanical properties of hydrogels influence neurite extension', *Journal of Biomedical Materials Research - Part A*, 72(1), pp. 91–97. doi: 10.1002/jbm.a.30203.

Gupta, D., Tator, C. H. and Shoichet, M. S. (2006) 'Fast-gelling injectable blend of hyaluronan and methylcellulose for intrathecal, localized delivery to the injured spinal cord', *Biomaterials*, 27(11), pp. 2370–2379. doi: 10.1016/j.biomaterials.2005.11.015.

Gutowski, S. M. *et al.* (2015) 'Protease-degradable PEG-maleimide coating with on-demand release of IL-1Ra to improve tissue response to neural electrodes', *Biomaterials*, 44, pp. 55–70. doi: 10.1016/j.biomaterials.2014.12.009.

Gwak, S. *et al.* (2016) 'Therapeutic Use of 3β-[N-(N',N'- Dimethylaminoethane) Carbamoyl] Cholesterol-Modified PLGA Nanospheres as Gene Delivery Vehicles for Spinal Cord Injury So-Jung', *PLOS ONE*, 11(1), pp. 1–14. doi: 10.1371/journal.pone.0147389.

Hackett, J. T., Ueda, T. and Snare, S. I. Á. S. Á. (2015) 'Glutamate Release', *Neurochemical Research*. Springer US, 40(12), pp. 2443–2460. doi: 10.1007/s11064-015-1622-1.

Haddad, Y. (2017) 'Trk Receptors and Neurotrophin Cross-Interactions : New Perspectives Toward Manipulating Therapeutic Side-Effects', *Frontiers in Molecular Neuroscience*, 10, pp. 1–7. doi: 10.3389/fnmol.2017.00130.

Hamid, S. and Hayek, R. (2008) 'Role of electrical stimulation for rehabilitation and regeneration after spinal cord injury : an overview', *Eur Spine J (2008)*, 17, pp. 1256–1269. doi: 10.1007/s00586-008-0729-3.

Han, F. *et al.* (2016) 'Cellular modulation by the elasticity of biomaterials', *Journal of Materials Chemistry B*. Royal Society of Chemistry, 4, pp. 9–26. doi: 10.1039/c5tb02077h.

Harris, J. M. and Chess, R. B. (2003) 'Effect of pegylation on pharmaceuticals', *Nature Reviews Drug Discovery*, 2(3), pp. 214–221. doi: 10.1038/nrd1033.

Hartman, A. L. (2009) 'Normal Anatomy of the Cerebrospinal Fluid Compartment', in Irani, D. N. B. T.-C. F. in C. P. (ed.) *Cerebrospinal Fluid in Clinical Practice*. Philadelphia: W.B. Saunders, pp. 5–10. doi: https://doi.org/10.1016/B978-141602908-3.50005-4.

Hatley, R. J. D. *et al.* (2018) 'An αv-RGD Integrin Inhibitor Toolbox: Drug Discovery Insight, Challenges and Opportunities', *Angewandte Chemie - International Edition*, 57(13), pp. 3298–3321. doi: 10.1002/anie.201707948.

He, X. . and Garcia, K. C. (2004) 'Structure of nerve growth factor complexed with the shared neurotrophin receptor p75. https://www.rcsb.org/pdb/explore/jmol.do?structureId=1sg1&bionumber=1&jmolMode=HTML5' , *Science*, 304, pp. 870–875. Available at: https://www.rcsb.org/pdb/explore/jmol.do?structureId=1sg1&bionumber=1&jmolMode=HTML5 (Accessed: 4 July 2019).

Henderson, K. J. *et al.* (2010) 'Ionically Cross-Linked Triblock Copolymer Hydrogels with High Strength', *Macromolecules*, pp. 6193–6201. doi: 10.1021/ma100963m.

Herndon, J. M., Tome, M. E. and Davis, T. P. (2017) 'Development and Maintenance of the Blood–Brain Barrier', in *Primer on Cerebrovascular Disease*. 2nd edn, pp. 51–56. doi: 10.1016/B978-0-12-803058-5.00009-6.

Hesse, E. *et al.* (2010) 'Collagen type I hydrogel allows migration , proliferation , and osteogenic differentiation of rat bone marrow stromal cells', *Journal of Biomedical Materials Research Part A*, 94A(2), pp. 442–449. doi: 10.1002/jbm.a.32696.

Hezaveh, H. *et al.* (2018) 'Encoding Stem-Cell-Secreted Extracellular Matrix Protein Capture in Two and Three Dimensions Using Protein Binding Peptides', *Biomacromolecules*, 19, pp. 721–730. doi: 10.1021/acs.biomac.7b01482.

Hidalgo San Jose, L. *et al.* (2018) 'Microfluidic Encapsulation Supports Stem Cell Viability, Proliferation, and Neuronal Differentiation', *Tissue Engineering - Part C: Methods*, 24(3), pp. 158–170. doi: 10.1089/ten.tec.2017.0368.

Hofer, H. R. and Tuan, R. S. (2016) 'Secreted trophic factors of mesenchymal stem cells support neurovascular and musculoskeletal therapies', *Stem Cell Research and Therapy*. Stem Cell Research & Therapy, 7(1), pp. 1–14. doi: 10.1186/s13287-016-0394-0.

Holyoak, D. T. *et al.* (2019) 'Injectable mechanical pillows for attenuation of load-induced post-traumatic osteoarthritis', *Regenerative Biomaterials*, 6(4), pp. 211–219. doi: 10.1093/rb/rbz013.

Hong, S. *et al.* (2012) 'Collagen microsphere production on a chip', *Lab on a Chip*, 12, pp. 3277–3280. doi: 10.1039/c2lc40558j.

Hoshino, K. *et al.* (2018) 'Network elasticity of a model hydrogel as a function of swelling ratio : from shrinking to extreme swelling states †', *Soft Matter*. Royal Society of Chemistry, 14, pp. 9693–9701. doi: 10.1039/c8sm01854e.

Hosseini, S. M. *et al.* (2018) 'Neuroscience Letters Concomitant use of mesenchymal stem cells and neural stem cells for treatment of spinal cord injury : A combo cell therapy approach', *Neuroscience Letters*. Elsevier, 668(January), pp. 138–146. doi: 10.1016/j.neulet.2018.01.008.

Hsu, J. C. *et al.* (2006) 'Matrix Metalloproteinase-2 Facilitates Wound Healing Events That Promote Functional Recovery after Spinal Cord Injury', *The Journal of Neuroscience*, 26(39), pp. 9841–9850. doi: 10.1523/JNEUROSCI.1993-06.2006.

Hu, W., Eaton, J. W. and Tang, L. (2019) 'Molecular basis of biomaterial-mediated foreign body reactions', *Blood*, 98(4), pp. 1231–1239.

Hu, W., Wang, Z. and Xiao, Y. (2019) 'Biomaterials Science Advances in crosslinking strategies of biomedical hydrogels', *Biomaterials Science*. Royal Society of Chemistry, 7, pp. 843–855. doi: 10.1039/c8bm01246f.

Huang, E. J. and Reichardt, L. F. (2001) 'Neurotrophins: Roles in Neuronal Development and Function', *Annu Rev Neurosci.*, 24, pp. 677–736. doi:

10.1146/annurev.neuro.24.1.677.Neurotrophins.

Huaping, T. *et al.* (2012) 'Hyaluronic acid-based hydrogels through a double crosslinking strategy', *J Tissue Eng Regen Med*, 5(10), pp. 790–797. doi: 10.1002/term.378.Controlled.

Huda, F. *et al.* (2016) 'Fusion of Human Fetal Mesenchymal Stem Cells with " Degenerating " Cerebellar Neurons in Spinocerebellar Ataxia Type 1 Model Mice', *PLOS ONE*, 11(11), pp. 1–18. doi: 10.1371/journal.pone.0164202.

Huebsch, N. and Mooney, David J. Mooney1, 3 (2010) 'Inspiration and application in the evolution of biomaterials', *Nature*, 462(7272), pp. 426–432. doi: 10.1038/nature08601.Inspiration.

Hutter, J. L. *et al.* (1998) 'Calibration of atomic-force microscope tips tips', *Review of Scientific Instruments*, 64(7), pp. 1868–1873. doi: 10.1063/1.1143970.

Hwang, J. J., Choi, S. Y. and Koh, J. Y. (2002) 'The role of NADPH oxidase, neuronal nitric oxide synthase and poly(ADP ribose) polymerase in oxidative neuronal death induced in cortical cultures by brain-derived neurotrophic factor and neurotrophin-4/5', *Journal of Neurochemistry*, 82(4), pp. 894–902. doi: 10.1046/j.1471-4159.2002.01040.x.

Hyun, J. K. and Kim, H. (2010) 'Clinical and Experimental Advances in Regeneration of Spinal Cord Injury', *Journal of Tissue Engineering*, 2010, pp. 1–20. doi: 10.4061/2010/650857.

Ivanova, E. P., Bazaka, K. and Crawford, R. J. (2014) 'Advanced synthetic polymer biomaterials derived from organic sources', in *New Functional Biomaterials for Medicine and Healthcare*, pp. 71–99. doi: 10.1533/9781782422662.71.

Jacobson, S. and Marcus, E. M. (2018) *Neuroanatomy for the Neuroscientist*. 3rd edn. Springer.

Jain, A. *et al.* (2006) 'In situ gelling hydrogels for conformal repair of spinal cord defects, and local delivery of BDNF after spinal cord injury', *Biomaterials*, 27(3), pp. 497–504. doi: 10.1016/j.biomaterials.2005.07.008.

Jain, E. *et al.* (2015) 'Fabrication of Polyethylene Glycol-Based Hydrogel Microspheres Through Electrospraying', *Macromolecular Materials and Engineering*, 300, pp. 823–835. doi: 10.1002/mame.201500058.

Jalali, S. *et al.* (2016) 'Regulation of Endothelial Cell Adherence and Elastic Modulus by Substrate Stiffness Regulation of Endothelial Cell Adherence and Elastic Modulus by Substrate', *Cell Communication & Adhesion*, 22, pp. 79–89. doi: 10.1080/15419061.2016.1265949.

Jans, K. *et al.* (2009) 'Chemical and biological characterization of thiol SAMs for neuronal cell attachment', *Langmuir*, 25(8), pp. 4564–4570. doi: 10.1021/la802217r.

Jansen, L. E., Galarza, S. and Shelly, R. (2019) 'Control of Thiol-Maleimide Reaction Kinetics in PEG Hydrogel Networks', *Acta Biomater.*, 70, pp. 120–128. doi: 10.1016/j.actbio.2018.01.043.Control.

Jin, X. (2014) 'Membrane resealing as a promising strategy for early treatment of neurotrauma', *Neural Regeneration Research*, 9(21), pp. 1876–1877. doi: 10.4103/1673-5374.145475.

Jones, C. F., Kwon, B. K. and Cripton, P. A. (2012) 'Mechanical indicators of injury severity are decreased with increased thecal sac dimension in a bench-top model of contusion type spinal cord injury', *Journal of Biomechanics*. Elsevier, 45(6), pp. 1003–1010. doi: 10.1016/j.jbiomech.2012.01.025.

Kakulas, A. B. (1999) 'A Review of the Neuropathology of Human Spinal Cord Injury with Emphasis on Special Features', *The Journal of Spinal Cord Medicine*, 22(2), pp. 119–124. doi: 10.1080/10790268.1999.11719557.

Kalaba, S. *et al.* (2016) 'Bioactive Materials Design strategies and applications of biomaterials and devices for Hernia repair', *Bioactive Materials*. Elsevier Ltd, 1(1), pp. 2–17. doi:

10.1016/j.bioactmat.2016.05.002.

Kapp, T. G. *et al.* (2017) 'A Comprehensive Evaluation of the Activity and Selectivity Profile of Ligands for RGD-binding Integrins', *Scientific reports*. Nature Publishing Group, 7, pp. 1–13. doi: 10.1038/srep39805.

Karamched, B. R. and Bressloff, P. C. (2015) 'Article Delayed Feedback Model of Axonal Length Sensing', *Biophysj*. Biophysical Society, 108(9), pp. 2408–2419. doi: 10.1016/j.bpj.2015.03.055.

Keefe, K. M., Sheikh, I. S. and Smith, G. M. (2017) 'Targeting Neurotrophins to Specific Populations of Neurons : NGF , BDNF , and NT-3 and Their Relevance for Treatment of Spinal Cord Injury', *International Journal of Molecular Sciences*, 18(548), pp. 1–17. doi: 10.3390/ijms18030548.

Khan, F. and Tanaka, M. (2018) 'Designing smart biomaterials for tissue engineering', *International Journal of Molecular Sciences*, 19(1), pp. 1–14. doi: 10.3390/ijms19010017.

Kim, B. J. *et al.* (2008) 'Colloid Surfactants for Emulsion Stabilization', *Advanced Materials*, 20, pp. 3239–3243. doi: 10.1002/adma.200800484.

Kim, H. J. *et al.* (2003) 'TrkB mediates BDNF-induced potentiation of neuronal necrosis in cortical culture', *Neurobiology of Disease*, 14(1), pp. 110–119. doi: 10.1016/S0969-9961(03)00103-7.

Kim, J. *et al.* (2016) 'Characterization of the crosslinking kinetics of multi-arm poly(ethylene glycol) hydrogels formed via Michael-type addition', *Soft Matter*. Royal Society of Chemistry, 12, pp. 2076–2085. doi: 10.1039/c5sm02668g.

Kim, Y. *et al.* (2018) 'Laminin peptide YIGSR enhances epidermal development of skin equivalents', *Journal of Tissue Viability*. Elsevier Ltd, 27(2), pp. 117–121. doi: 10.1016/j.jtv.2018.02.001.

Kimpinski, K., Campenot, R. B. and Mearow, K. (1997) 'Effects of the neurotrophins nerve growth factor, neurotrophin-3, and brain-derived neurotrophic factor (BDNF) on neurite growth from adult sensory neurons in compartmented cultures', *Journal of Neurobiology*, 33(4), pp. 395–410. doi: 10.1002/(SICI)1097-4695(199710)33:4<395::AID-NEU5>3.0.CO;2-5.

Kingsley, D. M. *et al.* (2019) 'Multi-modal characterization of polymeric gels to determine the influence of testing method on observed elastic modulus', *Journal of the Mechanical Behavior of Biomedical Materials*. Elsevier Ltd, 92(January), pp. 152–161. doi: 10.1016/j.jmbbm.2019.01.003.

Kirshblum, S. C. *et al.* (2011) 'International standards for neurological classification of spinal cord injury (Revised 2011) International standards for neurological classification of spinal cord injury (Revised 2011)', *The Journal of Spinal Cord Medicine*, 34(6), pp. 535–546. doi: 10.1179/204577211X13207446293695.

Koch, D. *et al.* (2012) 'Strength in the Periphery : Growth Cone Biomechanics and Substrate Rigidity Response in Peripheral and Central Nervous System Neurons', *Biophysical Journal*. Biophysical Society, 102(3), pp. 452–460. doi: 10.1016/j.bpj.2011.12.025.

Kong, L. *et al.* (2017) 'Role of mesenchymal stem cells in osteoarthritis treatment', *Journal of Orthopaedic Translation*. Elsevier Ltd, 9, pp. 89–103. doi: 10.1016/j.jot.2017.03.006.

Koo, J. *et al.* (2018) 'Wireless bioresorbable electronic system enables sustained nonpharmacological neuroregenerative therapy', *Nature Medicine*. Springer US, 24(December). doi: 10.1038/s41591-018-0196-2.

Koopmans, G. C. *et al.* (2005) 'The Assessment of Locomotor Function in Spinal Cord Injured Rats : The Importance of Objective Analysis of Coordination', *Journal of Neurotrauma*, 22(2), pp. 214–225.

Koser, D. E. *et al.* (2016) 'Mechanosensing is critical for axon growth in the developing brain', *Nature Neuroscience*, 19(12), pp. 1592–1604. doi: 10.1038/nn.4394.

Krames, E. S. (2014) 'The Role of the Dorsal Root Ganglion in the Development of Neuropathic Pain', *Pain Medicine*, 15, pp. 1669–1685.

Krassioukov, A. V, Furlan, J. C. and Fehlings, M. G. (2003) 'Medical co-morbidities, secondary complications, and mortality in elderly with acute spinal cord injury', *J Neurotrauma*, 20(0897–7151), pp. 391–399. doi: 10.1089/089771503765172345.

Kreutzberg, G. W. (1995) 'Microglia: a sensor for pathological events in the CNS', *Journal of Neuroscience*, 2236, pp. 471–474.

Krinke, G. J. and Weber, K. (2012) 'Histology', in Hedrich, H. J. B. T.-T. L. M. (Second E. (ed.) *The Laboratory Mouse*. Boston: Academic Press, pp. 161–192. doi: https://doi.org/10.1016/B978-0-12-382008-2.00008-8.

Krishna, V. *et al.* (2013) 'A Contusion Model of Severe Spinal Cord Injury in Rats', *JOVE*, 78, pp. 1–5. doi: 10.3791/50111.

Kudva, A. K., Luyten, F. P. and Patterson, J. (2017) 'RGD-functionalized polyethylene glycol hydrogels support proliferation and in vitro chondrogenesis of human periosteum-derived cells', *Journal of Biomedical Materials Research Part A*, 106(1), pp. 33–42. doi: 10.1002/jbm.a.36208.

Kumar, S. *et al.* (2018) 'Sizes and Sufficient Quantities of MSC Microspheres for Intrathecal Injection to Modulate Inflammation in Spinal Cord Injury', *Nano Life*, 5(4), pp. 1–22. doi: 10.1142/S179398441550004X.Sizes.

Lampe, K. J., Antaris, A. L. and Heilshorn, S. C. (2013) 'Acta Biomaterialia Design of three-dimensional engineered protein hydrogels for tailored control of neurite growth Elastin-like', *Acta Biomaterialia*. Acta Materialia Inc., 9(3), pp. 5590–5599. doi: 10.1016/j.actbio.2012.10.033.

Lan, L. *et al.* (2017) 'Implantable porous gelatin microspheres sustained release of bFGF and improved its neuroprotective effect on rats after spinal cord injury', *PLOS ONE*, 12(3), pp. 1–16.

Lanzalaco, S. and Armelin, E. (2017) 'Poly(N-isopropylacrylamide) and Copolymers: A Review on Recent Progresses in Biomedical Applications', *Gels*, 3(4), p. 36. doi: 10.3390/gels3040036.

Lashkaripour, A. *et al.* (2019) 'Performance tuning of microfluidic flow-focusing droplet generators', *Lab on a Chip*. Royal Society of Chemistry, 19, pp. 1041–1053. doi: 10.1039/c8lc01253a.

Lazarini, F. *et al.* (2012) 'Early Activation of Microglia Triggers Long-Lasting Impairment of Adult Neurogenesis in the Olfactory Bulb Franc', *Journal of Neuroscience*, 32(11), pp. 3652–3664. doi: 10.1523/JNEUROSCI.6394-11.2012.

Le, D. *et al.* (2018) 'A novel method for quantifying axon degeneration', *PLOS ONE*, 13(7), pp. 1–9.

Lee, B. B. *et al.* (2014) 'The global map for traumatic spinal cord injury epidemiology: update 2011, global incidence rate.', *Spinal cord*. Nature Publishing Group, 52(2), pp. 110–6. doi: 10.1038/sc.2012.158.

Lee, F. H. F. *et al.* (2018) 'Specific Alterations in Astrocyte Properties via the GluA2-GAPDH Complex Associated with Multiple Sclerosis', *Scientific Reports*. Springer US, 8(1), pp. 1–17. doi: 10.1038/s41598-018-31318-4.

Lee, J. B. *et al.* (2012) 'A mechanical metamaterial made from a DNA hydrogel.', *Nature nanotechnology*. Nature Publishing Group, 7(12), pp. 816–20. doi: 10.1038/nnano.2012.211.

Lee, S., Tong, X. and Yang, F. (2014) 'The effects of varying poly (ethylene glycol) hydrogel crosslinking density and the crosslinking mechanism on protein accumulation in three-dimensional hydrogels', *Acta Biomaterialia*. Acta Materialia Inc., 10(10), pp. 4167–4174. doi: 10.1016/j.actbio.2014.05.023.

Leszczyńska, A. N. *et al.* (2015) 'Thoracic Hemisection in Rats Results in Initial Recovery Followed by a Late Decrement in Locomotor Movements , with Changes in Coordination Correlated with Serotonergic Innervation of the Ventral Horn', *PLoS ONE*, 10(11), pp. 1–28. doi: 10.1371/journal.pone.0143602.

Levi, A. D. *et al.* (2010) 'Clinical Outcomes Using Modest Intravascular Hypothermia After Acute Cervical Spinal Cord Injury', *NEUROSURGERY*, 66(4), pp. 670–677. doi: 10.1227/01.NEU.0000367557.77973.5F.

Levi, A. D. *et al.* (2019) 'Clinical Outcomes from a Multi-Center Study of Human Neural Stem Cell Transplantation in Chronic Cervical Spinal Cord Injury', *Journal of Neurotrauma*, 902, pp. 891–902. doi: 10.1089/neu.2018.5843.

Lewis, C. L. *et al.* (2010) 'Microfluidic fabrication of hydrogel microparticles containing functionalized viral nanotemplates', *Langmuir*, 26(16), pp. 13436–13441. doi: 10.1021/la102446n.

Li *et al.* (2014) 'Surgical decompression in acute spinal cord injury: A review of clinical evidence, animal model studies, and potential future directions of investigation Yiping', *Front Biol (Beijing)*, 9(2), pp. 127–136. doi: 10.1007/s11515-014-1297-z.Surgical.

Li, G., Yang, P. and Huang, N. (2011) 'Layer-by-layer construction of the heparin / fibronectin coatings on titanium surface : stability and functionality', *Physics Procedia*, 18, pp. 112–121. doi: 10.1016/j.phpro.2011.06.068.

Li, H. Y. *et al.* (2013) 'Host reaction to poly(2-hydroxyethyl methacrylate) scaffolds in a small spinal cord injury model', *Journal of Materials Science: Materials in Medicine*, 24(8), pp. 2001–2011. doi: 10.1007/s10856-013-4956-8.

Li, K. *et al.* (2014) 'Overexpression of the astrocyte glutamate transporter GLT1 exacerbates phrenic motor neuron degeneration, diaphragm compromise, and forelimb motor dysfunction following cervical contusion spinal cord injury', *Journal of Neuroscience*, 34(22), pp. 7622–7638. doi: 10.1523/JNEUROSCI.4690-13.2014.

Li, X. *et al.* (2014) 'Short Laminin Peptide for Improved Neural Stem Cell Growth', *STEM CELLS TRANSLATIONALMEDICINE*, 3(5), pp. 662–670.

Liddelow, S. A. and Barres, B. A. (2017) 'Reactive Astrocytes: Production, Function, and Therapeutic Potential Shane', *Immunity*. Elsevier Inc., 46(6), pp. 957–967. doi: 10.1016/j.immuni.2017.06.006.

Liebl, D. J. *et al.* (2001) 'Regulation of Trk receptors following contusion of the rat spinal cord', *Experimental Neurology*, 167(1), pp. 15–26. doi: 10.1006/exnr.2000.7548.

Lin, C. and Anseth, K. S. (2009) 'PEG Hydrogels for the Controlled Release of Biomolecules in Regenerative Medicine', *Pharmaceutical Research*, 26(3), pp. 631–643. doi: 10.1007/s11095-008-9801-2.

Lin, L. *et al.* (2014) 'Extracellular matrix-mimetic poly (ethylene glycol) hydrogels engineered to regulate smooth muscle cell proliferation in 3-D', *Acta Biomaterialia*. Acta Materialia Inc., 10(12), pp. 5106–5115. doi: 10.1016/j.actbio.2014.08.025.

Lin, Y. *et al.* (2014) 'Tuning Chemical and Physical Crosslinks in Silk Electrogels for Morphological Analysis and Mechanical Reinforcement', *Biomacromolecules*, 14(8), pp. 2629–2635. doi: 10.1021/bm4004892.Tuning.

Lindsay, S. L. *et al.* (2017) 'Human Olfactory Mesenchymal Stromal Cell Transplants Promote Remyelination and Earlier Improvement in Gait Co-ordination after Spinal Cord Injury', *Glia*, 65, pp. 639–656. doi: 10.1002/glia.23117.

Liu, A. L. and Garcia, A. J. (2016) 'Methods for Generating Hydrogel Particles for Protein Delivery', *Annals of Biomedical Engineering*, 44(6), pp. 1946–1958. doi: 10.1007/s10439-016-1637-z.

Liu, L. *et al.* (2016) 'A New Method for Preparing Mesenchymal Stem Cells and Labeling with Ferumoxytol for Cell Tracking by MRI', *Nature Publishing Group*. Nature Publishing Group, (February), pp. 1–10. doi: 10.1038/srep26271.

Liu, S. *et al.* (2018) 'Biomaterial-supported cell transplantation treatments for spinal cord injury: Challenges and perspectives', *Frontiers in Cellular Neuroscience*, 11(January), pp. 1–19. doi: 10.3389/fncel.2017.00430.

Lizarraga-Valderrama, L. R. *et al.* (2019) 'Unidirectional neuronal cell growth and differentiation on aligned polyhydroxyalkanoate blend microfibres with varying diameters', *J Tissue Eng Regen Med.*, 2019, pp. 1–14. doi: 10.1002/term.2911.

Loy, D. N. *et al.* (2002) 'Temporal Progression of Angiogenesis and Basal Lamina Deposition After Contusive Spinal Cord Injury in the Adult Rat', *THE JOURNAL OF COMPARATIVE NEUROLOGY*, 445(December 2001), pp. 308–324. doi: 10.1002/cne.10168.

Lu, P. *et al.* (2012) 'Long-Distance Growth and Connectivity of Neural Stem Cells after Severe Spinal Cord Injury', *Cell*, 150, pp. 1264–1273. doi: 10.1016/j.cell.2012.08.020.

Lu, S. and Anseth, K. S. (2000) 'Release behavior of high molecular weight solutes from poly(ethylene glycol)-based degradable networks', *Macromolecules*, 33(7), pp. 2509–2515. doi: 10.1021/ma9915024.

Lu, X. *et al.* (2018) 'Polyethylene glycol in spinal cord injury repair: A critical review', *Journal of Experimental Pharmacology*, 10, pp. 37–49. doi: 10.2147/JEP.S148944.

Lukovic, D. *et al.* (2015) 'Concise Review : Reactive Astrocytes and Stem Cells in Spinal Cord Injury : Good Guys or Bad Guys ?', *Stem Cells*, 33, pp. 1036–1041.

Luo, L. *et al.* (2018) 'Molecular Mechanisms of Transdifferentiation of Adipose-Derived Stem Cells into Neural Cells : Current Status and Perspectives', *Stem Cells International*. Hindawi, 2018, pp. 1–14. doi: 10.1155/2018/5630802.

Lynskey, J. V., Belanger, A. and Jung, R. (2008) 'Activity-dependent plasticity in spinal cord injury', *Journal of Rehabilitation Research & Development*, 45(2), pp. 229–240. doi: 10.1682/JRRD.2007.03.0047.Activity-dependent.

Ma, Y. H. *et al.* (2018) 'Perineurium-like sheath derived from long-term surviving mesenchymal stem cells confers nerve protection to the injured spinal cord', *Biomaterials*. Elsevier Ltd, 160, pp. 37–55. doi: 10.1016/j.biomaterials.2018.01.015.

Macaya, D. J. *et al.* (2013) 'Astrocyte infiltration into injectable collagen-based hydrogels containing FGF-2 to treat spinal cord injury', *Biomaterials*. Elsevier Ltd, 34(14), p. 3602. doi: 10.1016/j.biomaterials.2012.12.050.

Mahoney, M. J. and Anseth, K. S. (2006) 'Three-dimensional growth and function of neural tissue in degradable polyethylene glycol hydrogels', *Biomaterials*, 27, pp. 2265–2274. doi: 10.1016/j.biomaterials.2005.11.007.

Mark, L. P. *et al.* (2001) 'Pictorial Review of Glutamate Excitotoxicity : Fundamental Concepts for Neuroimaging', *AJNR Am J Neuroradiol*, 22(December), pp. 1813–1824.

Martens, P. and Anseth, K. S. (2000) 'Characterization of hydrogels formed from acrylate modified poly (vinyl alcohol) macromers', *Polymer*, 41, pp. 7715–7722.

Martino, F. *et al.* (2018) 'Cellular Mechanotransduction : From Tension to Function', *Frontiers in Physiology*, 9(July), pp. 1–21. doi: 10.3389/fphys.2018.00824.

Mather, B. D. *et al.* (2006) 'Michael addition reactions in macromolecular design for emerging technologies', 31, pp. 487–531. doi: 10.1016/j.progpolymsci.2006.03.001.

Matsumoto, M. *et al.* (2016) 'A Water-Based Chitosan – Maleimide Precursor for Bioconjugation : An Example of a Rapid Pathway for an In Situ Injectable Adhesive Gel', *Macromol. Rapid Commun.*, 37, pp. 1618–1622.

Matute, C. *et al.* (2007) 'Excitotoxic damage to white matter', *J. Anat.*, 210, pp. 693–702. doi: 10.1111/j.1469-7580.2007.00733.x.

Mauri, E. *et al.* (2018) 'Biomaterials Science hydrogels as 3D neural stem cell culture systems †', *Biomaterials Science*. Royal Society of Chemistry, 6, pp. 501–510. doi: 10.1039/c7bm01056g.

Maynard, F. M. *et al.* (1997) 'International Standards for Neurological and Functional Classification of International Standards for Neurological and Functional Classi ® cation of Spinal Cord Injury', *Spinal Cord*, 35, pp. 266–274. doi: 10.1038/sj.sc.3100432.

Mccanney, G. A. *et al.* (2019) 'The Use of Myelinating Cultures as a Screen of Glycomolecules for CNS Repair', *Biology*, 8(52), pp. 1–15.

Mccormick, D. A. (2014) 'Membrane Potential and Action Potential', in *From Molecules to Networks*. 3rd edn, pp. 351–376. doi: 10.1016/B978-0-12-397179-1.00012-9.

Mcdonald, J. C. *et al.* (2000) 'Review General Fabrication of microfluidic systems in poly (dimethylsiloxane)', *Electrophoresis*, 21, pp. 27–40.

McDonald, J. W. and Sadowsky, C. (2002) 'Spinal cord injury', *The Lancetncet*, 359, pp. 417–425.

Mcever, R. P. and Luscinskas, F. W. (2018) 'Cell Adhesion', in *Hematology*. Seventh Ed. Elsevier Inc., pp. 127–134. doi: 10.1016/B978-0-323-35762-3.00012-3.

McKinnon, D. D., Kloxin, A. M. and Anseth, K. S. (2013) 'Synthetic hydrogel platform for three-dimensional culture of embryonic stem cell-derived motor neurons', *Biomaterial Science*, 4830(5), pp. 449–548. doi: 10.1039/c3bm00166k.

Meijering, E. *et al.* (2004) 'Design and Validation of a Tool for Neurite Tracing and Analysis in Fluorescence Microscopy Images', *Cytometry Part A*, 58(2), pp. 167–176. doi: 10.5040/9781474229050.0007.

Mendoza, J. E. and Foundas, A. L. (2008) *Clinical Neuroanatomy : A Neurobehavioral Approach*. Springer.

Merrill, E. W., Dennison, K. A. and Sung, C. (1993) 'Partitioning and diffusion of solutes in hydrogels of poly(ethylene oxide)', *Biomaterials*, 14(15), pp. 1117–1126. doi: 10.1016/0142-9612(93)90154-T.

Microchem (2000) 'SU-8 3000 Permanent Epoxy', *Product Datasheet*. doi: 10.1146/annurev.matsci.28.1.153.

Middendorp, J. J. Van *et al.* (2011) 'Diagnosis and Prognosis of Traumatic Spinal Cord Injury', in *Globabl Spine Journal*, pp. 1–7.

Milner, R. and Campbell, I. L. (2002) 'The Integrin Family of Cell Adhesion Molecules Has Multiple Functions Within The CNS', *Journal of Neuroscience Research*, 69, pp. 286–291. doi: 10.1002/jnr.10321.

Mohamad, C. A. C. (2014) *Human embryonic stem cell-derived mesenchymal stem cells as a therapy for spinal cord injury*. University of Glasgow.

Morpurgo, M. and Veronese, F. M. (2004) 'Conjugates of Peptides and Proteins to Polyethylene Glycols', in Niemeyer, C. M. (ed.) *Bioconjugation Protocols: Strategies and Methods*. Totowa, NJ: Humana Press, pp. 45–70. doi: 10.1385/1-59259-813-7:045.

Moses, J. E. and Moorhouse, A. D. (2007) 'The growing applications of click chemistry', *Chemical Society Reviews*, 36(8), pp. 1249–1262. doi: 10.1039/b613014n.

Moshayedi, P., Costa, L. F. and Christ, A. (2010) 'Mechanosensitivity of astrocytes on optimized polyacrylamide gels analyzed by quantitative morphometry', *J. Phys.: Condens. Matter*, 22, pp. 1–11. doi: 10.1088/0953-8984/22/19/194114.

Mosley, M. C. *et al.* (2016) 'Neurite extension and neuronal differentiation of human induced pluripotent stem cell derived neural stem cells on polyethylene glycol hydrogels containing a continuous Young ' s Modulus gradient', *JOURNAL OF BIOMEDICAL MATERIALS RESEARCH A*, 105A(3), pp. 824–833. doi: 10.1002/jbm.a.35955.

Mukhamedshina, Y. O. *et al.* (2018) 'Mesenchymal stem cells and the neuronal microenvironment in the area of spinal cord injury', *Neural Regeneration Research*, (1), pp. 227–237. doi: 10.4103/1673-5374.244778.

Myers, J. P., Santiago-medina, M. and Gomez, T. M. (2011) 'Regulation of Axonal Outgrowth and Pathfinding by Integrin – ECM Interactions', *Developmental Neurobiology*, 71(11), pp. 901–923. doi: 10.1002/dneu.20931.

Naghdi, P. *et al.* (2016) 'Survival , proliferation and differentiation enhancement of neural stem cells cultured in three-dimensional polyethylene glycol – RGD hydrogel with tenascin', *JOURNAL OF TISSUE ENGINEERING AND REGENERATIVE MEDICINE*, (October 2014), pp. 199–208. doi: 10.1002/term.

Nagoshi, N., Nakashima, H. and Fehlings, M. G. (2015) 'Riluzole as a Neuroprotective Drug for Spinal Cord Injury: From Bench to Bedside', *Molecules*, 20, pp. 7775–7789. doi: 10.3390/molecules20057775.

Nair, D. P. *et al.* (2014) 'The Thiol-Michael Addition Click Reaction: A Powerful and Widely Used Tool in Materials Chemistry', *Chem. Mater.*, 26, pp. 724–744. doi: 10.1021/cm402180t.

Nair, L. S. and Laurencin, C. T. (2007) 'Biodegradable polymers as biomaterials', *Progress in Polymer Science*, 32, pp. 762–798. doi: 10.1016/j.progpolymsci.2007.05.017.

Nakae, A. *et al.* (2011) 'The Animal Model of Spinal Cord Injury as an Experimental Pain Model', *Journal of Biomedicine and Biotechnology*, 2011, pp. 1–11. doi: 10.1155/2011/939023.

Nardo, T. *et al.* (2017) 'Synthetic Biomaterial for Regenerative Medicine Applications', in Orlando, G., Remuzzi, G., and Williams Bioengineering and Regeneration, D. F. B. T.-K. T. (eds) *Kidney Transplantation, Bioengineering and Regeneration*. Academic Press, pp. 901–921. doi: https://doi.org/10.1016/B978-0-12-801734-0.00065-5.

Naser, P. V and Kuner, R. (2018) 'Molecular , Cellular and Circuit Basis of Cholinergic Modulation of Pain', *Neuroscience*. The Authors, 387, pp. 135–148. doi: 10.1016/j.neuroscience.2017.08.049.

Nathan, F. M. and Li, S. (2017) 'Environmental cues determine the fate of astrocytes after spinal cord injury', *Neural Regeneration Research*, 12(12), pp. 1964–1970. doi: 10.4103/1673-5374.221144.

Nguyen, K. T. and West, J. L. (2002) 'Photopolymerizable hydrogels for tissue engineering applications', *Biomaterials*, 23, pp. 4307–4314.

Nguyen, L. H. *et al.* (2017) 'Three-dimensional aligned nanofibers-hydrogel scaffold for controlled non-viral drug / gene delivery to direct axon regeneration in spinal cord injury treatment', *Scientific reports*, 7(42212), pp. 1–12. doi: 10.1038/srep42212.

Nieberler, M. *et al.* (2017) 'Exploring the Role of RGD-Recognizing Integrins in Cancer', *Cancers*, 9(116), pp. 1–33. doi: 10.3390/cancers9090116.

Nieuwenhuis, B. *et al.* (2018) 'Integrins promote axonal regeneration after injury of the nervous system', *BIological Reviews*, 1346, pp. 1339–1362. doi: 10.1111/brv.12398.

Noback, C. R. *et al.* (2005) *The Human Nervous System*. 6th Editio. Edited by T. Catanese. Totowa:

Human Press.

Norenberg, M. D., Smith, J. O. N. and Marcillo, A. (2004) 'The Pathology of Human Spinal Cord Injury ':, *JOURNAL OF NEUROTRAUMA*, 21(4), pp. 429–440.

Northrop, B. H., Frayne, S. H. and Choudhary, U. (2015) 'Thiol–maleimide "click" chemistry: evaluating the influence of solvent, initiator, and thiol on the reaction mechanism, kinetics, and selectivity', *Polymer Chemistry*. Royal Society of Chemistry, 6, pp. 3415–3430. doi: 10.1039/c5py00168d.

Novikova, L. N., Novikov, L. N. and Kellerth, J. (2000) 'Survival effects of BDNF and NT-3 on axotomized rubrospinal neurons depend on the temporal pattern of neurotrophin administration', *European Journal of Neuroscience*, 12, pp. 776–780.

Okada, S. (2016) 'The pathophysiological role of acute inflammation after spinal cord injury', *Inflammation and Regeneration*, 36(1), p. 20. doi: 10.1186/s41232-016-0026-1.

Osseward, P. J. and Pfaff, S. L. (2019) 'Cell type and circuit modules in the spinal cord', *Current Opinion in Neurobiology*. Elsevier Ltd, 56, pp. 175–184. doi: 10.1016/j.conb.2019.03.003.

Othman, R., Vladisavljević, G. T. and Nagy, Z. K. (2015) 'Preparation of biodegradable polymeric nanoparticles for pharmaceutical applications using glass capillary microfluidics', *Chemical Engineering Science*, 137, pp. 119–130. doi: 10.1016/j.ces.2015.06.025.

Ouyang, L. I. U. *et al.* (2019) 'MMP - sensitive PEG hydrogel modified with RGD promotes bFGF , VEGF and EPC - mediated angiogenesis', *Experimental and Therapeutic Medicine*, 18, pp. 2933–2941. doi: 10.3892/etm.2019.7885.

Oyinbo, C. A. (2011) 'Secondary injury mechanisms in traumatic spinal cord injury : a nugget of this multiply cascade', *Acta Neurobiol Exp*, 71, pp. 281–299.

Paluch, E. K. *et al.* (2015) 'Mechanotransduction : use the force (s)', *BMC Biology*. BMC Biology, 13(47), pp. 1–14. doi: 10.1186/s12915-015-0150-4.

Park, H. *et al.* (2010) 'Effect of Swelling Ratio of Injectable Hydrogel Composites on Chondrogenic Differentiation of Encapsulated Rabbit Marrow Mesenchymal Stem Cells In Vitro', *Biomacromolecules*, 10(3), pp. 541–546. doi: 10.1021/bm801197m.Effect.

Park, J. *et al.* (2009) 'Nerve regeneration following spinal cord injury using matrix metalloproteinase-sensitive, hyaluronic acid-based biomimetic hydrogel scaffold containing brain-derived neurotrophic factor', *Journal of Biomedical Materials Research Part A*, 9999A, p. NA-NA. doi: 10.1002/jbm.a.32519.

Patterson, J. and Hubbell, J. A. (2010) 'Enhanced proteolytic degradation of molecularly engineered PEG hydrogels in response to MMP-1 and MMP-2', *Biomaterials*. Elsevier Ltd, 31(30), pp. 7836–7845. doi: 10.1016/j.biomaterials.2010.06.061.

Patterson, J. and Hubbell, J. A. (2011) 'Biomaterials SPARC-derived protease substrates to enhance the plasmin sensitivity of molecularly engineered PEG hydrogels', *Biomaterials*. Elsevier Ltd, 32(5), pp. 1301–1310. doi: 10.1016/j.biomaterials.2010.10.016.

Pellegatta, M. *et al.* (2013) 'α6β1 and α7β1 Integrins Are Required in Schwann Cells to Sort Axons', *The Journal of Neuroscience*, 33(46), pp. 17995–18007. doi: 10.1523/JNEUROSCI.3179-13.2013.

Peng, H. *et al.* (2007) 'Integrins and Dystroglycan Regulate Astrocyte Wound Healing : The Integrin b 1 Subunit is Necessary for Process Extension and Orienting the Microtubular Network'. doi: 10.1002/dneu.20593.

Phelps, E. A. *et al.* (2012) 'Maleimide Cross-Linked Bioactive PEG Hydrogel Exhibits Improved Reaction Kinetics and Cross-Linking for Cell Encapsulation and In Situ Delivery', *Advanced*

Materials, 24(1), pp. 64–70. doi: 10.1002/adma.201103574.

Pirko, I. and Noseworthy, J. H. (2007) 'Demyelinating Disorders of the Central Nervous System', in Goetz, C. G. B. T.-T. of C. N. (Third E. (ed.) *Textbook of Clinical Neurology*. 3rd edn. Philadelphia: W.B. Saunders, pp. 1103–1133. doi: https://doi.org/10.1016/B978-141603618-0.10048-7.

Placone, A. F. *et al.* (2016) 'Remain Quiescent in a Novel 3D Matrix', *Biomaterials*, 42, pp. 134–143. doi: 10.1016/j.biomaterials.2014.11.046.Human.

Platen, M. *et al.* (2015) 'Poly (2-oxazoline) -Based Microgel Particles for Neuronal Cell Culture', *Biomacromolecules*, 16, pp. 1516–1524. doi: 10.1021/bm501879h.

Poo, M. (2001) 'NEUROTROPHINS AS SYNAPTIC MODULATORS', *Nature Reviews Neuroscience*, 2(January), pp. 24–32.

Poole, L. B. (2015) 'The Basics of Thiols and Cysteines in Redox Biology and Chemistry', *Free Radic Biol Med.*, 0, pp. 148–157. doi: 10.1016/j.freeradbiomed.2014.11.013.The.

Poon, P. C. *et al.* (2007) 'Clip Compression Model Is Useful for Thoracic Spinal Cord Injuries Histologic and Functional Correlates', *Spine*, 32(25), pp. 2853–2859.

Popovich, P. G., Jakeman, L. B. and McTigue, D. M. (2009) 'Glial Responses to Injury', in Squire, L. R. B. T.-E. of N. (ed.) *Encyclopedia of Neuroscience*. Oxford: Academic Press, pp. 853–859. doi: https://doi.org/10.1016/B978-008045046-9.00018-8.

Powell, E. M. *et al.* (1997) 'Mechanisms of astrocyte-directed neurite guidance', *Cell and Tissue Research*, 290, pp. 385–393.

Powell, E. M. and Geller, H. M. (1999) 'Dissection of Astrocyte-Mediated Cues in Neuronal Guidance', *Glia*, 26, pp. 73–83.

Puranen, J. S. *et al.* (2003) 'α11β1 Integrin Recognizes the GFOGER Sequence in Interstitial Collagens', *THE JOURNAL OF BIOLOGICAL CHEMISTRY*, 278(9), pp. 7270–7277. doi: 10.1074/jbc.M210313200.

Purves, D. *et al.* (2001) 'The Internal Anatomy of the Spinal Cord.', in *Neuroscience*.

Qu, J. and Zhang, H. (2017) 'Review Article Roles of Mesenchymal Stem Cells in Spinal Cord Injury', *Stem Cells International*. Hindawi, 2017(5251313), pp. 1–12. doi: 10.1155/2017/5251313.

Radi, B., Wellard, R. M. and George, G. A. (2013) 'Effect of dangling chains on the structure and physical properties of a tightly crosslinked poly(ethylene glycol) network', *Soft Matter*, 9, pp. 3262–3271. doi: 10.1039/c3sm27819k.

Raeber, G. P., Lutolf, M. P. and Hubbell, J. A. (2005) 'Molecularly Engineered PEG Hydrogels : A Novel Model System for Proteolytically Mediated Cell Migration', *Biophysical Journal*. Elsevier, 89(2), pp. 1374–1388. doi: 10.1529/biophysj.104.050682.

Rao, S. R. *et al.* (2016) 'Differentiation of human gingival mesenchymal stem cells into neuronal lineages in 3D bioconjugated injectable protein hydrogel construct for the management of neuronal disorder', *Experimental & Molecular Medicine*. Nature Publishing Group, 48(2), pp. e209-11. doi: 10.1038/emm.2015.113.

Raper, J. and Mason, C. (2019) 'Cellular Strategies of Axonal Pathfinding', *Cold Spring Harb Perspect Biol*, 2, pp. 1–22.

Rauch, F. M. *et al.* (2010) 'Engineering angiogenesis following spinal cord injury: A coculture of neural progenitor and endothelial cells in a degradable polymer implant leads to an increase in vessel density and formation of the blood-spinal cord barrier', *Eur J Neurosci.*, 29(1), pp. 132–145. doi: 10.1111/j.1460-9568.2008.06567.x.Engineering.

Rehmann, M. S. *et al.* (2017) 'Tuning and Predicting Mesh Size and Protein Release from Step

Growth Hydrogels', *Biomacromolecules*, 18(10), pp. 3131–3142. doi: 10.1021/acs.biomac.7b00781.

Repic, T. *et al.* (2016) 'Characterization of dorsal root ganglion neurons cultured on silicon micro-pillar substrates', *Scientific Reports*. Nature Publishing Group, 6, pp. 1–10. doi: 10.1038/srep39560.

Rezaie, H. R., Bakhtiari, L. and Öchsner, A. (2015) *Biomaterials and Their Applications*. Berlin: Springer International Publishing.

Richardson, S. M. *et al.* (2016) 'Mesenchymal stem cells in regenerative medicine : Focus on articular cartilage and intervertebral disc regeneration', *Methods*. Elsevier Inc., 99, pp. 69–80. doi: 10.1016/j.ymeth.2015.09.015.

Roa, J. J. *et al.* (2011) 'Calculation of Young's Modulus Value by Means of AFM', *Recent Patents on Nanotechnology*, 5, pp. 27–36. doi: 10.1016/0041-0101(83)90155-1.

Robinson, R. . *et al.* (1999) 'The structures of the neurotrophin 4 homodimer and the brain-derived neurotrophic factor/neurotrophin 4 heterodimer reveal a common Trk-binding site. https://www.rcsb.org/pdb/explore/jmol.do?structureId=1b8m&bionumber=1&jmolMode=HTML5', *Protein Sci.*, 8, pp. 2589–2597. Available at: https://www.rcsb.org/pdb/explore/jmol.do?structureId=1b8m&bionumber=1&jmolMode=HTML5 (Accessed: 4 July 2019).

Rocha, L. A. *et al.* (2018) 'The Role of Biomaterials as Angiogenic Modulators of Spinal Cord Injury : Mimetics of the Spinal Cord , Cell and Angiogenic Factor Delivery Agents', *Frontiers in Pharmacology*, 9(164), pp. 1–7. doi: 10.3389/fphar.2018.00164.

Rogers, S. *et al.* (1983) 'Neurite Extension by Peripheral and Central Nervous System Neurons in Response to Substratum-Bound Fibronectin and Laminin '', *Developmental Biology*, 220, pp. 212–220.

Rose, J. C. *et al.* (2017) 'Nerve Cells Decide to Orient inside an Injectable Hydrogel with Minimal Structural Guidance', *Nano Letters*, 17, pp. 3782–3791. doi: 10.1021/acs.nanolett.7b01123.

Rosner, J. *et al.* (2012) 'The Potential for Cellular Therapy Combined with Growth Factors in Spinal Cord Injury', *Stem Cells International*, 2012, pp. 1–11. doi: 10.1155/2012/826754.

Ruel-Gariépy, E. and Leroux, J. C. (2004) 'In situ-forming hydrogels - Review of temperature-sensitive systems', *European Journal of Pharmaceutics and Biopharmaceutics*, 58(2), pp. 409–426. doi: 10.1016/j.ejpb.2004.03.019.

Ruoslahti, E. and Pierschbacher, M. D. (1987) 'New Perspectives in Cell Adhesion : RGD and Integrins', *Science*, 238(4826), pp. 491–497.

Rust, R. and Kaiser, J. (2017) 'Insights into the Dual Role of Inflammation after Spinal Cord Injury', *The Journal of Neuroscience*, 37(18), pp. 4658–4660. doi: 10.1523/JNEUROSCI.0498-17.2017.

Saha, K. *et al.* (2008) 'Substrate Modulus Directs Neural Stem Cell Behavior', *Biophysical Journal*, 95(November), pp. 4426–4438. doi: 10.1529/biophysj.108.132217.

Salgado, A. J. *et al.* (2015) 'Mesenchymal stem cells secretome as a modulator of the neurogenic niche : basic insights and therapeutic opportunities', *Frontiers in Cellular Neuroscience*, 9(July), pp. 1–18. doi: 10.3389/fncel.2015.00249.

Salimath, A. S. *et al.* (2012) 'Dual Delivery of Hepatocyte and Vascular Endothelial Growth Factors via a Protease-Degradable Hydrogel Improves Cardiac Function in Rats', *PLOS ONE*, 7(11), pp. 1–12. doi: 10.1371/journal.pone.0050980.

Salter, M. W. and Stevens, B. (2017) 'Microglia emerge as central players in brain disease', *Nature Medicine*. Nature Publishing Group, 23(9), pp. 1018–1027. doi: 10.1038/nm.4397.

Santos, D. *et al.* (2016) 'Dose-Dependent Differential Effect of Neurotrophic Factors on in Vitro and in Vivo Regeneration of Motor and Sensory Neurons', *Neural Plasticity*, 2016, pp. 1–13. doi: 10.1155/2016/4969523.

Sarkar, K., Yingfei, X. and Sant, S. (2017) *The Immune Response to Implanted Materials and Devices Chapter 5: Host Response to Synthetic Versus Natural Biomaterials*. Edited by B. Corradetti. Springer.

Sawicka, K. M. *et al.* (2015) 'Fibronectin Interaction and Enhancement of Growth Factors : Importance for Wound Healing Fibronectin Interaction and Enhancement of Growth Factors : Importance for Wound Healing', *Advances in Wound Care*, 4(8), pp. 1–10. doi: 10.1089/wound.2014.0616.

Saxena, A. *et al.* (2012) 'Trehalose-enhanced isolation of neuronal sub-types from adult mouse brain', *Biotechniques*, 52(6), pp. 381–385. doi: 10.2144/0000113878.

Saxena, T. *et al.* (2012) 'Mechanical characterization of the injured spinal cord after lateral spinal hemisection injury in the rat.', *Journal of neurotrauma*, 29(9), pp. 1747–57. doi: 10.1089/neu.2011.1818.

Schneider, A. *et al.* (2006) 'Polyelectrolyte Multilayers with a Tunable Young ' s Modulus : Influence of Film Stiffness on Cell Adhesion', *Langmuir*, 22(6), pp. 1193–1200. doi: 10.1021/la0521802.

Schneider, C. A., Rasband, W. S. and Eliceiri, K. W. (2012) 'NIH Image to ImageJ: 25 years of image analysis', *Nature Methods*, 9, p. 671*675. Available at: https://www.nature.com/articles/nmeth.2089.

Schultz, K. M. and Anseth, K. S. (2013) 'Monitoring degradation of matrix metalloproteinases-cleavable PEG hydrogels via multiple particle tracking microrheology', *Soft Matter*, 9, pp. 1570–1579. doi: 10.1039/c2sm27303a.

Schultz, K. M., Kyburz, K. A. and Anseth, K. S. (2015) 'Measuring dynamic cell – material interactions and remodeling during 3D human mesenchymal stem cell migration in hydrogels', *PNAS*, 112(29), pp. E3757–E3764. doi: 10.1073/pnas.1511304112.

Schwab, J. M. *et al.* (2015) 'The paradox of chronic neuroinflammation, systemic immune suppression and autoimmunity after traumatic chronic spinal cord injury', *Exp Neurol.*, 258, pp. 121–129. doi: 10.1016/j.expneurol.2014.04.023.The.

Schweigreiter, R. and Bandtlow, C. E. (2006) 'Nogo in the Injured Spinal Cord', *JOURNAL OF NEUROTRAUMA*, 23(3), pp. 384–396.

Scuteri, A. *et al.* (2010) 'Mesenchymal Stem Cells Neuronal Differentiation Ability : A Real Perspective for Nervous System Repair ?', *Current Stem Cell Research & Therapy*, 6, pp. 82–92. doi: 10.2174/157488811795495486.

Seidlits, S. K. *et al.* (2010) 'The effects of hyaluronic acid hydrogels with tunable mechanical properties on neural progenitor cell differentiation', *Biomaterials*. Elsevier Ltd, 31(14), pp. 3930–3940. doi: 10.1016/j.biomaterials.2010.01.125.

Seliktar, D. *et al.* (2004) 'MMP-2 sensitive, VEGF-bearing bioactive hydrogels for promotion of vascular healing', *J Biomed Mater Res A*, 68(4), pp. 704–716. doi: 10.1002/jbm.a.20091.

Sengul, G. and Watson, C. (2015) 'Ascending and Descending Pathways in the Spinal Cord', in *The Rat Nervous System*. Fourth Edi. Elsevier Inc., pp. 115–130. doi: 10.1016/B978-0-12-374245-2.00008-5.

Seong, Y. J. *et al.* (2019) 'Hyaluronic Acid-Based Hybrid Hydrogel Microspheres with Enhanced Structural Stability and High Injectability', *ACS Omega*, 4(9), pp. 13834–13844. doi: 10.1021/acsomega.9b01475.

Sezer, N. (2015) 'Chronic complications of spinal cord injury', *World Journal of Orthopedics*, 6(1), p. 24. doi: 10.5312/wjo.v6.i1.24.

Shahdoost, S. *et al.* (2014) 'Towards a Miniaturized Brain-Machine-Spinal Cord Interface (BMSI) for Restoration of Function after Spinal Cord Injury', pp. 486–489.

Sherman, V. R., Yang, W. and Meyers, M. A. (2015) 'The materials science of collagen', *Journal of Mechanical Behavior of Biomedical Materials*. Elsevier Ltd, 52, pp. 22–50. doi: 10.1016/j.jmbbm.2015.05.023.

Siddiqui, A. M., Khazaei, M. and Fehlings, M. G. (2015) *Translating mechanisms of neuroprotection, regeneration, and repair to treatment of spinal cord injury*. 1st edn, *Progress in Brain Research*. 1st edn. Elsevier B.V. doi: 10.1016/bs.pbr.2014.12.007.

Siesjo, B. K. (1972) 'The regulation of cerebrospinal fluid pH', *Kidney International*, 1, pp. 360–374. doi: 10.1038/ki.1972.47.

Silva, N. A. *et al.* (2014) 'From basics to clinical: A comprehensive review on spinal cord injury', *Progress in Neurobiology*, 114, pp. 25–57. doi: 10.1016/j.pneurobio.2013.11.002.

Singh, A. *et al.* (2014) 'Global Prevalence and incidence of traumatic spinal cord injury', *Clinical Epidemiology*, 6(February 2015), pp. 309–331. doi: 10.2147/CLEP.S68889.

Singh, S. P. *et al.* (2015) 'A peptide functionalized poly(ethylene glycol) (PEG) hydrogel for investigating the influence of biochemical and biophysical matrix properties on tumor cell migration', *Biomater Sci.*, 2(7), pp. 1024–1034. doi: 10.1039/C4BM00022F.A.

Sloan, S. A. *et al.* (2017) 'Human Astrocyte Maturation Captured in 3D Cerebral Cortical Spheroids Derived from Pluripotent Stem Cells', *Neuron*, 95, pp. 779–790. doi: 10.1016/j.neuron.2017.07.035.

Smith, L. J. *et al.* (2018) 'Diels-Alder Click-Cross-Linked Hydrogels with Increased Reactivity Enable 3D Cell Encapsulation', *Biomacromolecules*, 19(3), pp. 926–935. doi: 10.1021/acs.biomac.7b01715.

Sofroniew, M. V (2009) 'Molecular dissection of reactive astrogliosis and glial scar formation', *Trends in Neurosciences*, 32(12), pp. 638–647. doi: 10.1016/j.tins.2009.08.002.

Sofroniew, M. V and Vinters, H. V (2010) 'Astrocytes : biology and pathology', *Acta Neuropathol (2010)*, 119, pp. 7–35. doi: 10.1007/s00401-009-0619-8.

Stobart, J. L. and Anderson, C. M. (2013) 'Multifunctional role of astrocytes as gatekeepers of neuronal energy supply', *Frontiers in Cellular Neuroscience*, 7(April), pp. 1–21. doi: 10.3389/fncel.2013.00038.

Straley, K. S. *et al.* (2010) 'Biomaterial Design Strategies for the Treatment of Spinal Cord Injuries', *Journal of Neurotrauma*, 27, pp. 1–19.

Sun, X. *et al.* (2018) 'Differentiation of adipose-derived stem cells into Schwann cell-like cells through intermittent induction: potential advantage of cellular transient memory function', *Stem Cell Research & Therapy*. Stem Cell Research & Therapy, 9(133), pp. 1–20.

Takeda, Y. S. and Xu, Q. (2015) 'Neuronal Differentiation of Human Mesenchymal Stem Cells Using Exosomes Derived from Differentiating Neuronal Cells', *PLOS ONE*, 10(8), p. 2015. doi: 10.1371/journal.pone.0135111.

Talac, R. *et al.* (2004) 'Animal models of spinal cord injury for evaluation of tissue engineering treatment strategies Animal models of spinal cord injury for evaluation of tissue engineering treatment strategies', *BIomaterials*, 25, pp. 1505–1510. doi: 10.1016/S0142-9612(03)00497-6.

Tan, H. *et al.* (2009) 'Novel multiarm PEG-based hydrogels for tissue engineering', *Journal of*

Biomedical Materials Research Part A, 92A(3), pp. 26–28. doi: 10.1002/jbm.a.32438.

Taran, R. *et al.* (2014) 'Review In vitro and in vivo neurogenic potential of mesenchymal stem cells isolated from different sources', *Journal of biosciences*, 39(January), pp. 157–169. doi: 10.1007/s12038-013-9409-5.

Temenoff, J. S. *et al.* (2001) 'Effect of poly (ethylene glycol) molecular weight on tensile and swelling properties of oligo (poly (ethylene glycol) fumarate) hydrogels for cartilage tissue engineering', *Journal of Biomedical Materials Research*, 59, pp. 429–437. doi: 10.1002/jbm.1259.

Temple, S. (2001) 'The development of neural stem cells', *Nature*, 414, pp. 112–117.

Thid, D. *et al.* (2008) 'Supported phospholipid bilayers as a platform for neural progenitor cell culture', *Journal of Biomedical Materials Research - Part A*, 84(4), pp. 940–953. doi: 10.1002/jbm.a.31358.

Thuret, S., Moon, L. D. F. and Gage, F. H. (2006) 'Therapeutic interventions after spinal cord injury.', *Nature reviews. Neuroscience*, 7(8), pp. 628–43. doi: 10.1038/nrn1955.

Tibbitt, M. W. and Anseth, K. S. (2009) 'Hydrogels as Extracellular Matrix Mimics for 3D Cell Culture', *Biotechnology and Bioengineering*, 103(4), pp. 655–663. doi: 10.1002/bit.22361.

Toft, A. *et al.* (2007) 'Electrophysiological evidence that olfactory cell transplants improve function after spinal cord injury', *Brain*, 130, pp. 970–984. doi: 10.1093/brain/awm040.

Toft, A. *et al.* (2013) 'A Comparative Study of Glial and Non-neural Cell Properties for Transplant-Mediated Repair of the Injured Spinal Cord', *Glia*, 61, pp. 513–528. doi: 10.1002/glia.22452.

Tonge, D. A. *et al.* (2012) 'Fibronectin supports neurite outgrowth and axonal regeneration of adult brain neurons in vitro', *Brain Research*. Elsevier B.V., 1453, pp. 8–16. doi: 10.1016/j.brainres.2012.03.024.

Turner, C. E. (2000) 'Paxillin and focal adhesion signalling', *Nature Cell Biology*, 2(December), pp. 231–236.

Turney, S. G. *et al.* (2007) 'Nerve growth factor stimulates axon outgrowth through negative regulation of growth cone actomyosin restraint of microtubule advance', *Molecular Biology of the Cell*, 27(3), pp. 500–517. doi: 10.1091/mbc.E15-09-0636.

Uchida, M. *et al.* (2019) 'Evaluation of the effects of cross-linking and swelling on the mechanical behaviors of hydrogels using the digital image', *Soft Matter*. Royal Society of Chemistry, 15, pp. 3389–3396. doi: 10.1039/c9sm00049f.

Ulndreaj, A., Badner, A. and Fehlings, M. G. (2017) 'Promising neuroprotective strategies for traumatic spinal cord injury with a focus on the differential effects among anatomical levels of injury [version 1 ; referees : 2 approved] Referee Status ':, *F1000 Research*, 6, pp. 1–13. doi: 10.12688/f1000research.11633.1.

Vanderhaeghen, P. and Cheng, H.-J. (2010) 'Guidance Molecules in Axon Pruning and Cell Death', *Cold Spring Harb Perspect Biol*, 2, pp. 1–18.

Varma, S. and Voldman, J. (2018) 'Caring for cells in microsystems: principles and practices of cell-safe device design and operation', *Lab on a Chip*. Royal Society of Chemistry, 18, pp. 3333–3352. doi: 10.1039/c8lc00746b.

Varone, A. *et al.* (2017) 'The potential of Antheraea pernyi silk for spinal cord repair', *Scientific Reports*. Springer US, 7(1), pp. 1–10. doi: 10.1038/s41598-017-14280-5.

Wang, J. and Pearse, D. D. (2015) 'Therapeutic Hypothermia in Spinal Cord Injury : The Status of Its Use and Open Questions', *International Journal of Molecular Sciences*, 16, pp. 16848–16879. doi: 10.3390/ijms160816848.

Wang, N., Ostuni, E. and Whitesides, G. M. (2002) 'Micropatterning Tractional Forces in Living Cells', *Cell Motility and the Cytoskeleton*, 106(February), pp. 97–106. doi: 10.1002/cm.10037.

Wang, N., Tytell, J. D. and Ingber, D. E. (2009) 'Mechanotransduction at a distance: mechanically coupling the extracellular matrix with the nucleus', *Nature Reviews*, 10, pp. 75–82.

Van Der Want, J. J. L. *et al.* (1998) 'Dendro-dendritic connections between motoneurons in the rat spinal cord : an electron microscopic investigation', *Breain Research*, 779, pp. 342–345.

Waxman, S. G. (2017) 'Conduction in Myelinated , and Demyelinated Fibers', 02215(1), pp. 1–5.

Webb, D. J., Parsons, J. T. and Horwitz, A. F. (2002) 'Adhesion assembly , disassembly and turnover in migrating cells – over and over and over again', *Nature Cell Biology*, 4, pp. 97–100.

Weber, L. M., Lopez, C. G. and Anseth, K. S. (2010) 'The effects of PEG hydrogel crosslinking density on protein diffusion and encapsulated islet survival and function', *J Biomed Mater Res A.*, 90(3), pp. 720–729. doi: 10.1002/jbm.a.32134.The.

Weightman, A. P. *et al.* (2014) 'Biomaterials An in vitro spinal cord injury model to screen neuroregenerative materials', *Biomaterials*. Elsevier Ltd, 35(12), pp. 3756–3765. doi: 10.1016/j.biomaterials.2014.01.022.

Wen, Y. *et al.* (2016) 'Spinal cord injury repair by implantation of structured hyaluronic acid scaffold with PLGA microspheres in the rat', *Cell Tissue Res*, 364, pp. 17–28. doi: 10.1007/s00441-015-2298-1.

Whetstone, W. D. *et al.* (2010) 'Blood-Spinal Cord Barrier After Spinal Cord Injury: Relation to Revascularization and Wound Healing', *J Neurosci Res.*, 74(2), pp. 227–239. doi: 10.1002/jnr.10759.Blood-Spinal.

Widenfalk, J. *et al.* (2003) 'Vascular Endothelial Growth Factor Improves Functional Outcome and Decreases Secondary Degeneration in Experimental Spinal Cord Contusion Injury', *Neuroscience*, 120, pp. 951–960. doi: 10.1016/S0306-4522(03)00399-3.

Wiesmann, C. *et al.* (1999) 'Crystal structure of nerve growth factor in complex with the ligand-binding domain of the TrkA receptor. https://www.rcsb.org/structure/1WWW', *Nature*, 401, pp. 184–188. doi: 10.2210/PDB1WWW/PDB.

Witten, J. and Ribbeck, K. (2017) 'The particle in the spider's web: transport through biological hydrogels', *Nanoscale*. Royal Society of Chemistry, 9, pp. 8080–8095. doi: 10.1039/c6nr09736g.

Wright, B. L. C., Lai, J. T. F. and Sinclair, A. J. (2012) 'Cerebrospinal fluid and lumbar puncture : a practical review', *J Neurol*, 259, pp. 1530–1545. doi: 10.1007/s00415-012-6413-x.

Wu, G. *et al.* (2018) 'Biomaterials Recovery of paralyzed limb motor function in canine with complete spinal cord injury following implantation of MSC-derived neural network tissue', *Biomaterials*. Elsevier Ltd, 181, pp. 15–34. doi: 10.1016/j.biomaterials.2018.07.010.

Wu, J. *et al.* (2015) 'Effect of micropatterned TiO 2 nanotubes thin film on the deposition of endothelial extracellular matrix : For the purpose of enhancing surface biocompatibility', *Biointerphases*, 10(4), pp. 1–9. doi: 10.1116/1.4928304.

Wu, Y., Satkunendrarajah, K. and Fehlings, M. G. (2014) 'RILUZOLE IMPROVES OUTCOME FOLLOWING ISCHEMIA – REPERFUSION INJURY TO THE SPINAL CORD BY PREVENTING DELAYED PARAPLEGIA', *Neuroscience*, 265, pp. 302–312. doi: 10.1016/j.neuroscience.2014.01.059.

Xi, W. *et al.* (2014) 'Click chemistry in materials science', *Advanced Functional Materials*, 24(18), pp. 2572–2590. doi: 10.1002/adfm.201302847.

Yao, S. *et al.* (2016) 'Co-effects of matrix low elasticity and aligned topography on stem cell neurogenic differentiation and rapid neurite outgrowth', *Nanoscale*. Royal Society of Chemistry, 8,

pp. 10252–10265. doi: 10.1039/c6nr01169a.

Ying, Y. *et al.* (2016) 'In Vitro Differentiation of Bone Marrow Mesenchymal stem cells into neuron-like cells by cerebrospinal Fluid improves Motor Function of Middle cerebral artery Occlusion rats', *Frontiers in Neurology*, 7(October), pp. 1–9. doi: 10.3389/fneur.2016.00183.

Yoshida, K. and Gage, F. H. (1991) 'Fibroblast growth factors stimulate nerve growth factor synthesis and secretion by astrocytes', *Brain Research*, 538, pp. 118–126.

Yousefi, A. *et al.* (2016) 'Prospect of Stem Cells in Bone Tissue Engineering : A Review', *Stem Cells International*, 2016, pp. 1–13.

Yu, C. *et al.* (2011) 'Early integrin binding to Arg-Gly-Asp peptide activates actin polymerization and contractile movement that stimulates outward translocation', *PNAS*, 108(51), pp. 20585–20590. doi: 10.1073/pnas.1109485108.

Yu, S. *et al.* (2016) 'Angiogenic microspheres promote neural regeneration and motor function recovery after spinal cord injury in rats', *Nature Publishing Group*. Nature Publishing Group, 6, pp. 1–13. doi: 10.1038/srep33428.

Yuan, Y. and He, C. (2013) 'The glial scar in spinal cord injury and repair', *Neurosci Bull*, 29(4), pp. 421–435. doi: 10.1007/s12264-013-1358-3.

Yunoki, S., Ohyabu, Y. and Hatayama, H. (2013) 'Temperature-Responsive Gelation of Type I Collagen Solutions Involving Fibril Formation and Genipin Crosslinking as a Potential Injectable Hydrogel', *International Journal of Biomaterials*, 2013, pp. 1–14.

Zaidel-bar, R., Kam, Z. and Geiger, B. (2005) 'Polarized downregulation of the paxillin-p130 CAS - Rac1 pathway induced by shear flow', *Journal of Cell Science*, 118, pp. 3997–4007. doi: 10.1242/jcs.02523.

Zhang, Q. *et al.* (2014) 'Stiff substrates enhance cultured neuronal network activity', *Scientific Reports*, 4, pp. 12–15. doi: 10.1038/srep06215.

Zhang, Y. *et al.* (2017) 'Thiol Specific and Tracelessly Removable Bioconjugation via Michael Addition to 5-Methylene Pyrrolones', *Journal of the American Chemical Society*, 139, pp. 6146–6151. doi: 10.1021/jacs.7b00670.

Zhang, Z. and Guth, L. (1997) 'Experimental Spinal Cord Injury : Wallerian Degeneration in the Dorsal Column Is Followed by Revascularization , Glial Proliferation , and Nerve Regeneration', *Experimental Neurology*, 171(147), pp. 159–171.

Zhu, J. (2011) 'Bioactive Modification of Poly(ethylene glycol) Hydrogels for Tissue Engineering', *Biomaterials*, 31(17), pp. 4639–4656. doi: 10.1016/j.biomaterials.2010.02.044.Bioactive.

Zustiak, S. P., Durbal, R. and Leach, J. B. (2010) 'Influence of cell-adhesive peptide ligands on poly(ethylene glycol) hydrogel physical , mechanical and transport properties', *Acta Biomaterialia*. Acta Materialia Inc., 6(9), pp. 3404–3414. doi: 10.1016/j.actbio.2010.03.040.

Zustiak, S. P. and Leach, J. B. (2010) 'Hydrolytically degradable poly(ethylene glycol) hydrogel scaffolds with tunable degradation and mechanical properties', *Biomacromolecules*, 11(5), pp. 1348–1357. doi: 10.1016/j.surg.2006.10.010.Use.